Model-based Optimization of Oil Recovery: Robust Operational Strategies

Model-based Optimization of Oil Recovery: Robust Operational Strategies

PROEFSCHRIFT

ter verkrijging van de graad van doctor
aan de Technische Universiteit Delft,
op gezag van de Rector Magnificus prof. ir. K.Ch.A.M. Luyben,
voorzitter van het College voor Promoties,
in het openbaar te verdedigen op
18 maart 2015 om 15:00 uur

door

Gijs Michiel VAN ESSEN

werktuigbouwkundig ingenieur
geboren te Amersfoort

Dit proefschrift is goedgekeurd door de promotoren:

Prof. dr. ir. J.D. Jansen
Prof. dr. ir. P.M.J. Van den Hof

Samenstelling promotiecommissie:

Rector Magnificus	voorzitter
Prof. dr. ir. J.D. Jansen	Technische Universiteit Delft, promotor
Prof. dr. ir. P.M.J. Van den Hof	Technische Universiteit Delft, promotor
Prof. dr. W.R. Rossen	Technische Universiteit Delft
Prof. dr. S. Weiland	Technische Universiteit Eindhoven
Prof. dr. ir. A.W. Heemink	Technische Universiteit Delft
Dr. P.J. van den Hoek	Shell International E & P
Dr. J.B. Jørgensen	Technical University of Denmark
Prof. dr. P.L.J. Zitha	Technische Universiteit Delft, reservelid

This research has been conducted in the framework of the ”Integrated System Approach for Petroleum Production” (ISAPP) programme. The knowledge center is a long-term co-operation of TNO, Shell and Delft University of Technology to increase hydrocarbon recovery through the application of innovative reservoir development and management technologies.

ISBN/EAN: 978-94-6108-949-6
Keywords: petroleum, reservoir engineering, systems and control, optimization

Printed by Gildeprint - The Netherlands.

Acknowledgements

Completing this thesis after spending four years in Delft working on my PhD research turned out to be very challenging. For the fact that it eventually did come together I owe thanks to a great many people.

First of all my gratitude goes out to my supervisors Jan Dirk and Paul. Your steer and feedback were at times just the thing I needed to keep my focus. I also truly value that you kept faith in me in bringing my PhD project to a proper end. I realize I may not have been the easiest PhD student to supervise, which makes my appreciation for your time and effort even greater. Special thanks also go out to Okko Bosgra who played an important role in defining the initial outline of my PhD project. His passing was and still is a great loss to the entire field of Systems & Control.

I would also like to thank my current and former Shell team leads Paul van den Hoek and Paul Gelderblom for allowing me to spend time on writing my thesis, without which I couldn't have finished. I also owe thanks to Maarten Zandvliet, who - as my MSc thesis supervisor - inspired me to also do a PhD and thus became a valuable colleague and friend. Similarly, I hold dear memories to the many useful and pleasant discussions I had with my Shell coworkers Jorn, Sippe, Gerard, Roald, Gosia and Aslı. My gratitude also goes out to Amin Rezapour for the contribution he made to this thesis through his MSc project.

I'd like to say thanks to my parents for supporting me and encouraging me to go on. Stijn, Koen and Jort, my *boeffies*, many thanks for the very much-needed and pleasant distractions. You've really helped me to put things into perspective. And finally and mostly I want to thank Daphne for being there for me and supporting me during hard times.

The Hague, March 2015
Gijs van Essen

Contents

Chapter 1

Introduction

The theoretical basis for solving large-scale dynamic optimization problems has been around for more than three centuries, starting with the calculus of variations, from which the conditions for optimality were defined. However, it wasn't until the uprise of the computer in the 1980s that these theories could really be exploited to their full extent. Nowadays, dynamic optimization is encountered in many different environments such as manufacturing, transportation, scheduling, financial markets and so on. In those circumstances where dynamic optimization is applied to find an optimal control strategy, it is often referred to as *optimal control*. Especially in process control, optimal control has made a significant contribution over the recent years to maximize revenues and minimize costs.

In the upstream oil industry, the process of depleting an oil reservoir can quite easily be poured into a mathematical description of a dynamic optimization or optimal control problem. As in any optimal control problem, three elements need to be defined: an objective function, a dynamic model and the constraints. The dynamic system involves the reservoir itself, of which the behavior can be manipulated by the controls present in the wells and the surface facilities. The objective function is often of an economic nature, although additional objectives may be involved, e.g. ultimate recovery. Various constraints act on the problem due to physical, environmental, contractual, technical, organizational or legal limitations.

In literature, the first reports on large-scale dynamic optimization of oil recovery over the life of a reservoir can be traced back to the work by Ramirez (1987), followed by, among others, Virnovski (1991), Zakirov et al. (1996) and Sudaryanto and Yortsos (2000, 2001). However, it wasn't until the advent of 'smart wells' and 'smart fields' technologies that the subject was truly picked up by the oil and gas research commu-

nity. These technologies significantly increased the possibility to measure and control the depletion process, causing a revival of interest in dynamic optimization using a variety of methods, see Yang et al. (2003), Brouwer and Jansen (2004), Saputelli et al. (2005), Thiele and Batycky (2006), Lorentzen et al. (2006) and Alhuthali et al. (2007). Initially, scalability of these methods from small-scale academic 2D problems to large-scale optimization problems using full-physics, large-scale reservoir models were limiting the deployment of these methods within oil companies. However, advances in these technologies, as well as the increased computational capacity of modern day computers have (partly) resolved that problem. The following field case study, presented in Van Essen et al. (2010a), demonstrates the application of model-based optimization to a complex realistically-sized reservoir model to aid the design of new smart wells. In this study, water flooding is considered as recovery mechanism. This secondary recovery mechanism involves the injection of water into the reservoir to increase production, using dedicated water injection wells. It serves two purposes: preserving a high enough pressure in the reservoir (pressure maintenance) and displacing the oil from the pore spaces (sweep).

Example 1. *St. Joseph is a mature oil field located 135km offshore Sabah, Malaysia. The stock tank oil initially in place (STOIIP) is estimated at 630 MMstb, of which 83% is located in the main reservoir package in the Northwest Flank. These reservoir units dip at an angle of approximately 20 degrees to the NW and have a strongly layered internal architecture, with only limited (vertical) communication between layers. The St. Joseph field has been on production since 1981. Until 1996 the recovery mechanism was natural depletion under gravity drainage. At the end of 1995, the field had produced 105 MMstb out of the total ultimate recovery estimated at 230 MMstb. Average pressure had fallen from 7.3 MPa to 4.1 MPa. Since May 1996, production has been supported by crestal gas injection. Gas is injected into the reservoir for two reasons: disposal of produced gas from St. Joseph and neighboring fields, and reservoir pressure maintenance.*

A feasibility study completed in the second quarter of 2006 concluded that water injection was not only feasible, but also required to safeguard developed reserves and to realize additional oil recovery from the field. A large redevelopment project was planned to facilitate water flooding, using six horizontal water injectors. The horizontal water injectors require a high degree of zonal control, because of the laminated nature of the reservoir and historical problems with controlling water and gas breakthrough in high permeability streaks. The selected concept for the water injection wells is a horizontal well, completed with multiple zones. Each zone will be fitted with an inflow control valve (ICV) and dual downhole pressure gauges to allow remote control.

The main objective of this waterflood optimization study is to determine the value of downhole control in the planned water injectors, in terms of incremental cumulative oil production. The maximum incremental oil production using downhole control is determined by finding the optimum configuration of perforation zones, where the injection rate into each zone is con-

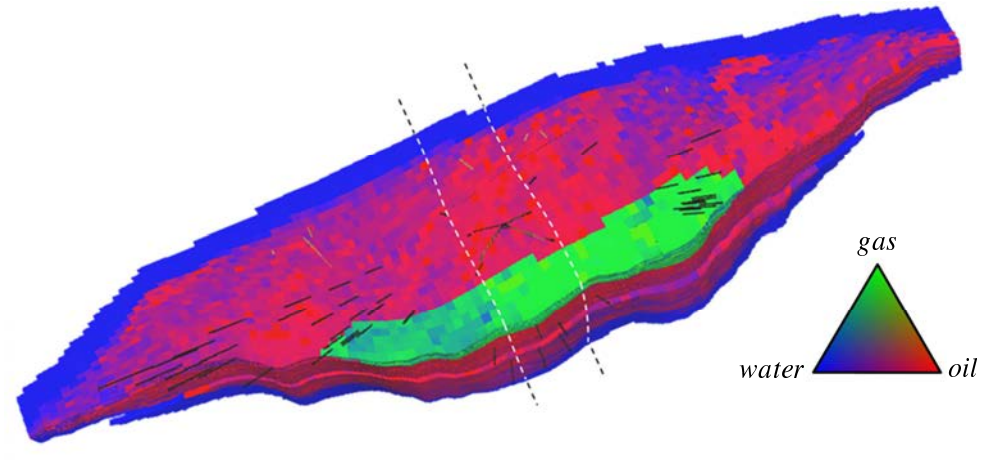

Figure 1.1 : Full Field Model showing saturations at start production in 1981. The location and size of the sector model are shown between dashed lines.

trolled by one ICV and the optimum operation of the ICVs. The valve settings (optimization parameters) can vary within a specified range, defined by a number of operational and physical constraints.

In this optimization study, to determine the value of a four-zone smart completion of the planned horizontal injectors, a 3D finite-difference model of the St. Joseph field was used. From this full field model a representative sector of size $28 \times 9 \times 711$ *grid blocks (GBs) was selected from the middle of the reservoir, as indicated in Figure 1.1. The sector model contains 12 production wells of which five have a dual completion. The planned water injector is a horizontal well that injects (treated) seawater at a fixed flow rate of 10,000 bbl/d. Its horizontal section is located below the initial oil-water contact. The completion is perforated over the entire horizontal section, which runs through all layers of the major sands, as can be observed in Figure 1.2. The perforation is initially divided into four perforation zones, which correspond to the predefined geological zones indicated by the B through E reservoir units. However, the number and length of the perforation zones are not fixed, but are regarded as variables within this optimization study. In the model, the horizontal section of the water injector passes through 102 grid blocks resulting in 102 perforation intervals in the reservoir model. A variable permeability-height product (KDH) multiplier is assigned to each perforation interval and they are used to simulate the use (and control) of ICVs, with a value of 0 relating to a fully closed valve and 1 to a fully open valve.*

In order to determine the maximum incremental production as a result of a smart completions, the study was conducted in three stages. Optimization was carried out using a gradient-based optimization technique, using a system of adjoint equations to determine the gradients, as described in Van Essen et al. (2009b).

1. *The first stage was aimed at finding the optimal values of all the 102 KDH-multipliers*

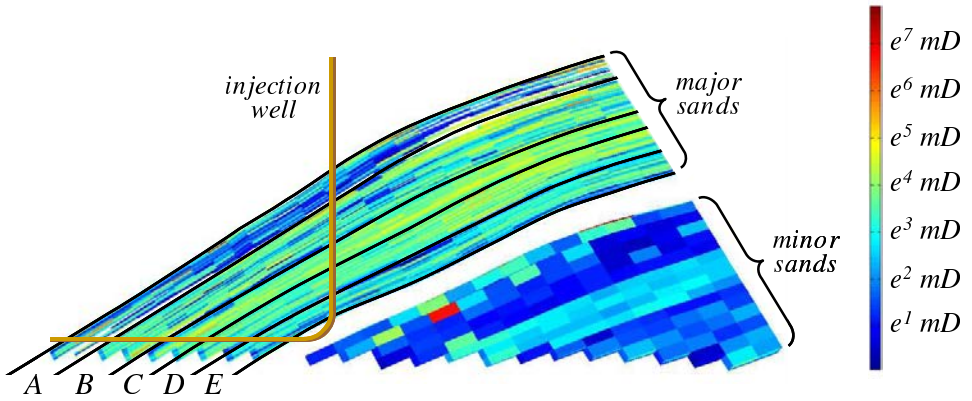

Figure 1.2 : Cross section of the St. Joseph sector model permeability field, showing the horizontal injection well and the minor and major sands, with its five identified geological layers A, B, C, D and E.

over time. In this 'ultimately smart' well case the only constraints on the control are the lower and upper bounds constraints, and its main purpose was to investigate the overall scope for optimization.

2. *In the second stage, the results of the first stage are used to identify the four optimal perforation zones. This is done through a visual inspection of the changes in the 102 KDH-multipliers over time.*

3. *In the third stage, the KDH-values are lumped together according to the defined optimal perforation zones such that they have the same value and act as if only one ICV is active for that zone. The lumped KDH-values are again optimized using the gradient-based optimization procedure used in the first stage.*

Four different cases were considered relating to the four different stages of the optimization procedure:

1. *No control. The no control case serves as base case and can be regarded as if using an ordinary completion instead of a smart completion.*

2. *Full 102 control. Serves as an reference case for the overall scope for optimization*

3. *Initial four-zone control. In this case the 102 KDH-multipliers are grouped according to the four predefined geological zones in the sector model and are labeled B, C, D and E.*

4. *Alternative four-zone control. In this case the 102 KDH-multipliers are grouped according to the optimal KDH-multipliers derived with Full 102 control, and are labeled B^*, C^*, D^*, E^*.*

Figure 1.3 shows the optimal control (time-varying KDH-multipliers), upon which are superimposed the standard (B, C, D and E) and alternative grouping (B^*, C^*, D^* and E^*) of

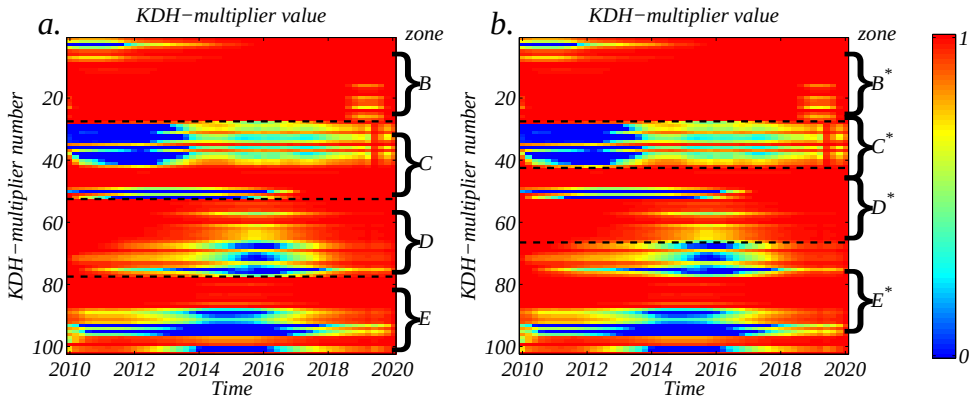

Figure 1.3 : Optimal time-varying KDH-multipliers for full 102 control. Left (a.) standard grouping according to predefined geological layers (B, C, D, E) of the sector model. Right (b.) alternative grouping (B^*, C^*, D^*, E^*).

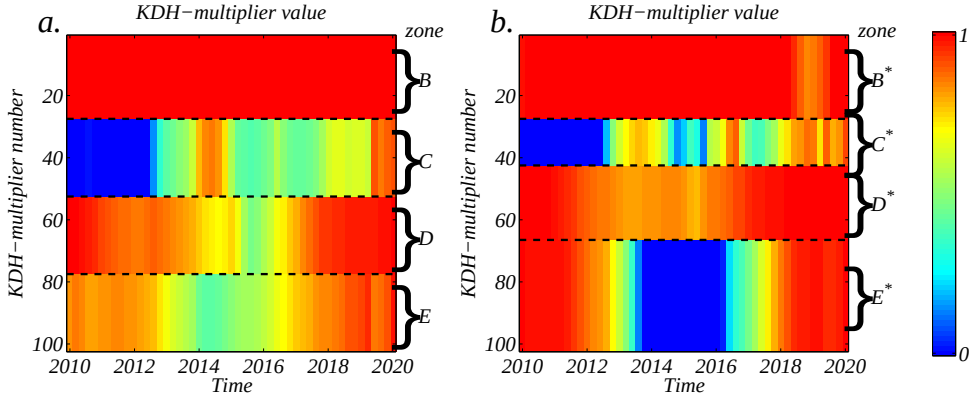

Figure 1.4 : Left (a.) Optimal time-varying KDH-multipliers for standard 4-zone control. Right (b.) Optimal time-varying KDH-multipliers for alternative 4-zone control.

*KDH-multipliers, based on similar behavior of the 102 KDH-multipliers over time. Figure 1.4.*a *shows the time-varying KDH-multipliers optimized for zones B, C, D and E and Figure 1.4.*b *shows the optimal time-varying KDH-multipliers for the alternative zones B^*, C^*, D^* and E^*. The results of these four cases with different control strategies are summarized in Table 1.1.*

As expected Full 102 control, which has the most degrees of freedom, yields the best results (11.7% increase in cumulative oil). Compared to Standard and Alternative four-zone control, both having much less freedom due to a reduction from 102 to four control valves, there is indeed a slight loss in performance. Furthermore, the results suggest that the alternative grouping used in Alternative four-zone control will yield better results than the standard grouping used in Standard four-zone control (10.0% versus 8.1%). The determined 'optimal'

Table 1.1 : *Cumulative oil production for different cases*

Case	*Cumulative oil [MMstb]*	*Increase [%]*
No control (base case)	11.47	-
Optimized water injection		
Full 102 control	12.82	11.7
Standard four-zone control	12.40	8.1
Alternative four-zone control	12.62	10.0

perforation zones do not correspond exactly to the geological zones defined using a static geological model. This result emphasizes the relevance of incorporating dynamic flow modeling into well design.

Despite the fact that the techniques for performing life-cycle optimization of oil and gas production have shown a large potential to increase economic performance and have shown to be able to handle the size of realistic problems, so far they haven't found their way into operational environments within the industry. This observation has lead to the following research objective of this PhD thesis.

1.1 Research Objective

Improve the operational applicability of model-based optimization of oil recovery

The reluctance by oil and gas companies to adopt the technology in their operational environments can mainly be attributed to the large uncertainties that come into play in optimizing production over the entire life of a field and - in effect - the lack of faith that exists in the available methods and models. These uncertainties are of varying nature and come from several different sources:

Modeling uncertainty

In order to perform life-cycle optimization a numerical, dynamic model is required to capture the dynamic behavior of the reservoir, wells and possibly the surface facilities. The reservoir model describes the dynamic behavior of the reservoir, i.e. how the fluids flow through the reservoir as a result op the depletion strategy. The well and surface facility models describe how these fluids behave flowing from subsurface

to surface and processing units. Especially reservoir models suffer from large uncertainties, both in the model structure as well as in the model parameters. The main contributor to that uncertainty is the lack of knowledge of the subsurface geology that defines the reservoir. Therefore, in many cases when uncertainty in reservoir models is addressed, only geological uncertainty is taken into consideration. However, uncertainty in the fluid properties and distribution can also contribute largely to the uncertainty in fluid flow behavior.

Often, the information that is available to model the geology in reservoir models is relatively accurate but very sparse (e.g. well logs or production measurements), and/or it is dense but very noisy and of low resolution (e.g. coming from (time-lapse) seismic surveys). Although geostatistics and geological insight can help to constrain the degrees of freedom of the model that the available data allow, the variations in possible model structures and parameters can still be vast. This freedom can have a serious impact on the economic performance that can be expected from the field, as the following example from Van Essen et al. (2010b) demonstrates.

Example 2. *In this example, we consider a three-dimensional oil reservoir model, introduced in Van Essen et al. (2009b). The reservoir model consists of 18,553 active grid blocks, as depicted in Figure 1.5, and has dimensions of* $480m \times 480m \times 28m$*. Its geological structure involves a network of fossilized meandering channels of high permeability. All remaining geological and fluid properties used in this example are presented in Table C.1. The reservoir model contains eight injection wells and four production wells. The injection wells are operated on injection flow rates, while the production wells operate on flowing bottomhole pressure.*

During the first 1.5 years of production from the reservoir, the bottomhole pressures of the producers were kept at a constant value of $39.5MPa$*. During that time, the injection rates of all eight injectors fluctuated monthly with a uniform probability distribution around an average value of* $5.52 \times 10^{-4} m^3/s$ *(300* bbl/day*). Monthly production measurements were taken of the flowing bottomhole pressures of the eight injectors and phase flow rate measurements of the four producers, on top of which no noise was superimposed. Thus, the total number of measurements added up to 288 data points.*

The goal of this example is to determine a lower and upper bound on expected economic performance over the remaining life of the field - from 1.5 to 6.0 years - by changing certain model properties, while the model stays compliant with historic data over the first 1.5 years of production. In this particular example, only permeability was adjusted using a homogeneous prior model of 1000 mDarcy. The remaining model properties were chosen identical to the 'truth' reservoir model. As economic performance measure, NPV was used, as described in Eq. C.4, with a constant water injection costs, water production costs and oil revenue of 0

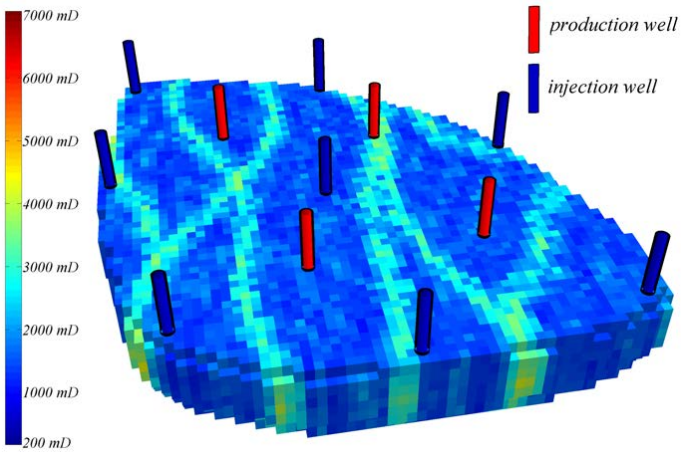

Figure 1.5 : 3-dimensional oil reservoir model with eight injection and four production wells, after Van Essen et al. (2009b).

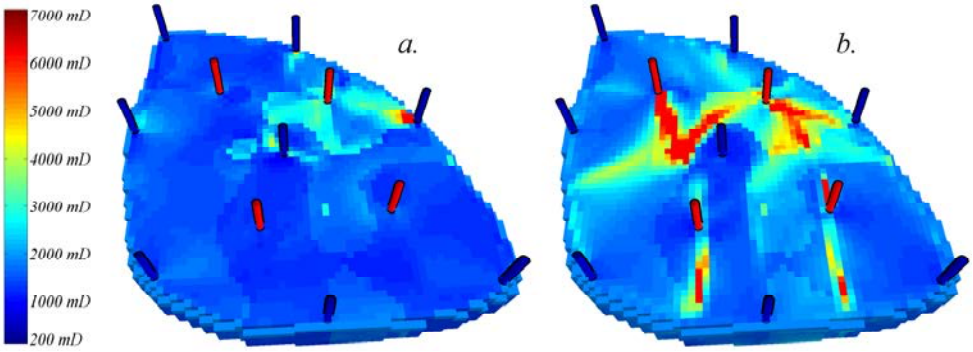

Figure 1.6 : Permeability fields of the lower bound 3D reservoir model (a.) and upper bound 3D reservoir model (b.) determined after the first 1.5 years of production.

$/m^3$, *-1* $/m^3$ *and 9* $/m^3$ *respectively.*

The upper and lower bounds of the NPV are determined for a given (fixed) control strategy $\bar{\mathbf{u}}$*. In this example, a reactive control approach is used that is evaluated on a field level. All injection wells are assumed to continuously operate on average historical rates and the production wells on a fixed bottomhole pressure of* 39.5*MPa. The instant the field watercut exceeds 0.90, all wells are shut-in. Note that this threshold is related to the ratio between oil revenues and water production costs. To determine the history-matched models that provide the lower and upper bound on NPV for the remaining production life, two hierarchical optimization procedures were initiated using the 'switching' method, as described in Van Essen et al. (2011). The procedures were terminated when the feasible updates no longer resulted in a significant change in NPV.*

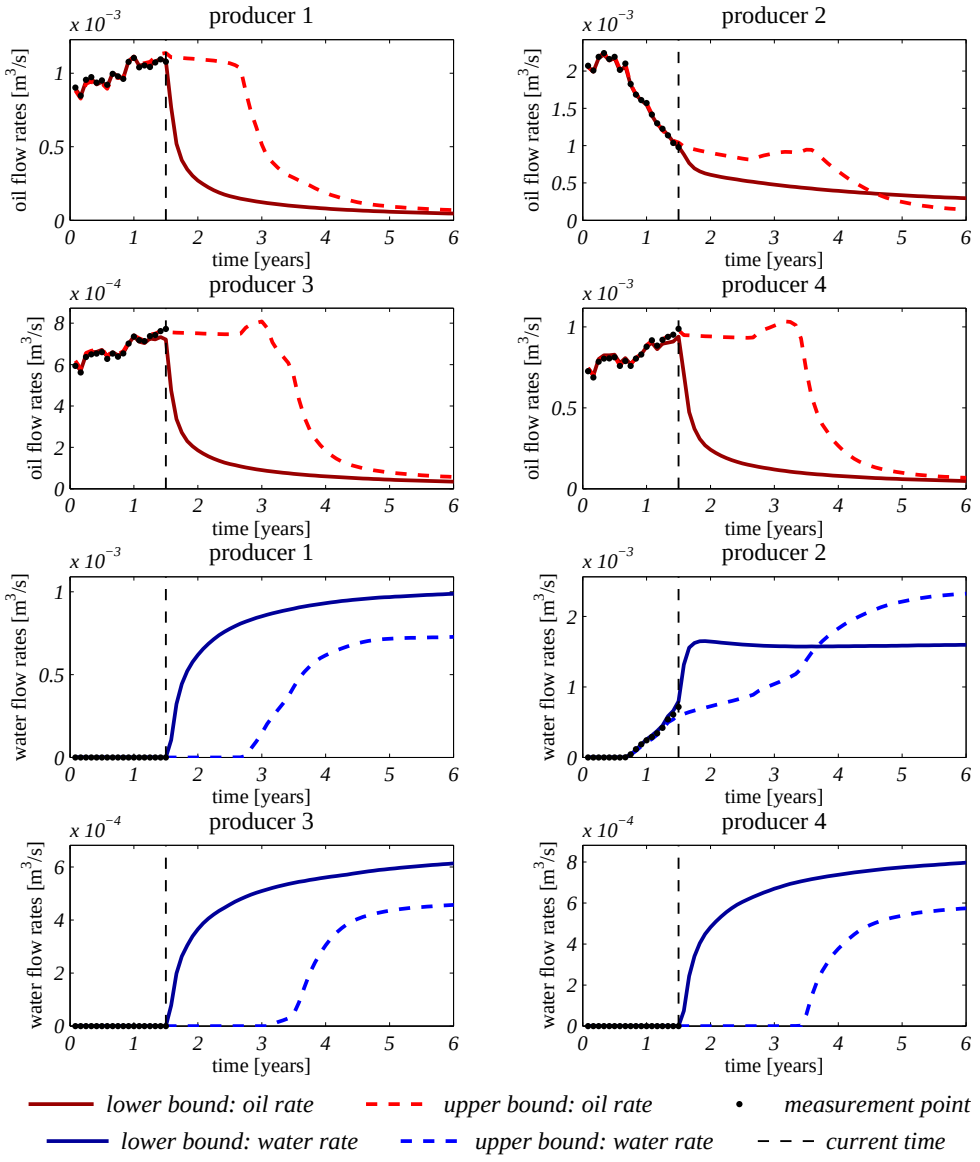

Figure 1.7 : Measured oil and water rates of the producers over first 1.5 years of production from the (synthetic) 3D reservoir, along with the simulated oil and water rates for the remaining 4.5 years of production until the end of the field's life, originating from the lower and upper bound models.

Table 1.2 : *Results*

	Lower Bound	*Upper Bound*	*Average*
Expected NPV over remaining 4.5 years	3.0 M$	13.2 m$	+ 8.1 M$
% deviation from average	-63%	+63%	-

In Figure 1.6 it can be observed that the permeability fields of the lower and upper bound model are quite different. However, in Figure 1.7 it is shown that for the first 1.5 years of production, the simulated production data is very close to the measured production data and hence both models show a very satisfactory history-match. Nevertheless, when the models are used for forecasting (from 1.5 years until the end of the life-cycle) the behavior of the models is quite different, as can be observed in Figure 1.7 as well. Table 1.2 shows that the upper and lower bounds of expected NPV over the remaining 4.5 years of production are respectively 63% above and below the average of the two bounds. This demonstrates that the degrees of freedom in permeability that the measured production data allow can have a significant impact on the expected economic performance.

The impact of modeling uncertainty on the performance of the depletion process generally doesn't increase with the length of the life-cycle. Rather the opposite is true, when the life of a reservoir is stretched over a longer period, more measurement data is gathered allowing for a reduction in the uncertainty.

Economic uncertainty

The objective of any oil and gas company is to turn its oil and gas reserves into economic value. The way to quantify the economic value of a petroleum reservoir over its entire life can range from very simple to very complex, but it is undoubtedly the price of oil and gas that is the most uncertain parameter in these equations. Figure 1.8 shows the evaluation of the price of oil since 1861 corrected for inflation, which clearly shows its erratic behavior. Unlike geological uncertainty, economic uncertainty grows exceedingly with time, and hence the length of the life-cycle of a reservoir.

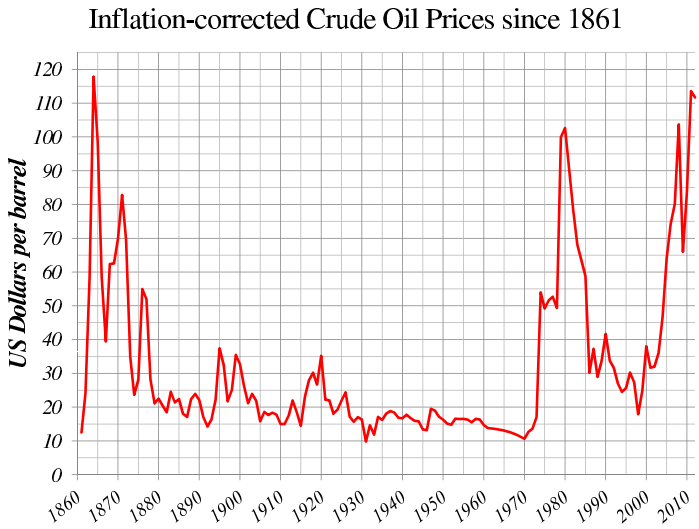

Figure 1.8 : Long term crude oil prices, corrected for inflation (1861-1944 US Average, 1945-1983 Arabian Light posted at Ras Tanura, 1984-2012 Brent dated. Source: BP Statistical Review of World Energy 2013).

Operational uncertainty

Operational conditions in oil and gas production are not stationary. Major changes may be involved in the number, type or capacity of wells due to e.g. infill drilling, well conversions, replacing equipment or work-overs. Also the capacity of the surface facilities may change when replacing separators, tubing or other. But even when these matters remain unchanged or if these changes are known upfront, operations suffer from all kind of disturbances over the life of the field due to e.g. equipment failure or environmental issues. Just as for economic uncertainty, operational uncertainty generally increases with the length of the life-cycle. A longer life-cycle allows for multiple field redevelopments, which generally take several years to realize. As time progresses, also operational disturbances become more likely, as equipment wears down.

Organizational uncertainty

Organizations are subject to changes over time. Generally, these changes evolve more rapidly than the duration of the life of an oil or gas field. The time horizons of performance related remunerations, like bonuses, often correlate with the frequency of these changes. For business or investment decisions that have a longer payback period, this type of reward system does not suffice and the chance of being rewarded

for long-term performance are much more uncertain. Besides this, organizational changes often involve a loss of knowledge on the reservoir and its operations, which increases uncertainty as well.

Political uncertainty

In any oil and gas project, (local) government is involved at some level. It might be as owner of the asset, because of tax regulations, because it obtains royalties, or through (environmental) regulation. The level of involvement varies considerably from location to location in the world. As a result, changing political circumstances may have a big impact on the progression of the depletion process and the resulting economic performance over the life of the field. Political stability of a country or region takes away some of the uncertainty, but nevertheless the uncertainty of the extent to which governments will impact the (economic) performance will grow with time.

Except for modeling or geologic uncertainties, most of the uncertainties listed above increase with time. Within many oil companies, this is a strong incentive to choose a production strategy aimed at having an as short as possible life-cycle. In fact, in many cases maximal production is adopted as objective of the production strategy design, which in effect leads to the shortest possible life-cycle. Even though, in hindsight, the value of many oil fields would have been much larger if a more ”restrained” production strategy had been implemented.

Summarizing the list above, the uncertainties acting on the life-cycle optimization problem of oil and gas production are of various nature and generally vast, especially considering the normally long time horizons. As mentioned earlier, these uncertainties form the main obstacles in implementing it in an operational environment. To that end, the following research question is addressed in this thesis.

1.2 Research Question

Can the performance of model-based life-cycle optimization of oil and gas production in realistic circumstances be improved by addressing uncertainty in the optimization problem?

In this work, mainly geological uncertainty and, to a lesser extent, economic uncer-

tainty and operational uncertainty will be addressed, since these uncertainties allow for a technical and quantitative solution. However, this is not necessarily a reflection of the importance of all uncertainties.

In this thesis, only optimization of oil production through waterflooding will be regarded as recovery mechanism. Attention is limited to waterflooding alone, because:

1. It is a common recovery mechanism.
2. A waterflooding strategy involves many decision variables.
3. The flooding process can be modeled reasonably accurately over long distances and periods of time.
4. There is generally a significant scope for improvement.

The methods presented in this thesis to address uncertainty in the optimization problem with the objective to improve (economic) life-cycle performance, can be subdivided into two main approaches depending on the choice of a *fixed* or an *adaptive* operational strategy.

1. In case of a fixed operational strategy, optimization of an (economic) life-cycle objective is only carried out once. The operational strategy is not updated over the life of the field. Uncertainty is explicitly incorporated in the design of the operational strategy and treated as undesired disturbances on performance during implementation
2. In case of an adaptive operational strategy, measurements are taken from the field during implementation and used to update the dynamic reservoir model. Re-optimization of the operational strategy is carried out during operation using the updated model, and the new operational strategy is implemented until the end of field life or until the next model update.

These two approaches will be discussed in more detail in Chapter 2 and Chapter 3 respectively. In Chapter 4 this thesis will be concluded and some recommendations for future research will be presented. Appendices A through E contain the papers on the different methods presented in Chapters 2 and 3 as they appeared in literature, which contain a more detailed description of the methods and examples.

Chapter 2

Robustness of Fixed Operational Strategies

In Chapter 1, different types of uncertainties were described that come into play when trying to optimize recovery from an oil or gas field. In this chapter, the question is addressed of how to reduce the impact of these uncertainties on economic life-cycle performance, given a fixed operational strategy that was designed *a priori*, i.e. before implementation. The measure of impact on performance is referred to as *robustness*. Robustness to uncertainties can be influenced by manipulating the control parameters of the operational strategy. However, this should be done without loosing sight of the main objective of the control strategy: maximizing the economic performance. The three methods presented in this chapter address this *dual-objective* problem, which are:

1. Hierarchical Optimization
2. Robust Optimization
3. Integrated dynamic optimization and feedback control

These methods will be presented in Section 2.1, 2.2 and 2.3 respectively, by incorporating the uncertainty in the optimization problem, either explicitly or implicitly. This chapter is concluded in Section 2.4.

2.1 Hierarchical Optimization

The dual nature of optimizing an operation strategy, in terms of economic performance and risk, can be expressed as a multi-objective optimization problem, in which

one objective function J_1 represents a quantitative measure of economic performance and another objective function J_2 a measure of robustness of the operational strategy (not necessarily in that order):

$$\max_{\mathbf{u}_{1:K}} \left(J_1\left(\mathbf{u}_{1:K}\right),\ J_2\left(\mathbf{u}_{1:K}\right)\right)^T \tag{2.1}$$

$$s.t. \quad \mathbf{g}_{k+1}\left(\mathbf{u}_k, \mathbf{x}_k, \mathbf{x}_{k+1}, \theta\right) = 0, \quad k = 0, \ldots, K-1, \quad \mathbf{x}_0 = \bar{\mathbf{x}}_0, \tag{2.2}$$

$$\mathbf{c}_{k+1}\left(\mathbf{u}_{k+1}, \mathbf{x}_{k+1}\right) \leq 0, \quad k = 0, \ldots, K-1, \tag{2.3}$$

where $\mathbf{u}$ is the control vector (input vector), $\mathbf{x}$ is the state vector (gridblock pressures and saturations), $\mathbf{g}$ is a vector-valued function that represents the system equations, $\mathbf{x}_0$ is a vector of the initial conditions of the reservoir with prescribed value $\bar{\mathbf{x}}_0$, the subscript k indicates discrete time, and K is the total number of timesteps. A colon in a subscript indicates a range [e.g., $\mathbf{u}_{1:K} = (\mathbf{u}_1, \mathbf{u}_2, \ldots, \mathbf{u}_K)$] The vector of inequality constraints $\mathbf{c}$ relates to the capacity limitations of the wells.

A common approach to solving the multi-objective optimization problem as described by Eq. (2.1) through (2.3) is through (linear) scalarization, where the multiple objective functions combined into a *balanced* single objective function with associated weights $\omega_i \in \mathbb{R}$; see Marler and Arora (2004):

$$J_{bal} = \omega_1 \cdot J_1 + \omega_2 \cdot J_2, \tag{2.4}$$

where J_{bal} is the balanced objective function. In Eq. (2.4), a different choice of weights ω_i leads to a different (Pareto) optimum, see Miettinen (1999). It is often difficult to *a priori* determine the weights ω_i that represent the decision-makers preference on the trade-off between economic performance and robustness. This is especially the case if the values of the multiple objective functions have different physical interpretations. A large number of trial-and-error runs with different weighting factors may be required to obtain a set of Pareto optimal solutions, from which the decision-maker can select the most satisfactory one.

In some cases, the objectives in a multiple-objective optimization problem can be prioritized, i.e. there is an order in which the decision-maker wishes to optimize the objective functions. If so, the multiple-objective optimization problem can be cast into a hierarchical or lexicographic optimization problem; see Haimes and Li (1988). In this structure, optimization of a secondary objective function J_2 is constrained by the requirement that the primary objective function J_1 must remain close to its (unconstrained) optimal value J_1^*. This structure can be expressed mathematically as:

$$\max_{\mathbf{u}_{1:K}} J_2(\mathbf{u}_{1:K}) \tag{2.5}$$

$$s.t. \quad \mathbf{g}_{k+1}(\mathbf{u}_k, \mathbf{x}_k, \mathbf{x}_{k+1}, \theta) = 0, \quad k = 0, \ldots, K-1, \quad \mathbf{x}_0 = \bar{\mathbf{x}}_0, \tag{2.6}$$

$$\mathbf{c}_{k+1}(\mathbf{u}_{k+1}, \mathbf{x}_{k+1}) \leq 0, \quad k = 0, \ldots, K-1, \tag{2.7}$$

$$J_1^* - J_1(\mathbf{u}_{1:K}) \leq \varepsilon, \quad k = 0, \ldots, K-1, \tag{2.8}$$

where ε can be used to specify how much the primary objective function is allowed to deviate from its optimal value to improve the secondary objective. In the case where the primary objective is economic performance and the secondary objective some measure of the robustness to uncertainty, determining a suitable value for ε comes down to the question how much economic performance (e.g. in terms of NPV) a decision-maker is willing to sacrifice to improve on the robustness of the production strategy. This is generally much easier to determine than suitable values for weights ω_1 and ω_2 in the balanced objective function setup, expressed by Eq. (2.4).

Redundant Degrees of Freedom Jansen et al. (2009) described that different solutions exist for the optimal control problem of maximizing an economic objective function over the life of the reservoir. The existence of multiple solutions was attributed to the ill-posedness of the optimal control problem. The ill-posedness also suggests that, even when optimality of an economic life-cycle objective is reached, not all degrees of freedom (DOF) of the decision variable space $\mathscr{U}$ are fixed. This means that there may exist redundant DOF in the optimization problem. These redundant DOF describe an optimal subspace or manifold (in case of nonlinear DOF) $\mathscr{U}^*$ of connected optimal solutions. Huesman et al. (2006, 2008) found similar results for economic dynamic optimization of plantwide operation. A consequence of these redundant DOF is that, even if ε in Eq. (2.8) is chosen equal to 0, DOF are left to improve the secondary objective function J_2. In this case where ε is equal to 0, inequality constraint (2.8) becomes an equality constraint and the hierarchical optimization problem can be rewritten into:

$$\max_{\mathbf{u}_{1:K} \in \mathscr{U}^*} J_2(\mathbf{u}_{1:K}) \tag{2.9}$$

$$s.t. \quad \mathbf{g}_{k+1}(\mathbf{u}_k, \mathbf{x}_k, \mathbf{x}_{k+1}, \theta) = 0, \quad k = 0, \ldots, K-1, \quad \mathbf{x}_0 = \bar{\mathbf{x}}_0, \tag{2.10}$$

$$\mathbf{c}_{k+1}(\mathbf{u}_{k+1}, \mathbf{x}_{k+1}) \leq 0, \quad k = 0, \ldots, K-1, \tag{2.11}$$

$$\tag{2.12}$$

where optimality constraint (2.8) is now represented by the condition that control vector $\mathbf{u}_{1:K}$ has to lie within optimal subspace or manifold $\mathscr{U}^*$.

As a result of the nonlinear nature of reservoir dynamics, the redundant DOF of an optimal operation strategy over the life of a field will also be nonlinear. However, within a small region around $\mathbf{u}_{1:K}$, the DOF can be assumed to be linear. In other words, a local linear approximation $\hat{\mathscr{U}}^*$ can be defined for the optimal subspace $\mathscr{U}^*$. This allows for an iterative approach to Eq. (2.9) - (2.11), where a new approximation $\hat{\mathscr{U}}^*$ to $\mathscr{U}^*$ needs to be determined for each iteration. The local linear approximation $\hat{\mathscr{U}}^*$ can be determined using a linear approximation of the redundant DOF and the definition of a region around $\mathbf{u}_{1:K}$ within which the approximation is adequate. This approach is analogous to trust region methods for optimization, see Conn et al. (2000).

Local linear approximation to redundant DOF In the following, we will use the short-hand notation $\mathbf{u}$ to indicate the input sequence $\mathbf{u}_{1:K} = (\mathbf{u}_1, \mathbf{u}_2, \ldots, \mathbf{u}_K)$. A solution $\mathbf{u}$ for which no constraints are active is an optimal solution $\mathbf{u}^*$ if and only if the gradients of J with respect to $\mathbf{u}$ are zero [i.e., $(\partial J/\partial \mathbf{u})^T = \mathbf{0}$]. As a result, at $\mathbf{u}^*$, the gradients do not provide any information on possible redundant DOF under the optimality condition on J. Second-order derivatives of J with respect to $\mathbf{u}$ are collected in the Hessian matrix $\mathbf{H} = \partial^2 J/\partial \mathbf{u}^2$. If $\mathbf{H}$ is negative definite, the considered solution $\mathbf{u}$ is an optimal solution, but no DOF are left when the optimality condition on J holds. If $\mathbf{H}$ is negative semidefinite, the Hessian does not have full rank. An orthonormal basis $\mathbf{B}$ for the undetermined directions of $\mathbf{H}$ can then obtained through a singular value decomposition.

$$\mathbf{H} = \mathbf{U} \cdot \Sigma \cdot \mathbf{V}^T. \tag{2.13}$$

The orthonormal basis $\mathbf{B}$ consists of those columns of $\mathbf{V}$ that relate to singular values of zero; i.e.

$$\mathbf{B} \triangleq \{\mathbf{v}_i \mid \sigma_i = 0, \qquad i = 1, \ldots, N_{\mathbf{u}}\}, \tag{2.14}$$

where $\mathbf{v}_i$ represents a column of $\mathbf{V}$ and $N_{\mathbf{u}}$ is the number of redundant DOF of the approximation. Note that, because of the symmetrical nature of the Hessian matrix $\mathbf{H}$, the singular value decomposition may be replaced by a computationally more efficient eigenvalue decomposition, in which case the eigenvectors relating to eigenvalues equal to zero span the orthonormal basis $\mathbf{B}$. The orthogonal directions spanned by the columns of $\mathbf{B}$ are a local linear approximation of the redundant DOF with respect to optimality of an economic life-cycle objective

In the following example, the hierarchical optimization of a primary (economic) objective and a secondary (robustness) objective is demonstrated. In this particular case,

improved robustness against economic and operational uncertainty is addressed implicitly by a secondary objective function that is aimed at shortening the life of the field, i.e. a speedup of production. The redundant DOF with respect to the primary objective are used to optimize the secondary objective, i.e. where $\varepsilon = 0$. A local linear approximation $\hat{\mathscr{U}}^*$ of the optimal solution space of the primary objective is determined iteratively using an orthonormal basis **B** as described above. A more detailed description of this approach can be found in Appendix C.

Example 3. *The 3D reservoir model in this example is identical to the 3D reservoir model that serves as truth model in Example 2 in Chapter 1 (after Van Essen et al. (2009b)), but deviates in the density and viscosity of the fluids. These properties can be found in Table C.1 in Appendix C. The life cycle of the reservoir covers a period of 3,600 days. The wells operate at a constant bottomhole pressure p_{wf} of 39.5 MPa (395 bar). In this example, only the flow rates of the injection wells can be manipulated directly (i.e., the control input* **u** *involves injection flow-rate trajectories for each of the eight injection wells). The minimum rate for each injection well is 0.0 m^3/day; the maximum rate is set at 79.5 m^3/day. The control input* **u** *is reparameterized in time using a zero-order-hold scheme with input parameter vector θ. For each of the eight injection wells, the control input* **u** *is reparameterized into four time periods t_θ of 900 days during which the injection rate is held constant at value θ_i. Thus, the input parameter vector θ consists of $8 \times 4 = 32$ elements.*

In this example, two objectives are specified that are improved upon by adjusting the initial control input from its initial guess. The first objective involves cumulative cash flow over the life of the field and is regarded as the primary goal of the updated control input. It is defined as in Eq. (C.4), with r_o = 126 \$/m^3, r_{wp} = 19 \$/m^3 and r_{wi} = 6 \$/m^3 and a discount rate b of 0. The secondary objective of the control vector addresses the risk of the project due to economic uncertainty. As mentioned in Chapter 1, the main contributor to economic uncertainty lies in the oil price fluctuations. These fluctuation are almost impossible to predict, but generally speaking, uncertainty in the oil price and hence economic risk increases with the length of the prediction horizon. Therefore, as a proxy, the secondary objective is aimed at maximizing the speed at which oil is produced. To that end, the secondary objective J_2 is defined to be identical to the primary objective function but with the addition of a very high annual discount rate b of 0.25. As a result, short-term production is weighed more heavily than future production.

The hierarchical optimization setup as defined by (2.5) - (2.7) first requires optimization of the primary objective J_1 alone to determine J_1^* and the associated optimal control vector $\mathbf{u}_{1:K}^*$ that serves as starting point to the hierarchical optimization. The optimization of the primary objective function was carried out using a gradient-based algorithm (steepest ascent), with the adjoint to calculate the gradients. The final optimal input $\mathbf{u}_\theta^*$ of the life-cycle optimization problem is shown in Fig. 2.1. The value of the objective function corresponding to input $\mathbf{u}_\theta^*$ is 47.6 $\times$ 10^6 \$.

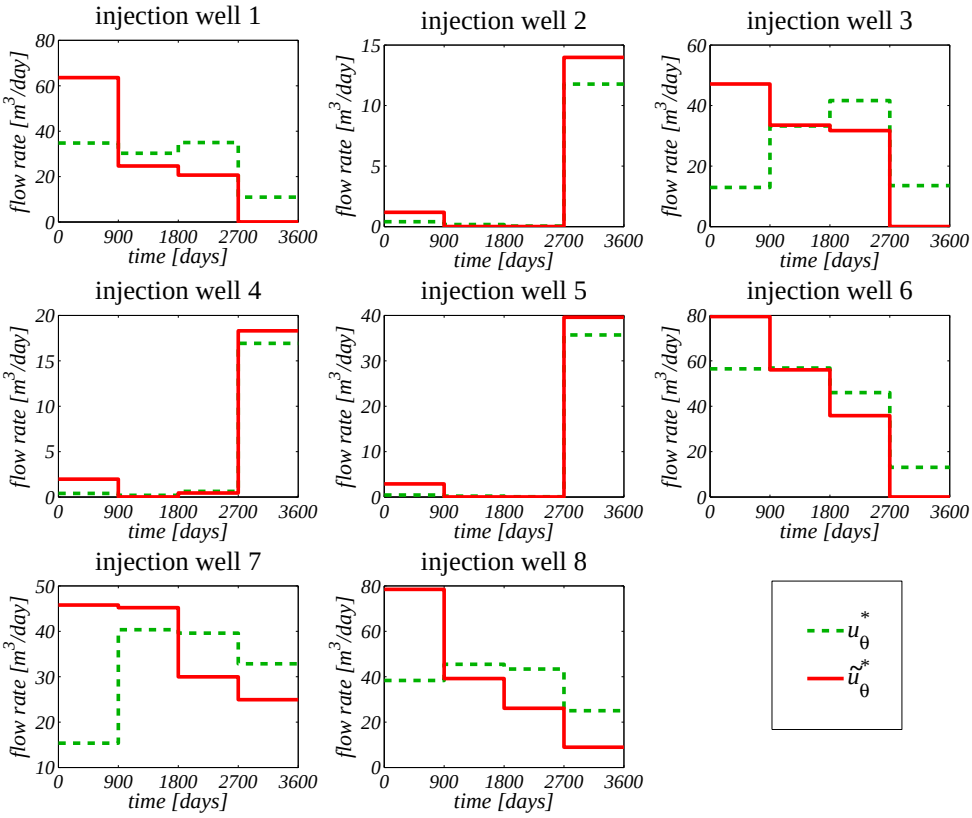

Figure 2.1 : Input trajectories for each of the eight injection wells for the initial optimal solution $\mathbf{u}^*_\theta$ to J_1 (green dashed line) and the optimal solution $\tilde{\mathbf{u}}^*_\theta$ after the constrained optimization of J_2 (red solid line)

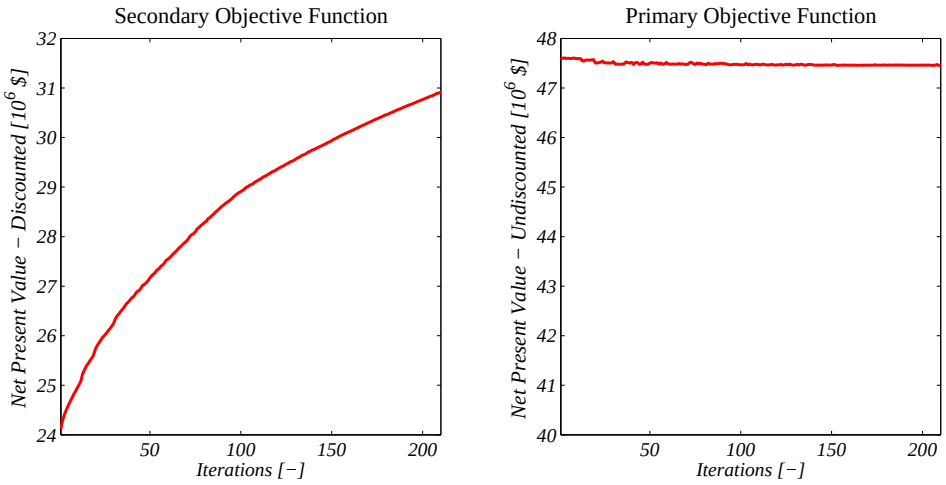

Figure 2.2 : Values of the secondary objective function J_2 and the primary objective function J_2 plotted against the iteration number for the constrained secondary optimization problem.

To determine a local linear approximation of the redundant DOFs, second-order derivatives with respect to the primary objective are required. However, the adjoint implemented in the reservoir simulator used in this example only provides first-order derivatives. As an alternative, the Hessian matrix can approximated using the gradients through a forward-difference scheme:

$$\frac{\partial^2 J}{\partial u_i \partial u_j} \approx \frac{\nabla J_i(\mathbf{u}+h_j\mathbf{e}_j)-\nabla J_i(\mathbf{u})}{2h_j}+\frac{\nabla J_j(\mathbf{u}+h_i\mathbf{e}_i)-\nabla J_j(\mathbf{u})}{2h_i}, \tag{2.15}$$

where ∇J_i is the ith element of the gradient $\nabla J = (\partial J/\partial \mathbf{u})^T$, $\mathbf{e}_i$ is a canonical unit vector (i.e., a vector with a 1 at element i and 0 elsewhere), and h_i is the perturbation step size that relates to parameter u_i of $\mathbf{u}$. The number of required simulations to determine the approximate Hessian matrix is equal to the number of elements in the input parameter vector θ plus 1. In this example that amounts to 33 simulations, which are processed concurrently on multiple CPU's. The local linear approximation of redundant DOF are determined through the singular value decomposition. After every iterative update of input vector $\mathbf{u}_\theta$, a new local linear approximation to the redundant DOF is determined.

Fig. 2.2 displays the values of J_1 and J_2 plotted against the iteration number for the hierarchical optimization problem. It shows a considerable increase of J_2 of 28.2% and a slight drop of J_1 of -0.3%. In Fig. 2.1, the input strategy after the final iteration step is presented. It can be observed that the injection strategy shows a substantial increase in injection rates at the beginning of the production life and a decrease at the end. As a comparison, we repeated the optimization of J_2 starting from $\mathbf{u}_\theta^*$ with the difference that it was no longer constrained by the requirement that J_1 remains close to J_1^* (i.e., Eq. (2.8) was omitted). The optimization procedure was terminated when the improvement of J_2 was equal to 28.2% (i.e., the final

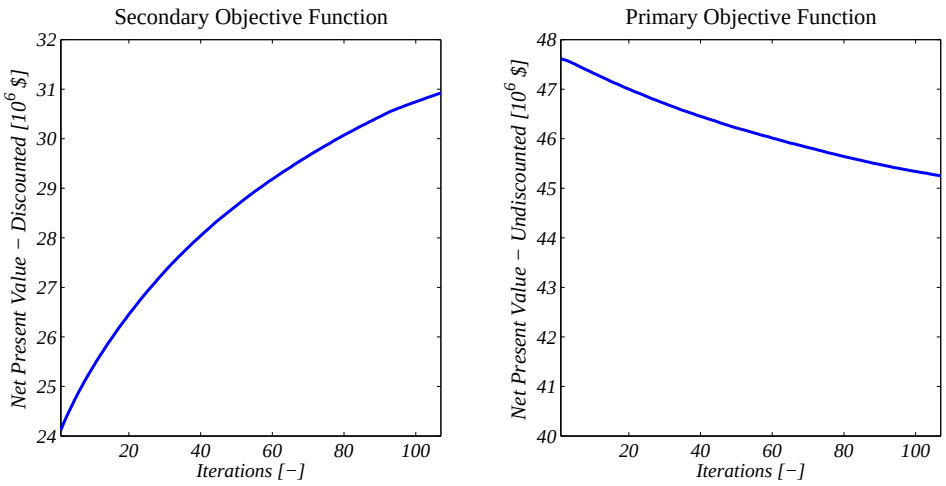

Figure 2.3 : Values of the secondary objective function J_2 and the primary objective function J_1 plotted against the iteration number for the secondary optimization problem, no longer constrained by local linear solution space $\hat{\mathscr{U}}^*$.

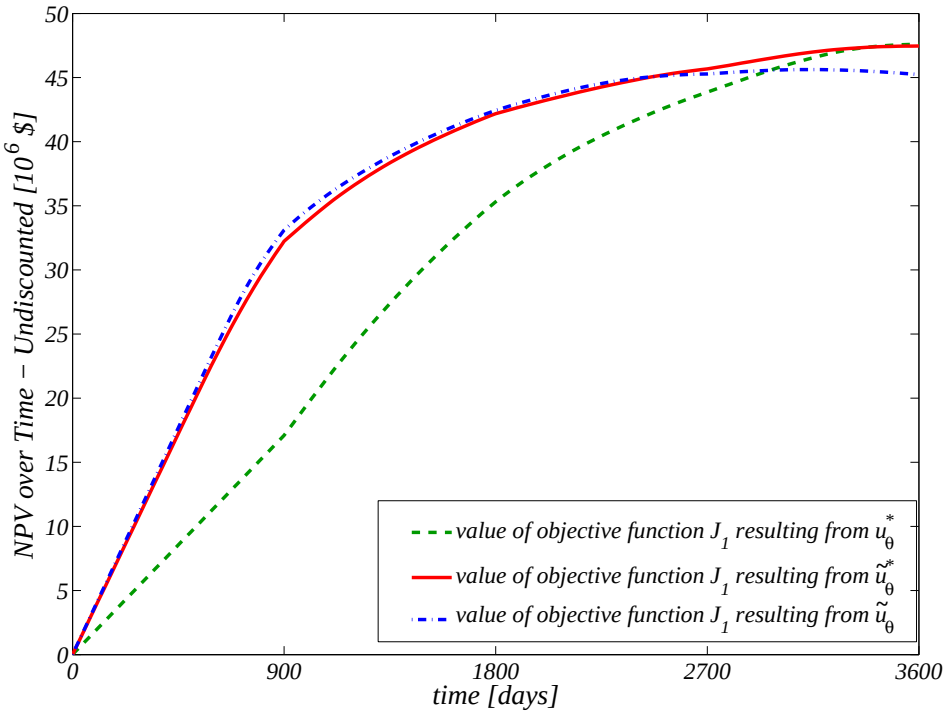

Figure 2.4 : Value of the primary objective function J_1 over time for initial optimal input $\mathbf{u}_\theta^*$ to J_1 (dashed green line), the optimal input $\tilde{\mathbf{u}}_\theta^*$ after the constrained optimization of J_2 (red solid line), and input $\mathbf{u}_\theta$ after the unconstrained optimization of J_2 (blue dashed/dotted line).

value of J_2 in the constrained optimization case). The values of J_1 and J_2 plotted against the iteration number for the unconstrained optimization of J_2 are shown in Fig. 2.3. Again an increase in J_2 of 28.2% is realized, but now at a cost of a decrease in J_1 of -5.0%. Finally, Fig. 2.4 shows the value of the primary objective function J_1 over time until the end of the producing reservoir life for $\mathbf{u}_\theta^*$, $\tilde{\mathbf{u}}_\theta^*$ and $\tilde{\mathbf{u}}_\theta$. Input $\tilde{\mathbf{u}}_\theta^*$ shows a steeper ascent of J_1 than $\mathbf{u}_\theta^*$, while their final values are nearly equal. Input $\tilde{\mathbf{u}}_\theta$ shows initially the same steep ascent, but J_1 drops toward the end of the life of the reservoir.

The presented hierarchical optimization approach using the Hessian matrix can be computationally very demanding and may become infeasible for more realistic reservoir models with an increased number of input parameters. It should be noted however, that execution of the hierarchical optimization procedure does not require knowledge of all redundant DOF explicitly. An alternative method to solve the hierarchical optimization problem without explicitly calculating the redundant DOF is through the use of a balanced objective function as described by Eq. (2.4), with the variation of using weighting functions Ω_1 and Ω_2 instead of weighting factors ω_1 and ω_2:

$$J_{bal} = \Omega_1 \cdot J_1 + \Omega_2 \cdot J_2, \tag{2.16}$$

where Ω_1 and Ω_2 are switching functions of J_1 and J_1^* that take on values of 1 and 0 or vice versa:

$$\Omega_1(J_1) = \begin{cases} 1 & \text{if } J_1^* - J_1 > \varepsilon \\ 0 & \text{if } J_1^* - J_1 \leq \varepsilon \end{cases} \tag{2.17}$$

$$\Omega_2(J_1) = \begin{cases} 0 & \text{if } J_1^* - J_1 > \varepsilon \\ 1 & \text{if } J_1^* - J_1 \leq \varepsilon \end{cases}. \tag{2.18}$$

Here, ε is the threshold value as defined in the inequality constraint Eq. (2.8). For gradient-based methods, the gradient of J_{bal} with respect to the input parameters $\mathbf{u}$ for iteration $n+1$ is then simply

$$\left.\frac{\partial J_{bal}}{\partial \mathbf{u}}\right|_{n+1} = \Omega_1(J_{1,n}) \cdot \left.\frac{\partial J_1}{\partial \mathbf{u}}\right|_{n+1} + \Omega_2(J_{1,n}) \cdot \left.\frac{\partial J_2}{\partial \mathbf{u}}\right|_{n+1}. \tag{2.19}$$

Execution of the optimization problem using balanced objective function Eq. (2.16) sequentially gives improving directions for either J_1 or J_2. With each iteration, the value of J_2 either increases while the value of J_1 decreases or vice versa, as the solution moves to and from the feasible region with respect to the inequality constraint

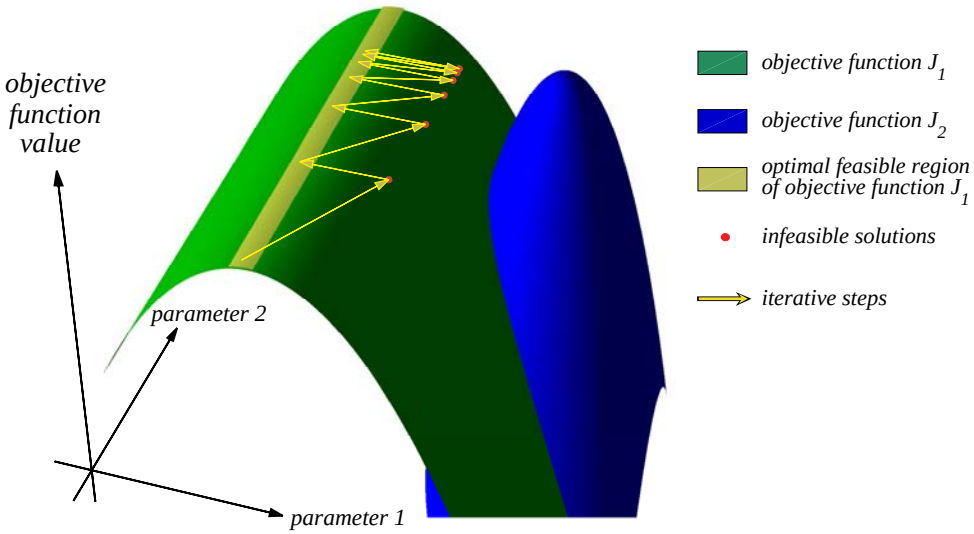

Figure 2.5 : Schematic representation of the iterative process of solving a hierarchical optimization problem using an objective function as described by Eqs. (2.16), (2.17) and (2.18). The process converges toward a final solution in a zigzag fashion, moving into and out of the feasible region bounded by the optimal solutions of the primary objective function J_1.

Eq. (2.8). When no redundant DOF are available, the control input would jump between two fixed solutions, of which only one would be feasible. However, in the case where redundant DOF do exist, improvement of J_2 is possible without compromising Eq. (2.8) and convergence of the hierarchical optimization will occur in a zigzag fashion, as schematically represented in Fig. 2.5.

This switching method has the advantage that numerous evaluations of the system and adjoint equations are avoided: Only two runs (in parallel execution) of the system and adjoint equations are necessary per iteration, regardless of the number of input parameters. Secondly, the method is straightforward to implement. A disadvantage of the method is the slow convergence because of the infeasible solution steps. Also, some tuning will be required to account for the fact that the Euclidean length of vectors $\partial J_1/\partial \mathbf{u}$ and $\partial J_2/\partial \mathbf{u}$ is different.

2.2 Robust Optimization

The concept behind robust optimization is to express the objective function in probabilistic terms, where the uncertainty in the optimization problem is expressed by stochastic variables. Adopting a probabilistic objective function will provide a production strategy which is optimal from a statistical point of view, see Ruppen et al. (1995); Terwiesch et al. (1998); Srinivasan et al. (2003).

A straightforward choice as robust optimization objective function J_{RO} is to take the expected value of an economic performance measure (J), e.g. NPV, given the uncertain parameters θ. Through this objective function a production strategy can be obtained that may not be optimal for any specific realization of the uncertain parameters, but on average gives the best performance. This can be expressed mathematically as:

$$J_{RO} \triangleq E_\theta \left[J(\mathbf{y}, \theta) \right], \tag{2.20}$$

where $\mathbf{y}$ is the output of the dynamic model, which contains for example the (cumulative) oil and water production. Alternatively, the variance of the economic performance measure given the uncertain parameters can be used as a measure for robustness. A production strategy that gives a small variance in the resulting economic performance measure is no longer sensitive against the considered uncertainty. Generally however, reducing the variance lowers the average performance, with the extreme case of no production giving a variance of 0. To that end, the measure of variance must be balanced against the expected value, which mathematically can be expressed as:

$$\begin{aligned} J_{RO} \triangleq E_\theta \left[J(\mathbf{y}, \theta) \right] - \gamma \cdot Var_\theta \left[J(\mathbf{y}, \theta) \right] = \\ E_\theta \left[J(\mathbf{y}, \theta) \right] - \gamma \cdot E_\theta \left[\left(J(\mathbf{y}, \theta) - E_\theta \left[J(\mathbf{y}, \theta) \right] \right)^2 \right], \end{aligned} \tag{2.21}$$

in which the balance between good average performance and a small variance can be adjusted through weight factor γ. It should be noted that:

$$E_\theta \left[J(\mathbf{y}, \theta) \right] \neq J(\mathbf{y}, E_\theta \left[\theta \right]). \tag{2.22}$$

In other words, the robust optimization problem cannot be converted into a nominal optimization problem by taking the expected value of the uncertain (stochastic) model parameters θ. In order to solve the robust optimization problem, the robust optimization objective function can be approximated trough sampling of the uncertain

parameter space Θ, resulting in a finite number N_r of realizations of the uncertain parameters θ. The approximation for the expected value, given a set θ_d of realizations θ_i can be expressed as:

$$E_\theta\left[J(\mathbf{y},\theta)\right] \approx E_{\theta_d}\left[J(\mathbf{y},\theta_d)\right] = \sum_{i=1}^{N_r} P_i \cdot J(\mathbf{y},\theta_i),$$
$$\theta_d \triangleq \{\theta_1,\ldots,\theta_{N_r}\}, \tag{2.23}$$

where P_i is the probability of each realization, where

$$\sum_{i=1}^{N_r} P_i = 1. \tag{2.24}$$

In the case of equiprobable samples, P_i is equal to $\frac{1}{N_r}$. Likewise, the variance can be approximated using a set of realizations through:

$$Var_\theta\left[J(\mathbf{y},\theta)\right] \approx Var_{\theta_d}\left[J(\mathbf{y},\theta_d)\right] = \sum_{i=1}^{N_r} P_i \cdot \left[J(\mathbf{y},\theta_i) - \sum_{i=1}^{N_r}\left(P_i \cdot J(\mathbf{y},\theta_i)\right)\right]^2,$$
$$\theta_d \triangleq \{\theta_1,\ldots,\theta_{N_r}\}. \tag{2.25}$$

In case of geological uncertainty, the samples of θ relate to different geological scenarios of the subsurface, but also economic uncertainty can be addressed through different scenarios, e.g. different scenarios of the evolution of the oil price.

Using the discrete form (2.25), the value of the robust objective function can simply be approximated by performing a reservoir simulation for all realizations of θ in the set. The goal of robust optimization is to design a production strategy that maximizes that value. For optimization methods that regard the reservoir simulator as a black box, like EnKF, Experimental Design, particle swarm optimization, or numerical perturbation methods, the complexity of the robust objective function is not an issue, even when a more complicated robust objective function is adopted than the one expressed in terms of mean and variance, see Almeida et al. (2007); Chen et al. (2009b); Su and Oliver (2010); Echeverra Ciaurri et al. (2011). Determining the update step for the production strategy just involves calculating the performance measure for all individual realizations. This sensitivity to the complexity of the objective function is different for gradient-based algorithm which depend on the Adjoint to determine the gradients. Since the objective function is hard-coded into the adjoint

equations, a more complex objective function requires (complicated) adaptation of the adjoint code, see Kraaijevanger et al. (2007); Jansen (2011). Fortunately, when the robust optimization objective function is only expressed in terms of mean and variance, the gradients of the robust objective function J_{RO} with respect to the control parameters $\mathbf{u}$, are a linear combination of the gradients of the individual realizations:

$$\frac{J_{RO}(\mathbf{y},\theta_d)}{\mathbf{u}} = \overbrace{\frac{\partial \bar{J}(\mathbf{y},\theta_d)}{\partial \mathbf{u}}}^{\textit{mean part}} - \underbrace{2\gamma \sum_{i=1}^{N_r} P_i \cdot (J_i(\mathbf{y},\theta_i) - \bar{J}(\mathbf{y},\theta_d)) \left(\frac{\partial J_i(\mathbf{y},\theta_i)}{\partial \mathbf{u}} - \frac{\partial \bar{J}(\mathbf{y},\theta_d)}{\partial \mathbf{u}} \right)}_{\textit{variance part}} \quad (2.26)$$

where

$$\bar{J}(\mathbf{y},\theta_d) \triangleq \sum_{i=1}^{N_r} P_i \cdot J_i(\mathbf{y},\theta_i),$$
$$\theta_d \triangleq \{\theta_1,\ldots,\theta_{N_r}\}, \quad (2.27)$$

and

$$\frac{\partial \bar{J}(\mathbf{y},\theta_d)}{\partial \mathbf{u}} = \sum_{i=1}^{N_r} P_i \cdot \frac{\partial J_i(\mathbf{y},\theta_i)}{\partial \mathbf{u}},$$
$$\theta_d \triangleq \{\theta_1,\ldots,\theta_{N_r}\}. \quad (2.28)$$

In the example below, the robust optimization method is demonstrated on an oil reservoir for which the geological uncertainty is represented by a set of different geological realizations. More details of the example can be found in Appendix D.

Example 4. *Again the waterflooding example of the 3D reservoir model is considered, as introduced in Van Essen et al. (2009b). The structural model, grid block properties and wells are identical to those of the model introduced in the example 1 of Section 1, but the model deviates in the density and viscosity of the fluids. These properties can be found in Table D.1 in Appendix D. As in the previous examples, the lack of information about the real geological structure was assumed to be the only contributor to the model uncertainty.*

Two different sets of 100 geological realizations of the reservoir were generated, based on geological insight. In other words, the geologist sketched them by hand. Each set of realizations represents the range of possible geological structures within the boundaries of the geological uncertainties. The number of 100 realizations is assumed to be large enough to be a good representation of this range. To check whether this is a reasonable assumption, the responses of the two sets of 100 realizations to identical control strategies were compared. It should be noted that similar responses (in a statistical sense) indicate that this assumption is plausible, but do not provide a conclusive validation. The manual method by which the different realizations were created does not give a classification between the members in the set. No information from seismic, production, or other data was assumed to be available to rank the realizations; therefore, they were assumed to be equiprobable. Fig. 2.6 displays the absolute-permeability field of six realizations randomly selected from the set without the wells.

Production Strategies. *Three production strategies are considered: a reactive approach, a nominal optimization (NO) approach, and a robust optimization (RO) approach. The control parameters for each of the strategies involve the injection and production flow rates. For each strategy, the maximum rate for each well was fixed at 64 m^3/d. Additionally a pressure maintenance constraint was adopted, which involved keeping reservoir pressure (more-or-less) constant, by enforcing the total injection rate to be equal to the total production rate at each time instant. The performance of each production strategy was evaluated using the objective function as defined in Eq. (D.1), with r_o = 126 \$/m^3, r_w = 19 \$/m^3, and r_i = 6 \$/m^3. However, because of the geological uncertainty, a deterministic estimate of performance cannot be given. Therefore, the performance of each of the three strategies was estimated in a probabilistic sense, using the set of 100 realizations. For each strategy, the 100 deterministic values of the objective function resulting from the set were used to determine a cumulative distribution function (CDF) and to estimate a probability density function (PDF).*

Reactive approach. *Using the reactive approach, each production well is simply shut in if production is no longer profitable, where the profitability threshold corresponds to a water cut of 87%. The production flow rates are initially fixed at their maximum capacity of 64 m^3/day. The injection flow rates are equal for each injection well and are initially fixed at 32 m^3/day to honor the balanced injection and production constraint. If a production well is shut in, the injection rate of each injection well is proportionally scaled down to meet the constraint.*

This reactive strategy is used as a benchmark for the optimal control strategies that need predictive reservoir models to determine a strategy. The advantage of a reactive strategy is that it is model-free. Thus, when applied to an actual field, it does not suffer from a wrong representation of the geological realizations, whereas model-based methods do. However, the disadvantage is that it usually does not lead to an optimal reservoir flooding in terms of life-cycle performance. In the field-development phase of a project, the performance of a reactive strategy versus a model-based strategy can be assessed by simulating the performance of both strategies on a set of realizations.

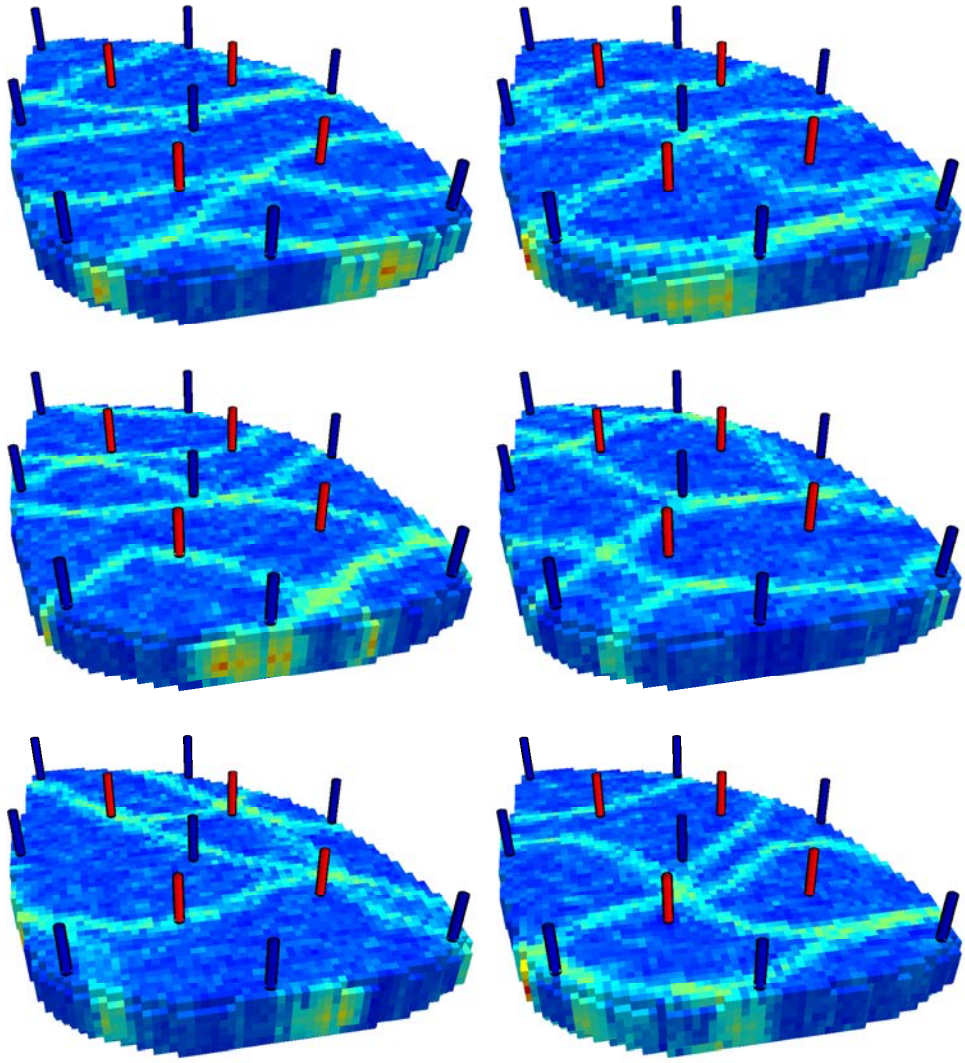

Figure 2.6 : Permeability field of six (randomly chosen) realizations out of a set of 100, showing alternative fluvial configurations.

Table 2.1 : *Results*

	Reactive Control	*NO (on average)*		*RO*	
Expected NPV	43.7 million $	46.3 million $	+5.9%	47.9 million $	+9.5%
Standard Dev.	1.20 million $	1.01 million $	-	0.79 million $	-

Applying the reactive control strategy to each of the 100 members resulted in 100 values of the objective function Eq. (D.1). The corresponding CDF and PDF, as depicted in Fig. 2.7, provide a probabilistic estimate of the performance of the reactive production strategy when applied to the true reservoir. The expected NPV and estimated standard deviation of the strategy are presented in Table 2.1.

Nominal Optimization *The NO approach is based on a single realization. However, because none of the realizations in the set of 100 is preferred over the others, the decision of which realization to use in the NO approach becomes an arbitrary one. To avoid the possibility of a biased choice, the NO procedure was performed on each of the 100 realizations in the set individually, resulting in 100 different NO production strategies. The initial injection and production flow rates were set constant over time and equal to 24 m^3/day and 48 m^3/day respectively. The injection and production flow rates were optimized with a gradient-based optimization algorithm, using the adjoint to determine the gradients of the objective function with respect to the injection and production flow rates.*

The performance of each of these 100 strategies on the entire ensemble was assessed by applying them to each member of the set. This resulted in 100×100 *values of the objective function, from which 100 CDFs and PDFs were determined, one for each strategy, as shown in Fig. 2.7. For each NO strategy, the expected NPV and the standard deviation were determined. The averages of these 100 expected NPV values and standard deviations are presented in Table 2.1.*

Robust Optimization *The RO approach uses the entire set of realizations to determine a control strategy that maximizes the expected NPV over the entire set of realizations. The robust optimal control strategy is determined using the same gradient-based optimization procedure and optimization parameters that were used in the NO approach. The RO control strategy was again applied to each realization in the set, and the value of the objective function was determined for each member. The resulting CDF and PDF are depicted in Fig. 2.7, and the expected NPV and standard deviation are presented in Table 2.1.*

Results

Fig. 2.7 and Table 2.1 show that the performance of the RO control strategy is greatly improved over the performance of the reactive control strategy. The expected NPV increases 9.5%. The standard deviation is also reduced considerably, although a reduction in variance is not part of the RO objective function. On average, the performance of the RO strategy is

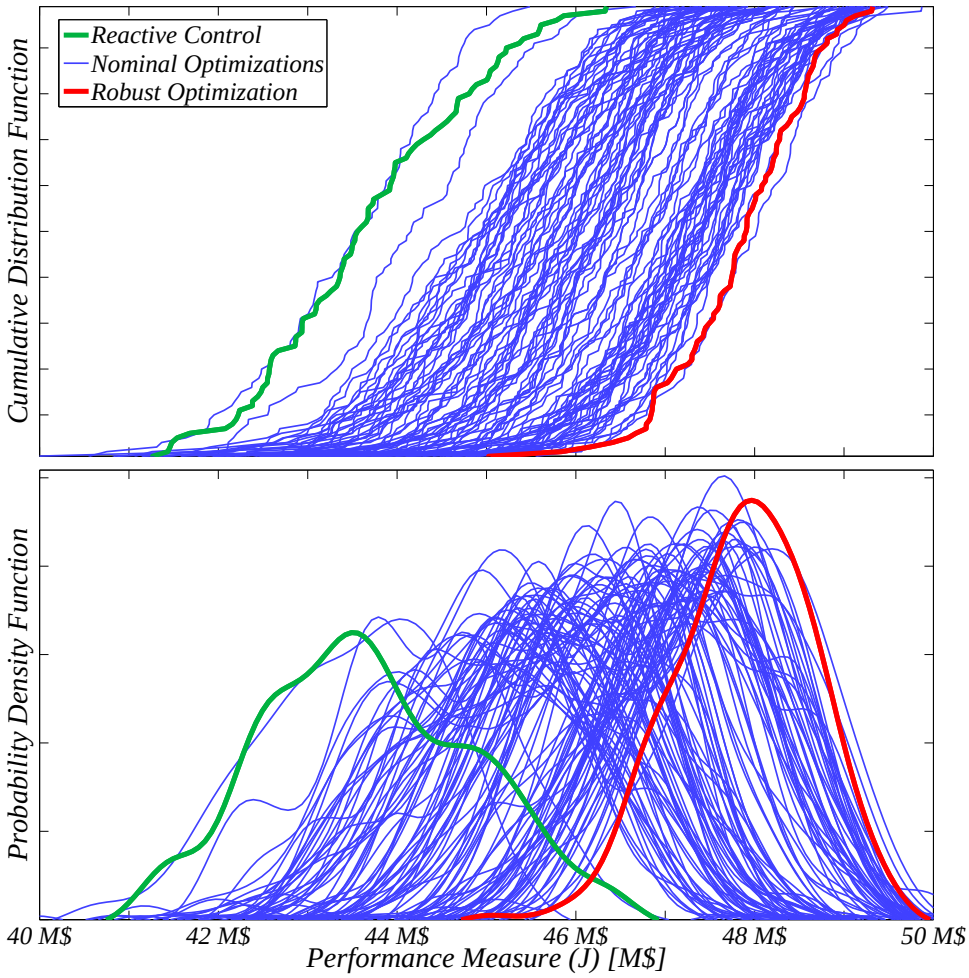

Figure 2.7 : Cumulative Distribution Function and Probability Density Functions based on the first set of 100 realizations of the reactive control strategy, the 100 nominal optimization strategies and the robust optimization strategy.

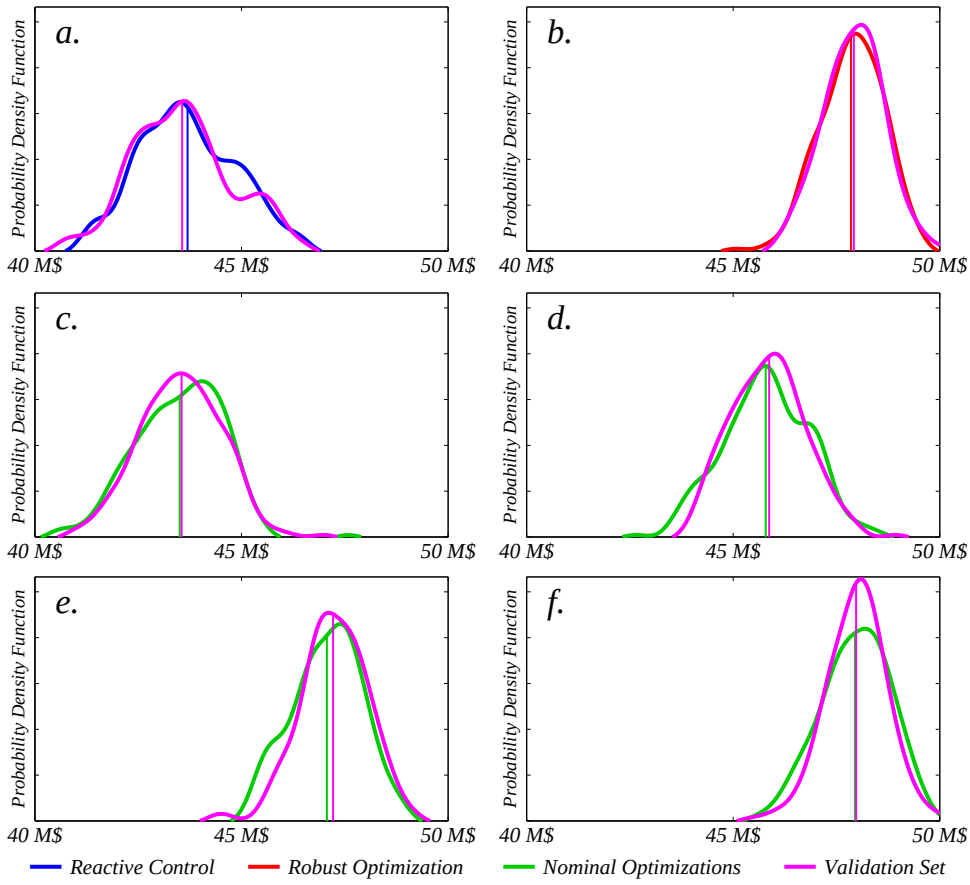

Figure 2.8 : Estimated PDFs of the reactive control strategy (a), the RO control strategy (b), the NO strategy with the lowest expected NPV (c), the highest expected NPV (f), and two intermediate values of expected NPV (d and e), applied to the original and the validation set of realizations.

also improved compared to the NO strategies. It performs better than 99 out of the 100 NO strategies, though the difference in the expected NPV of the best NO control strategy and the RO control strategy is very small. This may be the effect of an RO procedure that was not fully converged or of the RO strategy leading to a local optimum in expected NPV.

Improved performance of the RO strategy against the actual underlying geological uncertainty can only be claimed if the set is, in fact, a proper representation of this uncertainty, as was assumed in the introduction of the example. To validate that this assumption is plausible, the different control strategies were checked against the second set of 100 realizations.

Table 2.2 presents the averaged expected NPV and standard deviation of the reactive, NO and

Table 2.2 : *Validation*

	Reactive Control	*NO (on average)*	*RO*
Expected NPV	43.6 million $	46.3 million $	47.9 million $
Standard Dev.	1.24 million $	0.93 million $	0.79 million $

RO strategies, applied to this second validation set. Figs. 2.8.a and 2.8.b show the estimated PDFs of the reactive control strategy and of the RO control strategy, respectively, applied to the original and the validation set. Figs. 2.8.c and 2.8.f show the PDFs of the NO strategy with the lowest expected NPV and with the highest expected NPV, respectively; Figs 2.8.d and 2.8.e show two intermediate values of expected NPV. Table 2.2 and Fig. 2.8 show that the responses of the strategies to the different sets are very similar. This indicates that the assumption of the set being a proper representation of the geological uncertainty is, in fact, plausible.

It should be noted that the robust optimization objective function Eq. (2.24) fits the generic balanced objective function definition (2.4) presented in Section 2.1. Also with the more specific robust optimization objective, determining a proper weighting in advance is difficult and generally requires some trial and error. In this case, hierarchical optimization, as presented in Section 2.1 may be a more suitable approach.

2.3 Integrated Dynamic Optimization and Feedback Control

The robust optimization method presented in the previous section is aimed at increasing robustness to uncertainty *a priori*. In other words, minimizing the impact of anticipated uncertainty on (economic) performance is part of the initial design of the operational control strategy, which can subsequently be applied to the real reservoir. The difficulty with such an a priori approach is:

1. It is often hard to design a representative ensemble of models to reflect the expected uncertainty.
2. Not all uncertainties and their impact can be represented accurately by the reservoir model, e.g. fast, local (near-wellbore) dynamics.
3. Some uncertainties are impossible to predict, e.g. operational events due to material failure. These uncertain events are often referred to as 'disturbances'.

Ideally one would like to monitor the impact of uncertainty on performance on-the-fly when applying the operational strategy to the field and take corrective measures

when performance is (negatively) impacted. Unfortunately, economic life-cycle performance in terms of NPV can only be evaluated at the end of field life due to its cumulative nature. On top of that, in waterfloods life-cycle performance is mainly determined by water production, which generally occurs late in the life of the field. Hence, a life-cycle performance measure can not be evaluated on-the-fly to take remedial actions.

To suppress the impact of uncertainty on economic performance during execution of an operational strategy, a certain output of the dynamic model ($\hat{\mathbf{y}}$) needs to be available of which its progression over time or *trajectory* can serve as a reference, from which deviations during operation correlate with a *change* in economic performance. Hence, robustness against uncertainties - which is evaluated at the end of the life-cycle - is replaced by a tracking control problem which is evaluated at every time instant. Thus, tracking performance of a reference trajectory $\mathbf{r}$ serves as an on-the-fly proxy for robustness. The advantage of that approach is that it allows for a feedback control approach, in which field outputs (measurements) $\mathbf{y}$ are directly used to adjust control strategy $\mathbf{u}$. In the next section, the tracking control problem is discussed in more detail.

It may not always be possible to determine a model output $\hat{\mathbf{y}}$ of which its trajectory serves as a good reference to suppress the impact of uncertainty on economic performance on-the-fly. It will depend on the field, what types of data are available and on the depletion strategy. Besides this, the reference trajectory has to meet the following two conditions:

1. It must be possible to measure or estimate model output $\hat{\mathbf{y}}$ in the field, i.e. from reservoir output $\mathbf{y}$. This conditions relates to the *observability* of the reservoir as a system. See Zandvliet et al. (2008); Van den Hof et al. (2012).

2. It must be possible to manipulate and control field output $\mathbf{y}$, which relates to the *controllability* reservoir system. See Zandvliet et al. (2008); Van den Hof et al. (2012).

Not every output $\mathbf{y}$ that is measured in the field can serve as an appropriate reference signal for a tracking control problem. For instance watercut data per well seems like a suitable choice as a reference trajectory, considering the impact of an early water breakthrough on the economic performance of a waterflood project. However, watercut data may not be available for every well and often lacks accuracy. More important however is that it is not an output that can be controlled on-the-fly, i.e. it doesn't honor condition 2. Alternatively, liquid flow rates per well can be considered as reference trajectories as these can be both monitored and controlled in the field, but because watercut data is not part of the reference, perfect tracking control does

not necessarily imply little variance around expected economic performance (robustness). Considering the fact however that waterflooding is essentially a displacement process, a measure that represents injected and extracted volumes from the reservoir over time, i.e. (cumulative) liquid rates per well can still serve as a good proxy. An interesting development is the use of ocean-bottom seismometers for permanent seismic monitoring or instantaneous 4D (Barkved et al. (2005), Stammeijer et al. (2013)). This allows for relatively high-frequency (in the order of monthly) updates of the moving oil-water front, which may serve as a very suitable reference trajectory for the tracking control problem.

2.3.1 Multilevel Optimization and Control

If a model output $\hat{\mathbf{y}}$ exists that can serve as a reference trajectory $\mathbf{r}$ and it meets the two conditions mentioned above, *robustness* of the economic objective function can be improved on-the-fly, but not the economic objective function itself. That can still only be addressed at the end of the life-cycle for which a predictive reservoir model is required. To address both objectives at the same time, an output of the (life-cycle) *optimized* dynamic model $\hat{\mathbf{y}}^*$ may be selected as reference trajectory $\mathbf{r}$. This integrated or multilevel approach of dynamic optimization and feedback control can be encountered in the process industry. Similar multi-level control structures have been proposed by e.g. Saputelli et al. (2006) and Foss and Jensen (2011) for use in upstream oil and gas operations. In similar control structures in the process industry the second and third levels are often referred to as dynamic real-time optimization (D-RTO) and model predictive control (MPC) respectively.

By tracking the reference trajectory $\mathbf{r}$, the impact of uncertainty on $\mathbf{y}$ is repressed during operation. However, that uncertainty is also a representation of the inaccuracy of the reservoir model, which means that the optimal output for the model $\hat{\mathbf{y}}^*$ deviates from actual (unknown) optimal output $\mathbf{y}^*$ and $\mathbf{r}$ is a sub-optimal reference trajectory. As a result, any control effort during operation to honor reference trajectory $\mathbf{r}$ is likely to improve robustness, but may hurt economic performance in the end. Whether or nor economic life-cycle performance is negatively impacted depends on the sensitivity of $\mathbf{y}$ to uncertainty, compared to the sensitivity of $\mathbf{y}^*$ to uncertainty. To be more specific, if the impact of uncertainty or disturbances on $\mathbf{y}$ is large, but the actual (unknown) optimal output trajectory $\mathbf{y}^*$ remains more or less the same, suppressing the impact uncertainty on $\mathbf{y}$ through tracking control of $\mathbf{r}$ will probably have a positive effect on economic life-cycle performance. Conversely, if the impact on $\mathbf{y}$ is small, but the (unknown) optimal $\mathbf{y}^*$ would change significantly due to uncertainty, tracking control would reduce the economic life-cycle performance more than the uncertainty would have done.

Experiences in the process industry show that a tracking control approach is effective when uncertainties are relatively small and disturbances are local in time or space. Another aspect that limits applicability of tracking control to cases where the uncertainties are small and the disturbances are local is effect of the constraints that act on the input (control) parameters **u**. The larger the deviations of **y** from reference trajectory **r**, the more control effort is required to steer **y** back to its reference value. Limits on the control parameters may considerable limit tracking performance and consequently limit the ability to minimize the impact of uncertainty on economic life-cycle performance.

2.3.2 Tracking Control

The tracking control problem can be expressed as a moving horizon optimization problem, contrary to closed-loop reservoir management which is essentially a shrinking horizon optimization problem, see Naevdal et al. (2006), Sarma et al. (2008), Chen et al. (2009a), Jansen et al. (2009) and Wang et al. (2009). The objective function of the tracking control problem is a (discrete) quadratic cost function V that is evaluated over the receding prediction horizon and can mathematically be expressed by:

$$V(\check{\mathbf{u}}_{k:k+N}) = \sum_{j=k}^{N} (\check{\mathbf{y}}_j - \mathbf{r}_j)^T \, \mathbf{R} \, (\check{\mathbf{y}}_j - \mathbf{r}_j) + (\check{\mathbf{u}}_j - \hat{\mathbf{u}}_j)^T \, \mathbf{Q} \, (\check{\mathbf{u}}_j - \hat{\mathbf{u}}_j), \tag{2.29}$$

where N is the number of time steps over the moving control horizon, $\check{\mathbf{u}}$ relates to the corrected inputs, $\check{\mathbf{y}}$ is the predicted output of the real output **y** and **R** and **Q** are optional weighing matrices. Note that here, for simplicity, it is assumed that the time steps k have the same length as those in life-cycle optimization problem. In reality, the time steps in (2.29) will be much smaller. The second term at the right-hand side of Eq. (2.29) ensures that the corrected inputs $\check{\mathbf{u}}$ do not deviate too much from the optimal inputs $\hat{\mathbf{u}}$ as computed in the life-cycle optimization step. Using cost function V, the moving horizon tracking control problem can mathematically be expressed as:

$$\min_{\mathbf{u}_{k:k+N}} (V) \tag{2.30}$$

$$s.t. \quad \check{\mathbf{g}}_{k+1} \left(\check{\mathbf{u}}_k, \check{\mathbf{x}}_k, \check{\mathbf{x}}_{k+1}, \check{\boldsymbol{\theta}} \right) = 0, \quad k = k, \ldots, k+N, \quad \check{\mathbf{x}}_{k-1} = \bar{\mathbf{x}}_{k-1}, \tag{2.31}$$

$$\check{\mathbf{c}}_{k+1} (\check{\mathbf{u}}_{k+1}, \check{\mathbf{x}}_{k+1}) \leq 0, \quad j = k-1, \ldots, k+N, \tag{2.32}$$

where $\check{\mathbf{u}}$ is the corrected control vector (input vector), $\check{\mathbf{g}}$ is a vector-valued function that represents the system equations which may differ from the dynamic model $\mathbf{g}$ used for the life-cycle optimization problem. Vector $\check{\mathbf{x}}$ is the state vector of model description $\check{\mathbf{g}}$, $\check{\boldsymbol{\theta}}$ a vector of model parameters, $\check{\mathbf{x}}_0$ is a vector of the initial conditions of model $\check{\mathbf{g}}$ with prescribed value $\overline{\mathbf{x}}_{k-1}$, the subscript k indicates discrete time, and N is the total number of time steps of the receding horizon. The vector of inequality constraints $\check{\mathbf{c}}$ relates to the capacity limitations of the wells.

The optimal corrected control vector $\check{\mathbf{u}}^*_{k:k+N}$ leads to a minimum of cost function V and best possible predicted tracking performance. Of $\check{\mathbf{u}}^*_{k:k+N}$ only $\check{\mathbf{u}}_k$ is implemented after which the minimization of V is carried out from time step $k+1$ until $k+N+1$ (receding horizon). To minimize cost function V a model is required that provides a predicted output $\check{\mathbf{y}}$ of the real output $\mathbf{y}$, given corrected input $\check{\mathbf{u}}$. However, the required prediction horizon being equal to N times k can be considerably shorter than the prediction horizon for life-cycle optimization problem. This allows for different modeling choices and requirements:

- Whereas long-term reservoir dynamic are governed by non-linear properties of the mixed fluid dynamics, on the short term these effects can be neglected since the oil-water front generally moves relatively slow (compared to pressure propagation). This allows for a *linear* model to describe outputs $\mathbf{y}$ of the reservoir system.

- On the short term, reservoir behavior is mainly determined by fast, localized (near-wellbore) dynamics and the pressure communication between wells. This can be determined from measurements, contrary to the saturation behavior (front movement) which over the long term is often dominated by reservoir features that can only be captured through first-principle modeling. This allows for *data-driven* modeling methods to obtain a short-term predictive model, which only rely on measurement data to capture the input-output behavior of the reservoir, see Rowan and Clegg (1963); Chierici et al. (1981); Liu et al. (2009); Sayarpour et al. (2009); Viberg (1995).

- Compared to long-term reservoir dynamics, the short-term dynamic behavior of the reservoir is much more dependent on the 'current' state of the reservoir (in terms of saturations and pressures) and less on reservoir characteristics (captured by the model parameters). Hence, estimation of the 'initial' state $\check{\mathbf{x}}_{k-1}$ of model $\check{\mathbf{g}}$ is essential in moving horizon setup (2.30)-(2.32).

In the following example, the optimal operational strategy to an economic life-cycle objective is determined using a reservoir model. In the application of the operational strategy to the 'true' field, uncertainty is present in the form of an error in the modeled geological features and the presence of fast, local (near-wellbore) dynamics around

the wells. From the life-cycle optimization, the (model-)optimal liquid flow rates for each well are chosen as reference trajectories for a tracking control setup to minimize the impact of the considered uncertainties on the actual economic life-cycle performance. The short-term reservoir model used for solving the on-the-fly tracking problem is based on input-output data alone using a data-driven modeling technique known as System Identification (Ljung (1999)). It should be noted that the specific choices for reference trajectories and short-term reservoir model made in this example are not necessarily the best or only ones possible. More research is required to answer those questions. Details of the presented example can be found in Appendix E, which was published before as Van Essen et al. (2013).

Example 5. *The reservoir considered in this example is similar to the one presented in Example 2 in Chapter 1, except for some of the fluid properties and its geological structure, which is dominated by two intersecting high-permeable channels. The remaining reservoir properties can be found in Table E.1 of Appendix E. The life-cycle of the reservoir covers a period of 11.5 years. Of this reservoir a dynamic reservoir model was created to serve as the synthetic 'truth'. In order to provide realistic predictions of short-term dynamic behavior of the reservoir, a very fine spatial discretization around the wells was adopted and a (relatively) very short time step size was chosen of 0.25 days. This truth model was used to generate synthetic (noise-free) production measurements, and to assess the 'true' production performance over the life of the reservoir. A second reservoir model was created which serves as the model to perform life-cycle optimization and design the identification experiment. No grid refinement around the wells was used and a time step size of 30 days was adopted. Besides the coarser discretization in space and time, the second model deviates from the 'truth' in its geological structure. In particular it has channels in a slightly different flow direction, such that different wells are inside the high-perm streaks; see Fig. 2.9.*

Optimization of economic life-cycle performance is carried out using an objective function in terms of NPV, with oil revenues r_o equal to 56.6 $\$/m^3$, water production costs r_{wp} of 6.3 $\$/m^3$, zero water injection costs, and an annual discount rate b equal to 0.1. The controls of the wells $\mathbf{u}$ *involve the injection flow rates of the eight injectors and the (flowing) bottom-hole pressures (BHPs) of the four injectors. Rate constraints are applied to the injectors (a maximum rate of 1,590 $\frac{m^3}{day}$) and pressure constraints to the producers (a minimum BHP of 37.5 MPa (375 bar), i.e. 2.5 MPa (25 bar) below the initial reservoir pressure). The life-cycle optimization problem was solved with the aid of a gradient-based algorithm for which the gradients were obtained with the adjoint formalism in the simulator. Solving the life-cycle optimization problem resulted in an expected maximum NPV of 596 $\cdot 10^6$ \$. From the life-cycle optimization, the flow rates* $\mathbf{q}_l$ *over time of the four production wells, which cannot be manipulated directly, are selected as reference trajectories for the implementation of the production strategy using reference tracking control.*

To obtain a local, linear model for tracking control, a data-driven model is derived using input (control) data and output (measurement) data of the first 75 days of production. The

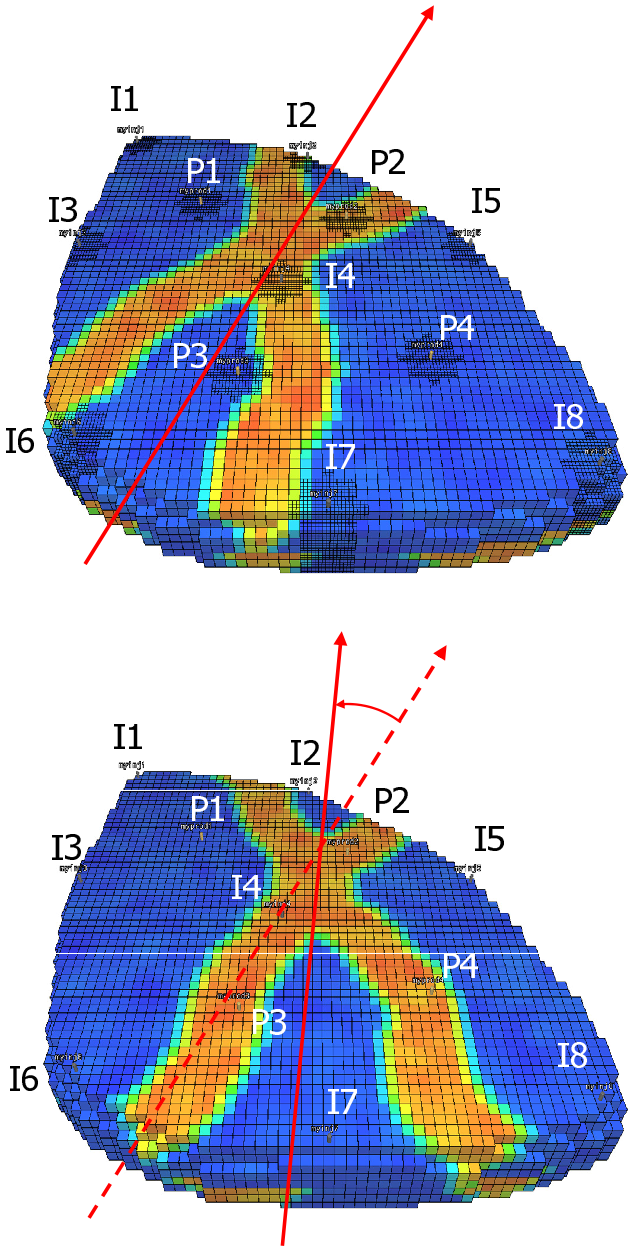

Figure 2.9 : (top) 3D reservoir model, used as synthetic 'truth', with 8 injection wells and 4 production wells. Its geological structure involves a network of meandering channels of high permeability. The model on the bottom is used for life-cycle optimization and differs from the model on the top in the direction of the channels, the absence of grid refinement, and the larger time-step size of 30 days.

inputs were the water injection rates of the eight injectors and the bottom-hole pressures of the four producers. The outputs are defined as the four total liquid rates in the producers. More details of the system identification experiment can be found in Appendix E. The tracking control problem involves minimization of a cost function as described by equation (2.29) by changing the inputs (injection flow rates and BHPs of the production wells). Matrix $\mathbf{W}_1$ *is taken as a unit matrix and weighting matrix* $\mathbf{W}_2$ *is chosen as a diagonal matrix with zeros and ones in positions corresponding to pressures and flow rates respectively. As a results,* $\mathbf{W}_2$ *only penalizes deviations of the optimal injection rates and not of the optimal production pressures, such that tracking is mainly realized through changes in the bottom-hole pressures in the production wells. The reason behind this choice is to aim for a higher penalty on changes in produced and injected volumes (with the aid of* $\mathbf{W}_1$ *and the nonzero elements of* $\mathbf{W}_2$ *respectively), than on changes in the corresponding pressures. In this experiment, the prediction horizon is chosen equal to one week. Each time step of 0.25 days, the minimization problem is solved for the (moving) prediction horizon, which involves two sequential steps: State estimation and quadratic programming (QP).*

1. State Estimation. *In this simulation study, no artificial noise was added to the measurements. As a result, the state estimation problem can be attacked quite straightforwardly using a Luenberger observer (Friedland (1986)); see Appendix E.2 for further details. Note however that alternative choices for state estimation may be considered as e.g. Kalman filtering.*

2. Quadratic Programming. *To solve the minimization of objective function V subject to the inequality constraints on the inputs, a QP problem needs to be solved. In this experiment, a gradient-based QP solver was used, implemented in the in-house reservoir simulator.*

It should be noted that the particular algorithmic choices for step 1 and 2 have little impact on the tracking procedure. The controls $\check{\mathbf{u}}_{k:k+N}$ *as determined by the tracking controller were re-calculated and applied to the 'real' reservoir at every 0.25 day time step; see Fig. 2.10.*

The results from inputs $\check{\mathbf{u}}$ *obtained with the additional tracking controller are compared to results from direct, open-loop application of optimal inputs* $\hat{\mathbf{u}}$ *from the life-cycle optimization. Performance is both evaluated in terms of tracking performance and NPV. Fig. 2.11 depicts the reference and output trajectories for both the open-loop and the reference tracking case for each of the four production wells over the life of the field. In each of the four plots, four different stages can be identified. In the first 75 days of production, the identification experiment is conducted where the optimal inputs* $\hat{\mathbf{u}}$ *serve as mean values. During this period the error is large because of the model error between the reservoir model and the 'truth', while tracking control is not active yet. From 75 days to approximately 500 days tracking performance is good due to activation of the tracking controller. After 500 days tracking performance decreases, however still outperforming open-loop control. This drop is the result of water breakthrough in the production wells, which has a strong nonlinear effect of the dynamics. After approximately 3,000 days tracking improves again, due to the fact that mainly water is produced resulting in a more linear response to the inputs. In Table 2.3, the NPVs of the open-loop application of* $\hat{\mathbf{u}}$ *and* $\check{\mathbf{u}}$ *are shown in comparison to the expected maximum NPV determined by the life-cycle optimizer. From the table it is clear that the application of*

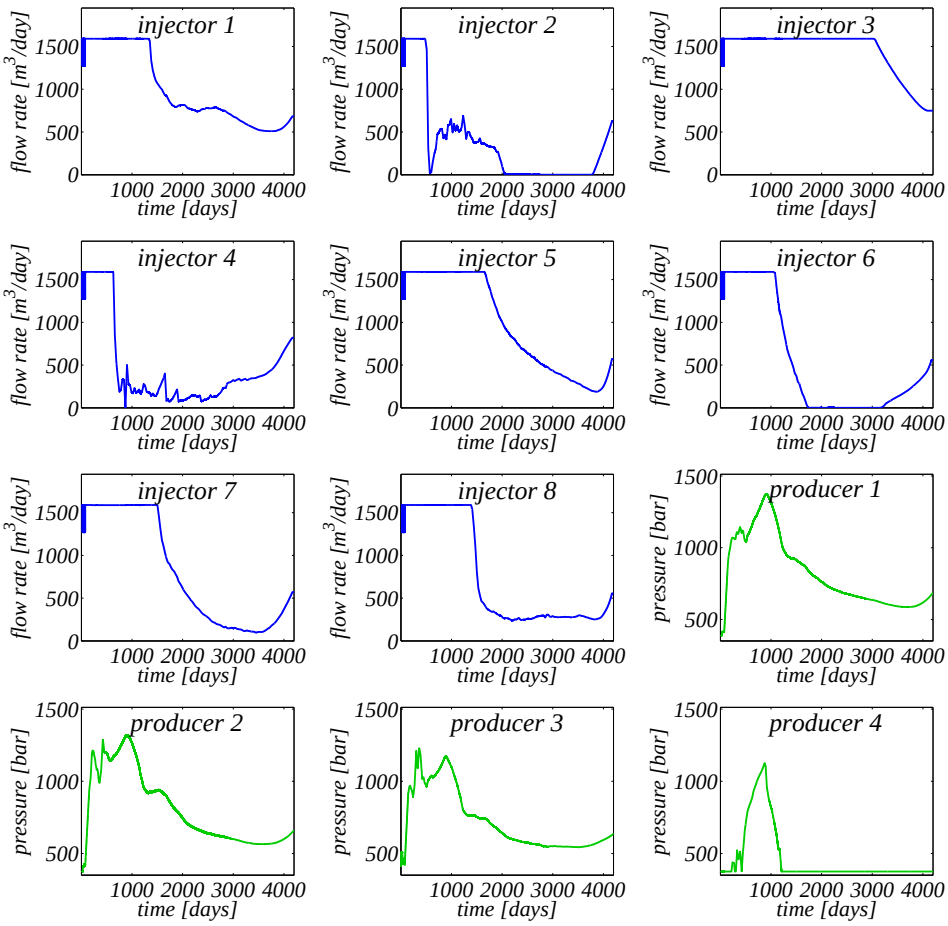

Figure 2.10 : Controls **ŭ** as determined by the tracking controller.

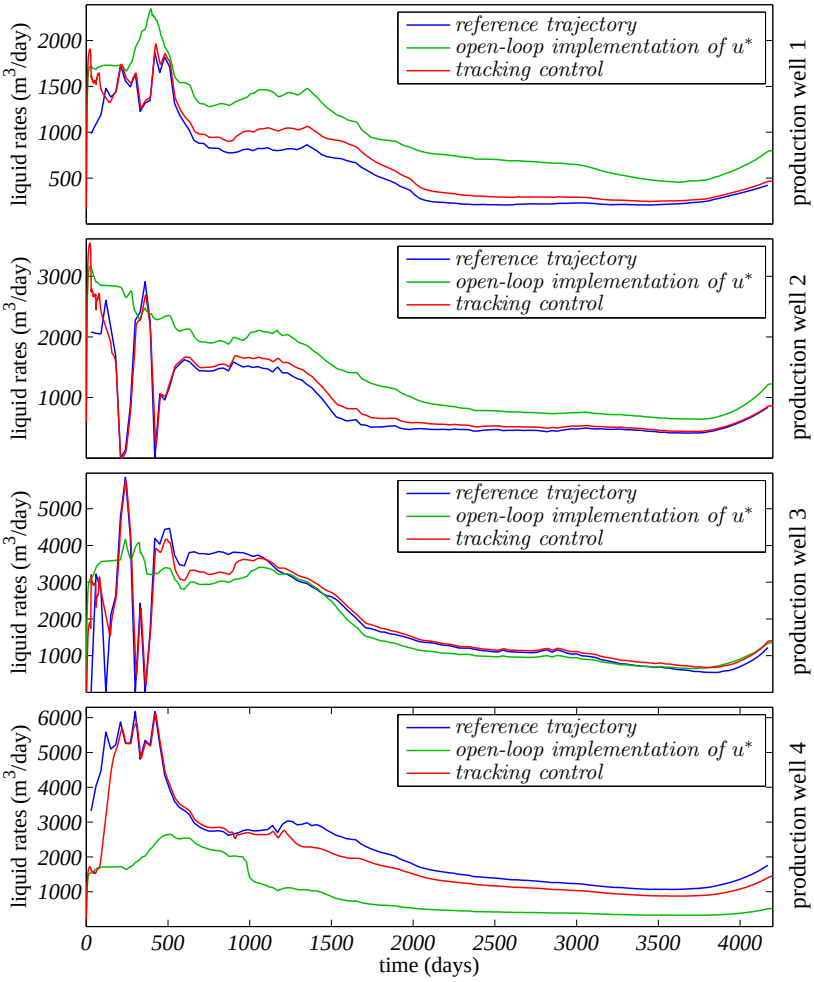

Figure 2.11 : Reference and output trajectories for the open-loop application and the tracked case for each of the four production wells over the life of the field.

Table 2.3 : *Economic Performance*

	NPV	*% change*
Maximum predicted	596×10^6\$	-
Open-loop application of $\hat{\mathbf{u}}$	558×10^6\$	-6.4%
MPC tracking using $\check{\mathbf{u}}$	594×10^6\$	-0.5%

the reference tracking controller improves the robustness of economic life-cycle performance against the considered uncertainties compared to direct application of the optimized input $\hat{\mathbf{u}}$ *from the life-cycle optimization (-0.5% drop in NPV versus -6.4%).*

2.4 Conclusion

In this chapter, three methods have been presented that can be used to increase the robustness of a production strategy when applied to more realistic circumstances in which uncertainty is present. In Section 2.1 hierarchical optimization was used to address uncertainty in the design of an operational (control) strategy. In the presented example, economic uncertainty was (implicitly) taken into account which resulted in a more robust control strategy by realizing maximal economic performance in the shortest possible time span. In section 2.2, robust optimization was presented, which uses a set of realizations of the uncertain parameters to explicitly incorporate the impact of uncertainty in the optimization problem. A 'robust' objective function was defined that addresses the design of an optimal operational strategy in probabilistic terms. In an illustrative example, geological uncertainty was captured using an ensemble of 100 geological realizations. In the integrated dynamic optimization and feedback control method presented in Section 2.3, the effect of uncertainty on the output was treated as undesired 'disturbance'. Using feedback control, the production strategy is adjusted to attenuate those effects, making the output less sensitive to the uncertainties and hence improve robustness. Although the examples used to illustrate the methods show promising results, more research and testing in realistic circumstances will be required to validate their effectiveness.

Chapter 3

Adaptive Operational Strategies

Through monitoring information is gathered over the production life of the field that can add to the understanding of the subsurface. This gained insight can be used to improve reservoir models and update the operational strategy which - in effect - increases the economic performance of the production process. The assimilation of measurement data to improve (dynamic) reservoir models is a broad and complex topic. This chapter does not address the use of measurements in economic life-cycle optimization in a very rigorous way, but in a more exploratory sense. A number of key aspects will be highlighted and some direction will be given to future research opportunities.

Building a dynamic model involves the integration of information and data on the subsurface from different sources, for example well logs, core plugs, seismic data and geological concepts. The information is often either accurate, but sparse (well logs, core plugs) or dense, but noisy or indistinct (seismic data, geological concepts). On top of that, the information is obtained at different spatial scales, such that an up- or downscaling step is required to apply the data to the dynamic model. As a result, obtaining an (initial) dynamic model that is consistent with all sources of information on all scales is already quite challenging. Figure 3.1 shows the modeling workflow that is generally followed to construct a dynamic reservoir model.

If a dynamic model is obtained that honors all available (static) data, its dynamic output can be compared to the dynamic output of the field itself, which involves all dynamic measurements data taken over the life of the field so far. Generally, for reservoir models created through first-principle modeling, the simulated and historical (measurement) data initially do not match within an acceptable range. To improve the predictive capacity of the model, the model parameters may be tuned in such a

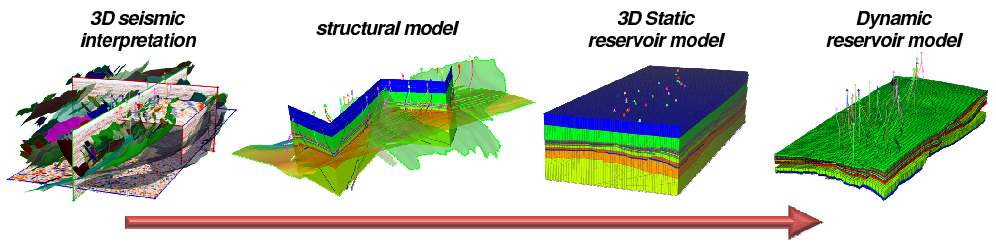

Figure 3.1 : Steps of the modeling workflow to construct a dynamic reservoir model from all sources of (static) subsurface data, involving the interpretation of seismic data and the construction of a structural model and static reservoir model. The static model contains all rock and fluid properties of the reservoir (and surroundings), but no dynamic response (in terms of pressure of saturation changes) can be calculated. The conversion to a dynamic model that can, generally requires an upscaling step of the static model properties to reduce the computational burden. After Kaleta et al. (2012).

way that the data are lined up. In reservoir engineering this inversion (calibration) process is referred to as *history matching*.

Although a lot of time is generally spent on history matching reservoir models, it is not the objective of the modeling process. When executed properly, it provides the means to reduce (geological) uncertainty and gain a better understanding of the subsurface, leading to more reliable model predictions. This in turn, may lead to better business decisions, e.g the drilling of new infill wells or the (re-)design of an operational strategy and hence improved economic life-cycle performance. While drilling new wells is usually a one-off event, an operational strategy can be adapted over the duration of its implementation whenever a more accurate model or models become available.

In many operational settings history matching is a manual process, in which understanding of basic reservoir physics is the main driver for model adjustments. However, over the recent years many different computer-assisted methods have been developed to aid the history matching process, e.g. the Ensemble Kalman Filter (EnKF), Experimental Design (ED), adjoint-based history matching and Particle Swarm Optimization (PSO), see e.g. Bennet (2002); Tarantola (2005); Evensen (2007); Oliver et al. (2008). Each of these methods involves a (number of) computer-based (mathematical) algorithms that aim to minimize the mismatch between simulated and measured historical data.

The development and improvement of history match algorithms is a research topic by itself. Giving a complete overview of all existing methods to date goes beyond the

scope of this thesis. This chapter focusses on two elements of the history matching process in view of improved predictions and (resulting) enhanced economic performance, in which the actually applied inversion algorithm plays a less essential role. These are:

1. The value of combining different (complementary) data sets

2. The value of increasing the model (and control) update frequency

These subjects will be discussed on a general level in Section 3.1 and 3.2 respectively. A more detailed description of the presented methods and examples can be found in Jansen et al. (2008) and Van Essen et al. (2012). In both papers, only geological uncertainty is addressed, however the method could be applied to other types of uncertainty as well. This chapter will be concluded in Section 3.3.

3.1 Combination of different data sets

During the production life of a reservoir, different measurements are taken to monitor the depletion process. With the development and improvement of measurement hard- and software, among which the use of smart or intelligent wells, the amount of data gathered from the field has increased considerably. Below, an overview is given of the (most common) measurements that monitor the dynamic behavior of a waterflooded reservoir.

Production data

Production data involve the measured flow rates coming from a well or group of wells. In many cases, the measurements are limited to *liquid* flow rates determined indirectly from flowing tubing head pressures (FTHP), with an occasional estimation of the phase fractions using a test separator. Phase flow meters that - on the fly - determine the phase flow rates are much more expensive and generally only used on high capacity wells. Since the (phase) flow rates are only gathered at the wells, the spatial resolution of the measurements is relatively low. However, flow meters generally measure continuously at high frequency (hours to days) so the temporal resolution of the data is high. When production data is used in history matching, the liquid flow rates are generally imposed as well constraints while the phase flow rates (or watercut) are used as the to-be-matched historical data .

Pressure data

Most wells are equipped with pressure gauges located at the surface, which record pressure data at a relatively high frequency. In order to get an estimate of the pressure at the bottom of a well, the data are corrected by the gravitational head. This is generally difficult to do accurately, since accurate estimates of the composition of the produced fluids are usually not available. Modern wells are sometimes equipped with a (permanent) downhole gauge as well (in case of smart wells even multiple) providing permanent and continuous measurements of pressures at the subsurface. Although the vertical (or along-well) resolution of (permanent) pressure devices in wells is somewhat higher, the spatial and temporal resolution of the data is comparable to those of production measurement data.

Well logs

Using wireline tools that are lowered into a well, logs can be generated of saturations and pressures along the trajectory of a well. A measurement point can be obtained every few feet, so high resolution data in the vertical direction is obtained. However, in order to take measurements the wells needs to be shut in, which makes it unattractive to do it often. In many cases, only one saturation and/or pressure log is available per well, taken before the start of production of that particular well. Production logging tools (”spinners”) can measure the flow rate while the well is producing, but are not always possible and/or are very expensive to be run.

Well tests

In well tests, streams of individual wells are lead through a test separator facility. From the test, the fractional flow rates of the well can be determined and in case of smart wells equipped with interval control valves (ICVs) even the fractional flow rates per zone. In a well test, also the well is shut in to record pressure transient effects inside the reservoir. These pressure transients effects can also provide information of the state on the field somewhat further away from the wells, but need very high recording frequencies to capture accurately (order of seconds to minutes).

4D seismic data

Time-lapse or 4D seismic data are obtained by looking at the difference signal of multiple (3D) seismic surveys. Since a lot of the ’noise’ that contaminates the 3D seismic survey is of a repeatable nature (originating from the unchanged subsurface), the difference signal is mainly determined by the dynamics in the reservoir. The quality of

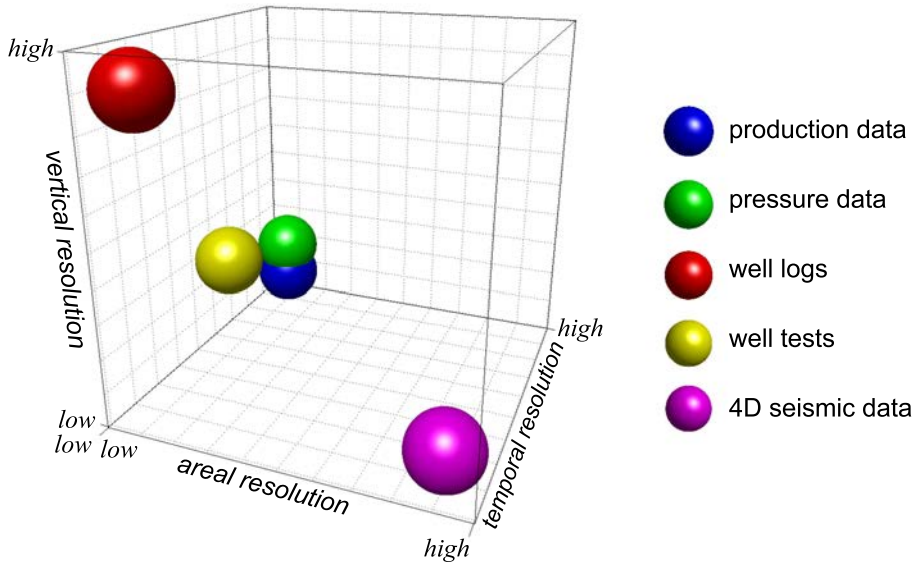

Figure 3.2 : Different measurement sources positioned on an areal, vertical and temporal resolution scale.

the signal largely depends on the ability to replicate the conditions of (a) previous survey(s) accurately. The difference signal can provide areal information on changes in the reservoir in terms of pressures, saturations or compaction, but distinguishing between these different causes can be hard. Seismic traces are generally stacked in bins of $25m \times 25m$ or $12.5m \times 12.5m$, which determines the horizon resolution (and influences the noise level) of the data. The resolution in the vertical direction is on the order of $10m$ depending on depth. The time between different surveys is usually in the order of years, so 4D seismic data is of low temporal resolution. See Calvert (2005) for more information on the subject of 4D seismic data.

In Figure 3.2, the different measurement sources are positioned on an areal, vertical and temporal resolution scale. The plot shows that although several sources of information on the depletion process are available, they generally only provide high resolution data on one of the scales. Hence, even when all data from a particular measurement source are honored by the dynamic model through history matching, much freedom on the other scales remains such that the predictions of the resulting model may still be far off from reality.

Although there is no (economically viable) method that can provide high resolution data on all scales, through combination of the data sources, the solution of the history

Table 3.1 : *Geological and fluid properties for the example*

Symbol	*Variable*	*Value*	*Units*
	Reservoir parameters		
Φ	Porosity	0.20	-
	Fluid parameters		
ρ_o	Oil density	900	kg/m^3
ρ_w	Water density	1000	kg/m^3
c_o	Oil compressibility	1.00×10^{-10}	$1/Pa$
c_w	Water compressibility	1.00×10^{-10}	$1/Pa$
μ_o	Dynamic oil viscosity	5.00×10^{-3}	$Pa \cdot s$
μ_w	Dynamic water viscosity	1.00×10^{-3}	$Pa \cdot s$
p_c	Capillary pressure	0	Pa

matching process can be constrained to (at least partly) honor reality on all scales. In effect this should lead to improved models, which give more accurate predictions. This is demonstrated in the following example.

Example 6. *In this example, the simultaneous history match of production and 4D seismic data is demonstrated on a synthetic model. The quality of the history matched model is evaluated based on the match with the historic data, the extent to which (the main geological features of) the 'true' permeability field is (are) retrieved and on the prediction accuracy over the remaining 7 years of production. A more detailed description the numerical example and the applied history matching algorithm and workflow can be found in Van Essen et al. (2012).*

This synthetic field case involves a three-dimensional oil reservoir model, introduced in Van Essen et al. (2009b). The reservoir model consists of 18,553 grid blocks, as depicted in Figure 3.3, and has dimensions of $480 \times 480 \times 28$*m. Its geological structure involves a network of fossilized meandering channels of high permeability. The reservoir boundaries and well locations are equal to those used in Van Essen et al. (2009b), but a coarser channelized structure is used to enhance the detectability of the oil-water front in the channels from time-lapse seismic. All remaining geological and fluid properties used in this example are presented in Table 3.1.*

The reservoir model contains eight injection wells and four production wells. The life-cycle of the reservoir covers a period of eight years and during that time the injection wells inject at maximum capacity of 55.2×10^{-3} m^3/s *(300 bbl/day), while the production wells operate at a fixed bottom-hole pressure of 39.9 MPa. During the first year of production, monthly production measurements were conducted of the flowing wellbore pressures (bottom-hole pressures), the water injection flow rates of the injectors, and the fractional flow rates of the production wells. After 1 year of production, a synthetic new seismic survey is conducted. The survey provides (exact) estimates of the saturation distribution at that time, mapped to a 2D areal chart, as shown in Figure 3.4.a. Based on these two data sources, three adjoint-based data history matching experiments were conducted, involving the:*

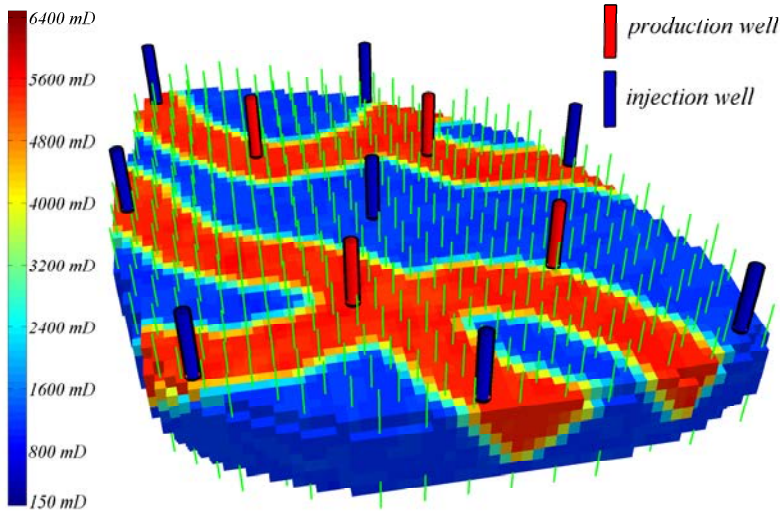

Figure 3.3 : 3-dimensional oil reservoir model with eight injection and four production wells, after Van Essen et al. (2009b). The saturation estimates from the synthetic seismic survey are averages over the thickness of the reservoirs. A subset of the 4D seismic measurement locations are shown as green lines (every other third measurement location) that penetrate the reservoir from top to bottom.

1. *History match of production data only.*
2. *History match of interpreted 4D seismic data only.*
3. *Simultaneous history match of production and 4D seismic data.*

Experiment 1: History match of production data only

The monthly measurements of the bottom-hole pressures of the 8 injection wells and fractional flow rates of the 4 production wells add up to 192 measurement points. An objective function was defined in terms of mean squared difference (MSD) between the measurements and simulated data points from the updated reservoir model. The properties of the prior model were taken identical to the 'true' model, except for the permeability field, which was considered homogeneous at a value of 700 mDarcy. Updates of the reservoir model to match historic data were limited to changes in the permeability field.

The grid block permeabilities were updated using a trust region optimization algorithm, which is a gradient-based method that searches for (the closest) minimum of the objective function. The gradients of the objective function with respect to grid block permeabilities, required for the gradient-based method, were determined using the adjoint functionality, which is described in more detail in Kraaijevanger et al. (2007).

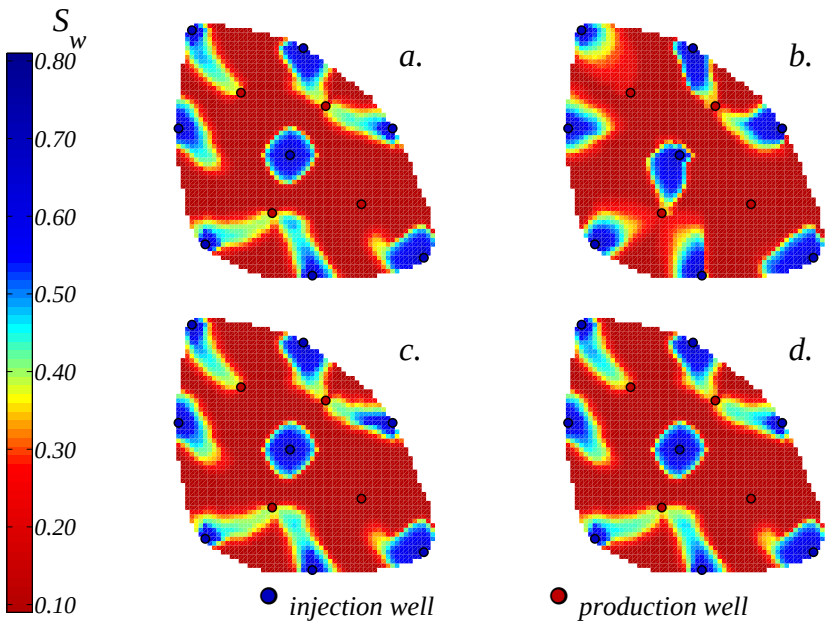

Figure 3.4 : 2D mapping of saturation distribution on the x-y-plane after one year of production from a.) the real (synthetic) field, b.) the model obtained through production data assimilation, c.) the model obtained through 4D seismic data assimilation, and d.) the model obtained through simultaneous production and 4D seismic data assimilation.

In Figure 3.5 and Figure 3.6 respectively the pressure measurements and fractional flow measurements of the 'true' field can be observed along with the simulated data originating from the updated model of experiment 1. The updated model obtained through assimilation of production data shows an excellent match with the historic data. However, the 2D mapping of saturation shown in Figure 3.4.b deviates considerably from the 2D map of the 'true' field shown in Figure 3.4.a. The updated permeability field, shown in Figure 3.7 shows high values of permeability around the well that are located in the high-permeability channels, but the structure and direction of the channels cannot be recognized. The predicted fractional flow rates, presented in Figure 3.8, show that the updated model gives relatively accurate predictions for production well 2 and 3, but are off for production well 1 and 4. Especially the predicted water breakthrough time for production well 4 is poor, since it cannot be sensed from historic production data.

Experiment 2: History match of interpreted 4D seismic data only

Experiment 2 was carried out in the same way as experiment 1 with the exception of the objective function, which uses the areal map of water saturation as measurements, corresponding to 2,491 data points. History-matching of these data points was again performed using the trust region method, with the adjoint functionality providing the gradient information. However, in order to mimic 4D seismic "measurements" such that the adjoint functionality could

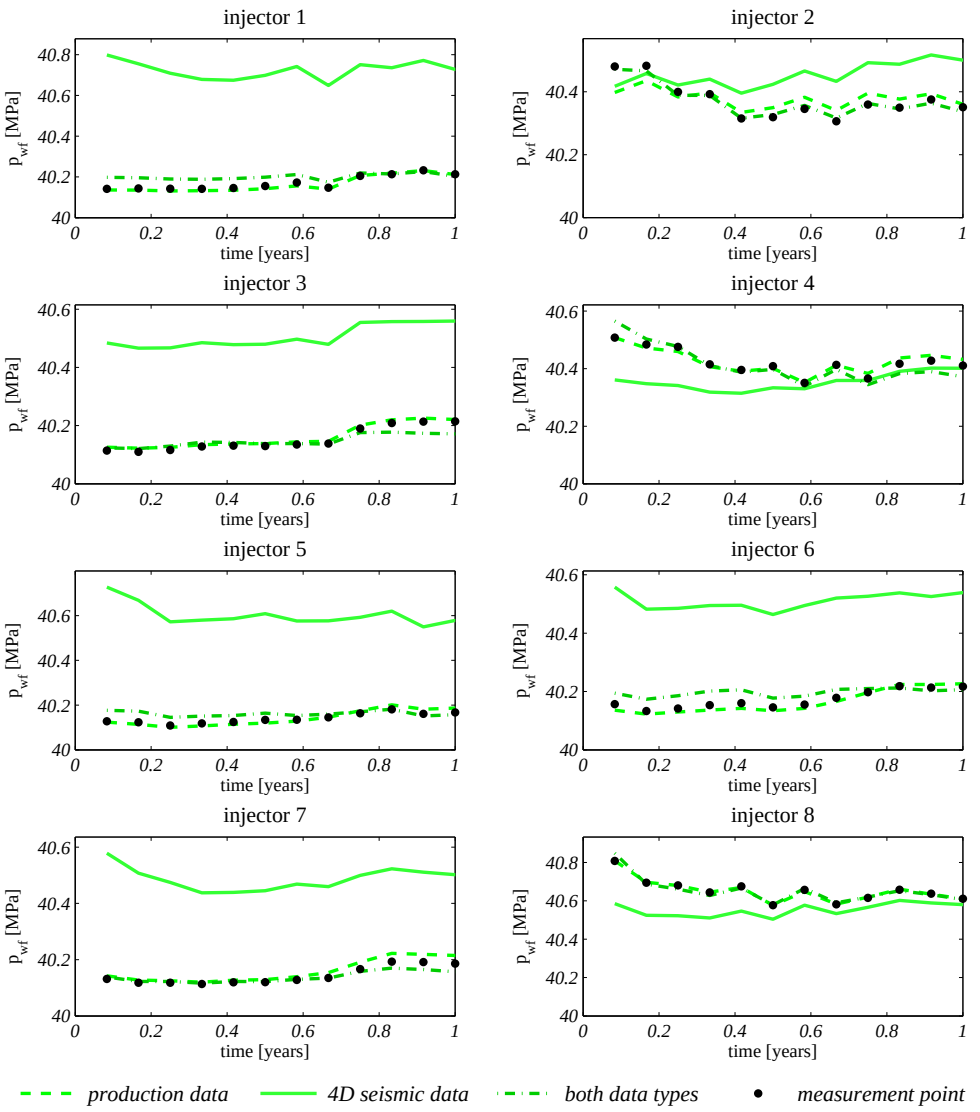

Figure 3.5 : Measured and simulated flowing bottom-hole pressures (p_{wf}) of the 8 injection wells from the 'true' model, and the three models obtained in the data-assimilation experiments.

be applied, pseudo-wells or virtual sensors were used in the model as can be observed in Figure 3.3. The use of virtual sensors to history-match 4D data using the adjoint is explained in more detail in Van Essen et al. (2012).

As can be observed in Figure 3.4.c, the 2D map of the saturation distribution of the updated model is very close to the 'true' 2D map. However, the simulated production data of the

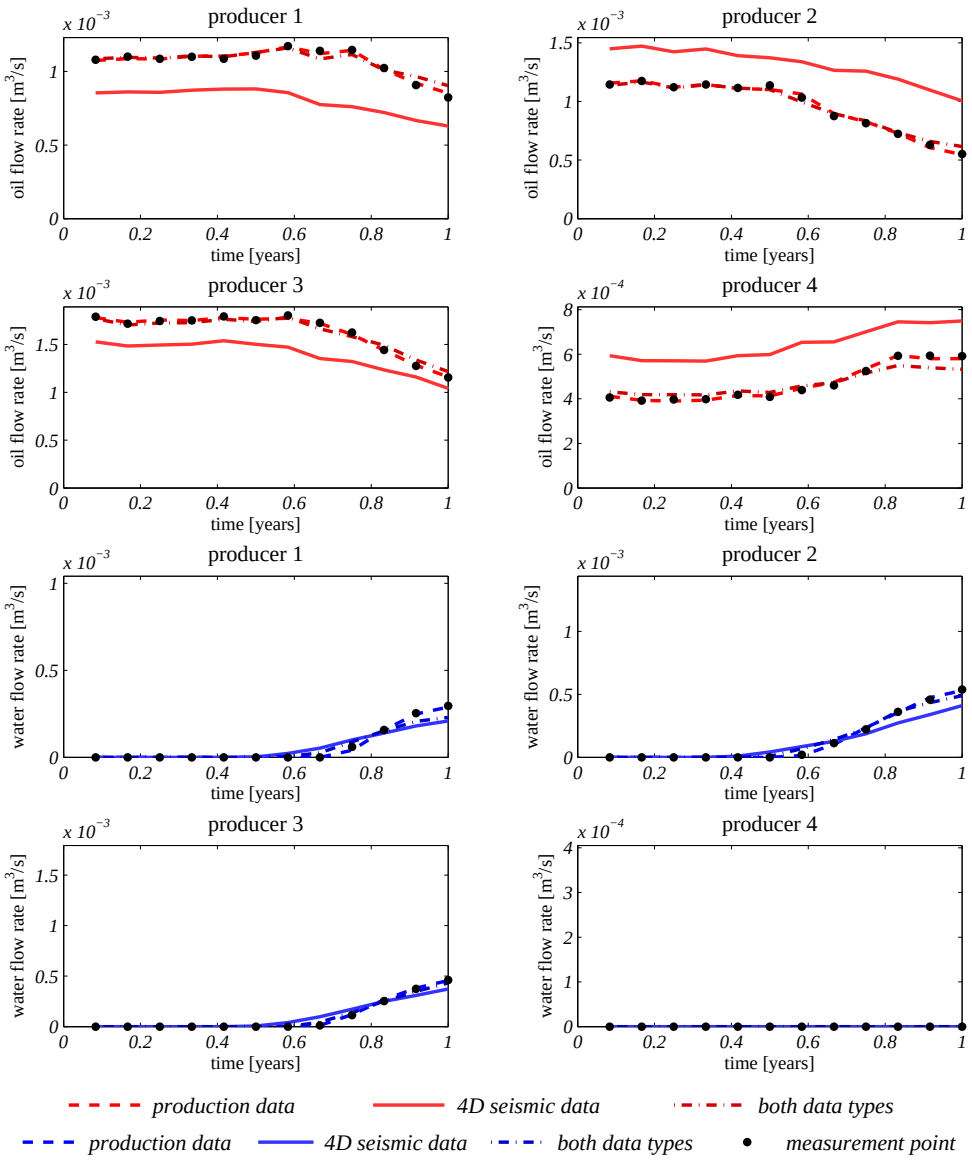

Figure 3.6 : Measured and simulated oil flow rates (red) and water flow rates (blue) of the 4 production wells from the 'true' model, and the three models obtained in the data-assimilation experiments.

updated model is far from the 'true' historic production data, as can be observed in Figure 3.5 and Figure 3.6. The updated permeability field, shown in Figure 3.7.c, shows that relatively small changes of the (homogeneous) prior model are required to realize a proper match of interpreted time-lapse seismic data. It should be noted that these updates are mainly at the location of the high-permeability channels, but further away from the well compared to model

obtained in experiment 1. The updated model obtained in this experiment also shows poorer predictive capacity compared to the model obtained in the first experiment, except for the prediction of the water breakthrough time of production well 4, as can be observed in Figure 3.8.

Experiment 3: Simultaneous history match of production and 4D seismic data

The assimilation procedure in experiment 3 was again initiated from a homogeneous permeability field of 700 mDarcy with an objective function in terms of MSD of both historic production measurements and (interpreted) time-lapse seismic measurements. In order to assign more-or-less the same weight to errors of production data and errors in areal data, a weighting factor was used. It was chosen such that the relative errors of both data types for the prior (homogeneous) model were of the same order of magnitude. The total amount of data points for experiment 3 equaled 2,683.

The comparison with historic production data in Figure 3.5 and Figure 3.6 shows only a slight loss in matching performance compared to the model obtained in experiment 1. Moreover, the match of the 2D map of the 'true' saturations is excellent, as can be observed in Figure 3.4.d. The updated permeability field in Figure 3.7.d shows that when the information contained in the two data sources is combined, the resulting model updates are close to the wells as well as further away from the wells. In the updated model, the main high-permeability geological features of the 'true' field (Figure 3.3.a) can also be recognized. From the models obtained in the three experiments, the last model demonstrates the best predictive capacity as can be observed in Figure 3.8 as well as in Table 3.2, which shows the MSD between the 'true' and simulated production data from 1 year to the end of the field life after 8 years.

Table 3.2 : *MSD between 'true' and predicted production data from year 1 - 8*

Experiment 1: History match of production data only	3.64
Experiment 2: History match of interpreted 4D seismic data only	6.33
Experiment 3: Simultaneous history match of production and 4D seismic data	1.67

The example demonstrates the value of a joint history match of two data sets. Adding additional data, especially data of higher vertical resolution e.g. coming from well logs, may improve the prediction quality of dynamic reservoir models even more. However, history matching of joint data sets of varying scale and nature poses new challenges in the history matching and will require further research to be solved efficiently.

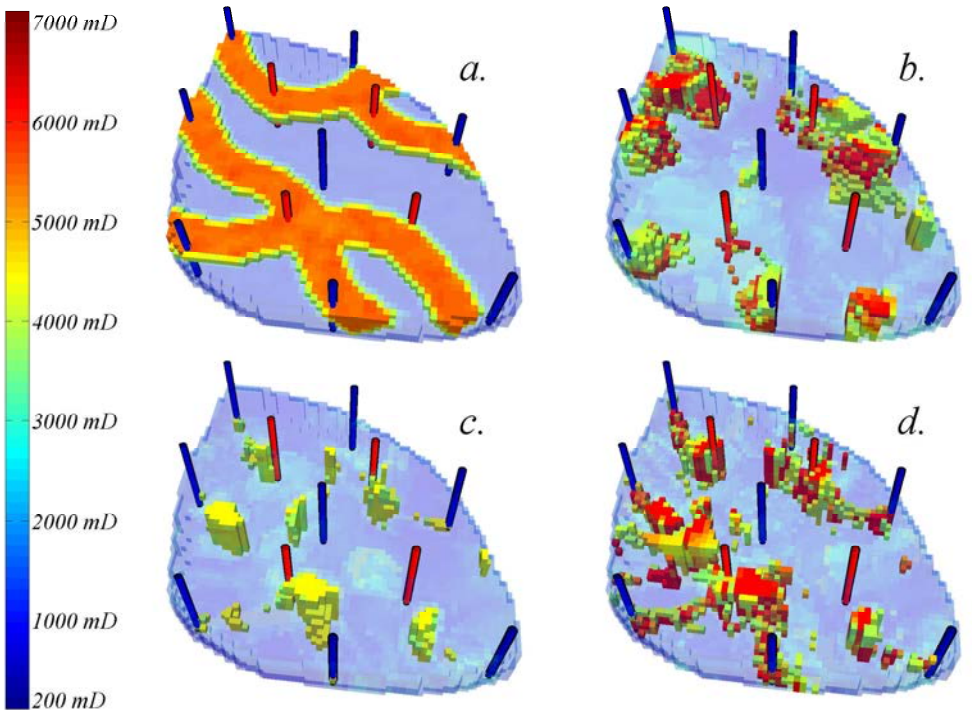

Figure 3.7 : Permeability field of a.) the 'true' (synthetic) field, b.) the model obtained through production data assimilation, c.) the model obtained through 4D seismic data assimilation, and d.) the model obtained through simultaneous production and 4D seismic data assimilation. Grid blocks with a permeability below 3,800 mDarcy have been made transparent.

3.2 Increasing the model update frequency

The production life of a reservoir may cover several decades. During the entire life-cycle, different measurements are gathered, as described in Section 3.1. On average every 3 to 5 years, the need arises to initiate a field re-development plan, which involves - amongst others - the design of a new production strategy. Reasons for such a field re-development may be to increase the production from the field or to mitigate a decline in production, e.g. as a result of a drop in reservoir pressure.

In order to design a field re-development plan, the dynamic reservoir models need to be history matched such that they are consistent with all the measurements gathered from the field, including the newly acquired data since the last model update. Based on the history matched model, the best field re-development plan and associated pro-

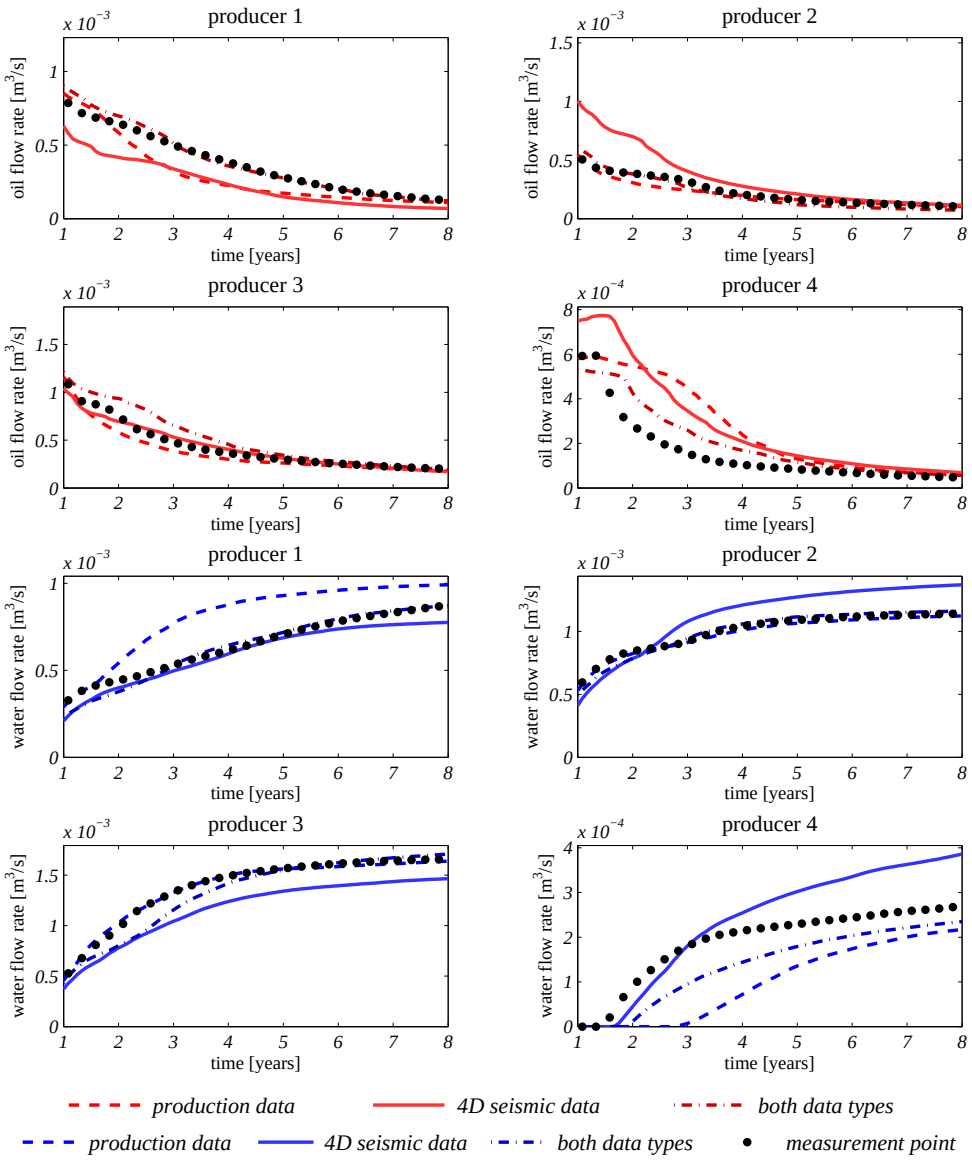

Figure 3.8 : Measured and predicted oil flow rates (red) and water flow rates (blue) of the 4 production wells from 1 year after start production until the end of the field life after 8 years, obtained using the 'true' model, and the three models obtained in the data-assimilation experiments.

duction strategy are chosen and implemented, after which the cycle is repeated after 3 to 5 years.

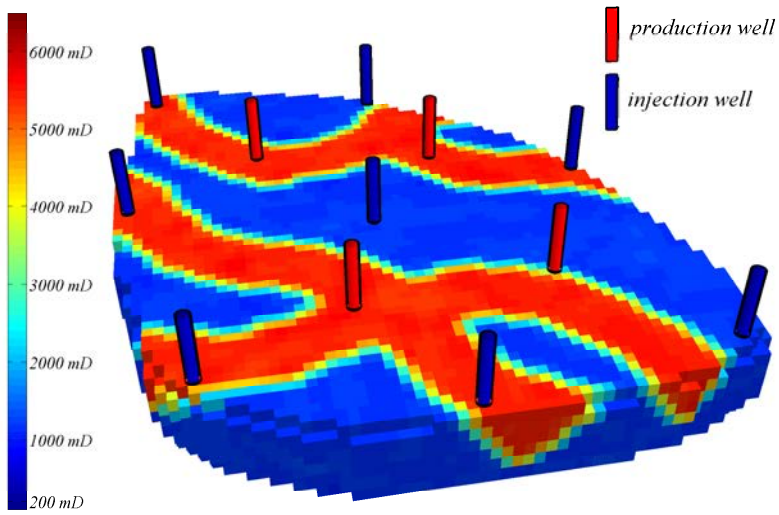

Figure 3.9 : 3-dimensional oil reservoir model with eight injection and four production wells, after Van Essen et al. (2009b).

During the period between field re-developments, the production strategy is executed as designed in the most recent plan. Hence, the control of the reservoir is essentially open-loop over long periods of time over the field's production life. If adjustments are made to the well controls that deviate from the designed production strategy it is generally done to improve (instant) well performance and not the (economic) performance of the entire field over a longer period of time.

The result of this workflow is that information on the subsurface, present in the data, is only used up to years later, at which point it might be too late to take mitigating actions against undesired events, like water breakthroughs. Increasing the frequency at which history matching (model updates) and production strategy design (control updates) are sequentially executed can significantly improve economic performance of a field over its life-cycle. This is demonstrated by the following example.

Example 7. *The objective of this example is to demonstrate that an increase of the frequency at which the consecutive update of the model en production strategy is executed improves the economic life-cycle performance of the field. The uncertainty considered within this example is limited to geological uncertainty only.*

The synthetic field case presented in this example is again based on the 3D reservoir model introduced in Van Essen et al. (2009b) and in fact identical to the 3D model used in Example 6 presented Section 3.1, including its geological and fluid properties. The 3D reservoir model

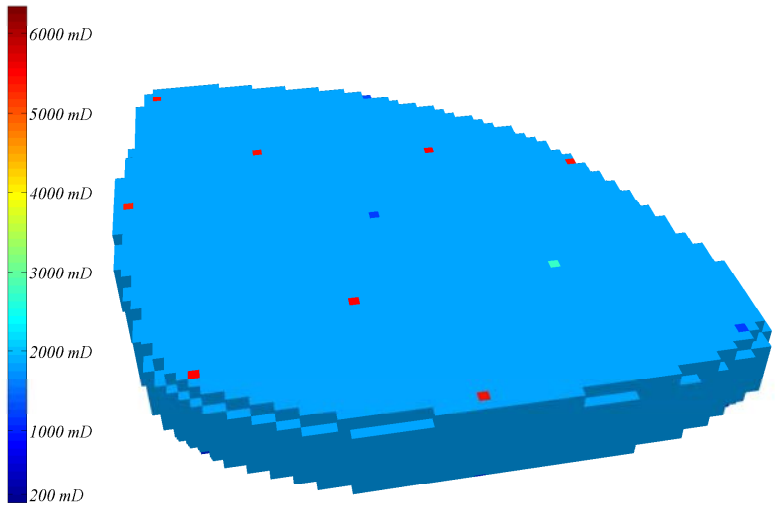

Figure 3.10 : Prior permeability field of the 3D reservoir model before history matching. Homogeneous permeability is assumed of 1000*mDarcy*, except in the grid blocks containing a well where the permeability is assumed to be known.

that serves as the "true" field with unknown permeability can be observed in Figure 3.9. The life-cycle of the field extends over a fixed period of 6 year exactly. The model available for predictions and optimization of the production strategy is identical to the 3D model used for the true field, but with homogenous permeability everywhere of 1000*mDarcy*, *except in the grid blocks that contain a well, where the permeability is assumed to be known. The prior model is displayed in Figure 3.10.*

From each of the 8 injection wells and 4 production wells, the (fractional) flow rates and bottomhole pressures (BHPs) are recorded with an interval of a month. In the history matching process, the injection rates and BHPs of the producers are used as constraints, while the remaining data (BHPs of the injectors and the fractional flow rates of the producers) are used in a mismatch objective function in terms of mean squared difference (MSD). The time horizon over which the history matching is performed increases with (production) time as the loop is repeated several times (growing horizon).

Control of the wells, as prescribed by the (optimized) production strategy, is done by adjusting the water injection rates of the injectors and the BHPs of the producers, which are held constant for periods of a month. The optimal production strategy is determined in tems of Net Present Value (NPV) over the life of the field, which is defined in discrete form as:

$$J = \sum_{k=1}^{k_T} \left[\frac{r_o \cdot q_{o,k} - r_w \cdot q_{w,k}}{(1+b)^{\frac{t_k}{\tau_t}}} \cdot \Delta t_k \right], \tag{3.1}$$

where r_o is the oil price, equal to $283\frac{\$}{m^3}$ and r_w the water production costs, equal to $31.5\frac{\$}{m^3}$, which are both assumed constant. k_T is the time step index relating to life-cycle time T and Δt_k the time interval of time step k. The term b represents the discount rate for a certain reference time τ_t. This term is added to take into account the time value of money. In this example, $b = 0.15$ and $\tau_t = 365.25$ days. Although the production strategy is determined over the life of the field, only the first part will actually be executed. The length of this part is determined by the time period until the next loop. Since, the historical controls are fixed, the time horizon over which needs to be optimized becomes smaller with time (shrinking horizon).

In this example, both the history matching of the data by adjusting the permeabilities, as the optimization of the well controls to maximize NPV were performed using a gradient-based optimization technique. For history matching a trust region methods was adopted, while the optimization of the production strategy was carried put using steepest ascent combined with a line-search algorithm. In both steps, the gradients of the objective function in terms of MSD and NPV respectively were calculated using the Adjoint.

A total of six experiments were conducted, which were evaluated by testing them on the "true" field with unknown permeability distribution and calculating the NPV. The 6 experiments involved:

1. *A **reactive control strategy**. This strategy involves injecting at maximum capacity and shutting in production wells that no longer produce profitably (when the watercut exceeds 0.90).*
2. *An **open-loop control strategy**. With this strategy, the optimal production strategy is determined on the prior model and applied to the "true" field without adjusting it over the life of the reservoir. Hence, the information present in the measurements on the "true" permeability is not used.*
3. *A **closed-loop control strategy** with a loop cycle of **3 years**.*
4. *A **closed-loop control strategy** with a loop cycle of **2 years**.*
5. *A **closed-loop control strategy** with a loop cycle of **1 years**.*
6. *A **closed-loop control strategy** with a loop cycle of **3 months**.*

In order to evaluate the (economic) performance of each experiment, the maximum NPV over the life of the field is determined by optimizing the production strategy on the "true" fields as well, although this can obviously not be done on a real field case.

Figure 3.11 shows a bar plot of the NPV determined on the true field of each of the six experiments as well as the maximum NPV that can be reached through adjusting the control

strategy. The biggest increase in performance can possibly be observed when moving from a reactive control strategy (experiment 1) to an optimized control strategy (experiments 2 through 6). However, the bar plot also shows a clear upward trend in NPV with increasing loop cycle frequency. It is likely that this trend will be even more pronounced with increased well spacing (in this example less than 100m) and/or stronger heterogeneities in between the wells. In Figure 3.12 and 3.13, the cumulative oil and water production of the 6 experiments and upper bound case are displayed. Note that a higher NPV is not necessarily the result of increased production. In this case, associated water production and discount factor play a more significant role.

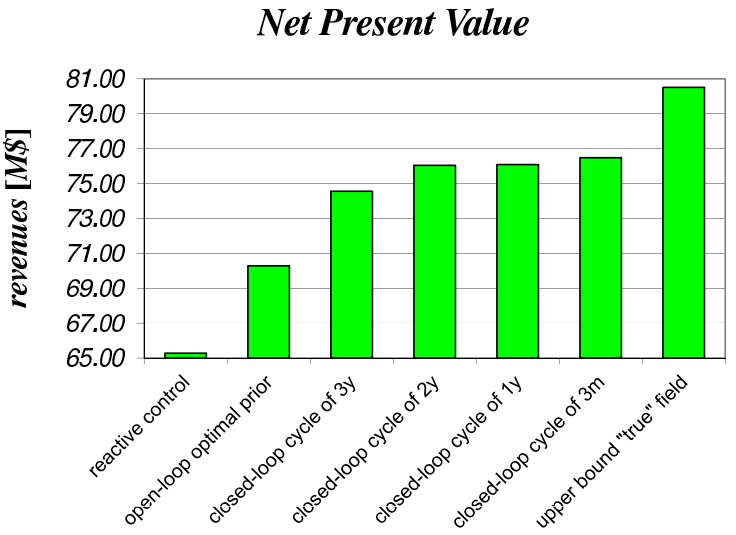

Figure 3.11 : Bar plot of the NPV determined on the ”true” field of each of the six experiments as well as the maximum NPV that can be reached through adjusting the control strategy.

From the example it becomes apparent that increasing the frequency at which dynamic reservoir model and production strategy are sequentially updated leads to improved economic life-cycle performance of the field. Similar results were reported by Jansen et al. (2009) based on the same synthetic reservoir model, but using a different data-assimilation technique and prior model.

In Foss and Jensen (2011) it was concluded that time delays between gathering measurement data and application of an updated production strategy may actually have a detrimental effect on performance compared to an open-loop application as feedback (closed-loop) control may introduce oscillatory behavior. It should be noted however that this conclusion was reached on the basis of single-phase flow and a performance

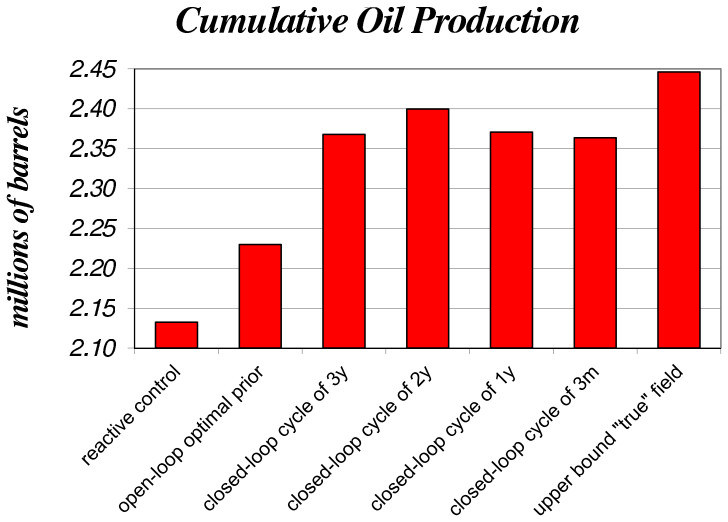

Figure 3.12 : Bar plot of the cumulative oil production of the ”true” field of each of the six experiments as well as the cumulative oil production of the optimal production strategy calculated on the ”true” model.

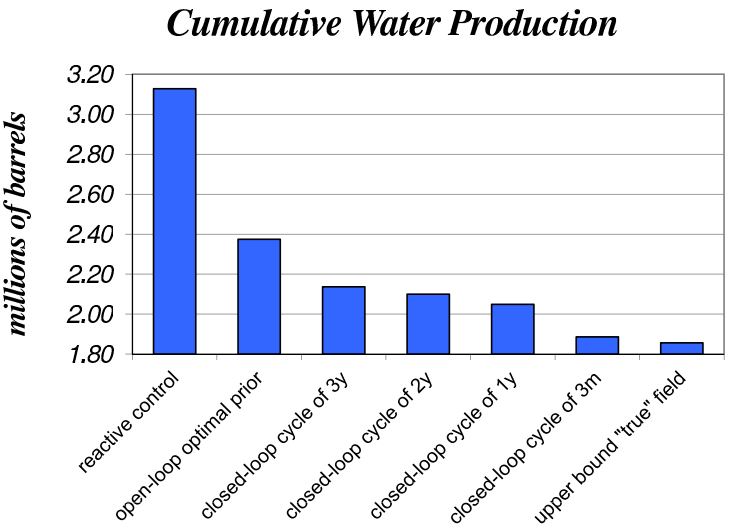

Figure 3.13 : Bar plot of the cumulative oil production of the ”true” field of each of the six experiments as well as the cumulative oil production of the optimal production strategy calculated on the ”true” model.

measure in terms of pressure control. Improved performance in a waterflooding setting are mainly reached through improved sweep efficiency and postponing water

breakthrough. The time constants associated with oil-water front movement are much bigger than those related to pressure behavior in the reservoir and hence a delay in such a closed-loop setup will likely not cause performance deterioration. However, more research into this subject is required.

Shortening the cycle times can partly be realized by computer-assisted methods that solve the history-matching and optimization problem faster and more efficiently. However, the technical issues are generally only a small part of the problem. In many oil companies, the major bottlenecks are caused by holdups in the applied workflows or decision-making processes. Hence, the biggest speedup in closed-loop reservoir management can be probably realized by streamlining these organizational processes, making them more efficient.

3.3 Conclusion

In this chapter, two components of using measurement data to reduce uncertainty in dynamic reservoir models and improve economic life-cycle performance of a field were discussed: the simultaneous history matching of multiple data (type) sets and the frequency at which reservoir model and production strategy are sequentially updated. These subjects are inherent to the history matching and closed-loop reservoir management problem, and not a consequence of the selected method to solve these problems. Although a combination of different data sets can reduce uncertainty considerably, more research is needed into how to do this efficiently and in such a way that all information present in the data is optimally used. Similarly in the case of increasing the update frequency, more research is required into how to determine an appropriate (minimal) frequency.

Chapter 4

Conclusion & Recommendations

In Chapter 1, the following research question was raised: Can the performance of model-based life-cycle optimization of oil and gas production in realistic circumstances be improved by addressing uncertainty in the optimization problem? In this thesis, four different methods were presented that address this research question. The first three methods, hierarchical optimization, robust optimization and multilevel control and optimization, are aimed at improving the robustness of a fixed operational (life-cycle) strategy when applied to the field. Of the fourth method, closed-loop reservoir management, two aspects were addressed in a more exploratory setting: the frequency of subsequent history matching and re-optimization and the combination of different data types in history matching.

4.1 Conclusions

Based on the presented methods and examples, the following conclusions can be drawn:

- Under the considered uncertainty, robust optimization, hierarchical optimization, multilevel optimization and control, and closed-loop reservoir management with increasing update frequency demonstrated better economic life-cycle performance compared to open-loop application of an optimized operational strategy based on a single realization and objective. Improved life-cycle performance through the use of multiple sources of data was demonstrated implicitly by showing improved prediction accuracy.
- The hierarchical optimization procedure provides a method to incorporate a robustness objective into the problem setting of maximizing economic life-cycle performance. In this structure, it is possibly to specify explicitly how much

economic performance a decision-maker is willing to sacrifice to improve the robustness of an operational strategy. Due to the ill-posedness of the life-cycle optimization problem, redundant DOFs in the input strategy with respect to the optimality of an economic life-cycle objective exist. This implies the existence of an optimal subset $\mathscr{S}$ of connected optimal solutions within the solution space $\mathscr{U}$. Using the redundant DOFs, a significant improvement of the secondary objective can be obtained without significantly compromising the primary objective in the hierarchical optimization structure, as was demonstrated by a numerical example. This suggests that $\mathscr{S}$ occupies a considerable space within decision variable space $\mathscr{U}$. The theoretically rigorous method to determine the redundant DOFs is computationally too demanding for application to realistically sized problems. However, nearly identical results can be obtained with the aid of a somewhat more pragmatic, but computationally much more efficient, switching method.

- Life-cycle performance of a operational strategy depends heavily on the particular realization of the uncertain parameters that is selected to perform the optimization on. In robust optimization, the life-cycle objective function is expressed in probabilistic terms (mean and variance), using an ensemble of realizations that serves as a representation of the uncertainty. In the example presented in this paper, the mean NPV from a set of geological realizations was used as robust objective. In the example, the robust optimization strategy was able to improve the mean NPV significantly compared a reactive strategy and a single-realization optimal strategy, regardless of which realization of the ensemble was selected.

- Robustness of an operational strategy can be improved by selecting a reservoir model output that can serve as a reference trajectory during implementation. It is required that in the field this output is both measurable and controllable on-the-fly. If so, any deviations of the reference trajectory in the operational phase due to uncertainty or disturbances can be attenuated through tracking control. In this approach, economic life-cycle performance can be addressed by selecting an output of the *optimized* dynamic model as reference trajectory, resulting in an integrated or multilevel approach of dynamic optimization and feedback control. In the presented example, tracking control was capable of quickly rejecting the disturbances resulting from small model errors in the form of neglected near-wellbore effects and a slightly erroneous channel orientation, resulting in a life-cycle production response that closely resembles the model-optimal results. In the example, System Identification proved to be an attractive method to create a linear data-driven reservoir model for tracking control.

- In the industry, on average every 3 to 5 years, the need arises to initiate a field re-development plan, which involves - amongst others - updating or rebuild-

ing the dynamic reservoir model and the design of a new production strategy. Closed-loop reservoir management aims to perform history-matching and optimization of the production strategy in a structural, continuous and computer-assisted way. One of the advantages of that approach is that the frequency at which these subsequent processes are executed can be increased. An example demonstrated that by increasing the frequency an increase in economic life-cycle performance can be realized in the field.

- During the production life of a reservoir, different measurements are taken to monitor the depletion process. These different measurements are generally conducted at a different areal, vertical or temporal resolution. The fact that every data type has low resolution in at least one of these three dimensions, provides much freedom (and hence remaining uncertainty) in history matching. By combining different sources of data, the solution of the history matching process can be constrained to (at least partly) honor reality on all scales. In effect this should lead to improved models, which give more accurate predictions. This simultaneous history matching of multiple types of data was demonstrated in an example where both production and (interpreted) 4D seismic data were available. Through the use of pseudo-wells, the computationally efficient adjoint method could be applied to both types of data. The history matched model of the combined data sets showed considerably better prediction accuracy, compared to history matched models using a single data set. Although not explicitly tested, the assumption is that this better prediction accuracy would also lead to better economic life-cycle performance after re-optimization of the operational strategy.

4.1.1 Discussion

- The redundant DOFs that can be used in hierarchical optimization, describe a connected space of optimal operational strategies with respect to an economic life-cycle objective. However, ill-posedness of the optimization problem does not imply that all optimal solutions are connected. Hence the operational strategy that provides the best possible performance to a secondary objective within the connected solution space may not necessarily be the true optimal solution to the hierarchical optimization problem.

- It should be stressed that the conclusion of improved performance of the robust optimization strategy compared to that of the single-realization and reactive strategy holds only if the used set of geological realizations is a good representation of the true modeling uncertainty. If not, it is impossible to say which of the considered strategies will perform better.

- In the robust optimization example, only the expected value in terms of NPV was used as a robust objective. Although the resulting strategy demonstrated smaller variance and hence more robustness when applied to all realizations in the ensemble, this may not always true. To that end, a robust objective function that has a (weighted) mean and a variance part more explicitly addresses the goal of robust optimization.
- In multilevel optimization and control, suppressing deviations from a model-optimal reference trajectory, while these deviations are a clear indication of an incorrect model seems paradoxical. It only makes sense if optimal solutions for a range of uncertainties have some 'universal' characteristics which are more-or-less invariant under the regarded uncertainties. From the presented example and experience in the process industry that seems to be true for small uncertainties and disturbances. But quantifying what constitutes to 'small' is a difficult matter. More research is required to understand what characteristics make an operational strategy optimal.
- In all the presented examples, gradient-based optimization was used to solve the optimization problem, using the computationally efficient adjoint method to calculate the gradients. Also gradients have been used to prove some of the aspects of the methods. However, the availability of gradients is not essential for applying the methods. Increased robustness through the use of a robust objective function or reference trajectory, the exploitation of redundant DOFs for multiple objectives and the improvement in economic performance due an increase of the model update frequency and data sources are properties of the life-cycle optimization problem itself and not of the used optimization method. Hence, similar results could be obtained with ensemble-based or derivative-free methods.

4.2 Recommendations

Although the methods presented in this thesis resolve some of the issues of improving the operational applicability of model-based optimization of oil recovery, the research in this area is far from finished. The following recommendations for future research are given.

- The presented methods to improve the performance of an optimized operational strategy under uncertainty were addressed and assessed separately. However, they do not exclude one another and any possible combination is feasible. In principle they could be combined into a single workflow, where multiple robust (ensemble-based) objective functions are solved through hierarchical optimization from which a reference (output) trajectory is derived that is tracked

in the field until enough measurement data is gathered to update the ensemble of reservoir models and re-optimize the operational strategy. It would be interesting to see if, and if so, how much economic life-cycle performance can be gained from such an integrated approach.

- The reservoir model used in the examples presented in this thesis has a 3-dimensional, asymmetric structure and is of considerable size, but is nonetheless completely synthetic. On top of that, only one type of uncertainty is considered at the same time and the well configuration is assumed to be fixed over the life of the field. To confirm with more certainty that the presented methods are indeed capable of improving economic life-cycle performance in realistic circumstances, additional experiments are required on more realistic models with combined uncertainties, where (infill) drilling of new wells is explicitly part of the to-be-optimized production strategy.

- In the examples presented in this thesis, the optimized operational strategies were applied as is. No analysis was performed on an operational strategy to try to understand why such a strategy would perform better than a reactive strategy. Understanding of the optimized strategy may prove to be essential in dealing with uncertainty in the field. It may lead to the identification of some general characteristics of the operational strategy, which - when observed in the field - can serve as sign to take operational action.

- All the examples presented in this thesis revolve around optimization of a waterflood. A waterflooding strategy does involve a large number of decision variables and can certainly be significantly optimized, but the scope for optimization is generally much larger for tertiary depletion processes. Enhanced oil recovery (EOR) methods such as polymer injection, steam injection, the use of foam or surfactants have much higher (variable) costs associated with them and may therefore benefit much more from an optimized operational strategy.

- In Example 2 in Chapter 1, hierarchical optimization was used to determine a history matched model (primary objective) that gives the best or worst *forecasted* life-cycle performance (secondary objective), given a predefined reactive strategy. The difference between the upper and lower bounds can be used as a measure of value of information (VoI). The same workflow can be applied when faced with different sets or types of data, where the range of forecasts - captured by the lower and upper bounds - serves as a measure to evaluate their (relative) added value.

- In the example used to demonstrate multilevel optimization and control, System Identification (SysID) was used to derive a data-driven, linear model of the reservoir. SysID is not an essential part of the multilevel optimization and control framework and other methods can be used to create a lower-order model

for short-term reservoir behavior. However, the short-term predictions of the SysID model turned out to be relatively accurate. It is worth investigating the use of SysID techniques in more detail to provide short-term simplified reservoir models to be applied in e.g. well and reservoir management decision-making.

Appendix A

Optimization Of Smart Wells in the St. Joseph Field

This appendix has been published before as "Van Essen, G.M., Jansen, J.D., Brouwer, D.R, Douma, S.G., Zandvliet, M.J., Rollett, K.I., and Harris, D. (2010a). Optimization of smart wells in the St. Joseph field. *SPE Reservoir Evaluation & Engineering*, 13(4), 588595. doi:10.2118/123563-PA".

A.1 Introduction

St. Joseph is a mature oil field located 135km offshore Sabah, Malaysia. The stock tank oil initially in place (STOIIP) is estimated at 630 MMstb, of which 83% is located in the main reservoir package in the Northwest Flank. These reservoir units dip at an angle of approximately 20 degrees to the NW and have a strongly layered internal architecture, with only limited (vertical) communication between layers. Sand porosities and permeabilities are high in the oil column, generally deteriorating down flank into an aquifer, which has a weak direct influx into the main reservoir, see Walsh et al. (1996). The St. Joseph field has been on production since 1981. Until 1996 the recovery mechanism was natural depletion under gravity drainage. At the end of 1995, the field had produced 105 MMstb out of the total ultimate recovery estimated at 230 MMstb. Average pressure had fallen from 7.3 MPa to 4.1 MPa. Since May 1996, production has been supported by crestal gas injection. Gas is injected into the reservoir for two reasons: disposal of produced gas from St. Joseph and neighboring fields and reservoir pressure maintenance.

A feasibility study completed in the second quarter of 2006 concluded that water in-

jection was not only feasible, but also required to safeguard developed reserves and to realize additional oil recovery from the field. A large redevelopment project is planned to facilitate water flooding. The total scope of the project includes the installation of a new platform for offshore living quarters, seawater treatment and injection facilities, and the drilling of six horizontal water injectors and five infill producer wells. The horizontal water injectors require a high degree of zonal control, because of the laminated nature of the reservoir and historical problems with controlling water and gas breakthrough in high permeability streaks. The selected concept for the water injection wells is a horizontal well injecting under fracturing conditions, completed with multiple zones. It is intended that injection will be into two zones simultaneously, alternating between zones several times a year. This concept is not feasible without the use of smart technology: each zone will be fitted with an inflow control valve (ICV) and dual downhole pressure gauges to allow remote control. At the time this study was conducted the number of zones was assumed to be limited to four as a result of physical and financial constraints. Currently however, the injection wells are planned to be equipped a five-zone smart completion.

There are significant benefits associated with a smart well completion over multiple zones. The increased control capability allows the potential optimization of the flooding process, thus maximizing total oil recovery. The main objective of this waterflood optimization study is to determine the value of down-hole control in the planned water injectors, in terms of incremental cumulative oil production. The maximum incremental oil production using downhole control is determined by finding the:

- Optimum configuration of perforation zones, where the injection rate into each zone is controlled by one ICV. Optimum operation of the ICVs over the producing life of the reservoir by dynamically changing the valve settings.
- The value of these parameters can vary within a specified range, defined by a number of financial, operational and physical constraints.

A.2 The St. Joseph sector model

In this optimization study, to determine the value of a four-zone smart completion of the planned horizontal injectors, a 3D finite-difference model of the St. Joseph field was used. As mentioned in the introduction, the St. Joseph field is a strongly layered reservoir, with only limited (vertical) communication. To adequately capture the layered structure in the reservoir model, a very high resolution grid in the z-direction is required compared to the x- and y-direction. As a result, the full-field model (FFM) consists of 28x117x711 = 2,329,236 grid blocks (GBs). A single forward reservoir simulation of the St. Joseph full-field model (FFM) takes approximately 24 hours.

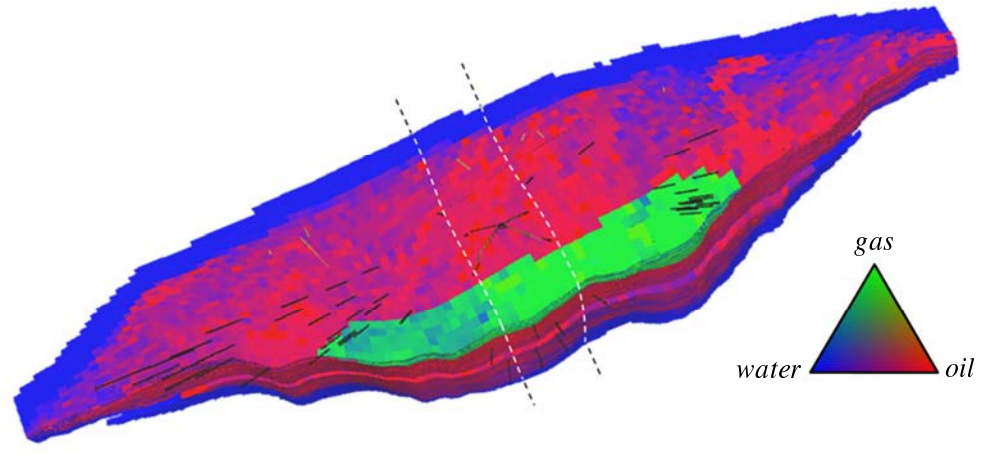

Figure A.1 : Full Field Model showing saturations at start production in 1981. The location and size of the sector model are shown between dashed lines.

Within this study this was deemed impractically long and therefore a computationally less demanding yet representative sector model of the St. Joseph field was used. This chapter deals with the main characteristics, assumptions and simplifications of the sector model.

From the FFM a representative sector of size 28x9x711 GBs was selected from the middle of the reservoir, as indicated in Figure A.2. This sector model was up-scaled in the z-direction using an in-house upscaling package to a size of 28x9x140 = 35.280 GBs with 21.909 GBs remaining active. The sector model is approximately 1600m x 500m x 450m with a dip of approximately 20 degrees. There is assumed to be no flow across the boundaries of the sector model. Aquifer support in this part of the reservoir is believed to be limited and is omitted in the sector model. Vertical communication between the layers is very limited. Below a threshold of 1 mD, connectivity is assumed to be zero and zero-transmissibility boundary in the z-direction is applied. Several grid blocks have vertical communication around this threshold, resulting in somewhat 'erratic' zero-transmissibilities.

A.2.1 Wells

The sector model, depicted in Figure A.2, contains 12 production wells of which five have a dual completion. The production wells are simulated under tubing-head pressure (THP) constraints. The flow rate of the production wells is the result of the difference between the reservoir pressure and the tubing head pressure, where the

pressure drop in the well is captured by individually assigned lift curves. The lift curves begin at a minimum flow rate of 40 bbl/d, below which the production rate is assumed to be no longer economically viable. When the pressure difference is no longer sufficient to realize a flow rate above 40 bbl/d, the well is shut-in. Within the sector model there are five production wells (one of these has dual completion) with completions perforated entirely inside the sector model. These are assumed to only produce from this sector of the field and are referred to as 'real' wells. There are an additional seven wells (including four with dual completions) that have completions either partly or entirely outside the sector model, but still contributing considerably to the total production from the sector. Because the total off-take of these wells is partly from the sector under consideration and partly from the neighboring sectors, they are referred to as 'dummy' wells. The dummy wells differ from the real wells in two respects:

1. Some of the dummy wells are not, or only just, perforated in the sector model. It is however assumed, that a large portion of their total off-take comes from the sector. For these wells the location has been altered somewhat such that the 'connection' to the reservoir improves.

2. The fraction of the total off-take of each dummy well that comes from the sector is unknown. Therefore, the so-called well fractions for each of the dummy wells were used as history matching parameters to achieve the desired sector-average pressure and gas-oil ratio (GOR) profiles and individual well bottom-hole pressure (BHP) and GOR's. Note that irrespective of the value of the well fractions, the drawdowns and constraints were correctly calculated for each well as if it were a 'full' well, and only the actual volumes produced (or injected) were scaled.

There is one gas injection well located in the sector model, which is perforated in the gas cap. The well is operated under a THP-constraint and the gas flow rate is calculated using a 'lift curve' accounting for the pressure drop.

The planned water injector is a horizontal well that injects (treated) seawater at a fixed flow rate of 10,000 bbl/d. Its horizontal section is located below the initial oil-water contact. The pressure drop in the well is implemented using a 'pressure drop' table. The completion is perforated over the entire horizontal section, which runs through all layers of the major sands, as can be observed in Figure A.3. The perforation is initially divided into four perforation zones, which correspond to the predefined geological zones indicated by the B through E reservoir units. The E reservoir is located at the heel of the horizontal injector and the B reservoir at the toe. Injection into the A reservoir was not considered feasible due to the pressure drop over the horizontal section. The number and length of the perforation zones are not fixed, but were regarded as variables within this optimization study.

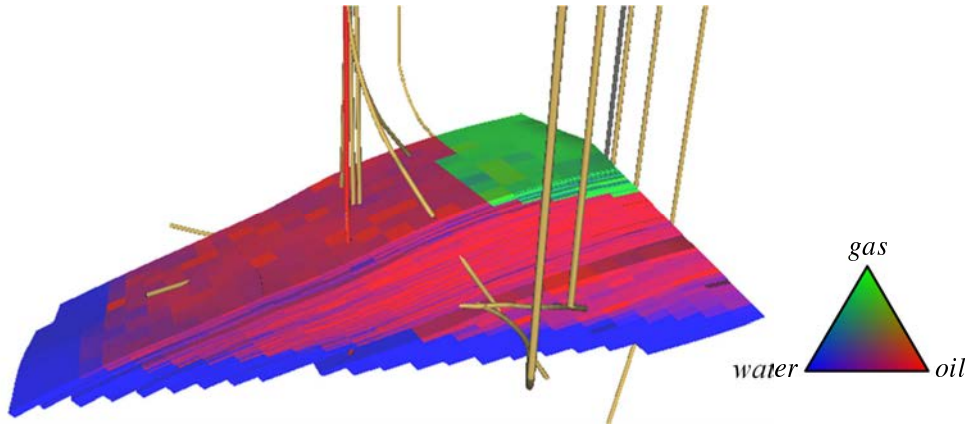

Figure A.2 : Sector model of the St. Joseph Field, showing 12 production wells (yellow), 1 water injection well (red) and 1 gas injection well (grey).

The injection of water into the stacked reservoir layers is believed to induce fracturing. However, within this study matrix injection is assumed instead of fracture injection. Modeling fracture injection using a (dynamic) fracture model coupled to the reservoir model was considered, but was not considered feasible due to:

1. The limited time frame to complete the case study. The limited experience with fracture models and the lack of good validation methods. The inability of the adjoint-based optimization to handle the coupled system.

2. Note however that optimization of a coupled dynamic fracture and reservoir model is possible, as shown by Van den Hoek et al. (2009). Static modeling of fractures, e.g. through negative skin factors, was considered as well. However, the implementation of a static fracture model was assumed to have little impact on the results, as the total injection rate of the injection wells is fixed and the ICVs only act as ”splitters” of the rate over the zones, and was therefore not pursued.

3. Although fracturing is not modeled in the sector model, it was accounted for by introducing an additional constraint on the injection policy, as described in the next section.

A.2.2 Well Inflow Control

In the model, the horizontal section of the water injector passes through 102 grid blocks resulting in 102 perforation intervals in the reservoir model. A variable permeability-

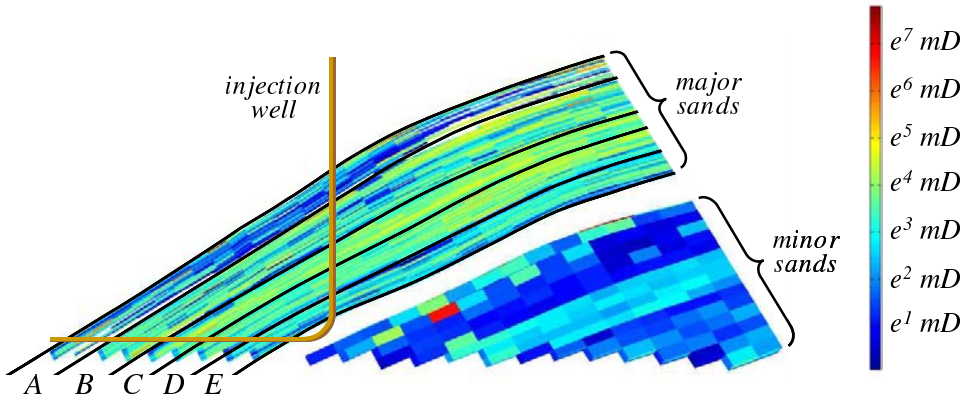

Figure A.3 : Cross section of the St. Joseph sector model permeability field, showing the horizontal injection well and the minor and major sands, with its five identified geological layers A, B, C, D and E.

height product (KDH) multiplier is assigned to each perforation interval. These variable KDH-multipliers are used to simulate the use (and control) of ICVs, with a value of zero relating to a fully closed valve and one to a fully open valve. This approach leads to a numerical upper bound for the number of ICVs and perforation zones of 102. The number of ICVs is in reality limited to four as a result of physical and financial constraints. A reduction from 102 ICVs to four can be modeled by lumping neighboring perforation intervals and assigning the same KDH-multiplier value to each interval in the zone. The number and size of the perforation zones can be changed by lumping differently.

A.3 Optimization Procedure

The St. Joseph field is operated under a Production Sharing Contract (PSC), which ends on the first of January 2020. The value of smart completions in the horizontal injection wells is in the incremental oil production that can be realized before the end of the PSC over and above what would be realized with only 'dumb' water injectors. Therefore, within this study ultimate recovery was selected as quantitative objective function. The production period under consideration extends from the initially planned date for start of production (first of October 2009) until the last day of the PSC (31st of December 2019). The optimization parameters are the 102 KDH-multipliers in the horizontal section of the water injector. The time steps of the reservoir simulator are equal to 0.2 years and as a result, the values of the KDH-multipliers can be changed with the same frequency. Since there are 51 time steps of 0.2 years between first of October 2009 and first of January 2020, the control input consists

of 51x102=5202 parameters. The goal of the waterflooding optimization problem is therefore to find the 5202 KDH-multipliers that maximize ultimate oil recovery. Due to practical and physical limitations, however, there are several constraints on the control, which have to be taken into account during the optimization procedure.

A.3.1 Constraints on the control

- *Lower and upper bound constraints*: All KDH-multipliers must stay between zero and one, since each KDH-multiplier represents the value of a downhole control valve. These valves can only vary between fully closed (zero) and fully open (one).
- *Equality constraints*: As mentioned in the previous section, the KDH-multipliers may be lumped together to simulate the operation of a single ICV for the entire zone. The 102 KDH-multipliers must therefore be lumped into four zones, as only four downhole control valves were assumed realistic. This means that the values of all KDH-multipliers within a particular zone must be equal.
- *Zonation constraints*: The four perforated zones of the injection well initially corresponded to the geological zones B through E, as depicted in Figure A.3. These initial perforation zones are referred to as p_1, p_2, p_3 and p_4. However, as mentioned in the introduction the location and length of each of the perforated zones were also part of the optimization problem. Still, the total perforation interval was limited to the heel of the horizontal section until the transition from zone A to B, i.e. perforation into zone A was discarded.
- *Switching constraints*: Although fractured water injection is planned and facilities have been designed with pressure capability based on a mini-frac conducted in 2006, matrix injection only has been assumed for this study. Under dynamic fracturing conditions, controlling injection into two zones simultaneously is assumed to be the upper limit due to the complexities associated with controlling both injection pressure and rate with the ICV's. Thus, within this study it was decided that at any particular time, two out of the four control valves had to be closed. Injection into all four zones thus required an alternating or switching control input.

A.4 Optimization Workflow

In order to determine the maximum incremental production as a result of a smart completions, the study was conducted in four stages. These relate to the increase in the number of constraints that were taken into account.

Stage 1

The first stage was aimed at finding the optimal values of all the 102 KDH-multipliers over time. In this 'ultimately smart' well case the only constraints on the control are the lower and upper bounds constraints, and its main purpose was to investigate the overall scope for optimization. If ultimate oil recovery cannot be increased using 102 control valves, it is unlikely that it can be increased using only four control valves. A gradient-based optimization procedure to determine the optimal values of the KDH-multipliers was used through the implementation of the adjoint functionality in the proprietary reservoir simulator used for this study, see Kraaijevanger et al. (2007). The adjoint allows a user to compute gradients of an objective function J with respect to the vector of control parameters $\mathbf{u}$ with a single run of the system equations and the adjoint equations. The use of the adjoint for control optimization in oil recovery was first described in Ramirez (1987) for the optimization of tertiary recovery. Subsequently, waterflooding optimization was addressed by Asheim (1988), followed by, among others, Virnovski (1991), Zakirov et al. (1996) and Sudaryanto and Yortsos (2000, 2001). Recently the method has been revived in the work of Brouwer and Jansen (2004) and Sarma et al. (2005) due to the computational burden no longer being such an obstacle. A vast number of gradient-based techniques exist. However, for reasons of simplicity and experience a Steepest Ascent (SA) algorithm was used, to optimize the control vector $\mathbf{u}$, which in this case study involved the 102 KDH-multipliers at each of the 51 time steps:

$$\mathbf{u}_{i+1} = \mathbf{u}_i + \tau \left(\frac{dJ}{d\mathbf{u}} \right)_i^T, \quad i = 1, \ldots, N \tag{A.1}$$

where i is an iteration counter, $\left(\frac{\partial J}{\partial \mathbf{u}} \right)^T$ is the gradient of the objective function J with respect to control vector $\mathbf{u}$, N is the number of iterations required to converge to the optimal KDH-multiplier values, and the step size τ is variable and determined using a line search.

Stage 2

In the second stage, the results of the first stage are used to identify the four optimal perforation zones. This is done through a visual inspection of the changes in the 102 KDH-multipliers over time. By grouping those KDH-multipliers that show similar dynamic behavior, the number of perforated zones and ICVs can be reduced. The number of zones that were identified was in this case equal to four. This well design concept using the optimal operation of an 'ultimately smart' well was first introduced

in Brouwer and Jansen (2004). The four 'optimal' perforation zones are referred to as p_1^*, p_2^*, p_3^* and p_4^*.

Stage 3

In the third stage, the KDH-values are lumped together according to the defined optimal perforation zones such that they have the same value and act as if only one ICV is active for that zone. The lumped KDH-values are again optimized using the gradient-based optimization procedure used in the first stage. The gradients of the objective function J with respect to the KDH-value of the entire perforation zone are defined as the cumulative gradient over all perforation intervals belonging to that zone:

$$\left(\frac{dJ}{d\mathbf{u}_p}\right)^T = \mathbf{W}\left(\frac{dJ}{d\mathbf{u}}\right)^T \tag{A.2}$$

where $\mathbf{u}_p$ is the control vector for the four perforations intervals in each of the 51 time steps and hence has dimensions 204×1. $\mathbf{W}$ is a sparse 204×5202 selection matrix that has ones at the elements corresponding to the relevant perforations and zeros elsewhere. Subsequently, all 102 KDH-values are updated in the following altered iterative SA scheme until convergence is reached:

$$\mathbf{u}_{p,i+1} = \mathbf{u}_{p,i} + \tau\left(\frac{dJ}{d\mathbf{u}_p}\right)_i^T, \quad i = 1,\ldots,N \tag{A.3}$$

Stage 4

In the fourth and final stage, all constraints were taken into account, including the switching constraints. To reduce the complexity of the optimization problem with switching, the choice was made to only allow simultaneous injection into either perforation zones 1 & 3, or perforation zones 2 & 4. Within this structure however, the ratio between the volumes injected into zones 1 & 3 (or 2 & 4) is still variable and was optimized using the (lumped) KDH-value for each zone. Two different switching strategies were considered:

1. Switching occurs after every time step. In other words, from one time step to the next, water injection is shifted from perforation zones 1 & 3 to 2 & 4 or vice versa. A total of 50 switches are defined in this case, equal to the number of time steps minus 1.

2. Switching is chosen such that the ratio between the total injection rate into zones 1 & 3 and zones 2 & 4 is matched against that same ratio determined

using the 'ultimately smart' well in stage 1. It is assumed that the injection ratio between zones 1 & 3 and 2 & 4 in the 'ultimately smart' well case is most favorable and is therefore imitated using the switching strategy. In the results section, the idea behind this second switching strategy becomes more apparent.

From these two switching strategies only the latter was investigated in this study.

A.5 Results

Six different cases were considered relating to the four different stages of the optimization procedure:

1. No control. The no control case serves as base case and can be regarded as if using an ordinary completion instead of a smart completion.
2. Full 102 control. Serves as an reference case for the overall scope for optimization
3. Initial four-zone control. In this case the 102 KDH-multipliers are grouped according to the four predefined geological zones in the sector model and are labeled p_1, p_2, p_3 and p_4.
4. Alternative four-zone control. In this case the 102 KDH-multipliers are grouped according to the optimal KDH-multipliers derived with Full 102 control, and are labeled p_1^*, p_2^*, p_3^*, p_4^*.
5. Initial four-zone switching control. In this case the 102 KDH-multipliers are grouped as in Standard four-zone control, but water injection must alter between zones p_1 & p_3 and p_2 & p_4, using the second switching strategy.
6. Alternative four-zone switching control. In this case the 102 KDH-multipliers are grouped as in Alternative four-zone control, but water injection must alter between zones p_1^* & p_3^* and p_2^* & p_4^*.

Table A.1 summarizes the waterflooding optimization results for the St. Joseph sector model for each of the six cases described above.

No control (base case)

Figure A.4 shows the injection rates for zones p_1, p_2, p_3 and p_4, as well as the cumulative oil and water production. Note that almost half of the 10.000 stb/day of water is injected into zone p_2. This is not proportional to the pressure profile in the

Table A.1 : *Cumulative oil production for different cases*

Case	*Cumulative oil [MMstb]*	*Increase [%]*
No control (base case)	11.47	-
Optimized water injection		
Full 102 control	12.82	11.7
Standard four-zone control	12.40	8.1
Alternative four-zone control	12.62	10.0
Standard four-zone switching control	12.65	10.3
Alternative four-zone switching control	12.38	7.9

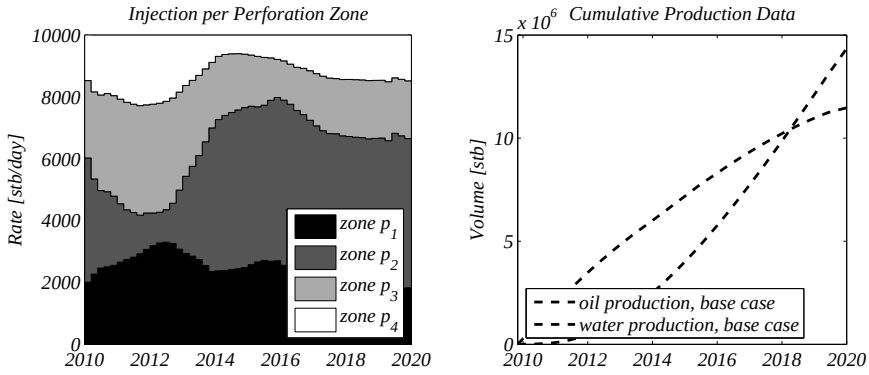

Figure A.4 : Base case results. Left: injection profile. Right: cumulative production.

well (the heel of the horizontal injector is in zone p_4, while the toe is in zone p_1), but can be explained by the higher permeability in geological layer p_2.

Full 102 control

Figure A.5 shows the injection rates for zones p_1, p_2, p_3 and p_4, and the cumulative oil and water production. Note that, compared to the base case, a lot of water is redirected from zone p_2 into other zones during the first few years, and that the injection profile varies significantly over time. The result is an 11.7% increase in cumulative oil production. The number of control valves in this study was limited to four instead of 102. Since there is no reason to assume that the 'standard' grouping according to predefined geological layers will yield the best results, an alternative grouping was investigated. Figure A.6 shows the optimal control (time-varying KDH-multipliers),

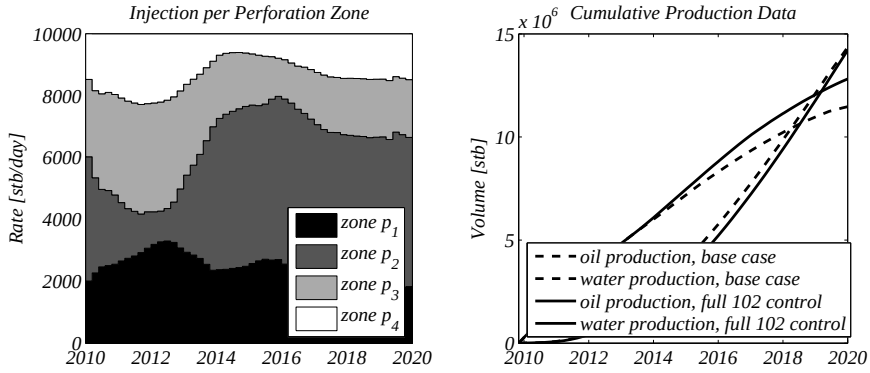

Figure A.5 : Full 102 control results. Left: injection profile. Right: cumulative production.

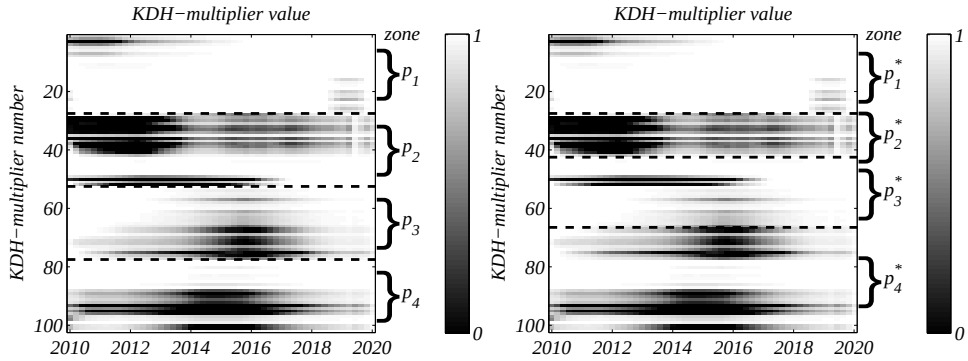

Figure A.6 : Optimal time-varying KDH-multipliers for full 102 control (black = fully closed; white = fully open). Left: standard grouping according to predefined geological layers (p_1, p_2, p_3, p_4) of the sector model. Right: alternative grouping (p_1^*, p_2^*, p_3^*, p_4^*).

upon which are superimposed the standard (p_1, p_2, p_3 and p_4) and alternative grouping (p_1^*, p_2^*, p_3^* and p_4^*) of KDH-multipliers used in the following sections.

Standard four-zone control

Figure A.7 shows the optimal time-varying KDH-multipliers, the injection rates for zones p_1, p_2, p_3 and p_4, and the cumulative oil and water production. Note that, as with the optimal full 102 control, a lot of water is redirected from zone p_2 into other zones during the first few years. Unfortunately, this results in only 8.l% (compared to 11.7%) increase in cumulative oil production.

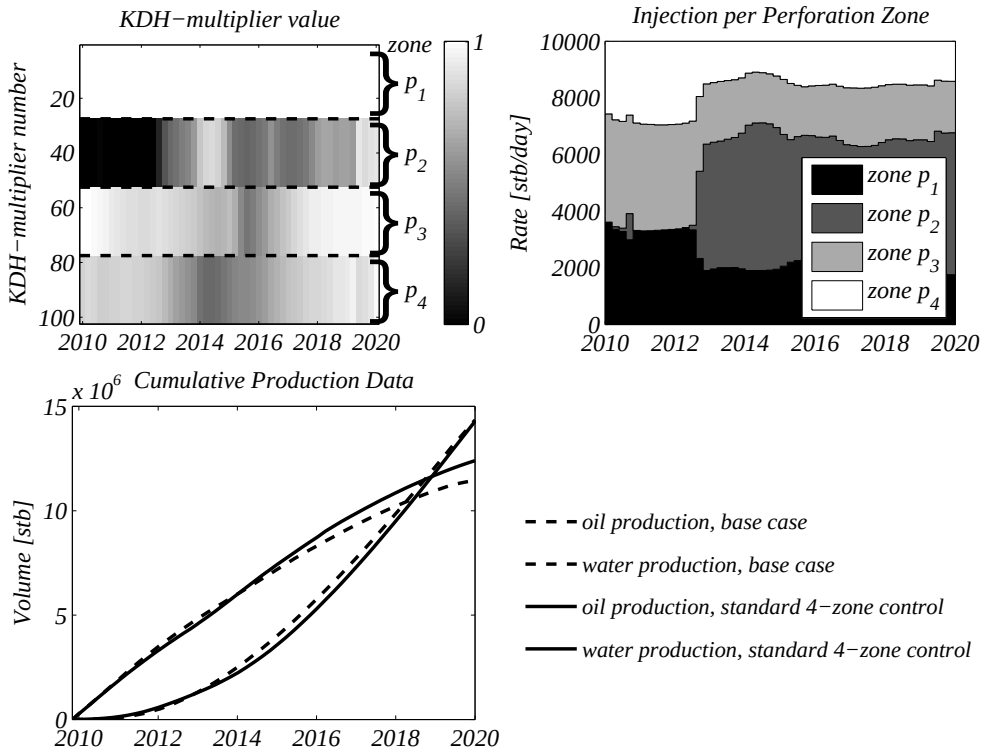

Figure A.7 : Standard four-zone control results. Left: optimal time-varying KDH-multipliers. Middle: injection profile. Right: cumulative production.

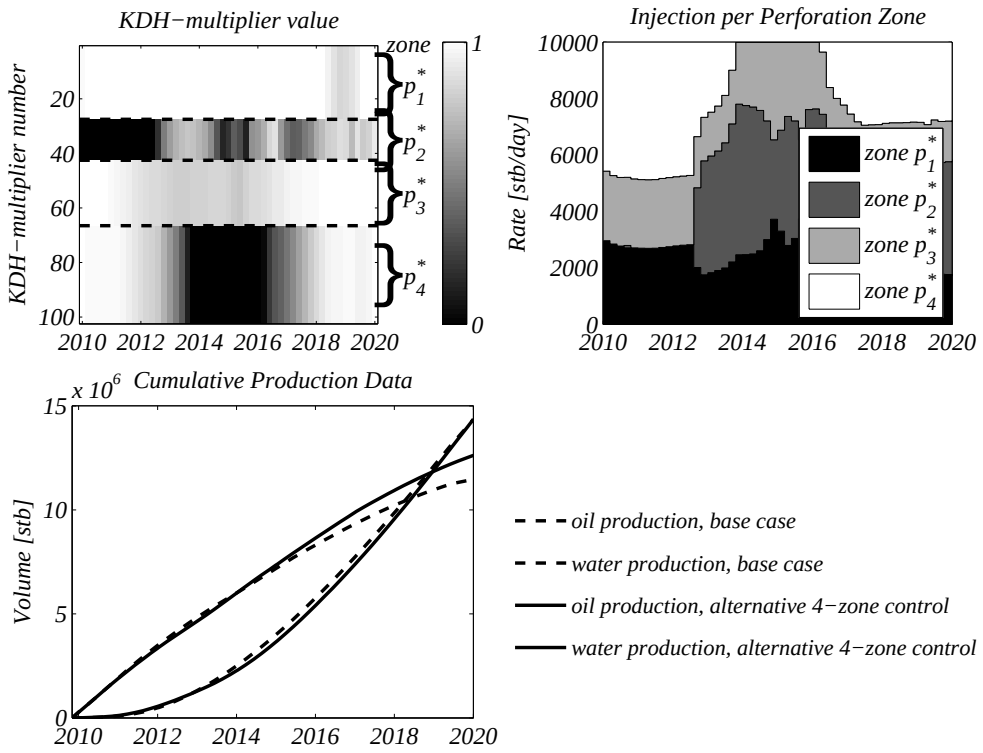

Figure A.8 : Alternative four-zone control results. Left: optimal time-varying KDH-multipliers. Middle: injection profile. Right: cumulative production.

Alternative four-zone control

Figure A.8 shows the optimal time-varying KDH-multipliers, the injection rates for zones p_1^*, p_2^*, p_3^* and p_4^*, and the cumulative oil and water production. As expected, the result is better than with standard grouping: 10.0% increase in cumulative oil. In other words, 1.7% of the scope for optimization is lost by going from 102 to four control valves.

To make control of the injection rates possible under fracturing conditions, a switching scheme is imposed upon the control strategy. Water injection must alter between zones p_1 & p_3 and p_2 & p_4 (when the standard grouping is used), or p_1^* & p_3^* and p_2^* & p_4^* (when the alternative grouping is used). In both cases the switching scheme is determined according to the optimal full 102 control injection profile. The switching profile can be observed in Figure A.9.

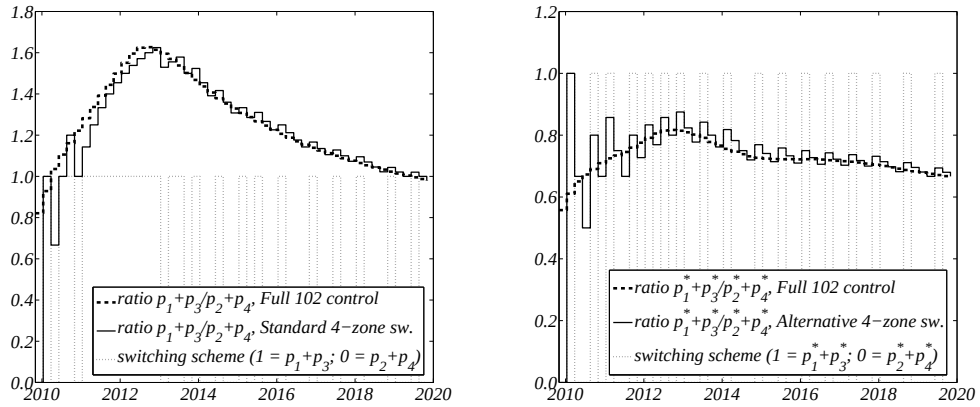

Figure A.9 : Injection ratios and resulting switching schemes. Left: standard grouping $(p_1+p_3)/\ (p_2+p_4)$. Right: alternative grouping $(p_1^*+p_3^*)/(\ p_2^*+p_4^*)$.

Standard four-zone switching control

Figure A.10 shows the optimal time-varying KDH-multipliers, the injection rates for zones p_1, p_2, p_3 and p_4, and the cumulative oil and water production. Surprisingly, the result is much better than for the standard four-zone control without the switching constraint: 10.3% increase in cumulative oil. Apparently, the optimization scheme had previously converged to a local optimum. This shows that, even when taking all of the practical constraints into account, there is significant scope to increase cumulative oil production in the St. Joseph sector model.

Alternative four-zone switching control

Figure A.11 shows the optimal time-varying KDH-multipliers, the injection rates for perforation zones p_1^*, p_2^*, p_3^* and p_4^*, and the cumulative oil and water production. Although it makes sense that the result should be worse than the alternative four-zone control without the switching constraint, it is surprising that the result is the worst yet: only 7.9% increase in cumulative oil production.

Discussion of results

As expected Full 102 control, which has the most degrees of freedom, yields the best results (11.3% increase in cumulative oil). Compared to Standard and Alternative four-zone control, both having much less freedom due to a reduction from 102 to four control valves, there is indeed a slight loss in performance. Furthermore, the results suggest that the alternative grouping used in Alternative four-zone control will yield

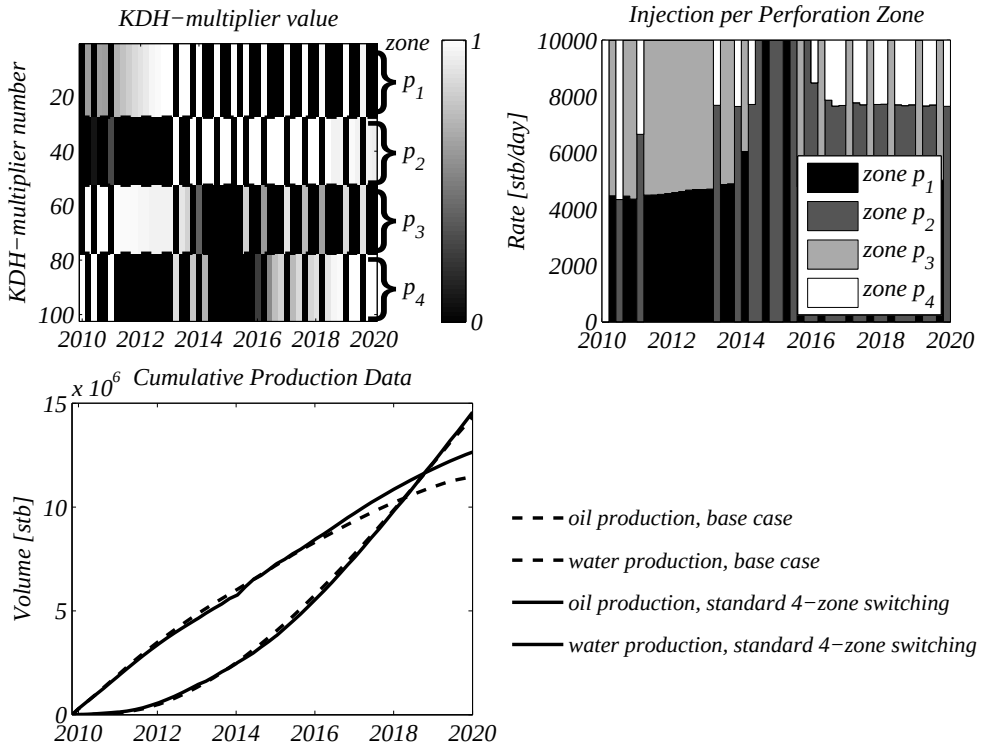

Figure A.10 : Standard four-zone switching control results. Left: optimal time-varying KDH-multipliers. Middle: injection profile. Right: cumulative production.

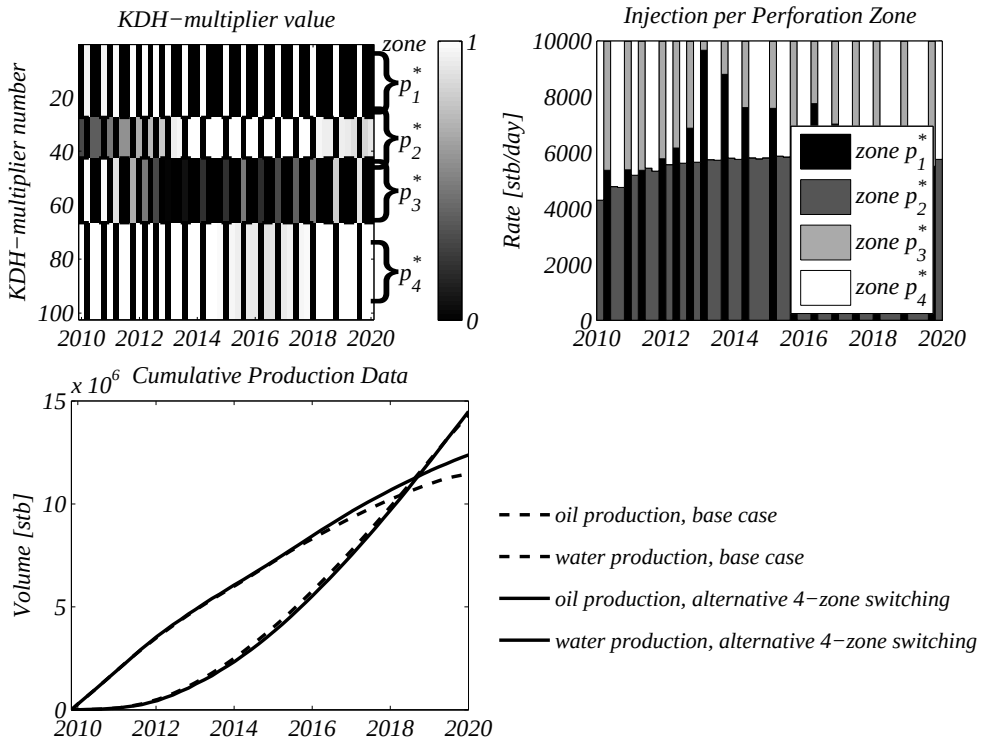

Figure A.11 : Alternative four-zone switching control results. Left: optimal time-varying KDH-multipliers. Middle: injection profile. Right: cumulative production.

better results than the standard grouping used in Standard four-zone control (10.0% versus 8.1%). It would make sense if Standard and Alternative four-zone switching control would again show a slight loss of performance, since these have even less freedom due to the switching constraint. Alternative four-zone switching control indeed shows this expected loss in performance (7.9%). However, the opposite is true for Standard four-zone switching control (10.3%): it is even higher than Alternative four-zone control. This is surprising, and suggests that the optimization procedure has converged to a local optimum for Standard four-zone control.

A.6 Discussion and Conclusions

A.6.1 Discussion

- Within this case study, use of ICVs was predetermined and therefore the dynamic flexibility of ICVs was used to optimize a dynamical waterflooding strategy. We note that the presented method can also be used to optimize f (static) interval control devices (ICDs) through the use of static instead of dynamic KDH-multipliers. The option to use ICDs was not investigated, because ICVs were preferred due to their larger flexibility to react to unforeseen events, and their capacity to control fracture growth through a switching strategy.
- We note that, in addition to valve setting optimization as addressed in our study, optimization of the valve configuration itself is an important topic. However coupled optimization of the valve operation and of the detailed valve design is not necessarily required, and the optimization exercises may be performed one after each other. Only if constraints resulting from the valve design optimization problem would limit the well to maintain the optimal injection rates per zone, coupling would be required, but normally this can be avoided through proper valve design (for which proper estimates of the expected rates are required).
- Within this work, matrix injection was assumed while fracturing is expected to occur in reality. Due to the switching control strategy and a fixed total injection rate for the injection well, sensitivity to fracturing is limited to the division of the total injection rates over two perforation zones simultaneously. The St. Joseph asset team believes that this is manageable in reality. A skin factor sensitivity study would give insight in the validity of this assumption, but was not performed within this case study.
- The optimization procedure presented, to determine the added value of smart completions for the planned water injection and infill wells, is based on the predictions of a dynamical reservoir model of the St. Joseph field. As with

any model-based decision-making procedure the decisions are only as good as the model. For time-restriction reasons, the representativeness of the sector model used within this study was not investigated thoroughly. This should be taken into consideration when evaluating the significance of the absolute values of the long-term predictions and consequently the incremental production. Using the full field model (FFM) would eliminate any issues concerning the representativeness of the sector model and therefore repeating the optimization exercise using the FFM is recommended. To improve convergence of the FFM optimization problem, the optimal valve settings of the sector model should be used as initial guess.

- As the number of constraints on the control increases, the number of degrees of freedom decreases. As a result, the optimal value of the objective function should remain equal or become smaller each time a constraint on the control is added. The reason that the results of our study do not reflect this is because of the used gradient-based optimization algorithm. Gradient-based solving of large-scale non-linear optimization problems always suffers from the risk of ending up in a local optimum. The use of multiple initial guesses increases the chance of finding the global optimum but certainly does not guarantee it. The risk of finding a local optimum is that a solution exists that gives better performance. In this particular case, it also means a global solution may exist that gives an alternative grouping of the perforation zones. However, all solutions presented in this work - albeit possibly locally optimal solutions - outperform an injection strategy using a conventional injection well by a margin of 8% or more and are therefore beneficial to implement. In fact, the concept of gradient-based optimization ensures that any (local) optimum is better than or equal to the starting point, but never worse. Moreover, Jansen et al. (2009) and Van Essen et al. (2009a) have observed that although multiple solutions to waterflooding optimization problems may exist, their corresponding values of the objective function are generally close to each other.

- The optimization procedure was performed on a single deterministic model of the St. Joseph field. The use of a representative ensemble of models may give a more realistic view of the added value of 'smartness' by means of a range of forecasts. The ensemble may e.g. represent the range of uncertainty in the geological structure of the reservoir, or the uncertainty in fracture growth parameters. With an ensemble of models, a robust optimization procedure can be performed, aimed at maximizing average performance over all members, see Van Essen et al. (2009b).

A.6.2 Conclusions

- The workflow using adjoint-based optimization provides a tool to assist in smart well design based on a dynamic reservoir model. It provides the capability to determine the added value of increasing levels of 'smartness', based on dynamic simulations. A predefined objective function can be determined that reflects actual field performance. Although the optimization procedure essentially provides an upper limit of the added value, it can serve as a valuable best-case reference.
- The determined 'optimal' perforation zones do not correspond exactly to the geological zones defined using a static geological model. This result emphasizes the relevance of incorporating dynamic flow modeling into well design.
- In this study, a sector model of the St. Joseph field was used to design the optimization approach instead of the full field model due to time constraints. Apart from the increase in simulation time, no major obstacles are expected in applying this approach to the full field model or any other model of considerable size and complexity.

Appendix B

Lower and Upper Bounds of Predicted Production

This appendix has been published before as "Van Essen, G.M., Jansen, J.D., and Van den Hof, P.M.J. (2010b). Determination of lower and upper bounds of predicted production from history-matched models. In *Proc.12th European Conference on the Mathematics of Oil Recovery* (*ECMOR XII*). Oxford, United Kingdom.".

B.1 introduction

It is a well-known fact that assimilation of historical production data into reservoir models is an ill-posed problem; see e.g. Watson et al. (1984), Tavassoli et al. (2004) or Zandvliet et al. (2008). This is mainly because generally the number of uncertain model parameters largely supersedes the number of measurements. Moreover, the measurements are strongly correlated since they originate from a relatively small number of sources: the wells. As a result, they contain less information on the true value of the model parameters than may be expected based solely on the number of data points. A relevant question in view of the purpose of large-scale, physics-based reservoir models is how the long-term predictions may vary because of the ill-posedness of the assimilation problem. In other words, what may be the economic consequences of the lack of information about the reservoir that is contained in the measurements?

In most practical circumstances, this question is addressed by constructing and history-matching a low and high case model, besides the nominal model. Alternatively, a set of model realizations can be used in a data-assimilation algorithm to obtain an entire

collection of predictions, as is the case with ensemble Kalman filter (EnKF) methods, see e.g. Naevdal et al. (2005), Evensen (2007) and Aanonsen et al. (2009). However, in either way the resulting history-matched models are heavily influenced by the prior information that went into the data-assimilation process. Hence, properly answering the question stated above requires either some (heuristic) method to translate static geological properties to flow behavior or economic performance, or requires very many forward simulation runs to obtain a proper low or high case prior model. These methods are either unreliable or impractical to provide a good measure of the economic consequences of the lack of knowledge about the true field. In this paper a procedure is introduced to search for a history-matched model that gives either a lower or an upper bound on predicted production (or any other economic objective) over the remaining life of the field, for a fixed production strategy. Such a production strategy may for instance involve a reactive control approach.

B.2 Problem

The problem of determining a history-matched model that provides either a lower or an upper bound on the predicted economic performance over the life of a reservoir is essentially a multi-objective optimization problem, see e.g. Marler and Arora (2004). The first objective is to find a certain realization of model parameters that minimizes the error between the measured and simulated production data, which can be expressed through a quantitative objective function V, e.g. mean square difference. The second objective relates to finding a set of parameter values that - for a certain future production strategy - minimizes or maximizes some economic cost function J, e.g. net present value (NPV).

However, the multiple objectives are not of the same importance; priority lies with obtaining a good history-match, while determining a lower bound or an upper bound on predicted economic performance serves as secondary objective. To that end, the multi-objective optimization problem may be cast into a hierarchical optimization problem, as presented in Haimes and Li (1988) and more recently specifically for oil production optimization in Van Essen et al. (2009a). In this structure, optimization of a (secondary) economic cost function J is constrained by the requirement that the (primary) quantitative history-matching cost function V must remain close to its minimal value V_{min}. This requires solving the following two (hierarchical) optimization problems:

$$V_{min} \triangleq \min_{\theta} V(\theta, \bar{\mathbf{u}}) \tag{B.1}$$

$$s.t. \quad \mathbf{g}_{k+1}(\bar{\mathbf{u}}_k, \mathbf{x}_k, \mathbf{x}_{k+1}, \theta) = 0, \quad k = 0, \ldots, K-1, \quad \mathbf{x}_0 = \bar{\mathbf{x}}_0, \tag{B.2}$$

$$\mathbf{c}_{k+1}(\bar{\mathbf{u}}_{k+1}, \mathbf{x}_{k+1}, \theta) \leq 0 \tag{B.3}$$

and:

$$\max_{\theta} J(\theta, \bar{\mathbf{u}}) \quad \text{or} \quad \min_{\theta} J(\theta, \bar{\mathbf{u}}) \tag{B.4}$$

$$s.t. \quad \mathbf{g}_{k+1}(\bar{\mathbf{u}}_k, \mathbf{x}_k, \mathbf{x}_{k+1}, \theta) = 0, \quad k = 0, \ldots, K-1, \quad \mathbf{x}_0 = \bar{\mathbf{x}}_0, \tag{B.5}$$

$$\mathbf{c}_{k+1}(\bar{\mathbf{u}}_{k+1}, \mathbf{x}_{k+1}, \theta) \leq 0 \tag{B.6}$$

$$V(\theta) - V_{min} \leq \varepsilon \tag{B.7}$$

where $\bar{\mathbf{u}}$ is the fixed control vector (input vector), $\mathbf{x}$ is the state vector (grid block pressures and saturations), $\mathbf{g}$ is a vector-valued function that represents the system equations, $\mathbf{x}_0$ is a vector of the initial conditions of the reservoir, the subscript k indicates discrete time, and $K$is the total number of time steps. The vector of inequality constraints $\mathbf{c}$ relates to the capacity limitations of the wells. The term ε is an arbitrary small value compared to V_{min}. In order to solve the secondary optimization problem (B.4)-(B.7) first a (single) optimal solution to the primary optimization problem (B.1)-(B.3) is required to determine V_{min}. The optimal solution to the primary problem can serve as feasible initial guess for the secondary problem. Because of the ill-posed nature of the inverse history-matching problem, there exists a vast null-space within the model parameter space. Any changes of the model parameters within that null-space will have no effect on the value of the used quantitative history-match quality indicator. Note that the search space of the secondary problem is constrained by the null-space of the primary objective function at a value of V_{min}, through inequality constraint (B.7). In other words, the redundant degrees of freedom (DOF) of the primary problem are the DOF of the secondary problem.

B.3 Method

In Van Essen et al. (2009a), the primary optimization problem is attacked using a gradient-based search algorithm. The gradients are obtained using a system of adjoint equations that is solved backwards in time once, regardless of the number of optimization parameters, see e.g. Brouwer and Jansen (2004), Sarma et al. (2005) and Kraaijevanger et al. (2007). Subsequently, the secondary optimization problem was also attacked using a gradient-based search algorithm. However, the secondary problem was executed with the addition of projecting the search direction

onto a second-order approximation of the null-space with respect to the optimality constraint defined in Eq. (B.7). The second-order approximation was explicitly determined through a forward difference scheme using first-order information obtained with the adjoint. Unfortunately, using this approach the number of forward and backward simulations is proportional to the number of optimization parameters. Hence, for the assimilation of production data this method is in most cases computationally infeasible.

In Van Essen et al. (2009a), also an alternative method is introduced to solve the hierarchical optimization problem without explicitly calculating the null-space with respect to Eq. (B.7). It uses a weighted objective function with weighting functions Ω_1 and Ω_2:

$$W = \Omega_1(V) \cdot V + \Omega_2(V) \cdot J, \tag{B.8}$$

where Ω_1 and Ω_1 are 'switching' functions of V and J that take on values of 1 and 0 or vice versa:

$$\Omega_1(V) = \begin{cases} 1 & \text{if } V - V_{min} > \varepsilon \\ 0 & \text{if } V - V_{min} \leq \varepsilon \end{cases}, \quad \Omega_2(V) = \begin{cases} 0 & \text{if } V - V_{min} > \varepsilon \\ 1 & \text{if } V - V_{min} \leq \varepsilon \end{cases}, \tag{B.9}$$

Here, ε is the threshold value as defined in inequality constraint (B.7). The gradients of W with respect to the model parameters θ for iteration $n+1$ is then simply:

$$\left.\frac{\partial W}{\partial \theta}\right|_{n+1} = \Omega_1(V_n) \cdot \left.\frac{\partial V}{\partial \theta}\right|_{n+1} + \Omega_2(J_n) \cdot \left.\frac{\partial J}{\partial \theta}\right|_{n+1} \tag{B.10}$$

Solving the secondary optimization problem using W as defined in Eq. (B.8), sequentially gives improving directions for either V or J. With each iteration, the value of J either increases while the value of V decreases or the other way around, as the solution moves to and from the feasible region with respect to inequality constraint (B.7). If there exist redundant DOF with respect to the primary problem, improvement of J is possible while satisfying Eq. (B.7) and convergence of the hierarchical optimization will occur in a 'zigzag' fashion, as schematically represented in Figure B.1.

To improve convergence speed, as presented above and in Van Essen et al. (2009a), a small adaptation to the switching algorithm can be made. By projecting the gradients of secondary objective function J onto the first-order approximation of the null-space

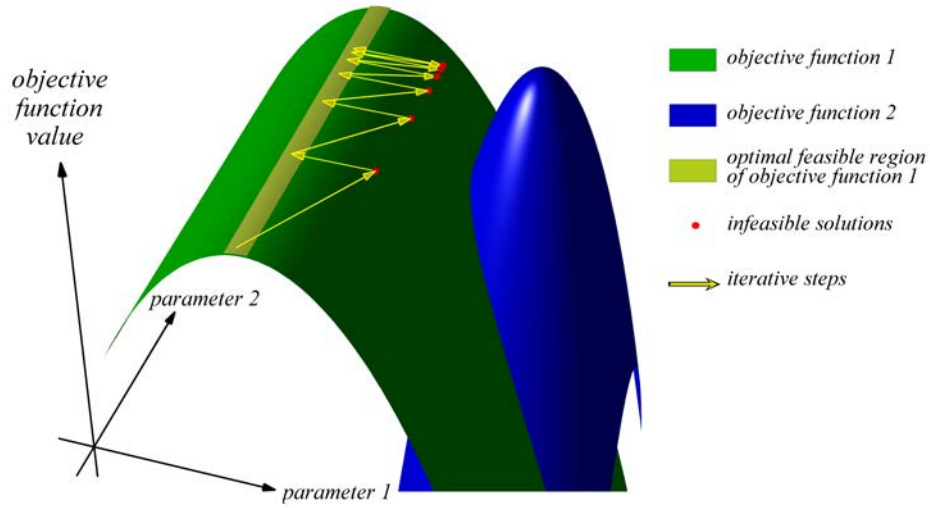

Figure B.1 : Schematic representation of the iterative process of solving a hierarchical optimization problem using a weighted objective function, as described by Eq. (X). The process converges towards a final solution in a 'zigzag'-fashion, moving into and out of the feasible region bounded by the optimal solutions of the primary objective function.

of the primary objective function V, the resulting update of θ will keep V closer to V_{min}. Mathematically this becomes:

$$\frac{\partial \tilde{J}}{\partial \theta} \triangleq \frac{\partial J}{\partial \theta} \cdot \left[I - \frac{\partial V}{\partial \theta}^T \cdot \frac{\partial V}{\partial \theta} \right], \tag{B.11}$$

Inserting of Eq. (B.11) in Eq. (B.8) gives an alternative switching search direction **d** for solving the hierarchical optimization problem:

$$\mathbf{d}_{n+1} = \Omega_1 (V_n) \cdot \left. \frac{\partial V}{\partial \theta} \right|_{n+1} + \Omega_2 (J_n) \cdot \left. \frac{\partial J}{\partial \theta} \right|_{n+1} \cdot \left[I - \frac{\partial V}{\partial \theta}^T \cdot \frac{\partial V}{\partial \theta} \right], \tag{B.12}$$

The switching algorithm using the projected gradient **d** was used in the following example to illustrate the performance of the method.

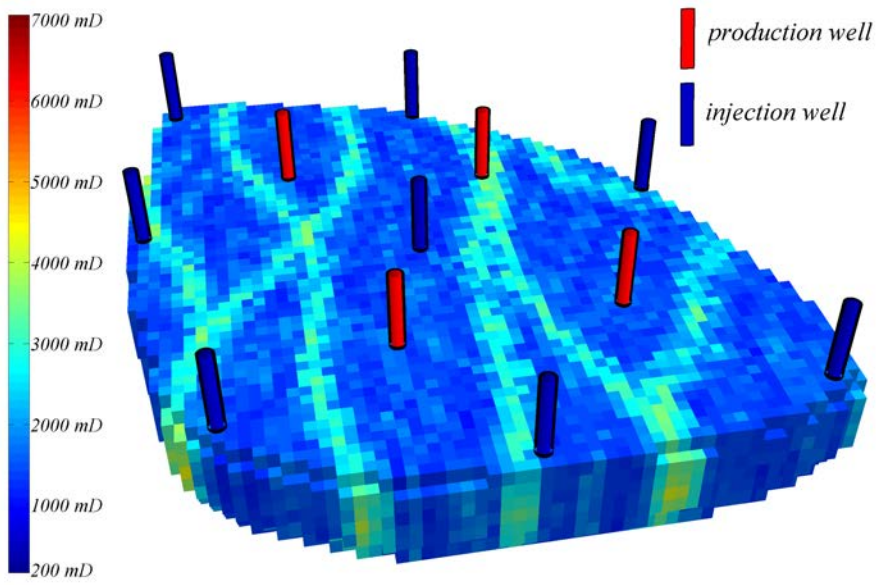

Figure B.2 : 3-dimensional oil reservoir model with eight injection and four production wells, after Van Essen et al. (2009b). Its geological structure involves a network of fossilized meandering channels of high permeability.

B.4 Example

In this example, we consider a three-dimensional oil reservoir model, introduced in Van Essen et al. (2009b). The reservoir model consists of 18,553 active grid blocks, as depicted in Figure B.2, and has dimensions of $480m \times 480m \times 28m$. Its geological structure involves a network of fossilized meandering channels of high permeability. The average reservoir pressure is 40.0 MPa. All remaining geological and fluid properties used in this example are presented in Table B.1. The reservoir model contains eight injection wells and four production wells. The near-wellbore flow is modeled using a Peaceman well model. The injection wells are operated on injection flow rates q_{wi}, while the production wells operate on flowing bottomhole pressure p_{wf}.

During the first 1.5 years of production from the reservoir, the bottomhole pressures of the producers were kept at a constant value of 39.5 MPa. During that time, the injection rates of all eight injectors fluctuated monthly with a uniform probability distribution around an average value of $5.52 \times 10^{-4} m^3/s$ (300 bbl/day) and a maximal offset $9.2 \times 10^{-4} m^3/s$ (50 bbl/day). Monthly production measurements were taken of the flowing bottomhole pressures of the eight injectors and fractional flow rate measurements of the four producers, on top of which no noise was superimposed.

Table B.1 : *Geological and fluid properties for the example*

Symbol	*Variable*	*Value*	*Units*
	Reservoir parameters		
Φ	Porosity	0.20	-
	Fluid parameters		
ρ_o	Oil density	800	kg/m^3
ρ_w	Water density	1000	kg/m^3
c_o	Oil compressibility	1.00×10^{-10}	$1/Pa$
c_w	Water compressibility	1.00×10^{-10}	$1/Pa$
μ_o	Dynamic oil viscosity	5.00×10^{-3}	$Pa \cdot s$
μ_w	Dynamic water viscosity	1.00×10^{-3}	$Pa \cdot s$
p_c	Capillary pressure	0	Pa

Thus, the total number of measurements added up to 288 data points.

The goal of this example is to determine a lower and upper bound on expected economic performance over the remaining life of the field - from 1.5 to 6.0 years - by changing certain model properties, while the model stays compliant with historic data over the first 1.5 years of production. In this particular example, only permeability was adjusted using a homogeneous prior model of 1000 *mDarcy*. The remaining model properties were chosen identical to the 'truth' reservoir model shown in Figure B.2, such that the reservoir volume, expressed as stock tank oil initially in place (STOIIP). for both the upper bound and lower bound model were equal to the 'true' STOIIP. As economic performance measure NPV was used:

$$J = \sum_{k=1}^{K} \left[\frac{\sum_{i=1}^{N_{inj}} r_{wi} \cdot (u_{wi,i})_k + \sum_{j=1}^{N_{prod}} \left[r_{wp} \cdot (y_{wp,j})_k + r_o \cdot (y_{o,j})_k \right]}{(1+b)^{\frac{t_k}{\tau_t}}} \cdot \Delta t_k \right] \tag{B.13}$$

where $u_{wi,i}$ are the control inputs relating to the water injection rate of well i, $y_{wp,j}$ the water production rate of well j, $y_{o,j}$ the oil production rate of well j. The water injection costs r_{wi}, the water production costs r_{wp} and the oil revenue ro are assumed constant at a value of 0 $\$/m^3$, -1 $\$/m^3$ and 9 $\$/m^3$ respectively. Δt_k is the time interval of time step k in days and the term b represents the discount rate for a certain reference time τ_t, which in this example was set to zero. The terms N_{inj} and N_{prod} relate to the number of injection wells and production wells respectively. In Eq.

(B.13), the output variables $y_{wp,j}$ and $y_{0,j}$ relate to the water production rate and oil production rate of well j, which form part of the output vector:

$$\mathbf{y}_{k+1} = \mathbf{h}\left(\mathbf{u}_{k+1}, \mathbf{x}_{k+1}\right), \quad k = 0, \ldots, K-1, \tag{B.14}$$

with $\mathbf{h}$ a vector-valued output function that relates $\mathbf{y}$ to the control vector (input vector) $\mathbf{u}$ and the state $\mathbf{x}$. The term $u_{wi,i}$ represents those elements of $\mathbf{u}$ that involve the water injection flow rates of well i.

The upper and lower bounds of the NPV can only be determined for a given (fixed) control strategy $\bar{\mathbf{u}}$. In this example, a reactive control approach is used that is evaluated on a field level. All injection wells are assumed to continuously operate on their average injection rate of $5.52 \times 10^{-4} m^3/s$ and the production wells on their fixed bottomhole pressure of 39.5 *MPa*. The instant the field watercut exceeds 0.90, all wells are shut-in. Note that this threshold is related to the ratio between oil revenue r_o and water production costs r_{wp}.

To determine the history-matched models that provide the lower and upper bound on NPV for the remaining production life, two hierarchical optimization procedures were initiated. The procedures were terminated when the feasible updates no longer resulted in a significant change in NPV. Figure B.3 and Figure B.4 show the measured production data, along with the simulated production data originating from the final lower and upper bound model, resulting from the hierarchical optimization method. They show that the error between measured and simulated bottomhole pressures of the injectors and fractional flow rates of the producers are very small for both the lower bound as the upper bound model.

Thus, the condition that the updated models maintain a good history match is met. However, in Figure B.5 it can be observed that the permeability fields of both models are quite different. These differences have a large impact on the predicted production data given the assumed reactive production strategy, as can be observed in Figure B.6 and Figure B.7.

Finally, Figure B.8 shows the actual lower and upper bound on predicted NPV over time. It can be observed that the upper and lower bound are respectively 63% above and below the average of the two bounds.

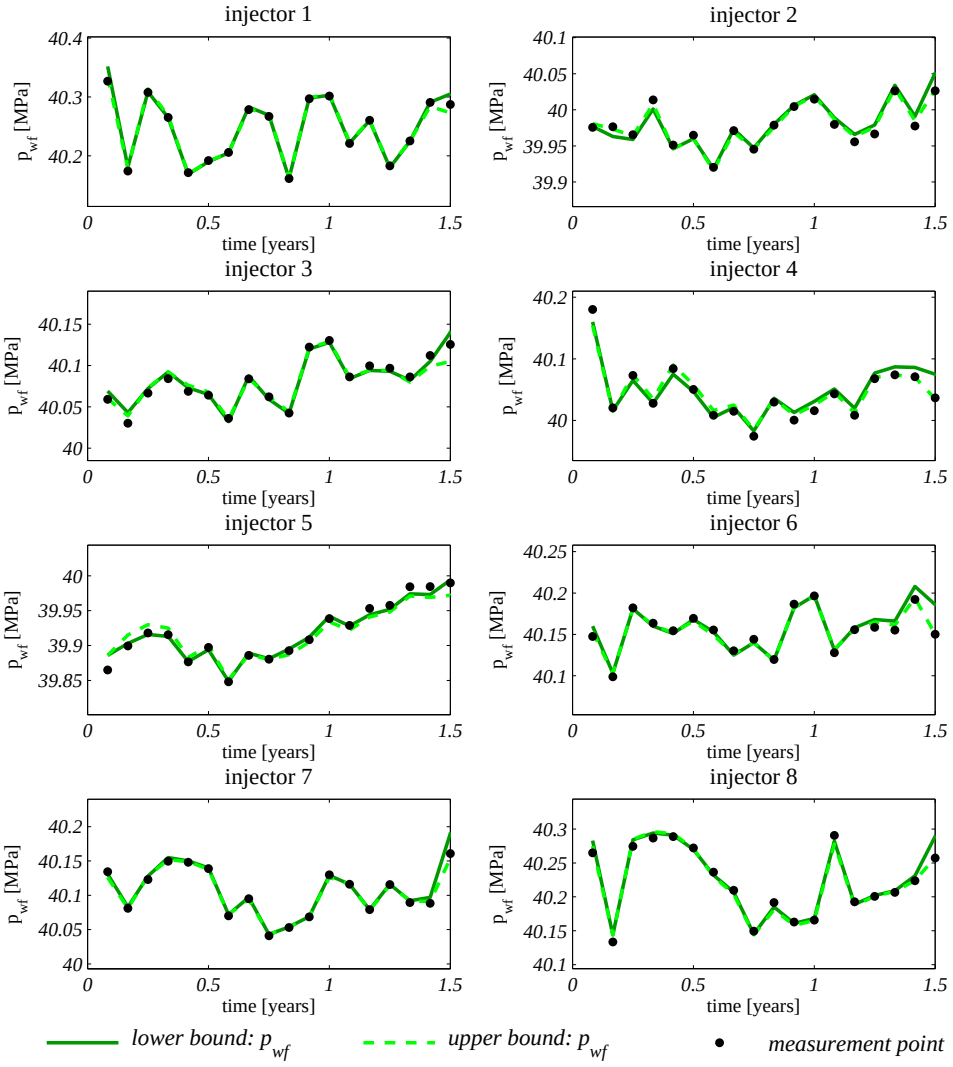

Figure B.3 : Measured flowing bottom-hole pressures of the injectors over the first 1.5 years of production from the (synthetic) 3D reservoir, along with the simulated bottom-hole pressures originating from the lower and upper bound models.

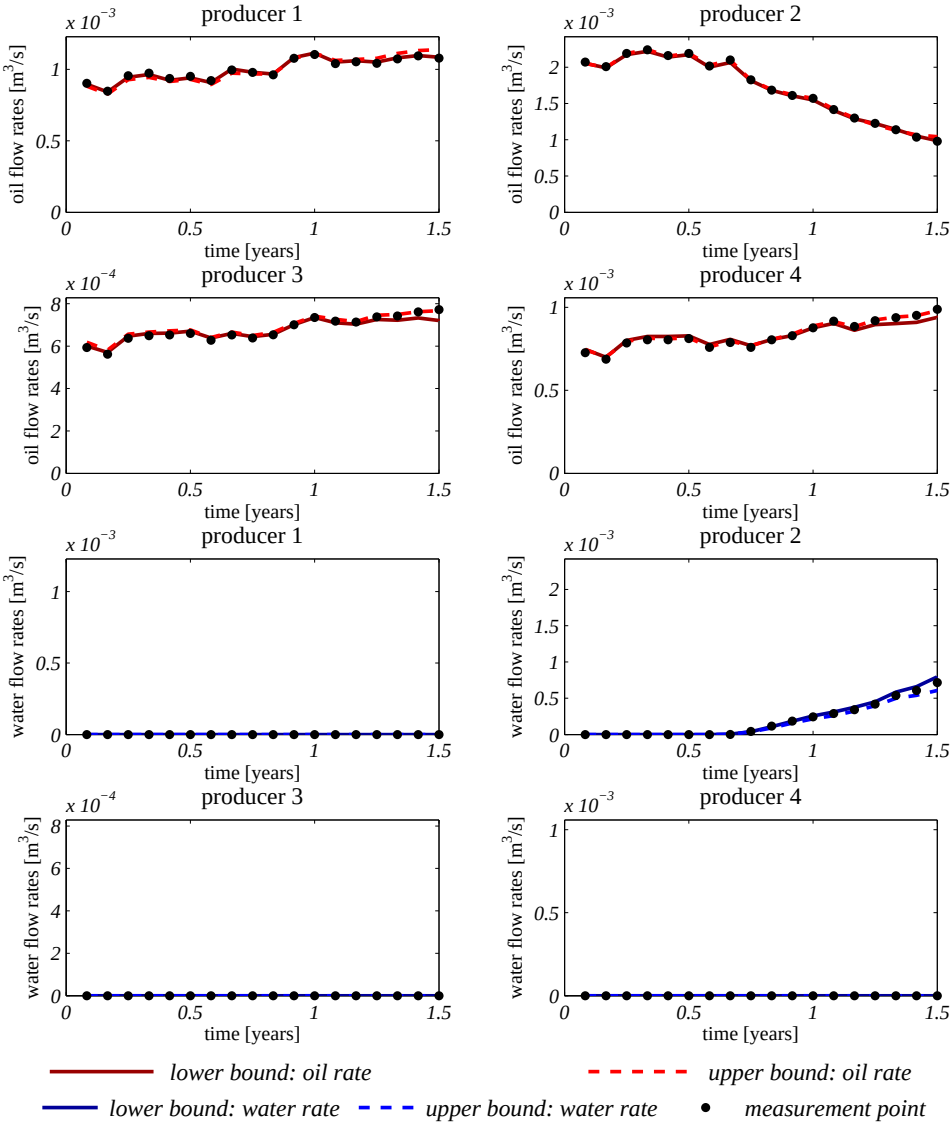

Figure B.4 : Measured oil and water rates of the producers over the first 1.5 years of production from the (synthetic) 3D reservoir, along with the simulated bottom-hole oil and water rates originating from the lower and upper bound models.

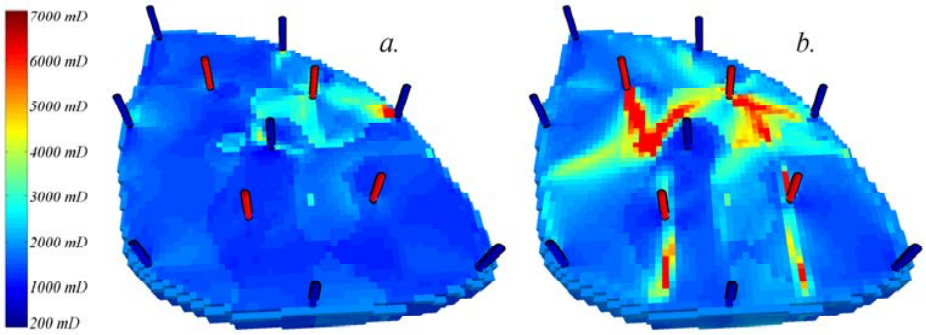

Figure B.5 : Permeability fields of the lower bound 3D reservoir model (a.) and upper bound 3D reservoir model (b.) determined after the first 1.5 years of production.

B.5 Discussion

The hierarchical procedure presented in this paper exploits the redundant DOF with respect to optimality of the primary objective. Updating the model parameters along these DOF to improve a secondary objective function is possible until there a no longer any DOF left or the update direction is tangent to the (optimality) constraint. If all (equal) optimal solutions to the primary problem are connected, the solution to the (constrained) secondary problem is in fact a global upper or lower bound. Unfortunately, this is infeasible to verify for large-scale problems. Hence, the range of (economic) predictions may still be larger than determined through the hierarchical optimization procedure. It should be noted that this is no artifact of the used gradient-based optimization approach, but the result of the strongly varying nature of the solution space to the primary problem. As a result, solving weighted objective function (B.8) with a gradient-free method may still suffer the same fate.

The iterative switching scheme used to address the hierarchical optimization problem may show very slow convergence, especially when the update direction is nearly tangent to the optimality constraint. As a result, many iterations may be required to find the lower and upper bound. Using a line search or trust region method, along with proper tuning of the algorithm parameters may possibly improve the convergence speed.

B.6 Conclusions

In this paper, we presented a hierarchical optimization method to determine the lower and upper bounds on predicted production from history-matched models. We con-

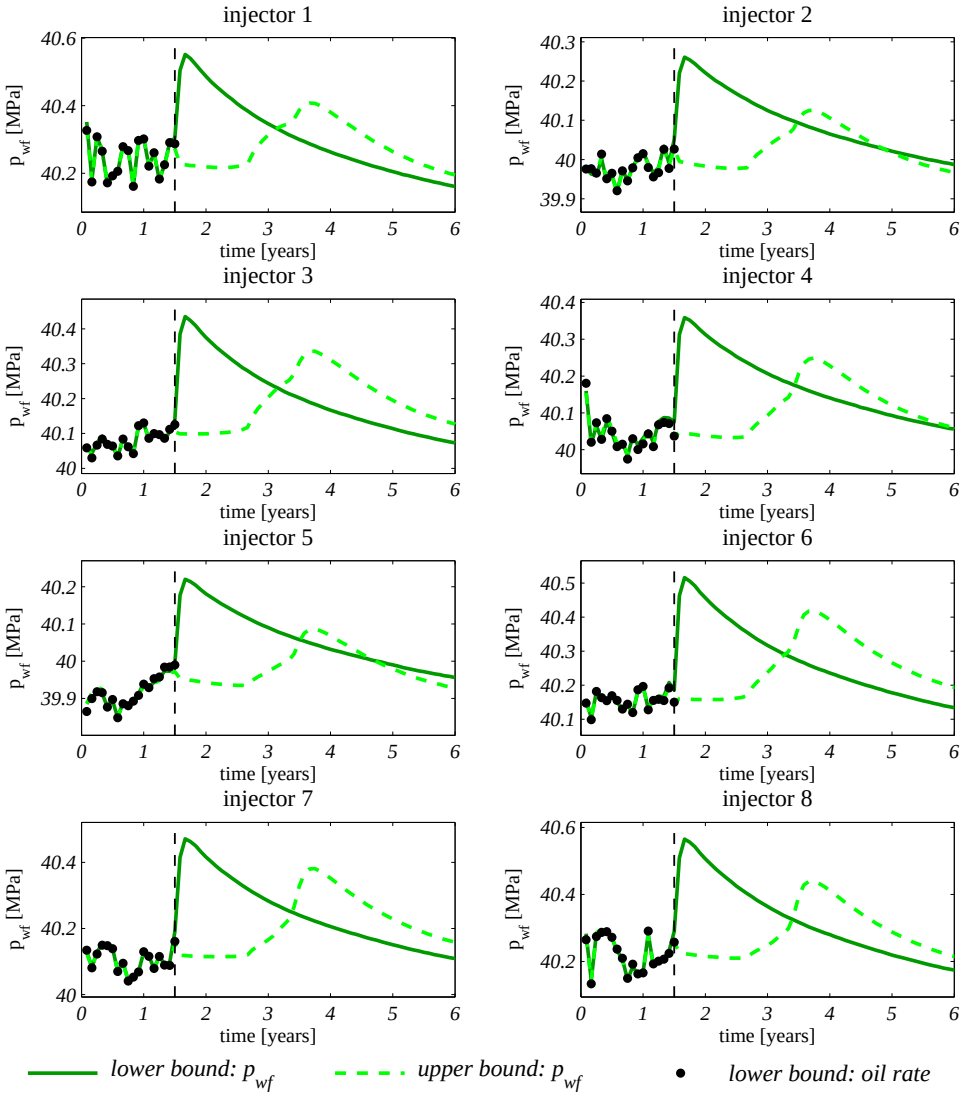

Figure B.6 : Measured flowing bottom-hole pressures of the injectors over first 1.5 years of production from the (synthetic) 3D reservoir, along with the simulated bottom-hole pressures for the remaining 4.5 years of production until the end of the field's life, originating from the lower and upper bound models.

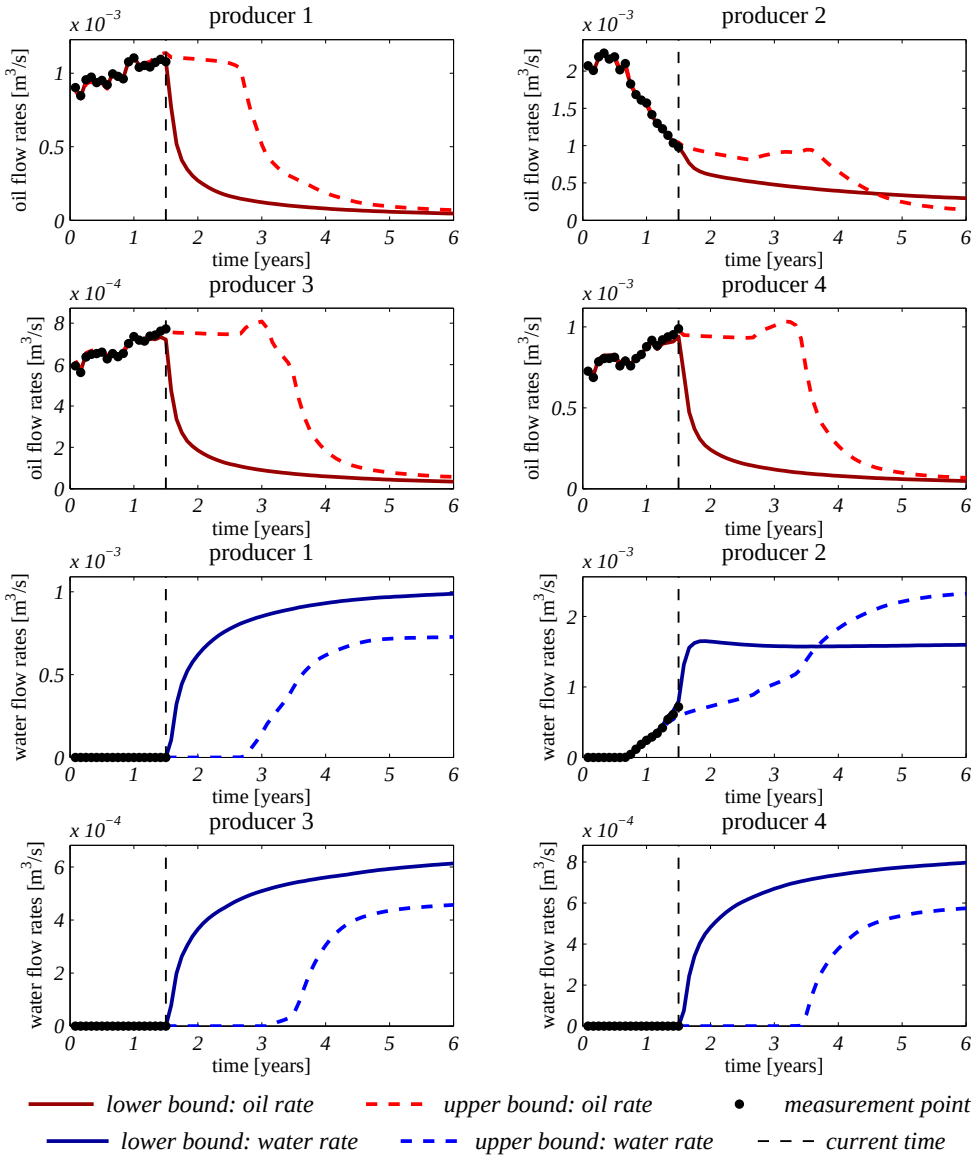

Figure B.7 : Measured oil and water rates of the producers over first 1.5 years of production from the (synthetic) 3D reservoir, along with the simulated oil and water rates for the remaining 4.5 years of production until the end of the field's life, originating from the lower and upper bound models.

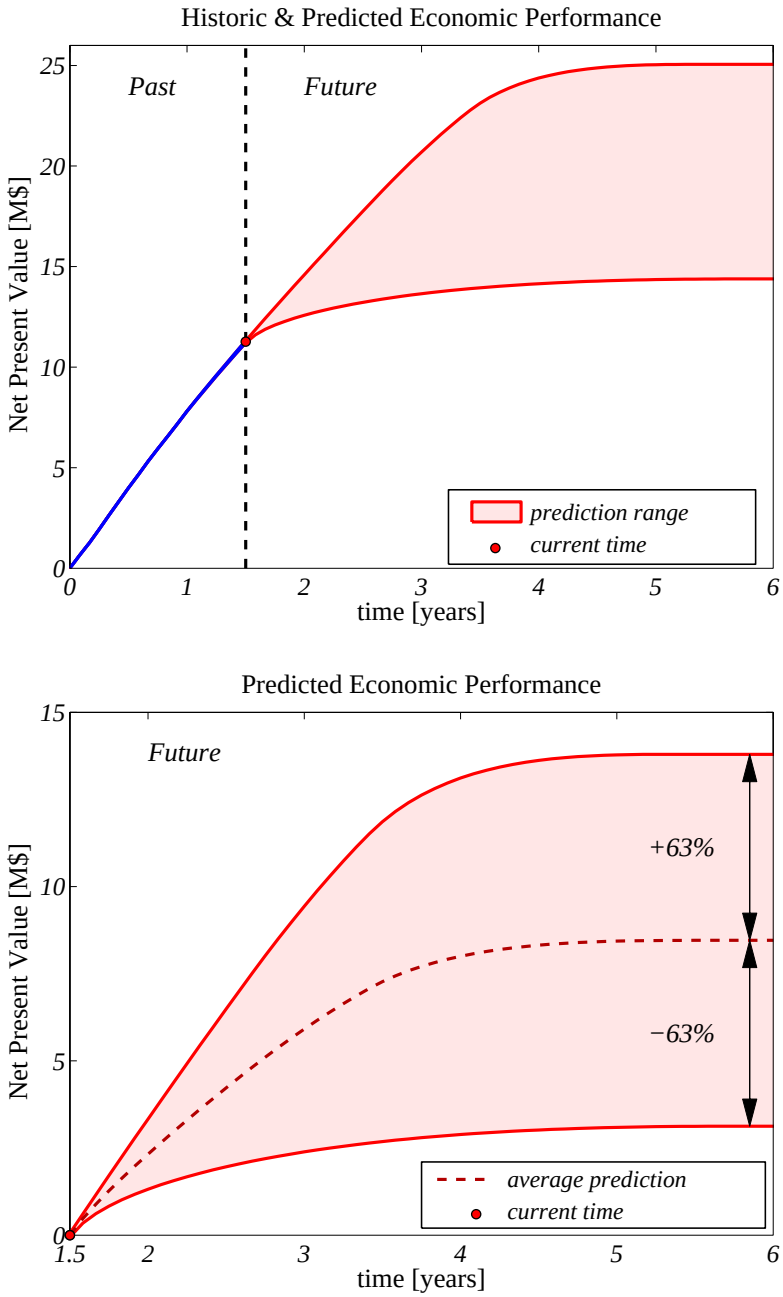

Figure B.8 : NPV over time for the lower and upper bound reservoir models. The plot on the top shows both the historic (first 1.5 year) and future (from 1.5 to 6 years) increase in NPV over time. The plot on the bottom only shows the economic performance (in terms of NPV) for the remaining (future) 4.5 years of production.

clude that:

- The method provides a way to gain more insight in the possible economic consequences of the lack of information contained in the measurement data. These consequences can be represented by total production, ultimate recovery, NPV or any other (economic) measure.

- This method can also be used to design a production strategy. Either a general strategy, by taking the range of outcomes into account: being conservative when the range is vast, while adopting a more risky approach when the range is small. Or by maximizing the lower bound, which can be a (rather conservative) alternative to the robust optimization approach, as presented in Van Essen et al. (2009b). It must be noted that designing a proper strategy requires sequential adaptation of the strategy and determination of the new bounds, as they are only valid for a fixed production scheme.

- The method is not limited to historic production data. Alternative data sources, e.g. time-lapse seismic data, can be used or added to determine the impact on the predicted economic performance. Hence, this method may also play a role in the quantification of the value of information.

B.7 Acknowledgements

This research was carried out within the context of the Integrated Systems Approach to Petroleum Production (ISAPP) knowledge centre. ISAPP is a joint project between Delft University of Technology (TUD), Shell International Exploration and Production (SIEP), and the Dutch Organization for Applied Scientific Research (TNO).

B.8 Nomenclature

b	=	*discount rate*
$\mathbf{d}$	=	*projected search direction*
n	=	*iteration index*
J	=	*economic objective function*
k	=	*time step counter*
q	=	*flow rate*
r	=	*revenues/costs*
t_k	=	*time at time step k*
$\mathbf{u}$	=	*input vector*
V	=	*history-match performance measure*
W	=	*weighted objective function*
$\mathbf{x}$	=	*state vector*
$\mathbf{x}_0$	=	*prescribed value of initial conditions*
$\mathbf{y}$	=	*output vector*
Δt_k	=	*time interval of time step k*
ε	=	*tolerance of optimality constraint*
θ	=	*vector of model parameters*
τ_t	=	*reference time*
Ω	=	*weighting function*
Subscripts		
o	=	*oil*
wf	=	*flowing well bore*
wp	=	*produced water*
wi	=	*injected water*
min	=	*minimum*
1	=	*primary*
Superscripts		
$*$	=	*optimal*

Appendix C

Hierarchical Long-Term and Short-Term Production Optimization

This appendix has been published before as "Van Essen, G.M., Van den Hof, P.M.J., and Jansen, J.D. (2011). Hierarchical long-term and short-term production optimization. *SPE Journal*, 16(1), 191199. doi:10.2118/124332-PA.".

C.1 Introduction

In recent years, improvements in dynamic reservoir modeling and measurement and control capabilities have lead to an increased interest in model-based operation of oil fields. Several studies have shown that there may be a significant scope for improving reservoir management by using reservoir models to optimize economic life- cycle performance [see, for example, Asheim (1988), Sudaryanto and Yortsos (2000), Brouwer and Jansen (2004), and Sarma et al. (2005)]. Especially combined with methods to reduce uncertainty - referred to as closed-loop reservoir management [see, for example, Naevdal et al. (2006), Sarma et al. (2008), Chen et al. (2009b), Jansen et al. (2009), and Wang et al. (2009)] - these (proactive) life-cycle optimization techniques seem to be promising alternatives to more reactive approaches, which are current practice.

However, in these studies on improved life-cycle performance, the importance of meeting short-term targets (e.g., maximizing revenues over a short time interval) is

generally neglected. As a result, many of the improvements in life-cycle performance are obtained at the expense of short-term objectives. In reality, however, it is often these short-term objectives that dictate the course of the operational strategy, especially in view of geological and economic uncertainties. Incorporating short-term goals into the life-cycle optimization problem, therefore, is an essential step in the route toward implementation of the closed-loop reservoir-management concept. To this end, Saputelli et al. (2005, 2006) proposed a multilevel hierarchical control structure, where the separation of the levels was based on different time scales and objectives.

Jansen et al. (2009) observed that significantly different optimized waterflooding strategies result in nearly equal values in NPV. They concluded that the life-cycle optimization problem is ill-posed and contains many more control variables than necessary. As a result, there exist multiple solutions to the optimization problem, and different initial guesses of an input $\mathbf{u}$ may lead to different solution points in an optimal subset $\mathscr{S}$ of the decision variable space $\mathscr{U}$.

The goal of this paper is to present a hierarchical optimization framework that is able to address both short-term and long-term objectives in a consistent manner. Although this framework is generic in nature, the presented approach is aimed at maximizing an economic life-cycle objective, in terms of NPV, without disregarding short-term performance. The existence and nature of multiple solutions in the life-cycle optimization problem are investigated because they provide the possibility to improve short-term operational goals while aiming for economic life-cycle optimality.

C.2 Life-Cycle Optimization Problem

The life-cycle (i.e., long-term) optimization problem does not impose any particular choice of depletion or modeling technique. It only requires the existence of at least one decision variable and the model being capable of providing relatively reliable long-term predictions. However, in many case studies, waterflooding is selected as the depletion method for a number of reasons:

- It is a common recovery mechanism.
- A waterflooding strategy involves many decision variables.
- The flooding process can be modeled reasonably accurately over long distances and periods of time.
- There is generally a significant scope for improvement.

For these reasons, waterflooding is also adopted as the production process within this work. However, the mathematical formulation is kept generic as far as possible. Because of the transient nature of the saturation distribution in an oil-producing reservoir, dynamic optimization must be performed over the entire life of the reservoir to improve economic life-cycle performance. This optimization problem can be expressed by the following mathematical formulation:

$$\max_{\mathbf{u}_{1:K}} J(\mathbf{u}_{1:K}) \tag{C.1}$$

$$s.t. \quad \mathbf{g}_{k+1}(\bar{\mathbf{u}}_k, \mathbf{x}_k, \mathbf{x}_{k+1}, \theta) = 0, \quad k = 0, \ldots, K-1, \quad \mathbf{x}_0 = \bar{\mathbf{x}}_0, \tag{C.2}$$

$$\mathbf{c}_{k+1}(\bar{\mathbf{u}}_{k+1}, \mathbf{x}_{k+1}) \leq 0, \quad k = 0, \ldots, K-1, \tag{C.3}$$

where $\mathbf{u}$ is the control vector (input vector), $\mathbf{x}$ is the state vector (gridblock pressures and saturations), $\mathbf{g}$ is a vector-valued function that represents the system equations, $\mathbf{x}_0$ is a vector of the initial conditions of the reservoir with prescribed value $\bar{\mathbf{x}}_0$, the subscript k indicates discrete time, and K is the total number of timesteps. A colon in a subscript indicates a range [e.g., $\mathbf{u}_{1:K} = (\mathbf{u}_1, \mathbf{u}_2, \ldots, \mathbf{u}_K)$] The vector of inequality constraints $\mathbf{c}$ relates to the capacity limitations of the wells. The objective function J is of an economic type, generally NPV:

$$J = \sum_{k=1}^{K} \left[\frac{\sum_{i=1}^{N_{inj}} r_{wi} \cdot (u_{wi,i})_k + \sum_{j=1}^{N_{prod}} \left[r_{wp} \cdot (y_{wp,j})_k + r_o \cdot (y_{o,j})_k \right]}{(1+b)^{\frac{t_k}{\tau_t}}} \cdot \Delta t_k \right] \tag{C.4}$$

where $u_{wi,i}$ is the control input representing the water-injection rate of Well i, $y_{wp,j}$ is the water-production rate of Well j, $y_{o,j}$ is the oil-production rate of Well j, r_{wi} is the water-injection costs (in USD/m^3), r_{wp} is the water-production costs (in USD/m^3), and r_o is the oil revenue (in USD/m^3), of which the latter three are assumed to be constant. Δt_k is the time interval of Timestep k in days. The term b represents the discount rate for a certain reference time τ_t. The terms N_{inj} and N_{prod} relate to the number of injection wells and production wells, respectively. In Eq. C.4, the output variables $y_{wp,j}$ and $y_{o,j}$ relate to the water-production rate and oil-production rate of Well j, respectively, which form part of the output vector

$$\mathbf{y}_{k+1} = \mathbf{h}(\mathbf{u}_{k+1}, \mathbf{x}_{k+1}), \quad k = 0, \ldots, K-1, \tag{C.5}$$

with $\mathbf{h}$ a vector-valued output function that relates $\mathbf{y}$ to the control vector (input vector) $\mathbf{u}$ and the state $\mathbf{x}$. The term $u_{wi,i}$ represents those elements of $\mathbf{u}$ that involve the

water-injection flow rates of Well *i*. An economic objective function such as Eq. C.4 does not necessarily provide a unique solution to the optimization problem. Although it relates to realistic business conditions, it may well cause ill-posedness of the problem.

Several methods exist to attack the dynamic optimization problem of batch-like processes [see, for example, Srinivasan et al. (2003)]. However, the size of the waterflooding optimization problem (Eqs. C.1 through C.3) limits the possibilities. Simultaneous methods or dynamic programming are impractical because of the usually very large number of states of reservoir models. The resulting long simulation times and large number of input variables also rule out search methods that require many function evaluations (e.g., genetic algorithms). A viable optimization technique is a gradient-based method using a set of adjoint equations to determine the gradients [see, for example, Brouwer and Jansen (2004), Sarma et al. (2005), and Kraaijevanger et al. (2007)]. This approach to life-cycle waterflooding optimization is encountered most often in literature and is also the method implemented in the proprietary reservoir simulator used in this study.

C.3 Hierarchical Optimization

Multiple Objectives. In the life-cycle waterflooding problem as expressed by Eqs. C.1 through C.3, the desire to aim for maximal short-term (daily) production is discarded. A balanced objective provides a possibility to address both objectives in a single function; see Marler and Arora (2004):

$$J_{bal} = \omega_1 \cdot J_1 + \omega_2 \cdot J_2. \tag{C.6}$$

Here J_{bal} is the balanced objective function constructed from the weighted long-term and short-term objective functions J_1 and J_2. The terms ω_1 and ω_2 are weighting factors of the short- and long-term objective, respectively. In the economic objective function (Eq. C.4) the discount rate b, apart from representing the time value of money, may also be used to weigh the importance of short-term against long-term performance. In that respect, the discount factor may also be seen as a weighting factor to balance the importance of multiple objectives. However, the difficulty in a balanced objective function lies in finding suitable weighting factors between the objectives. This is especially the case if the values of the multiple objective functions have different physical interpretations. Because the weighting factors strongly determine the characteristics of the optimal solution, a large number of trial-and-error runs with different weighting factors may be required to obtain a satisfactory one.

As an alternative, we propose a hierarchical optimization structure - sometimes referred to as the lexicographic method - that requires a prioritization of the multiple objectives, as described in Haimes and Li (1988). In this structure, optimization of a secondary objective function J_2 is constrained by the requirement that the primary objective function J_1 must remain close to its optimal value J_1^*. This structure can be expressed mathematically as

$$\max_{\mathbf{u}_{1:K}} J(\mathbf{u}_{1:K}) \tag{C.7}$$

$$s.t. \quad \mathbf{g}_{k+1}(\bar{\mathbf{u}}_k, \mathbf{x}_k, \mathbf{x}_{k+1}, \theta) = 0, \quad k = 0, \ldots, K-1, \quad \mathbf{x}_0 = \bar{\mathbf{x}}_0, \tag{C.8}$$

$$\mathbf{c}_{k+1}(\bar{\mathbf{u}}_{k+1}, \mathbf{x}_{k+1}) \leq 0, \quad k = 0, \ldots, K-1, \tag{C.9}$$

$$J_1^* - J_1(\mathbf{u}_{1:K}) \leq \varepsilon, \quad k = 0, \ldots, K-1, \tag{C.10}$$

where ε an arbitrary small value compared to J_1. Solving Eqs. C.7 through C.10 requires the knowledge of J_1^*, which is obtained through solving the optimization-problem equations (Eqs. C.1 through C.3). In the hierarchical optimization structure (Eqs. C.7 through C.10), the optimum value of the life-cycle objective function J_1 constrains optimization of the short-term objective. It should be noted that this ordering of long and short term by no means is unique. Alter- natively, one may want to optimize life-cycle performance under the condition that certain short-term production targets are met. In that case, the short-term goals act as constraints on the life-cycle optimization problem.

Redundant DOFs. Jansen et al. (2009) described that different solutions exist for the optimal control problem of maximizing an economic objective function over the life of the reservoir. The existence of multiple solutions was attributed to the ill-posedness of the optimal control problem. The ill-posedness also suggests that, even when optimality of an economic life-cycle objective is reached, not all DOFs of the decision variable space $\mathscr{U}$ are fixed and not all solution points in the optimal subset $\mathscr{S}$ are connected. This means that there may exist redundant DOFs in the optimization problem. Huesman et al. (2006, 2008) found similar results for economic dynamic optimization of plantwide operation. A consequence of these redundant DOFs is that, even if ε in Eq. C.10 is chosen equal to 0, DOFs are left to improve the secondary objective function J_2. A straightforward way of investigating this is to imbed Eq. C.10 as an equality constraint in the adjoint formulation by means of an additional Lagrange multiplier. Unfortunately, the adjoint functionality in the simulator used in our study was not yet capable of dealing with (additional) state constraints. Alternatively, unconstrained gradient information can be used to investigate the redundant DOFs, as described in the next section.

Quadratic Approximation of the Objective Function. In the following, we will use the short-cut notation $\mathbf{u}$ to indicate the input sequence $\mathbf{u}_{1:K} = (\mathbf{u}_1, \mathbf{u}_2, \ldots, \mathbf{u}_K)$. A solution $\mathbf{u}$ for which no constraints are active is an optimal solution $\mathbf{u}^*$ if and only if the gradients of J with respect to $\mathbf{u}$ are zero [i.e., $(\partial J/\partial \mathbf{u}) = 0$]. As a result, at $\mathbf{u}^*$, the gradients do not provide any information on possible redundant DOFs under the optimality condition on J. Second-order derivatives of J with respect to $\mathbf{u}$ are collected in the Hessian matrix $\mathbf{H} = \partial^2/\partial \mathbf{u}^2$. If $\mathbf{H}$ is negative definite, the considered solution $\mathbf{u}$ is an optimal solution, but no DOFs are left when the optimality condition on J holds. If $\mathbf{H}$ is negative semidefinite, the Hessian does not have full rank. An orthonormal basis $\mathbf{B}$ for the undetermined directions of $\mathbf{H}$ can then obtained through a singular value decomposition:

$$\mathbf{H} = \mathbf{U} \cdot \Sigma \cdot \mathbf{V}^T \tag{C.11}$$

The orthonormal basis $\mathbf{B}$ consists of those columns of $\mathbf{V}$ that relate to singular values of zero; i.e.

$$\mathbf{B} \triangleq (\mathbf{v}_i \mid \sigma_i = 0, \qquad i = 1, \ldots, N_{\mathbf{u}}) \tag{C.12}$$

where $N_{\mathbf{u}}$ is the number of DOFs in the input. Note that, because of the symmetrical nature of the Hessian matrix $\mathbf{H}$, the singular value decomposition may be replaced by a computationally more efficient eigenvalue decomposition, in which case the eigenvectors relating to eigenvalues equal to zero span the orthonormal basis $\mathbf{B}$.

Not all orthogonal directions spanned by the columns of $\mathbf{B}$ will be redundant DOFs. These directions are redundant DOFs if they are linear and if all higher-order derivatives are zero also, which, at this point in time, is impossible to prove for reservoir models. $\mathbf{B}$, however, is a basis for redundant DOFs for a quadratic approximation $\hat{J}$ of objective function J. Because $\hat{J}$ J can be considered to be an acceptable approximation for small deviations from $\mathbf{u}^*$, $\mathbf{B}$ can be regarded as an acceptable basis for the redundant DOFs for small deviations from $\mathbf{u}^*$.

Approximate Hessian Matrix. Unfortunately, no reservoir-simulation package is currently capable of calculating second-order derivatives. However, using the gradient information, second-order derivatives can be approximated. In our study, we used a forward-difference scheme:

$$\frac{\partial^2 J}{\partial u_i \partial u_j} \approx \frac{\nabla J_i(\mathbf{u} + h_j \mathbf{e}_j) - \nabla J_i(\mathbf{u})}{2h_j} + \frac{\nabla J_j(\mathbf{u} + h_i \mathbf{e}_i) - \nabla J_j(\mathbf{u})}{2h_i}, \tag{C.13}$$

where ∇J_i is the ith element of the gradient $\nabla J = (\partial J/\partial \mathbf{u})^T$, $\mathbf{e}_i$ is a canonical unit vector (i.e., a vector with a 1 at element i and 0 elsewhere), and h_i is the perturbation step size that relates to parameter u_i of $\mathbf{u}$. In total, $N_{\mathbf{u}+1}$ simulations (function evaluations) are required to obtain the approximate Hessian matrix $\hat{\mathbf{H}}$ at a particular optimal solution $\mathbf{u}^*$.

Alternatively, a reduced Hessian method could be used that approximates only that portion of the Hessian relevant for the subspace in which the Hessian is negative (or positive) definite; see Byrd and Nocedal (1990). If the Hessian is negative (or positive) semidefinite, the tangent space of this subspace will be equal to the null space of the complete Hessian matrix. This could lead to a significant reduction in computational burden, especially when the dimensions of the null space are large.

Hierarchical Optimization Method. Adopting the approximation of $\mathbf{H}$ as described in the preceding subsection, the following iterative procedure is proposed to attack the hierarchical optimization problem (Eqs. C.7 through C.10) with $\varepsilon = 0$:

1. Find a (single) optimal strategy u * that maximizes the primary objective function J_1 and use $\mathbf{u}_n = \mathbf{u}^*$, with $n = 0$, as a starting point in the secondary optimization problem, where n is the iteration index.

2. Approximate the Hessian matrix $\mathbf{H}$ of J_1 with respect to the input variables at (initial input) $\mathbf{u}_n$, and determine an orthonormal basis $\mathbf{B}$ for the null space of $\hat{\mathbf{H}}$

3. Find the improving direction $\mathbf{s}$ for the secondary objective function J_2 (e.g., the gradients $\partial J_2/\partial \mathbf{u}_n$.

4. Project $\mathbf{s}$ onto the orthonormal basis $\mathbf{B}$ to obtain projected direction $\mathbf{d}$, such that $\mathbf{d}$ is an improving direction for J_2 but does not affect J_1. The projection is performed using projection matrix $\mathbf{P}$ according to

$$\mathbf{d} = \mathbf{P} \cdot \mathbf{s}^T \tag{C.14}$$

$$\mathbf{P} = \mathbf{B}\mathbf{B}^T \tag{C.15}$$

5. Update $\mathbf{u}_n$ using projected direction $\mathbf{d}$ in a steepest-ascent method,

$$\mathbf{u}_{n+1} = \mathbf{u}_n + \tau \cdot \mathbf{d} \tag{C.16}$$

   where τ is an appropriately small step size such that the quadratic approximation of J_1 is justified.

6. Perform Steps 2 through 5 until convergence of J_2.

Note that, for the improving direction **s** for secondary objective function J_2, alternatives exist besides the steepest-ascent direction $\partial J_2/\partial \mathbf{u}$ (e.g., using a quasi-Newton or conjugate gradient method). This does not change the steps of the hierarchical optimization method but may speed up convergence of the procedure. In the next section, a numerical example will be presented in which the iterative hierarchical optimization structure is tested on a 3D heterogeneous reservoir model.

C.4 Example

We applied the hierarchical optimization procedure to a 3D oil- reservoir model, introduced in Van Essen et al. (2009b). The life cycle of the reservoir covers a period of 3,600 days. The reservoir model consists of 18,553 gridblocks, as depicted in Fig. C.1, and has dimensions of $480 \times 480 \times 28m$. Its geological structure involves a network of fossilized meandering channels. The average reservoir pressure is 400 bar. All remaining geological and fluid properties used in this example are presented in Table C.1. The reservoir model contains eight injection wells and four production wells. The production wells are modeled using a standard Peaceman well model, which relates the source (output) term **y** to the difference between the well pressure and gridblock pressure:

$$y_k^j = w_j \cdot \left(p_{wf,k}^j - p_k^j \right), \tag{C.17}$$

where p_{wf} is the flowing wellbore pressure (bottomhole pressure), j is the index of the gridblock containing the well, and p_k^j is the pressure of the gridblock in which the well is located. The well index w_j is a constant, which contains the well's geometric factors and the rock and fluid properties of the reservoir directly around the well. The wells operate at a constant bottomhole pressure p_{wf} of 395 bar. The flow rates of the injection wells can be manipulated directly (i.e., the control input **u** involves injection flow-rate trajectories for each of the eight injection wells). The minimum rate for each injection well is 0.0 m^3/d; the maximum rate is set at 79.5 m^3/d. The control input **u** is reparameterized in time using a zero-order-hold scheme with input parameter vector θ. For each of the eight injection wells, the control input **u** is reparameterized into four time periods t_θ of 900 days during which the injection rate is held constant at value θ_i. Thus, the input parameter vector θ consists of $8 \times 4 = 32$ elements.

Life-Cycle Optimization. The objective function for the life-cycle optimization was defined in terms of NPV, as defined in Eq. C.4, with r_o = 126 USD/m^3, $r_w p$ = 19

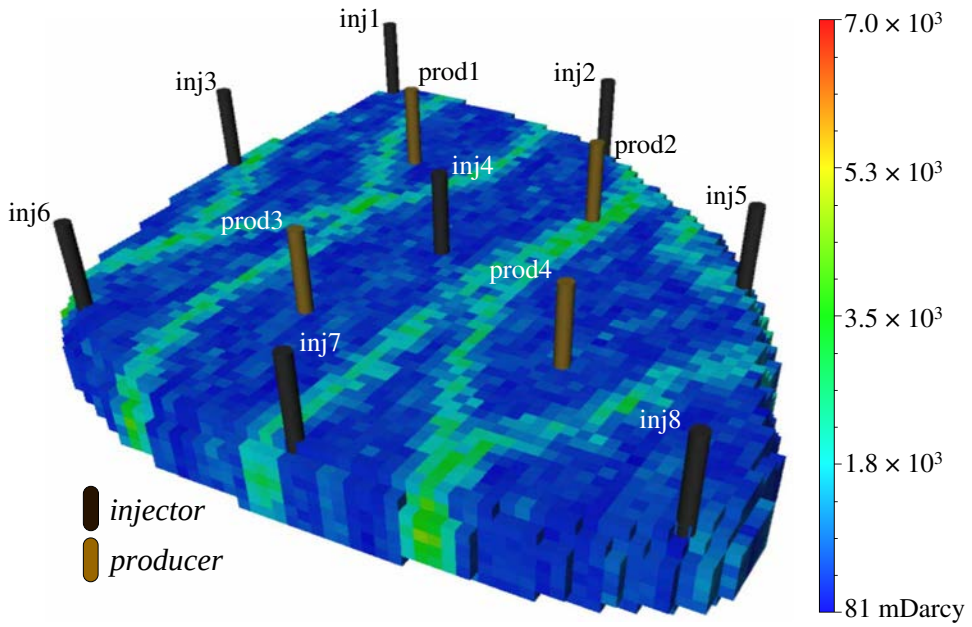

Figure C.1 : 3D oil-reservoir model (Van Essen et al. (2009b)).

Table C.1 : *Geological and fluid properties for example*

Property	*Value*	*Units*
Φ	0.20	-
ρ_o (at 1 bar)	900	kg/m^3
ρ_w (at 1 bar)	1000	kg/m^3
c_o	1.00×10^{-5}	$1/bar$
c_w	1.00×10^{-5}	$1/bar$
μ_o	5.00×10^{-3}	$Pa \cdot s$
μ_w	1.00×10^{-3}	$Pa \cdot s$
p_{cow}	0	bar

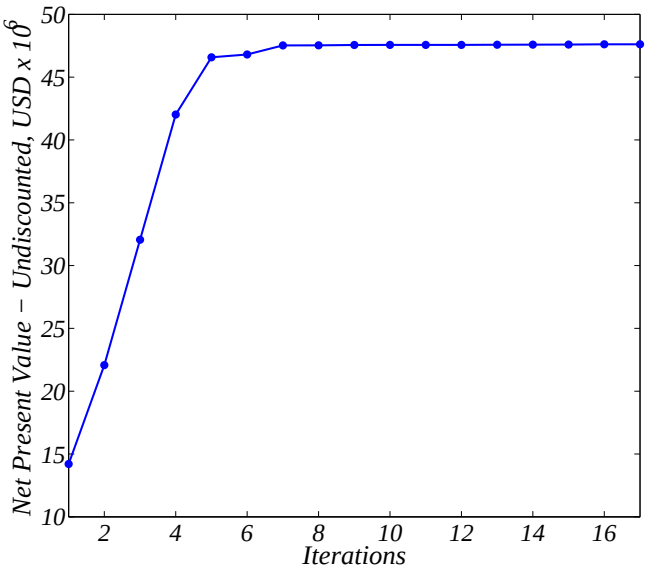

Figure C.2 : Plot of the value of the objective function (NPV) against the iteration number of the life-cycle optimization problem. The iterations of the line-search algorithm are not shown in this plot.

USD/m^3 and $r_w i$ = 6 USD/m^3. The discount rate b was set to 0. Thus, the life-cycle objective relates to undiscounted cumulative cashflow. The optimal input - denoted by $\mathbf{u}_\theta^*$ - was obtained using a steepest-ascent scheme together with a line-search algorithm. It was terminated after 17 iterations (excluding the iterations of the line search) when the line-search algorithm was not able to find a significant improvement in NPV. Convergence to the optimal solution of the life-cycle optimization problem may be speeded up using a quasi-Newton or conjugate gradient method. However, as efficiency of the optimization algorithm was not the objective of this study, the more simplistic steepest-ascent scheme was used. The value of NPV against the iteration number can be observed in Fig. C.2. The final optimal input $\mathbf{u}_\theta^*$ of the life-cycle optimization problem is shown in Fig. C.3.Note that none of the input constraints (Eq. C.9) is active for $\mathbf{u}_\theta^*$. The value of the objective function corresponding to input $\mathbf{u}_\theta^*$ is USD 47.6×10^6.

Hierarchical Optimization. In a realistic setting, short-term pro- duction optimization will be aimed at maximizing the oil production over the short time horizon of interest, while repeating this exercise as time goes by (i.e., using a moving-horizon approach). In view of the simplicity of the presented example, this short-term production objective, which involves successive re-optimization, is replaced by an objective

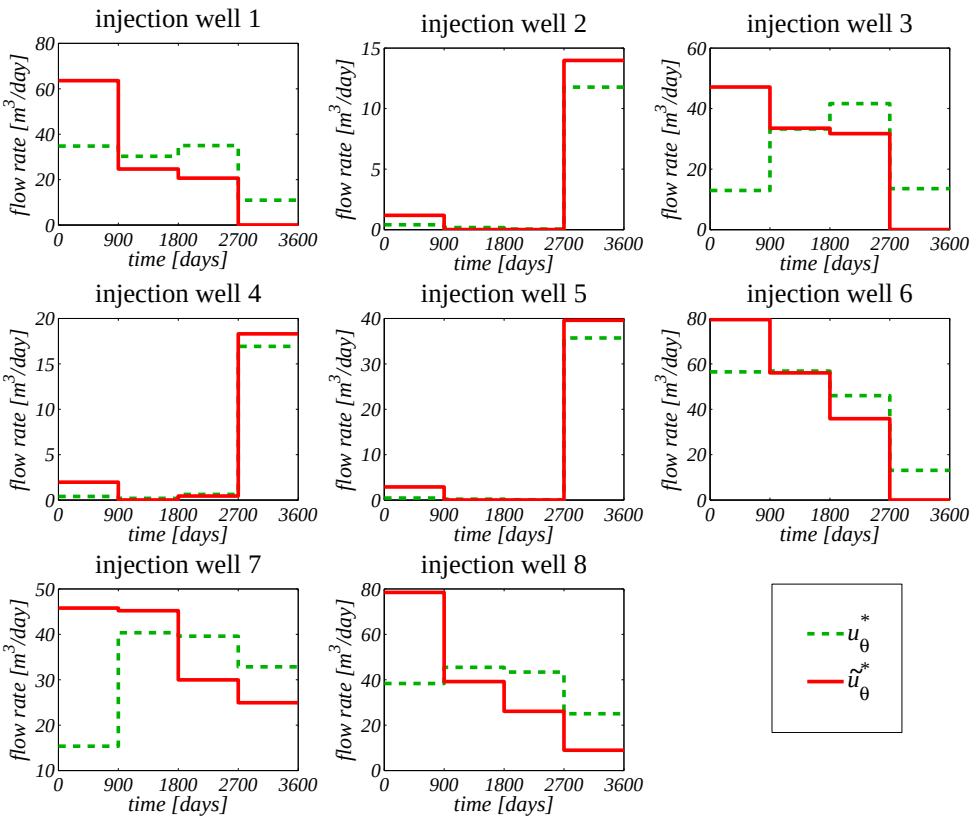

Figure C.3 : Input trajectories for each of the eight injection wells for the initial optimal solution $\mathbf{u}^*_\theta$ to J_1 (green dashed line) and the optimal solution $\tilde{\mathbf{u}}^*_\theta$ after the constrained optimization of J_2 (red solid line)

that does not require re-optimization over the production life, while still emphasizing the importance of short-term production. Therefore, we chose the secondary objective J_2 to be identical to the primary objective function but with the addition of a very high annual discount rate b of 0.25. As a result, short-term production is weighed much more heavily than future production. However, as stated before, the particular choice of primary and secondary objective has no effect on the hierarchical procedure itself. Note that, because of the very high discount rate, the actual value of J_2 no longer has a realistic meaning in an economic sense.

Next, we applied the hierarchical approach as presented in the preceding subsection. The total number of simulation runs needed to approximate the Hessian $\hat{\mathbf{H}}$ was 33, but the overall simulation time was kept within acceptable limits by parallel processing the simulations. Because this example involves a numerical model and an

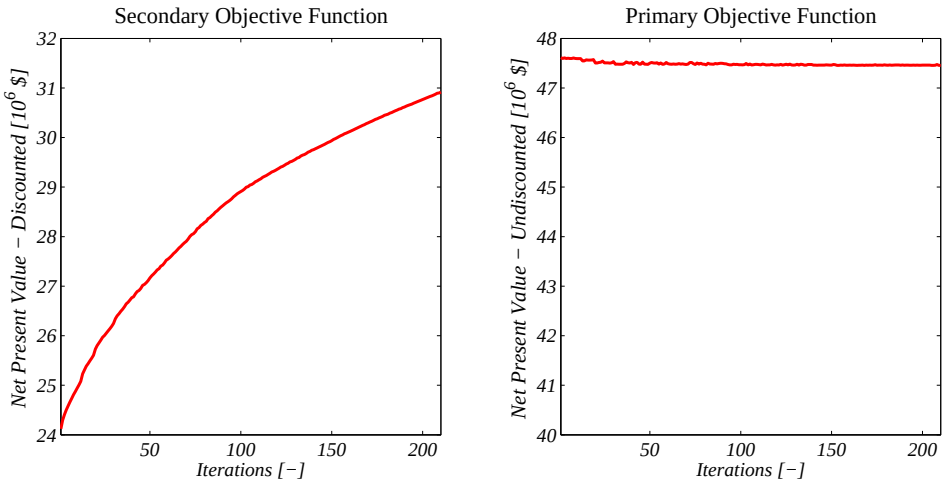

Figure C.4 : Values of the secondary objective function J_2 and the primary objective function J_2 plotted against the iteration number for the constrained secondary optimization problem.

approximation of the second-order derivatives, we relaxed the selection criterion for **B**. Those columns $\mathbf{v}_i$ of **V** were selected that correspond to singular values for which $\sigma_i/\sigma_1 < 0.02$ instead of $\sigma_i = 0$. The projected gradients **d** were again used in a steepest-ascent scheme. In order to ensure that $\mathbf{u}_{\theta,n+1}$ remains close to $\mathbf{u}_{\theta,n}$, **d** was normalized by dividing **d** by its largest absolute element. A step size τ of 1 was used in the steepest-ascent scheme, such that the largest update in the water-injection rates remained equal to 1. Through trial-and-error, this step size was considered appropriately small such that the quadratic approximation of J_1 was justified. The step size was kept constant during execution of the hierarchical optimization procedure because no downscaling was required to find an improving control input for J_2. Because of computing time restrictions, the hierarchical optimization of J_2 was terminated after 210 iterations, with final control input $\tilde{\mathbf{u}}^*_\theta$. The relatively slow convergence was because of the small step size required to allow for the quadratic approximation of J_1, but convergence may improve when a better improving direction for J_2 is used. At the start of the hierarchical optimization, the number of redundant DOFs was equal to 19, out of a total of 32 DOFs. During the 210 iterations, this number remained more or less constant.

To evaluate the results of the hierarchical optimization, the optimization of J_2 was also performed without projection on **B**. As a result, the obtained control input - denoted by $\tilde{\mathbf{u}}_\theta$ - in that case does not ensure optimality of J_1. Fig. C.4 displays the values of J_1 and J_2 plotted against the iteration number for the hierarchical optimization problem. It shows a considerable increase of J_2 of 28.2% and a slight drop of J_1 of -0.3%. In Fig. C.3, the input strategy after the final iteration step is presented. It

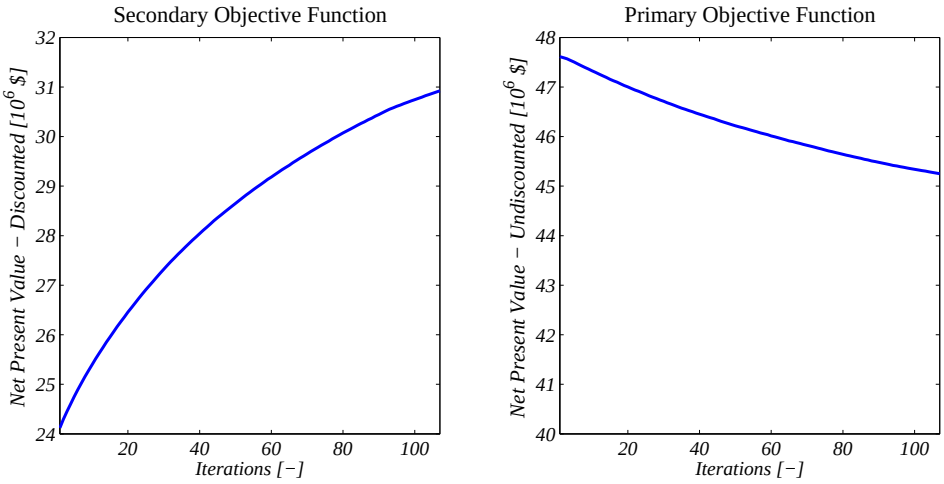

Figure C.5 : Values of the secondary objective function J_2 and the primary objective function J_1 plotted against the iteration number for the secondary optimization problem, no longer constrained by the orthonormal basis **B**.

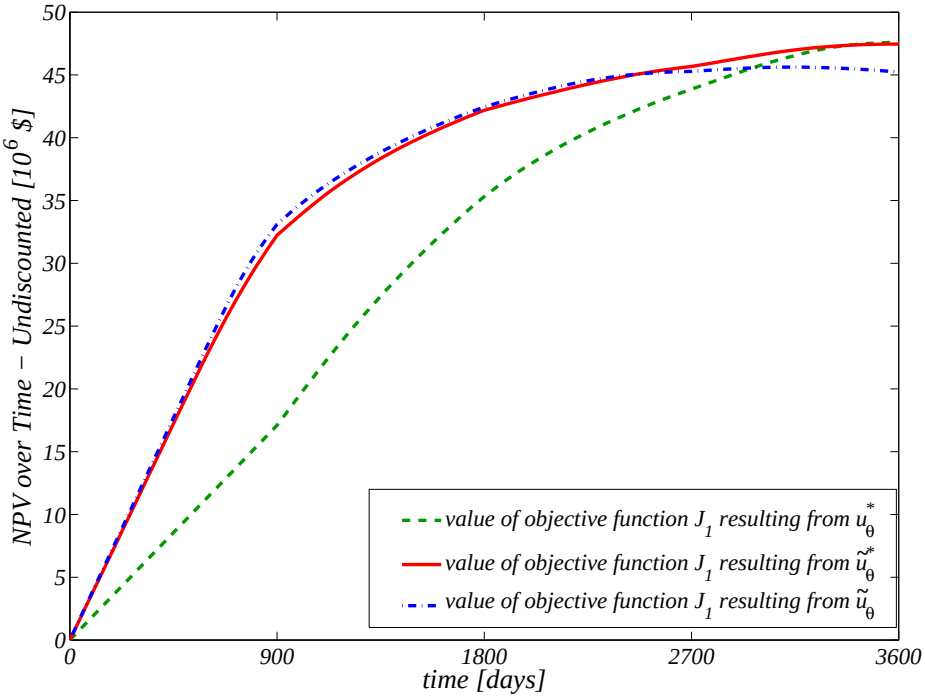

Figure C.6 : Value of the primary objective function J_1 over time for initial optimal input $\mathbf{u}_\theta^*$ to J_1 (dashed green line), the optimal input $\tilde{\mathbf{u}}_\theta^*$ after the constrained optimization of J_2 (red solid line), and input $\mathbf{u}_\theta$ after the unconstrained optimization of J_2 (blue dashed/dotted line).

can be observed that the injection strategy shows a substantial increase in injection rates at the beginning of the production life and a decrease at the end.

As a comparison, we repeated the optimization of J_2 starting from $\mathbf{u}_\theta^*$ with the difference that it was no longer constrained by the requirement that J_1 remain close to J_1^* (i.e., Eq. C.10 was omitted). The optimization procedure was terminated after 107 iterations when the improvement of J_2 was equal to 28.2% (i.e., the final value of J_2 in the constrained optimization case). The values of J_1 and J_2 plotted against the iteration number for the unconstrained optimization of J_2 are shown in Fig. C.5. Again an increase in J_2 of 28.2% is realized, but now at a cost of a decrease in J_1 of -5.0%. Finally, Fig. C.6 shows the value of the primary objective function J_1 over time until the end of the producing reservoir life for $\mathbf{u}_\theta^*$, $\tilde{\mathbf{u}}_\theta^*$ and $\tilde{\mathbf{u}}_\theta$. Input $\tilde{\mathbf{u}}_\theta^*$ shows a steeper ascent of J_1 than $\mathbf{u}_\theta^*$, while their final values are nearly equal. Input $\tilde{\mathbf{u}}_\theta$ shows initially the same steep ascent, but J_1 drops toward the end of the life of the reservoir.

C.5 Alternative Methods

The presented hierarchical optimization approach is computationally very demanding and becomes infeasible for more realistic reservoir models with an increased number of input parameters, even when reduced-Hessian techniques are used. It should be noted, however, that execution of the hierarchical optimization procedure does not require knowledge of all redundant DOFs explicitly. In theory, the inequality constraint (Eq. C.10) could be incorporated in the adjoint formulation through the use of an additional Lagrange multiplier, by which the calculation of second-order derivatives is avoided altogether. However, this would require modifications to the reservoir simulator, and, therefore, we did not pursue this route. An alternative method to solve the hierarchical optimization problem without explicitly calculating the redundant DOFs is through the use of a balanced objective function as described by Eq. C.6, with the variation of using weighting functions Ω_1 and Ω_2 instead of weighting factors ω_1 and ω_2:

$$J_{bal} = \Omega_1 \cdot J_1 + \Omega_2 \cdot J_2, \tag{C.18}$$

where Ω_1 and Ω_2 are switching functions of J_1 and J_1^* that take on values of 1 and 0 or vice versa:

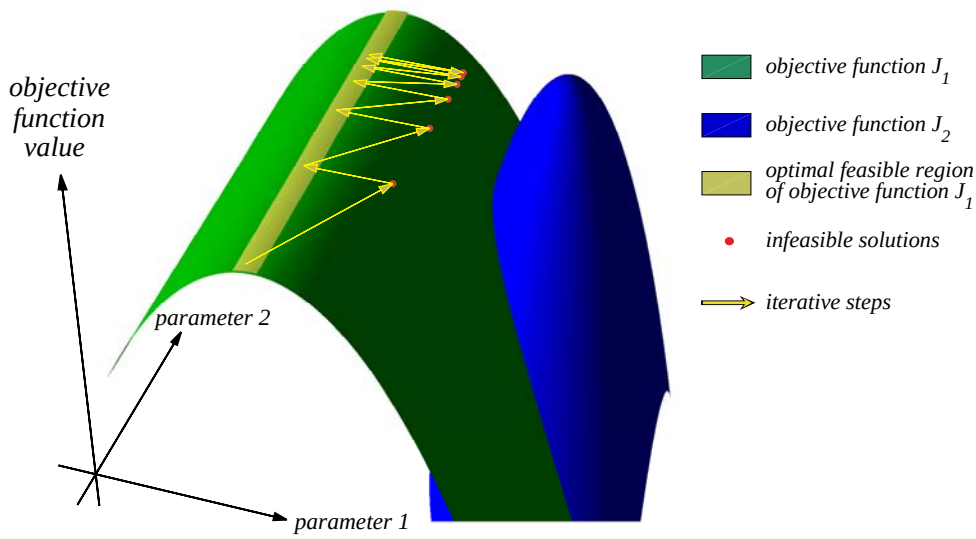

Figure C.7 : Schematic representation of the iterative process of solving a hierarchical optimization problem using an objective function as described by Eqs. C.18, C.19 and C.20. The process converges toward a final solution in a zigzag fashion, moving into and out of the feasible region bounded by the optimal solutions of the primary objective function J_1.

$$\Omega_1(J_1) = \begin{cases} 1 & \text{if } J^* - J_1 > \varepsilon \\ 0 & \text{if } J^* - J_1 \leq \varepsilon \end{cases} \tag{C.19}$$

$$\Omega_2(J_1) = \begin{cases} 0 & \text{if } J^* - J_1 > \varepsilon \\ 1 & \text{if } J^* - J_1 \leq \varepsilon \end{cases} \tag{C.20}$$

Here, ε is the threshold value as defined in the inequality constraint (Eq. C.10). The gradient of J_{bal} with respect to the input parameters $\mathbf{u}$ for iteration $n+1$ is then simply

$$\left.\frac{\partial J_{bal}}{\partial \mathbf{u}}\right|_{n+1} = \Omega_1(J_{1,n}) \cdot \left.\frac{\partial J_1}{\partial \mathbf{u}}\right|_{n+1} + \Omega_2(J_{1,n}) \cdot \left.\frac{\partial J_2}{\partial \mathbf{u}}\right|_{n+1} \tag{C.21}$$

Execution of the optimization problem using balanced objective function (Eq. C.18) sequentially gives improving directions for either J_1 or J_2. With each iteration, the value of J_2 either increases while the value of J_1 decreases or vice versa, as the solution moves to and from the feasible region with respect to the inequality constraint (Eq. C.10). When no redundant DOFs are available, the control input would jump between two fixed solutions, of which only one would be feasible. However, in the

case where redundant DOFs do exist, improvement of J_2 is possible without compromising Eq. C.10 and convergence of the hierarchical optimization will occur in a zigzag fashion, as schematically represented in Fig. C.7.

This switching method has the advantage that numerous evaluations of the system and adjoint equations are avoided: Only two runs (in parallel execution) of the system and adjoint equations are necessary per iteration, regardless of the number of input parameters. Second, the method is straightforward to implement. Finally, it provides the possibility to set a bound explicitly on the deviation of J_1 from J_1^* by choosing an appropriate value for ε. A disadvantage of the method is the slow convergence because of the infeasible solution steps. Also, some tuning of τ will be required to account for the fact that the Euclidean length of vectors $\partial J_1/\partial \mathbf{u}$ and $\partial J_2/\partial \mathbf{u}$ is different. As with the null-space approach, replacing the gradient vector $\partial J_2/\partial \mathbf{u}$ with an improving direction $\mathbf{s}$ for J_2 (obtained through, for example, a quasi-Newton or conjugate gradient method) may speed up convergence.

Example. The switching method was again applied to the 3D oil- reservoir model. Although the number of input parameters does not pose a problem to the switching method, again the control input was parameterized using 32 parameters to allow for a fair comparison with previous results. For the choice of threshold value ε, the maximum deviation of J_1 from J_1^* from the null-space method was used (-0.3%) (i.e., $\varepsilon = 0.997 \times J_1^*$). Just as in the null-space example, optimization of J_2 using the objective function (Eq. C.18) was started from $\mathbf{u}_\theta^*$. The optimization procedure was again terminated when a feasible solution $\tilde{\mathbf{u}}_{\theta,sw}^*$ was found that gave an improvement of J_2 of 28.2%. The results of the hierarchical optimization problem using the switching method as shown in Fig. C.7.

Fig. C.8 shows that the switching method is able to give results for the hierarchical optimization problem similar to those of the null- space method, while requiring much fewer evaluations of the system and adjoint equations per iteration (2 vs. 33). The fact that the switching method also needs fewer iterations to reach the same level of improvement of J_2 is the result of better tuning of the algorithm's parameters and is not inherent to the method. In Fig. C.9 the feasible input strategy $\tilde{\mathbf{u}}_{\theta,sw}^*$ reached after the final iteration step of the switching method is presented, together with the initial input strategy $\mathbf{u}_\theta^*$ and the final input strategy $\tilde{\mathbf{u}}_\theta^*$ of the null-space method.

C.6 Discussion and Conclusions

Discussion. In the hierarchical approach presented in this paper, long-term (life-cycle) recovery optimization was selected as the primary objective, while short-term

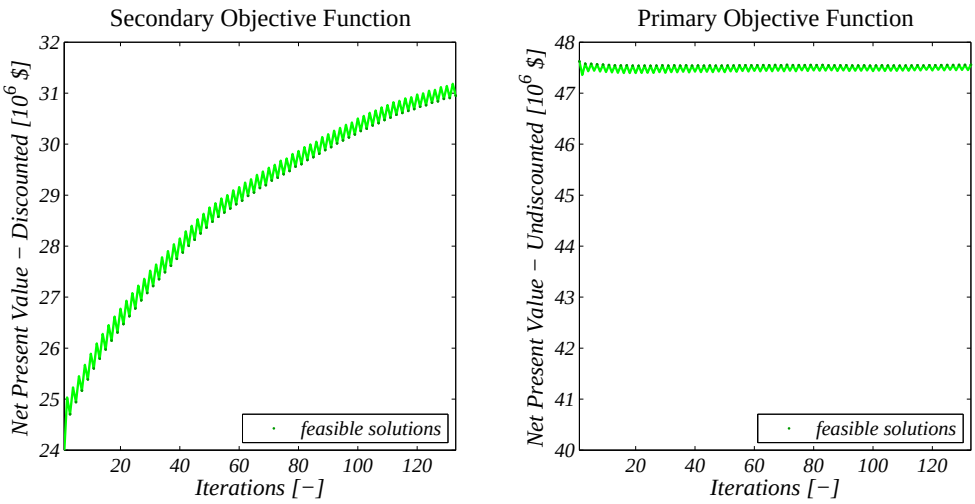

Figure C.8 : Values of the secondary objective function J_2 and the primary objective function J_1 plotted against the iteration number for the secondary optimization problem, using the switching method. The "feasible solutions" marks relate to those solutions that are feasible with respect to the inequality constraint (Eq. C.10).

production optimization served as the secondary objective. However, the concept of using the redundant DOFs of the primary objective to improve a secondary objective is not limited to this specific choice. Alternatively, the secondary objective function may be used, for example, to search for a smoother production profile, a bang/bang production profile [see Zandvliet et al. (2007)], or a persistently exciting production profile [see Zandvliet et al. (2008)]. Also, a different primary objective function may be chosen (e.g., ultimate recovery or short- term production), provided that it offers enough redundant DOFs to improve a secondary objective function.

In this paper, gradient information was used to prove the existence of redundant DOFs with respect to a life-cycle objective function. Moreover, gradients were at the heart of the presented null-space method to solve the hierarchical optimization problem. It should be noted, however, that there is no need to explicitly determine the null space using the gradients, as was shown using the switching method. Consequently, the optimization method used to attack the hierarchical optimization problem does not necessarily have to be gradient-based, which implies that alternative optimization methods (e.g., genetic algorithms) may also be considered.

Conclusions. We addressed the issue of multiple (long-term and short-term) objectives in oil-production optimization and investigated a hierarchical approach by means of a numerical experiment. On the basis of this experiment, we conclude that

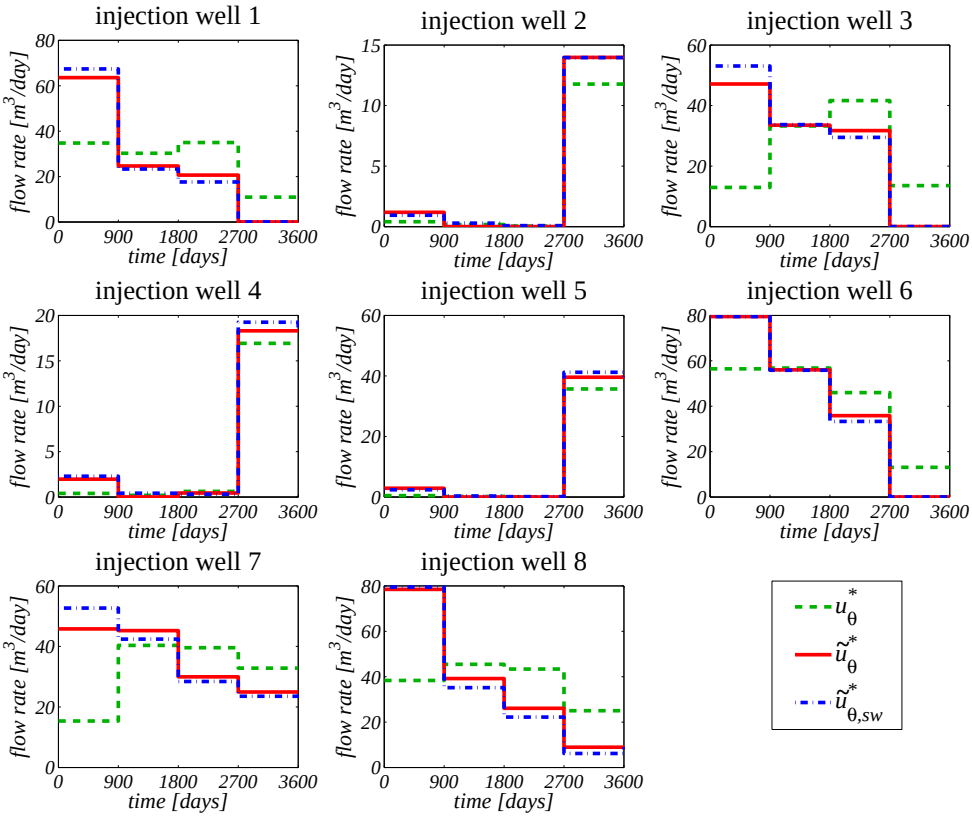

Figure C.9 : Input trajectories for each of the eight injection wells for the initial optimal solution $\mathbf{u}^*_\theta$ to J_1 (green dashed line), the final solution $\tilde{\mathbf{u}}^*_\theta$ of the null-space method (red solid line), and the final solution $\tilde{\mathbf{u}}^*_\theta$ of the switching method (blue dashed/dotted line).

- There exist redundant DOFs in the input strategy u with respect to the optimality of the long-term objective. This implies the existence of an optimal subset $\mathscr{S}$ of connected optimal solutions within the solution space $\mathscr{U}$.

- The redundant DOFs create enough freedom to improve a secondary, short-term objective function significantly. Moreover, the difference between the initial and final input strategy to the secondary optimization problem is substantial. This suggests that $\mathscr{S}$ occupies a considerable space within decision variable space $\mathscr{U}$.

- The presented hierarchical optimization procedure provides a method to incorporate short-term performance objectives into the problem setting of maximizing life-cycle performance of oil recovery. Using the hierarchical structure, optimization of the secondary objective can be obtained without significantly compromising the primary objective.

- A theoretically rigorous method to select the redundant DOFs in the primary objective function requires computation of the Hessian of the objective function with respect to the control variables. This makes the theoretically rigorous method computationally too demanding for application to realistically sized problems.

- Nearly identical results can be obtained with the aid of a somewhat more pragmatic, but computationally much more efficient, switching method that, starting from an optimal long-term strategy, alternately optimizes the primary and secondary objective functions.

C.7 Nomenclature

b	=	*discount rate*
$\mathbf{B}$	=	*basis for redundant DOFs*
c	=	*compression*
$\mathbf{d}$	=	*projected search direction on* $\mathbf{B}$
$\mathbf{H}$	=	*Hessian matrix*
$\hat{\mathbf{H}}$	=	*approximate Hessian matrix*
J	=	*objective function*
$\hat{J}$	=	*second-order approximation of* J
k	=	*time step counter*
n	=	*iteration index*
p	=	*pressure*
$\mathbf{P}$	=	*projection matrix*
r	=	*revenues/costs*
$\mathbf{s}$	=	*improving direction for* J_2
S	=	*saturation*
t_k	=	*time at time step* k
$\mathbf{u}$	=	*input vector*
$\mathbf{u}^*_\theta$	=	*optimal* $\mathbf{u}$ *for* J_1
$\tilde{\mathbf{u}}^*_\theta$	=	$\mathbf{u}$ *optimized for* J_2 *constrained by* $\mathbf{B}$
$\tilde{\mathbf{u}}_\theta$	=	$\mathbf{u}$ *optimized for* J_2 *not constrained by* $\mathbf{B}$
w	=	*well constant*
$\mathbf{x}$	=	*state vector*
$\bar{\mathbf{x}}_0$	=	*prescribed value of initial conditions*
$\mathbf{y}$	=	*output vector*
Δt_k	=	*time interval of Timestep* k
ε	=	*tolerance of optimality constraint*
μ	=	*viscosity*
τ	=	*step size of algorithm*
τ_t	=	*reference time*
ϕ	=	*porosity*
ω	=	*weighting factor*
Ω	=	*weighting function*
$\mathscr{S}$	=	*optimal subset of* $\mathscr{U}$
$\mathscr{U}$	=	*decision variable space*

Subscripts

cow	=	*oil/water capillary*
o	=	*oil*
wf	=	*flowing well bore*
wi	=	*injected water*
wp	=	*produced water*
1	=	*primary*
2	=	*secondary*

Superscripts

$*$	=	*optimal*

C.8 Acknowledgements

This research was carried out within the context of the Integrated Systems Approach to Petroleum Production (ISAPP) knowledge centre. ISAPP is a joint project between Delft University of Technology, Shell International Exploration and Production, and the Dutch Organization for Applied Scientific Research.

Appendix D

Robust Waterflooding Optimization

This appendix has been published before as "Van Essen, G.M., Zandvliet, M.J., Van den Hof, P.M.J., Bosgra, O.H., and Jansen, J.D. (2009). Robust waterflooding optimization of multiple geological scenarios. *SPE Journal*, 14(1), 202210. doi:10.2118/102913-PA. SPE 102913-PA.".

D.1 Introduction

In this paper, we consider the secondary-recovery phase of a petroleum reservoir using waterflooding. In this case, a number of injection and production wells are drilled to preserve a steady reservoir pressure and sweep the reservoir. The use of smart wells expands the possibilities to manipulate and control fluid-flow paths through the oil reservoir. The ability to manipulate (to some degree) the progression of the oil/water front provides the possibility to search for a control strategy that will result in maximization of ultimate oil recovery.

Dynamic optimization of waterflooding using optimal control theory has significant potential to increase ultimate recovery by delaying water breakthrough and increasing sweep, as has been shown in various studies (Brouwer and Jansen (2004)). However, optimal control strategies often lack robustness to geological uncertainties. By discarding these uncertainties, the sensitivity to a possibly large system/model mismatch is not taken into account within the optimization procedure. As a result, the optimal control strategy may cease to be optimal or may even result in very poor performance.

Dealing with uncertainty is a topic encountered in many fields related to modeling and control. It can essentially be divided into two different strategies, which are not mutually exclusive: reducing the uncertainty itself using measurements [i.e., history matching (Landa and Horne (1997), Li et al. (2003)] and reducing the sensitivity to the uncertainty. In this paper, we consider a situation in which no production data are assumed to be available, which rules out any history-matching approach to reduce the geological uncertainty. Our study forms part of a larger research project to enable closed- loop, model-based reservoir management (Jansen et al. (2005)).

A suggested approach from the process industry, to optimization problems that suffer from vast uncertainty and limited measurement information, is the use of a so-called RO technique (Srinivasan et al. (2003), Terwiesch et al. (1998), Ruppen et al. (1995)). In RO, the optimization procedure is performed over a set of realizations, actively accounting for the influence of the uncertainty. The implementation of multiple realizations within the optimization process has been addressed by Yeten et al. (2002). However, their study deviates in the way the realizations are incorporated in the objective function, in the optimization method, and in the number of realizations. The goal of our paper is to present an RO procedure on the basis of a set of 100 realizations of a 3D oil/water reservoir, which leads to a control strategy that accounts explicitly for geological uncertainty.

D.2 Theory

Optimal Control. We consider an optimal control problem in which the injection-flow rates and production-flow rates are manipulated directly (i.e., a rate-constrained scenario). The objective is to maximize the simple NPV of the cumulative oil and water production over a fixed time horizon. The objective function (or cost function) is thus given by (Brouwer and Jansen (2004)):

$$J\left(\mathbf{q}_{1:k}\right)=\sum_{k=1}^{K}J_K\left(\mathbf{q}_{1:K}\right)=\sum_{k=1}^{K}\frac{\Delta_{t_k}\left[-r_o\cdot q_{o,k}(\mathbf{q}_{1:k})+r_{wp}\cdot q_{wp,k}(\mathbf{q}_{1:k})-r_{wi}\cdot q_{wi,k}(\mathbf{q}_{1:k})\right]}{\left(1+b_\tau\right)^{\frac{t_k}{\tau}}} \tag{D.1}$$

where r_o is the oil revenue, r_{wp} the water production costs, and r_{wi} the water injection costs, which are all assumed constant. The variable $q_{o,k}$ represents the total flow rate (i.e. summed over all wells) of produced oil, $q_{wp,k}$ is the total flow rate of produced water and q_{wi} is the total flow rate of injected water, at discrete time k. We use the convention that injection rates are positive, and production rates negative, such that

the oil revenues in the objective function (D.1) are positive and the costs are negative. The term K represents the total number of time steps k, Δt_k the time interval of time step k and t_k the cumulative time until k. The term represents the total flow rate (i.e. summed over all wells) of produced oil, the total flow rate of produced water, and the total flow rate of injected water, at discrete time k. The variable $\mathbf{q}_k$ is a vector of the liquid flow rates in all wells at discrete time k, which act as the control variables (input variables) in our optimization problem, at discrete time k. The colon in the subscript is used to indicate a sequence (i.e. $\mathbf{q}_{1:K}$ implies q_k, $k = 1,\ldots,K$). The oil and water production rates $q_{o,k}$ and $q_{wp,k}$ at discrete time k are functions of the total flow rates $\mathbf{q}_k$ through their dependence on the (saturation-dependent) fractional flow in the well grid blocks. The saturations are in turn functions of the current and all previous inputs $\mathbf{q}_{1:k}$, such that $q_{o,k}$ and $q_{wp,k}$ become complex functions of $\mathbf{q}_{1:k}$. The parameter b in the denominator of equation (D.1) is the discount rate per time unit τ, and is considered to be equal to zero within this paper. The optimization problem involves finding the optimal injection and production flow rates $\mathbf{q}_{1:K}$ that maximize the performance measure $J(\mathbf{q}_{1:K})$, while honoring the dynamic system equations. We use a gradient-based optimization algorithm to converge to the (possibly locally) optimal flow rates. The gradients are the transposes of the derivatives, i.e. , and the derivatives. We use a gradient-based optimization algorithm to converge to the (possibly locally) optimal flow rates. The gradients are the transposes of the derivatives (i.e. $\nabla J_k = (\frac{\mathrm{d}J}{\mathrm{d}\mathbf{q}_k})^T$, and the derivatives

$$\frac{\mathrm{d}J}{\mathrm{d}\mathbf{q}_k} = \sum_{\kappa=k}^{K} \frac{\partial J_\kappa}{\partial \mathbf{q}_k}, \quad k = 1,\ldots,K \tag{D.2}$$

are obtained by solving a system of adjoint equations as described by e.g. Brouwer and Jansen (2004) and Sarma et al. (2005). (See Appendix A for a brief description of the adjoint-based method to obtain the gradient information). The gradients are used in a steepest ascent (SA) algorithm to iteratively converge to the optimal input trajectory:

$$\mathbf{q}_k^{i+1} = \mathbf{q}_k^i + \alpha \left(\frac{\mathrm{d}J}{\mathrm{d}\mathbf{q}_k} \right)^T, \quad k = 1,\ldots,K, \tag{D.3}$$

where α is the step size of the algorithm, and i is the iteration counter. A line search to find the optimal step size along the direction of the greatest ascent could be used to speed up the iterative procedure, but because this study is not aimed at improving convergence speed, we used a fixed α for simplicity's sake.

Using Eq. (D.3), a situation may occur in which the new flow rates $\mathbf{q}_k^{i+1}$, $k = 1,\ldots,K$ do not obey the constraint equations as addressed in more detail in equations (A.7)

and (A.8) in Appendix A. In order to ensure that they comply with the constraints, feasible search directions $\mathbf{d}_k$ of the gradient vectors $(\frac{\mathrm{d}J}{\mathrm{d}\mathbf{q}_k})^T$ need to be determined. Sarma et al. (2008) propose an effective, but rather complicated method to obtain feasible directions if there are state constraints. de Montleau et al. (2006) and Kraaijevanger et al. (2007) also discuss production optimization under state constraints, however, because we are dealing with linear equality and inequality constraints on the input variables only, we can simply apply the gradient projection method as described in Luenberger (1984), to determine $\mathbf{d}_k$. Using $\mathbf{d}_k$, the SA algorithm thus becomes:

$$\mathbf{q}_k^{i+1} = \mathbf{q}_k^i + \alpha \cdot \mathbf{d}_k \tag{D.4}$$

Determining a feasible search direction $\mathbf{d}_k$ however does still not guarantee that $\mathbf{q}_k^{i+1}$ is feasible, given the fixed step size α. It merely ensures that a certain $\alpha > 0$ exists for which it is feasible. For this reason, after $\mathbf{d}_k$ is determined, it is subsequently checked for its feasibility. If this is not the case, is scaled down until a feasible $\mathbf{q}_k^{i+1}$ is reached. Reducing the step size slows down the convergence rate of the steepest ascent method. However, we note that checking if feasibility of the input (flow rates) is violated and subsequently finding a reduced step size that ensures feasibility does not require any additional simulation runs.

Geological scenarios. The need to model uncertainty is an inevitable result of the modeling process itself; it is simply impractical or impossible to capture all dynamics and properties of a real dynamical system. Often, adopting an uncertain model description in a model-based control scheme does not create problems. The modeling error may be small, and output and measurement data can be used to correct the predicted state and parameter values to their real values.

Unfortunately, this does not hold for control strategies based on reservoir models. The geological uncertainty is generally profound, due to the noisy and sparse nature of seismic data, core samples and borehole logs. Besides, during production this uncertainty can be reduced only marginally, as the measurement and output data provide only limited information on the true values of the (large number of) states and model parameters.

The consequence of a large number of uncertain model parameters (θ) is the broad range of possible models that may satisfy the seismic and core sample data. Nevertheless, in many cases, for reasons of simplicity, a single reservoir model is adopted in which the uncertain parameters θ are converted to deterministic parameters η by taking their expected values (i.e. $\eta := E[\theta]$. However, because we are looking at the

NPV (denoted by J) as a measure of performance, we are far more interested in the expected NPV over the uncertainty space Θ (spanned by the uncertain parameters θ). It should be noted that this is generally not the same as taking the expected value of the uncertain parameters:

$$E_\theta\left[J(\mathbf{q}_{1:K},\theta)\right] \neq J(\mathbf{q}_{1:K},E_\theta[\theta]), \quad \theta \in \Theta \tag{D.5}$$

A better approximation of the expected NPV may be obtained by discretizing the uncertainty space Θ, resulting in a finite number (N_r) of realizations of θ and calculating the expected value over the discretized uncertainty space:

$$E_\theta\left[J(\mathbf{q}_{1:K},\theta)\right] \approx E_{\theta_d}\left[J(\mathbf{q}_{1:K},\theta_d)\right], \quad \theta_d \triangleq \{\theta_1,\ldots,\theta_{N_r}\} \tag{D.6}$$

where θ_d is the finite set of (deterministic) realizations of θ. In the special case that the realizations are equiprobable, the right-hand side of equation (D.6) is simply the average of the Js, given by:

$$E_{\theta_d}\left[J(\mathbf{q}_{1:K},\theta_d)\right] = \frac{1}{N_r}\sum_{i=1}^{N_r} J\left(\mathbf{q}_{1:K},\theta_i\right) \tag{D.7}$$

If the realizations are not equiprobable, a weighted average of the Js can be used, by applying different weighting factors to the Js resulting from each realization. If we assume that the modeling uncertainty is limited to uncertainty caused by a lack of information on the true geological structure of the reservoir, the realizations of θ are usually referred to as geological scenarios. Several methods are available to create an ensemble of geological scenarios. A geologist may create a number of scenarios based on his own knowledge and experience with comparable reservoirs. The uncertainty space thus provides the geologist with the boundaries within which he/she can design possible realizations. The advantage of such a method is that geological realism of the scenarios is guaranteed. It is, however, a rather subjective process; therefore, the set may be biased. A geostatistics-based method, such as multiple-point geostatistics (Strebelle (2000); Caers et al. (2003)), incorporates statistical information on geological parameters and, consequently, does not suffer from this problem. It is, however, more difficult to generate geologically realistic structures in this manner. Alternatively, geological realizations may be created with object-based or process-based algorithms, which usually produce realistic geological structures but are difficult to condition to well data (Gross and Small (1998); Viseur (1999); Deutsch and Tran (2002); Thomas and Nicholas (2002)).

RO. The use of an ensemble of geological scenarios to determine the expected revenues from a reservoir given a specified production strategy is not uncommon. Implementing such an ensemble in an optimization scheme has, however, not found its way into oil recovery optimization methods yet. Using a set of realizations to account for the effect of uncertainty within optimization problems, which suffer from uncertainty and limited measurement information, is not uncommon in the downstream petroleum industry. These optimization procedures are referred to as RO techniques. Within RO, the set of realizations may be used in different ways to account for the effect of uncertainty. These different approaches are represented by RO objectives (Ruppen et al. (1995); Terwiesch et al. (1998); Srinivasan et al. (2003)). The most straightforward RO objective is using the expected outcome over the set of realizations, which is, in our case, equivalent to Eq. (D.7). Other objectives may involve incorporating the variance of the outcomes or a worst-case approach. In this work, however, we limit ourselves to the expected NPV, represented by the robust objective function J_{rob}:

$$J_{\text{rob}}\left(\mathbf{q}_{1:K}\right) = \frac{1}{N_r}\sum_{i=1}^{N_r} J\left(\mathbf{q}_{1:K}, \theta_i\right) \tag{D.8}$$

This results in the following RO problem:

$$\max_{\mathbf{q}_{1:K}} J_{\text{rob}}\left(\mathbf{q}_{1:K}\right) \tag{D.9}$$

From this formulation follows that calculating the expected NPV, (i.e. the value of J_{rob}) involves a linear operation. As a result, calculating the gradients of Eq. (D.9) involves a linear operation in terms of the gradients of each realization:

$$\frac{\mathrm{d}J_{\text{rob}}}{\mathrm{d}\mathbf{q}_k} = \frac{1}{N_r}\sum_{i=1}^{N_r} \frac{\mathrm{d}J(\mathbf{q}_{1:K}, \theta_i)}{\mathrm{d}\mathbf{q}_k} \tag{D.10}$$

The fact that calculating the mean gradients $\frac{\mathrm{d}J_{\text{rob}}}{\mathrm{d}\mathbf{q}_k}$ involves a linear operation has the advantage that the gradients of each realization can be determined separately. As a result, the gradients can be calculated in a sequentially instead of simultaneously, which would result in a considerable computational burden, limiting the number of realizations to be used. Calculating the gradients sequentially solves this problem, but it does lead to an extended simulation time by a factor N_r. However, the fact that the calculations are decoupled allows for parallel calculations on multiple processors.

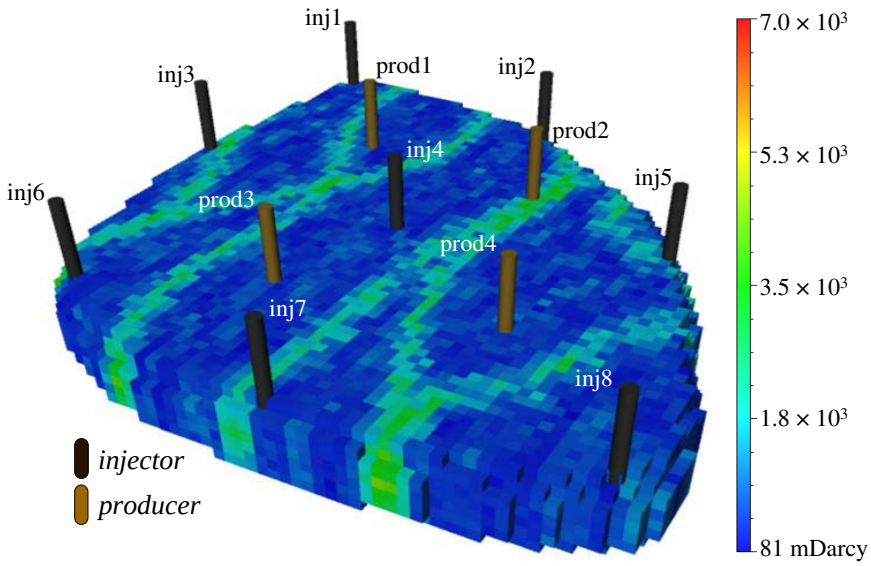

Figure D.1 : Permeability field and well locations of Realization Number 1 of a set of 100 realizations.

D.3 Example

We considered a waterflooding example of a 3D oil/water-reservoir model containing eight injection wells and four production wells. Production from the reservoir was simulated over a time horizon of 10 years, with timesteps of $\frac{1}{16}$ year. The model contains 18,553 gridblocks $8 \times 8 \times 4m$ in size, and there are seven vertical layers. The average reservoir pressure was set at 400 bar, and the initial water saturation was taken to be uniform over the reservoir at a value of 0.1. The remaining geological and fluid properties used in this example are presented in Table D.1. The reservoir is located in a fluvial depositional environment with known main-flow direction. Seismic and core-sample data from appraisal wells were assumed to provide no specific knowledge on the meandering structure of the fluvial depositions. In this example, the lack of information about the real geological structure was assumed to be the only contributor to the modeling uncertainty.

Two different sets of 100 geological realizations of the reservoir were generated, based on geological insight rather than a geostatistical method. In other words, the geologist sketched them by hand. Although it may be argued that a more sophisticated method is to be preferred in practice, the method of creating realizations is unrelated to the optimization strategy presented in this paper. Each set of realizations

Table D.1 : *Geological and fluid properties example*

Property	*Value*	*Units*
Φ	0.20	-
ρ_o (at 1 bar)	1000	kg/m^3
ρ_w (at 1 bar)	1000	kg/m^3
c_o	1.00×10^{-5}	$1/bar$
c_w	1.00×10^{-5}	$1/bar$
μ_o	1.00×10^{-3}	$Pa \cdot s$
μ_w	1.00×10^{-3}	$Pa \cdot s$
p_{cow}	0	bar

represents the range of possible geological structures within the boundaries of the geological uncertainties. The number of 100 realizations is assumed to be large enough to be a good representation of this range. To check whether this is a reason- able assumption, the responses of the two sets to identical control strategies were compared. It should be noted that similar responses (in a statistical sense) indicate that this assumption is plausible, but do not provide a conclusive validation. The manual method by which the different realizations were created does not give a classification between the members in the set. No information from seismic, production, or other data was assumed to be available to rank the realizations; therefore, they were assumed to be equiprobable.

The absolute-permeability field and well locations of the first realization of the set are depicted in Fig. D.1. Fig. D.2 displays the absolute-permeability field of six realizations randomly selected from the set without the wells. The minimum rate for each well was chosen equal to 0.02 m^3/d because setting the rate equal to 0 m^3/d presented numerical problems when solving the system of adjoint equations. The maximum rate for each well was fixed at 64 m^3/d. To keep the reservoir pressure constant, the total injection rate must be equal to the total production rate at each time instant.

Production Strategies. We considered three production strategies: a reactive approach, an NO approach, and an RO approach. Their performances were evaluated using the objective function as defined in Eq. D.1, with r_o = USD 126 /m^3, r_w = USD 19 /m^3, and r_i = USD 6 /m^3. However, because of the geological uncertainty, a deterministic estimate of performance cannot be given. Therefore, the performance of each of the three strategies was estimated in a probabilistic sense, using the set of 100 realizations. For each strategy, the 100 deterministic values of the objective func-

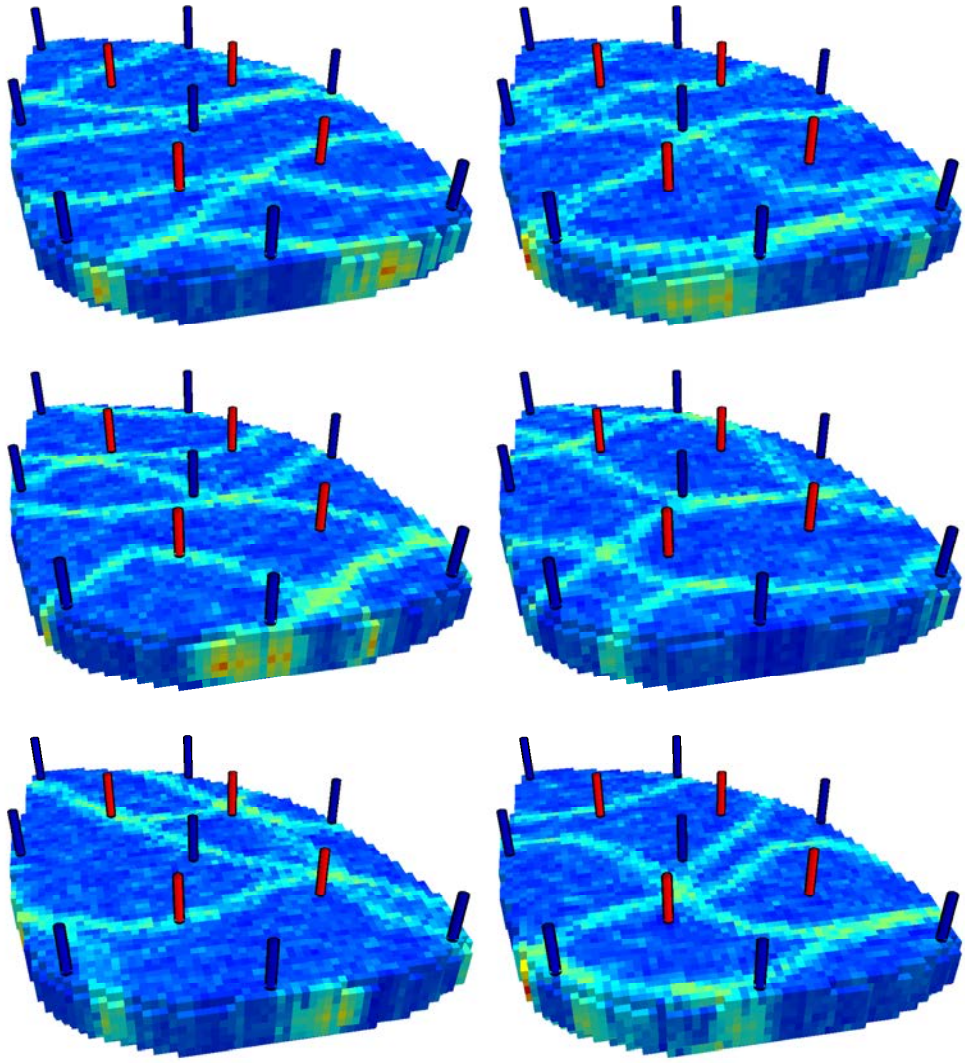

Figure D.2 : Permeability field of six (randomly chosen) realizations out of a set of 100, showing alternative fluvial structures.

Table D.2 : *Results*

	Reactive Control	*NO (on average)*		*RO*	
Expected NPV	USD 43.7m	USD 46.3m	+5.9%	USD 47.9m	+9.5%
Standard Dev.	USD 1.20m	USD 1.01m	-	USD 0.79m	-

tion resulting from the set were used to determine a cumulative distribution function (CDF) and to estimate a probability density function (PDF).

Reactive approach. Using the reactive approach, each production well is simply shut in if production is no longer profitable, where the profitability threshold corresponds to a water cut of 87%. The production flow rates are initially fixed at their maximum capacity of 64 m^3/d. The injection flow rates are equal for each injection well and are initially fixed at 32 m^3/d to honor the balanced injection and production. If a production well is shut in, the injection rate of each injection well is proportionally scaled down to meet the equality constraint, described in Appendix A by Eq. D.18. This reactive strategy will be used as a benchmark for the optimal control strategies that need predictive reservoir models to determine a strategy. The advantage of a reactive strategy is that it is model-free. Thus, when applied to an actual field, it does not suffer from a wrong representation of the geological realizations, whereas model-based methods do. However, the disadvantage is that it usually does not lead to an optimal reservoir flooding in terms of life-cycle performance. In the field-development phase of a project, we can assess the performance of a reactive strategy vs. a model-based strategy by simulating the performance of both strategies on a set of realizations. This assessment is valid only under the assumption that the set is a good representation of the true modeling uncertainty and, thus, can reflect the truth. If the used set is far from the truth, it is impossible to say which of the considered control strategies will perform better. We applied the reactive control strategy to each of the 100 members of the set of realizations. Fig. D.3 displays the response of the four production wells in terms of water cut over time for each of the 100 realizations. The large spread in water-breakthrough times gives an indication of the level of variability that the realizations are meant to represent. Note that the production wells are shut in when the profit- ability threshold of 87% water cut is reached. Applying the reactive control strategy to each of the 100 members also resulted in 100 values of the objective function (Eq. D.1). The corresponding CDF and PDF, as depicted in Fig. D.4, provide a probabilistic estimate of the performance of the reactive production strategy when applied to the true reservoir. The expected NPV and estimated standard deviation of the strategy are presented in Table D.2.

NO. The NO approach is based on a single realization. However, because none of the

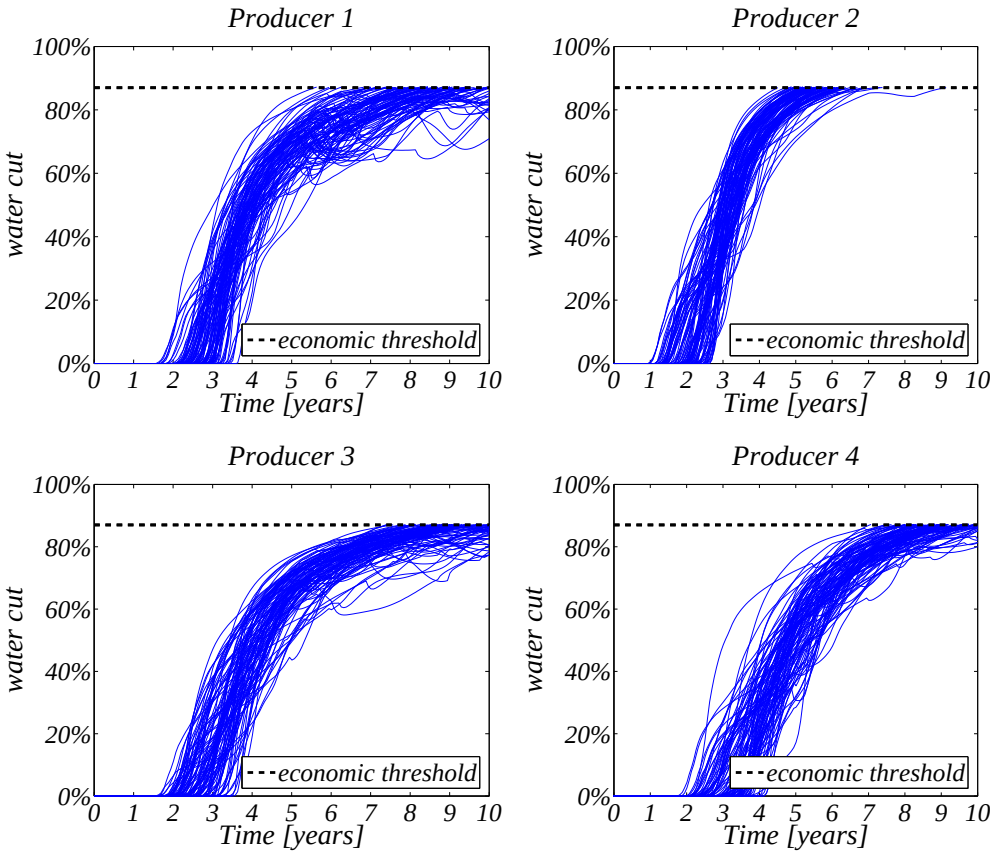

Figure D.3 : Response of the four production wells to the reactive control strategy in terms of water cut over time, for each of the 100 realizations. The production wells are shut in when the profitability threshold of 87% water cut is reached.

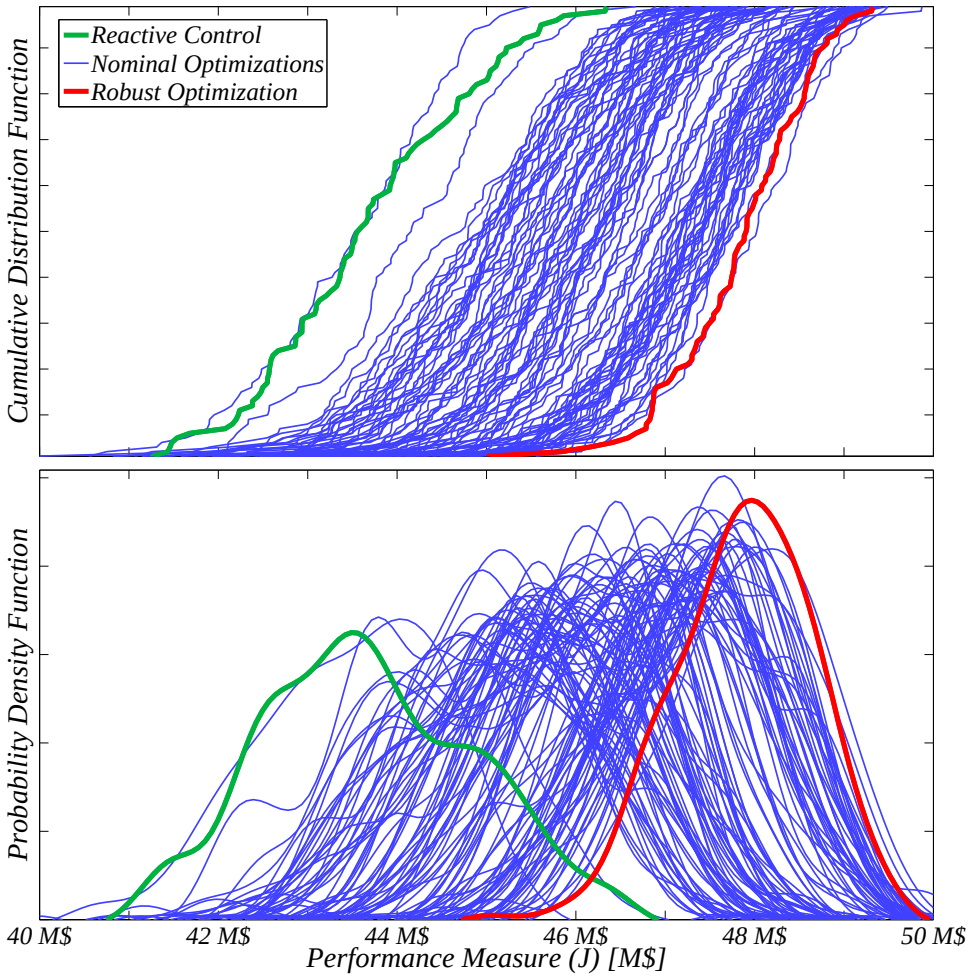

Figure D.4 : Cumulative Distribution Function and Probability Density Functions based on the first set of 100 realizations of the reactive control strategy, the 100 nominal optimization strategies and the robust optimization strategy.

realizations in the set of 100 is preferred over the others, the decision of which realization to use in the NO approach becomes an arbitrary one. To avoid the possibility of a biased choice, the NO procedure was performed on each of the 100 realizations in the set individually, resulting in 100 different NO production strategies. The number of control parameters for the optimization procedure is equal to the number of timesteps times the number of wells, which comes to 1,920 parameters. However, by using the adjoint method to obtain the gradients, the number of control parameters is not an issue because it requires only a single adjoint simulation to compute the gradients to all control parameters. The initial injection and production flow rates were set constant over time and equal to 24 m^3/d and 48 m^3/d respectively. In the SA algorithm, a fixed step size t is used of 3×10^{-4}, which was chosen on the basis of a number of trial runs.

The optimization was brought to an end after 80 iterations, at which point the incremental change of the objective function was less than 0.04% for all cases. The optimization procedure required a little more than 3 hours to converge to the optimal solution on a single computer for a single realization. Using a different optimization scheme or better constraint handling, we could have reached the convergence faster. However, improved convergence was not the goal of this study and was, therefore, not investigated further.

The optimal injection and production flow rates resulting from the NO procedure based on Realization Number 1 have been displayed in Fig. D.5. The performance of each of these 100 strategies on the entire ensemble was assessed by applying them to each member of the set. This resulted in 100×100 values of the objective function (Eq. D.1), from which 100 CDFs and PDFs were determined, one for each strategy, as shown in Fig. D.4. For each NO strategy, the expected NPV and the standard deviation were determined. The averages of these 100 expected NPV values and standard deviations are presented in Table D.2.

RO. The RO approach uses the entire set of realizations to determine a control strategy that maximizes the expected NPV over the entire set of realizations. The robust optimal control strategy is determined using the same gradient-based optimization procedure and optimization parameters that were used in the NO approach. However, calculating the robust gradient information requires calculating the gradients for each realization individually. Hence, the simulation time is approximately 100 times longer than the time needed for the NO approach (i.e., approximately 2 weeks). The RO control strategy was again applied to each realization in the set, and the value of the objective function was determined for each member. The resulting CDF and PDF are depicted in Fig. D.4, and the expected NPV and standard deviation are presented

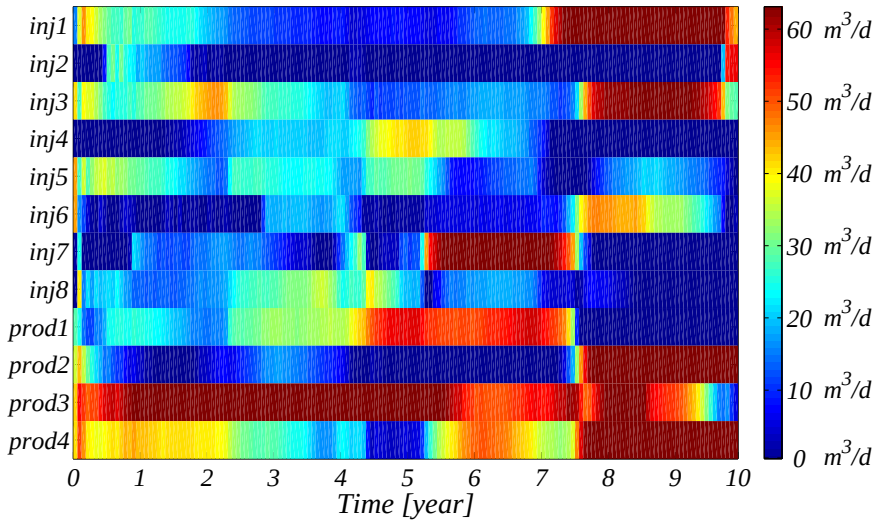

Figure D.5 : Injection and production flow rates resulting from the nominal optimization of realization nr. 1.

in Table D.2.

D.4 Results

The first observation from Fig. D.4 is that, given the set of realizations used in this example, a different choice of realization as a basis for the NO procedure can have a profound effect on the performance of the resulting NO strategy. A bad choice may lead to a drop of almost 10% in terms of expected NPV, compared to the expected NPV of a good choice. A second observation from Fig. D.4 is that, in this example, almost all NO control strategies perform better than the reactive control strategy. Table D.2 shows that, on average, the expected NPV of the NO control strategies is 5.9% higher than the expected NPV of a reactive control strategy. Also, the standard deviation is, on average, smaller than that of the reactive approach. This indicates that the NO control strategies, on average, show an increased robustness to the effect of the considered geological uncertainty.

Fig. D.4 and Table D.2 show that the performance of the RO control strategy is greatly improved over the performance of the reactive control strategy. The expected NPV increases 9.5%. The standard deviation is also reduced considerably, although a reduction in variance is not part of the objective function (Eq. D.1). On average, the performance of the RO strategy is also improved compared to the NO strategies.

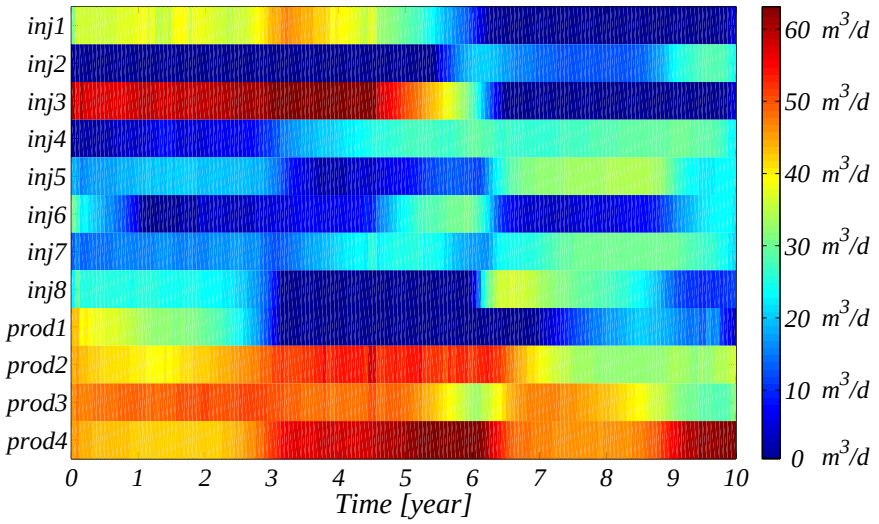

Figure D.6 : Injection and production flow rates resulting from the robust optimization of realization nr. 1.

It performs better than 99 out of the 100 NO strategies, though the difference in the expected NPV of the best NO control strategy and the RO control strategy is very small. This may be the effect of an RO procedure that was not fully converged or of the RO strategy leading to a local optimum in expected NPV. This was not investigated further. Finally, using the mean gradients $(\mathrm{d}J_{rob}/\mathrm{d}\mathbf{q})^T$ in the RO procedure has a regularizing effect on the resulting control strategy, as can be seen in Fig. D.6. The RO control strategy shows less-frequent and much smoother changes of the flow rates compared to the NO control strategy of Realization Number 1, as depicted in Fig. D.5.

D.5 Validation

The results show that the RO control strategy leads to an increase in expected NPV and reduced variance against the considered set of realizations. Improved performance of the RO strategy against the actual underlying geological uncertainty can only be claimed if the set is, in fact, a proper representation of this uncertainty, as was assumed in the introduction of the example. To validate that this assumption is plausible, the different control strategies were checked against the second set of 100 realizations. If both sets are large enough to give a good representation of the range of possible geological structures, the different strategies should lead to similar responses in a statistical sense.

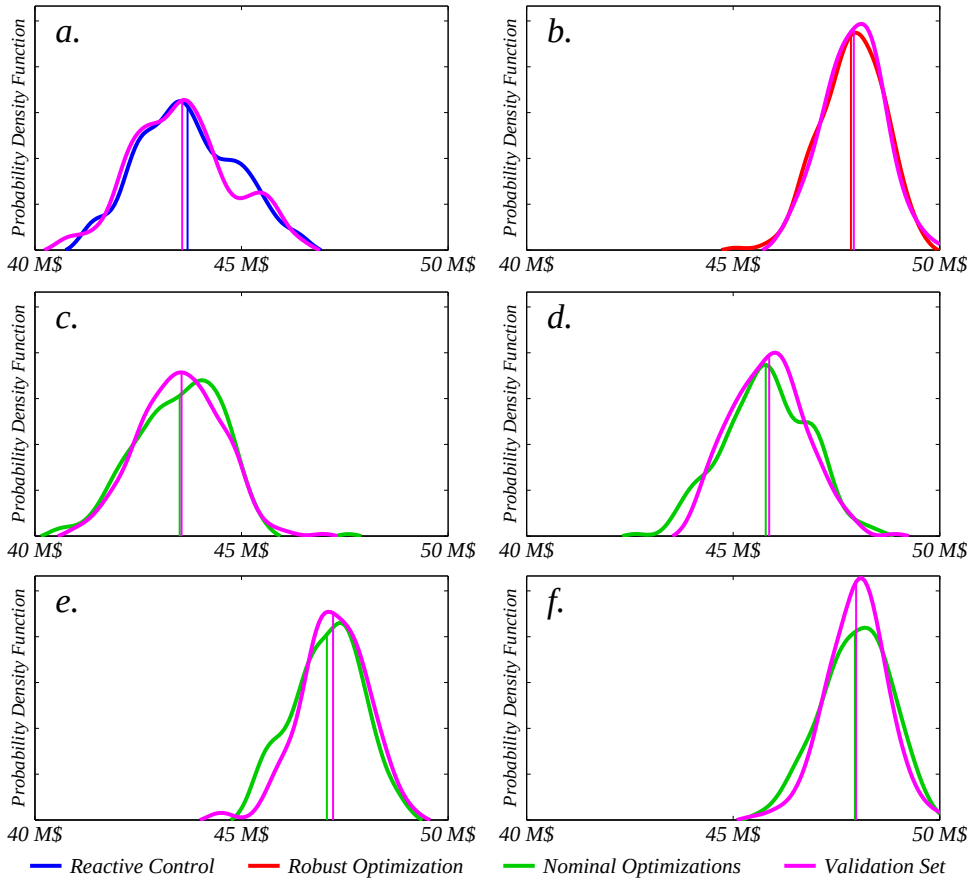

Figure D.7 : Estimated PDFs of the reactive control strategy (a), the RO control strategy (b), the NO strategy with the lowest expected NPV (c), the highest expected NPV (f), and two intermediate values of expected NPV (d and e), applied to the original and the validation set of realizations.

Table D.3 : *Validation*

	Reactive Control	*NO (on average)*	*RO*
Expected NPV	USD 43.6 million	USD 46.3 million	USD 47.9 million
Standard Dev.	USD 1.24 million	USD 0.93 million	USD 0.79 million

Table D.3 presents the averaged expected NPV and standard deviation of the reactive, NO and RO strategies, applied to this second validation set. Figs. D.7.a and D.7.b show the estimated PDFs of the reactive control strategy and of the RO control strategy, respectively, applied to the original and the validation set. Figs. D.7.c and D.7.f show the PDFs of the NO strategy with the lowest expected NPV and with the highest expected NPV, respectively; Figs D.7.d and D.7.e show two intermediate values of expected NPV. Table D.3 and Fig. D.7 show that the responses of the strategies to the different sets are very similar. This indicates that the assumption of the set being a proper representation of the geological uncertainty is, in fact, plausible.

D.6 Remarks

Within this work, injection and production flow rates are used to manipulate the progression of the oil/water front in the reservoir. The equality constraint, resulting from using flow rates as control variables, limits the search space of the optimization algorithm. Alternatively, the optimization may be performed using bottom-hole pressures or control-valve settings as control variables, which would require the use of well-inflow models. In that case, the use of an equality constraint to enforce balanced injection and production would no longer be necessary. Moreover, in this study, no measurement information was assumed to be available. Additional measurement information could be used, however, to reduce the geological uncertainty associated within the reservoir model. In future research on RO of reservoir flooding, a more integrated approach is advised, in which measurements are used to narrow the set of realizations or to improve the quality of the set through history matching.

D.7 Conclusions

An RO technique is an attractive approach to oil-recovery- optimization problems because it creates a bridge between two aspects of the E&P industry: geological uncertainty and maximizing oil recovery revenues. We tested its expected performance against those of NO strategies and reactive strategies by simulating a waterflooding example using 100 realizations of a fluvial reservoir. From the results of the example, we conclude that

- The performance of the NO strategy depends heavily on the particular realization that is selected to base the optimization on. In the example, there is no motivation to regard one geological structure to be more likely than the others, but the results of the resulting NOs are very different and nearly always worse than the result of the RO strategy.

- The RO strategy is able to improve the expected NPV significantly compared to the NO and reactive strategies, and it results in a smaller range of possible NPV outcomes (variance reduction) when tested using the initial set of realizations. The improved performance is maintained when the RO strategy is tested using a second (validation) set of realizations. This indicates that the set of 100 realizations is likely to be a proper representation of the geological uncertainty considered in this example.

- The advantage of a reactive strategy is that it is model-free. Thus, when applied to an actual field, it does not suffer from a wrong representation of the geological realizations, whereas the model-based RO and NO methods do. However, the disadvantage is that it usually does not lead to an optimal reservoir flooding in terms of life-cycle performance.

- It should be stressed that the conclusion of improved performance of the RO strategy compared to those of the NO and reactive strategies holds only if the used set of geological realizations is a good representation of the true modeling uncertainty. If the used set is far from accurate, it is impossible to say which of the considered strategies will perform better.

D.8 Nomenclature

$\bar{J}$	=	*modified objective function, M, USD*
k	=	*timestep counter*
K	=	*total number of timesteps*
N_r	=	*total number of realizations*
p	=	*pressure, m/(Lt^2), Pa*
$\mathbf{q}$	=	*vector of flow rates, L^3/t, m^3/s*
r	=	*price per unit volume, M/L^3, USD/m^3*
t	=	*time, t, seconds*
$\mathbf{x}$	=	*state vector*
α	=	*weight factor (step size)*
η	=	*vector of averages of model parameters*
θ	=	*vector of uncertain model parameters*
Θ	=	*uncertainty space*
κ	=	*dummy variable in summation*
λ	=	*Lagrange-multiplier vector*
μ	=	*viscosity, m/Lt, Pa·s*
ρ	=	*density, m/L^3, kg/m^3*
τ	=	*reference time for discounting, t, seconds*
ϕ	=	*porosity*

Subscripts

$_{cow}$	=	*oil/water capillary*
$_{d}$	=	*deterministic*
$_{max}$	=	*maximum*
$_{min}$	=	*minimum*
$_{o}$	=	*oil*
$_{r}$	=	*realization*
$_{rob}$	=	*robust*
$_{w}$	=	*water*
$_{wp}$	=	*produced water*
$_{wi}$	=	*injected water*

D.9 Appendix A - Gradient Calculations Using a System of Adjoint Equations

We consider the usual equations for multiphase flow through porous media on the basis of conservation of mass and Darcys law, equations of state and the empirical

closure equations for capillary pressure, and relative permeabilities Aziz and Settari (1979) some form of spatial discretization, such as a finite-volume or finite-element method, and an implicit time discretization, we obtain discrete-time system equations that can be expressed as

$$\mathbf{g}_{k+1} = (\mathbf{u}_{k+1}, \mathbf{x}_{k+1}, \mathbf{x}_k) \tag{D.11}$$

where $\mathbf{g}$ is a vector-valued function and $\mathbf{x}$ is the state vector containing pressures and phase saturations (or component accumulations) in each gridblock (i.e., finite volume or finite element). In general, the input vector $\mathbf{u}$ contains well flow rates, well pressures, or valve settings in those gridblocks that are penetrated by wells. In this paper, we restrict the input variables to total flow rates. Therefore, we can write

$$\mathbf{g}_{k+1} = (\mathbf{q}_{k+1}, \mathbf{x}_{k+1}, \mathbf{x}_k) \tag{D.12}$$

To complete the model, we specify the initial conditions

$$\mathbf{x}_0 = \check{\mathbf{x}}_0 \tag{D.13}$$

Next, we consider the flooding-optimization problem

$$\max_{\mathbf{q}_{1:K}} J(\mathbf{q}_{1:K}), \tag{D.14}$$

with objective function

$$J(\mathbf{q}_{1:K}) = \sum_{k=1}^{K} J_k(\mathbf{q}_{1:k}), \tag{D.15}$$

where J_k represents the contribution to J in each timestep as defined in more detail in Eq. D.1. Note that we could formally write Eq. D.15 as

$$J(\mathbf{q}_{1:K}) = \sum_{k=1}^{K} J_k(\mathbf{q}(\mathbf{x}(\mathbf{q}_{1:k}))) \tag{D.16}$$

to reflect the dependence on earlier inputs through the recurrence relationship (Eq. D.11), but we will refrain from doing so to keep the notation tractable. The injection and production rates are subject to inequality constraints as they are bounded by a minimum ($\mathbf{q}_{min}$) and maximum ($\mathbf{q}_{max}$) rate. An additional equality constraint is required stating that the total water injection rate $\mathbf{q}_{wi}$ must equal the negative of

the total production rate ($\mathbf{q}_o + \mathbf{q}_{wp}$) at each timestep k, such that reservoir pressure remains constant:

$$\mathbf{q}_{min} \leq \mathbf{q}_k \leq \mathbf{q}_{max} \tag{D.17}$$

and

$$\mathbf{q}_{o,k} + \mathbf{q}_{wp,k} = -\mathbf{q}_{wi,k} \tag{D.18}$$

The optimization problem can now be formulated as finding the input vector $\mathbf{q}_k$ that maximizes J over the time interval $k = 1, \ldots, K$, subject to system Eq. D.12, initial conditions Eq. D.13, and constraints Eqs. D.17 and D.18. We aim to compute the optimal control $\mathbf{q}_{1:K}$ with the aid of a gradient-based algorithm, which requires the derivatives of J with respect to $\mathbf{q}_{1:K}$. The complex dependence of J on $\mathbf{q}_{1:K}$ can be taken into account by considering Eqs. D.12 and D.13 as additional constraints to the optimization problem, and applying the technique of Lagrange multipliers to solve the constrained optimization problem:

$$\bar{J}(\mathbf{q}_{0:K}, \mathbf{q}_{0:K}, \lambda_{0:K}) = \sum_{k=0}^{K-1} \left[J_{k+1}(\mathbf{q}_{0:K}) + \lambda_0^T (\mathbf{x}_0 - \check{\mathbf{x}}_0)\, \delta_k + \lambda_{k+1}^T \mathbf{g}_{k+1}(\mathbf{q}_{k+1}, \mathbf{x}_k, \mathbf{x}_{k+1}) \right], \tag{D.19}$$

where the constraints have been adjoined to J with the aid of vectors of Lagrange multipliers λ. The Kronecker delta δ_k ensures that the initial-condition constraint is included in the summation. We note that the ordinary constraints Eqs. D.17 and D.18 are not included in this formulation because they are taken care of with the aid of the gradient projection method, as described in the body of the text. We can obtain a first-order description $\frac{\partial \bar{J}}{\partial \mathbf{q}_k}$ of the effect of changing $\mathbf{q}_k$ on the magnitude of *barJ* through taking the first variation of Eq. D.19. A necessary condition for an optimum is stationarity of $\bar{J}$ for all variations, which leads to the following set of equations:

$$\frac{\partial J_{k+1}}{\partial \mathbf{q}_{k+1}} + \lambda_{k+1}^T \frac{\partial \mathbf{g}_{k+1}}{\partial \mathbf{q}_{k+1}} = \mathbf{0}^T, \tag{D.20}$$

$$\lambda_1^T \frac{\partial \mathbf{g}_1}{\partial \mathbf{x}_0} + \lambda_0^T = \mathbf{0}^T, \tag{D.21}$$

$$\lambda_{k+1}^T \frac{\partial \mathbf{g}_{k+1}}{\partial \mathbf{x}_k} + \lambda_k^T \frac{\partial \mathbf{g}_k}{\partial \mathbf{x}_k} = \mathbf{0}^T, \tag{D.22}$$

$$\lambda_K^T \frac{\partial \mathbf{g}_K}{\partial \mathbf{x}_K} = \mathbf{0}^T, \tag{D.23}$$

$$(\mathbf{x}_0 - \check{\mathbf{x}}_0) = \mathbf{0}^T, \tag{D.24}$$

and

$$\mathbf{g}^T\left(\mathbf{q}_{k+1}, \mathbf{x}_k, \mathbf{x}_{k+1}\right) = \mathbf{0}^T \tag{D.25}$$

The last two equations are identical to system equation Eq. D.12 and initial-condition equation Eq. D.13 and are, therefore, automatically satisfied. Eq. D.23 reveals that the Lagrange-multiplier vector λ_K for the final discrete time K is equal to 0, and the discrete- time differential equation Eq. D.22 allows us to recursively compute the multipliers λ_K for $k = 1, \ldots, K$ (i.e., backward in time). Eq. D.21 represents the effect of changing the initial condition $\mathbf{x}_0$ on the value of the objective function, while keeping all other variables fixed. However, because we prescribed the initial condition through Eq. D.13, in our case, this term is of theoretical relevance only. Finally, Eq. D.20 represents the effect of changing the control on the value of the objective function while keeping all other variables fixed. For a nonoptimal control, this term is not equal to zero, but then its residual is just the gradient that we require to obtain iteratively the optimal control using a gradient-based algorithm. Solution of the optimization problem now consists of choosing an initial control vector $\mathbf{q}_{1:K}$ and repeating the following steps until the optimal control vector $\mathbf{q}_{1:K}$ has been found:

- Compute the states $\mathbf{x}_{1:K}$ using Eq. D.12, starting from initial conditions equation Eq. D.13.
- Compute the value of the objective function J using Eq. D.15. If converged, stop; otherwise continue.
- Compute the Lagrange multipliers $\lambda_{1:K}$ using Eqs. D.23 and D.22.
- Compute the derivatives (transposed gradients) of the objective function to the controls from the residuals of Eq. D.20 according to:

$$\frac{\mathrm{d}J}{\mathrm{d}\mathbf{q}_{k+1}} = \frac{\partial \bar{J}}{\partial \mathbf{q}_{k+1}} = \frac{\partial J_{k+1}}{\partial \mathbf{q}_{k+1}} + \lambda_{k+1}^T \frac{\partial \mathbf{g}_{k+1}}{\partial q_{k+1}} \tag{D.26}$$

- Compute an improved estimate of the control vector $\mathbf{q}_{1:K}$, using the derivatives as obtained from Eq. D.26 and a gradient- based minimization routine of choice (e.g., the SA method as described in Eq. D.3).

Because of its computational efficiency in calculating the gradients of the objective function, adjoint-based optimization is particularly attractive for problems with a large number of control parameters.

Appendix E

Integrated Dynamic Optimization and Control

This appendix has been published before as "Van Essen G.M., Van den Hof, P.M.J. and Jansen, J.D. (2013). A two-level strategy to realize life-cycle production optimization in an operational setting. *SPE Journal*, 18(6), 1057-1066. doi:10.2118/149736-PA".

E.1 Introduction

Several studies have shown that there is considerable scope to improve reservoir management by using reservoir models for the optimization of economic life-cycle performance. This type of model-based life-cycle optimization is also referred to as 'flooding optimization', 'recovery optimization', 'sweep optimization', or 'production optimization', although the latter name is conventionally reserved for more short-term operational optimization without the use of a reservoir simulation model. A very efficient way to perform model-based life-cycle optimization is with the aid of gradient-based methods where the gradient is obtained through an adjoint technique; see e.g. Asheim (1988), Sudaryanto and Yortsos (2000), Brouwer and Jansen (2004), Sarma et al. (2005), or Kraaijevanger et al. (2007). For further references we refer to the review paper by Jansen (2011). Alternative methods, which are generally less efficient but much easier to implement, use a variety of methods such as streamline techniques (Alhuthali et al. (2007), approximate-gradient methods such as ensemble techniques (Chen et al. (2009b); Su and Oliver (2010) or stochastic techniques (Wang et al. (2009)), or truly gradient-free methods including evolutionary techniques (Almeida et al. (2007)) and pattern-based search algorithms (Echeverra Ciaurri et al. (2011)). In all these studies the objective function is typically ultimate recovery or net present

value (NPV) while the controllable input is a set of well controls in the form of prescribed bottom hole pressures, flow rates or valve settings. In practice the optimal inputs, as obtained from the optimization, cannot be directly applied in production operations because:

1. There is uncertainty in reservoir flow parameters, and the real reservoir response will always be different from the simulated response.
2. The optimal inputs, in terms of life-cycle economic performance, are often suboptimal during the early phase of reservoir production in terms of instantaneous production rates.
3. Reservoir simulation models are usually much too coarse to represent near-well bore reservoir dynamics such as gas or water coning.
4. Unforeseen operational activities such as breakdown maintenance or well interventions cannot be accounted for in the reservoir simulator.

To a certain extent limitation 1), i.e. the effect of uncertainties in the reservoir flow parameters, can be counteracted by performing the optimization in a 'robust' fashion using an ensemble of reservoir models; see e.g. Van Essen et al. (2009b). A further step to counteract uncertainties is through frequent model updating with the aid of computer-assisted history matching (CAHM). Such a combination of life-cycle optimization and CAHM is sometimes called 'closed-loop reservoir management' (CLRM) or 'closed-loop' production optimization', and we refer to e.g. Naevdal et al. (2006), Sarma et al. (2008), Chen et al. (2009b), Jansen et al. (2009) and Wang et al. (2009) for further information. Limitation 2), i.e. the sub-optimal nature, from a production perspective, of 'optimal' life-cycle settings can to a certain extent be alleviated by sequential optimization or multi-objective optimization; see e.g. Van Essen et al. (2011) or Chen et al. (2012). However, limitations 3) and 4) are often too local (either in time or in space) to be captured in a reservoir simulation model, but may nevertheless have a negative (cumulative) effect on the life-cycle performance. Moreover, CAHM, and therefore CLRM, are usually time-consuming exercises which may limit the frequency with which the reservoir model can be updated.

E.2 Multi-level optimization and control

Similar difficulties to practical implementation of long-term optimal control strategies occur in the process industry and the standard solution is to use a multi-level control structure in which the results of a higher level serve as optimal reference for the next lower level. Such a 'disturbance rejection' strategy can quickly correct for small local disturbances that may have a negative (cumulative) effect on the long-term production strategy. Similar multi-level control structures have been proposed

by e.g. Saputelli et al. (2006) and Foss and Jensen (2011) for use in upstream oil and gas operations. The latter paper describes a four-level structure that makes a distinction between 'asset management', 'reservoir management', 'production optimization' and 'control and automation'. Here we consider the second and the third level. At the second level we apply model-based life-cycle optimization to a single reservoir model. At the third level we use a relatively simple data driven model in combination with a tracking control algorithm to determine well settings in the production optimization domain. We note that in similar control structures in the process industry the second and third levels are often referred to as dynamic real-time optimization (D-RTO) and model predictive control (MPC) respectively. Fig. 1 represents a schematic of our proposed two-level strategy. The box at the very top of the figure represents the 'real world', i.e. the system consisting of reservoir, wells and facilities. The box at the bottom of the figure (below the dotted line) represents the reservoir simulation model and the life-cycle optimization tool. The other boxes, above the dotted line, represent elements of the model-predictive production control. Their meaning will be described in detail below.

E.3 Reservoir Modeling using Linear Data-Driven Models

The introduction of advanced (subsurface) production measurement devices in new wells has opened the way for data-driven modeling techniques. The measurement frequency of these devices is quite high (in the order of seconds to minutes) in relation to the time step size of physics-based reservoir simulation models (in the order of days to months). Before the data are assimilated into these simulation models, they are therefore resampled and post-processed to match the time step size, by which all information on fast, localized dynamics is lost. However, using the high-resolution data in data-driven modeling, the fast dynamics are captured such that short-term predictions are better, compared to those of physics-based reservoir models. There exists a wide variety of data-driven modeling methods that create a model based on the input and output data it has been given, e.g. neural networks, genetic algorithms or polynomial interrelations. Early attempts to apply data driven modeling techniques to hydrocarbon reservoirs have been described by Rowan and Clegg (1963) and Chierici et al. (1981), while more recent attempts include extended Kalman filtering (Liu et al. (2009)) and capacitance-resistance modeling (e.g. Sayarpour et al. (2009)).

We use a so-called 'system identification' technique to determine a linear data-driven model. System identification, which has its origins in the downstream oil industry, is a black-box method, i.e. it creates a model solely based on measured data (Ljung (1999)). The order of the (linear) model, i.e. the number of dominant dynamic de-

grees of freedom represented in the identified model, is inferred from the data itself. During the modeling process the order of the model is increased until the residual error between modeled and measured data shows no evidence (within a predefined tolerance) of uncaptured dynamics. We note that the parameters of such an identified model usually have no direct physical interpretation and can therefore not be used to update the parameters of the physics-based reservoir model used for the life cycle optimization. In the example presented in this paper, a special sub-class of system identification has been used known as 'subspace identification' (SubID). SubID was used because of its simple structure, which is well suited for multiple input - multiple output systems, and because of its computational efficiency. A conceptual description of the method is given in Appendix A, while for further information we refer to Viberg (1995) and Van Overschee and De Moor (1996). For earlier SubID applications to reservoir modeling, see Markovinovic et al. (2002) andHeijn et al. (2004).

The data-driven model determined through SubID was subsequently used as prediction model for the model predictive controller. In the example described in this paper we consider a reservoir with eight water injection wells and four production wells, each equipped with devices to measure total flow rates (i.e. the sum of oil and water rates) and down hole pressures. We chose an input vector with twelve elements:

$$\mathbf{u} = \begin{bmatrix} u_1 & u_2 & \cdots & u_{12} \end{bmatrix}^T = \begin{bmatrix} p_{wf,1} & \cdots & p_{wf,4} & q_{wi,5} & \cdots & q_{wi,12} \end{bmatrix}^T \quad \text{(E.1)}$$

where $p_{wf,1}, \ldots, p_{wf,4}$ represent the bottom hole pressures in the producers, and $q_{w,5}, \ldots, q_{w,12}$ are the flow rates in the injectors. The output vector was chosen as

$$\mathbf{y} = \begin{bmatrix} y_1 & y_2 & y_3 & y_4 \end{bmatrix}^T = \begin{bmatrix} q_{t,1} & q_{t,2} & q_{t,3} & q_{t,4} \end{bmatrix}^T \quad \text{(E.2)}$$

where the four elements $q_{t,1}, \ldots, q_{t,4}$ are the total flow rates in the producers. As mentioned above, the identified model has degrees of freedom the number of which determines the order of the model, and which can be represented as state variables $\mathbf{x}$, linearly related to the inputs $\mathbf{u}$ and the outputs $\mathbf{y}$. Unlike in a physics-based reservoir simulation model, where the state variables are pressures, saturations or component concentrations, the states in an identified model do not have a direct physical interpretation. To capture all relevant dynamics in the identified model, the input $\mathbf{u}$ must be 'persistently exciting' during the length of the identification experiment, meaning that all relevant reservoir dynamics need to be stimulated by the inputs (Ljung (1999)). Design of such an experiment, in terms of the amplitude, frequencies and length of the input u, can be done on the basis of a physics-based large-scale reservoir simulation model and subsequently applied to the real reservoir. This approach was

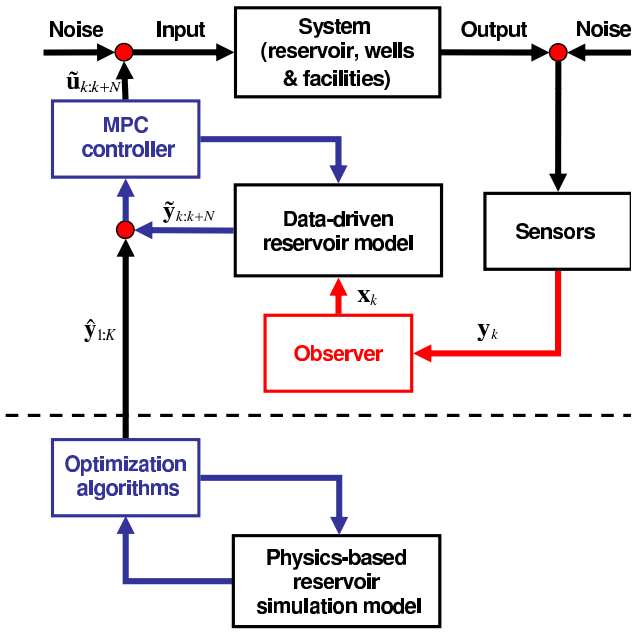

Figure E.1 : Two-level strategy to combine life-cycle optimization (bottom part of the figure) with MPC tracking of production (top part of the figure).

conceptually also adopted in the example presented in this paper, although we used a synthetic 'truth' in the form of a second, more detailed, reservoir simulation model.

E.4 Model Predictive Control in Water Flooding

The model predictive controller, as indicated in Fig. E.1, acts as a tracking controller for the reference variables obtained from the life-cycle optimization. As usual, the life-cycle optimization aims at maximizing NPV defined as an economic objective function J which for our example becomes

$$J = \sum_{k=1}^{K} \left[\frac{\sum_{i=1}^{8} r_{wi} \cdot (q_{wi,i})_k + \sum_{j=1}^{4} \left[r_{wp} \cdot (q_{wp,j})_k + r_o \cdot (q_{o,j})_k \right]}{(1+b)^{\frac{t_k}{\tau_t}}} \cdot \Delta t_k \right] \tag{E.3}$$

where $k = 1, 2, \ldots, K$ are the time steps in the simulator, $q_{wi,i}$ are the water injection rates of well i, $q_{wp,j}$ are the water production rate of well j, $q_{o,j}$ are the oil production

rates of well j, r_{wi} are the water injection costs, r_{wp} are the water production costs, r_o is the oil revenue, Δt_k is the time interval of time step k, and b is the discount rate (expressed as a fraction) for a reference time τt. During the life-cycle optimization procedure, the input vectors $\mathbf{u}_{1:K}$ are iteratively changed until a maximum value of J is obtained. (The notation $\mathbf{u}_{1:K}$ indicates the set of input vectors over the entire simulation period: $\mathbf{u}_{1:K} = \{\mathbf{u}_1, \mathbf{u}_2, \ldots \mathbf{u}_K\}$). Usually the optimal input vector $\mathbf{u}_{1:K}$ (where the hat indicates optimality with respect to the life-cycle reservoir model) is the desired result of the life-cycle optimization procedure. Here, however, we choose the corresponding optimal output $\hat{\mathbf{y}}_{1:K}$ as the result and use this set of optimal total flow rates as the reference variables for the model-predictive controller. The controller now attempts to find corrected inputs $\tilde{\mathbf{u}}$ such that the difference between the data driven model outputs $\tilde{\mathbf{y}}$ model and the life-cycle model-optimal outputs $\hat{\mathbf{y}}$ is minimal. This is achieved by minimizing the following objective function over a relatively short-time moving horizon:

$$V(\tilde{\mathbf{u}}_{k:k+N}) = \sum_{j=k}^{k+N} (\tilde{\mathbf{y}}_j - \hat{\mathbf{y}}_j)^T \mathbf{W}_1 (\tilde{\mathbf{y}}_j - \hat{\mathbf{y}}_j) + (\tilde{\mathbf{u}}_j - \hat{\mathbf{u}}_j)^T \mathbf{W}_2 (\tilde{\mathbf{u}}_j - \hat{\mathbf{u}}_j) \tag{E.4}$$

where N is the number of time steps over the moving control horizon, and $\mathbf{W}_1$ and $\mathbf{W}_2$ are optional weighing matrices. Note that here, for simplicity, it is assumed that the time steps k for the life-cycle optimization have the same length as those in the model predictive controller. In reality, the latter will use much smaller time steps. The second term at the right-hand side of equation E.12 ensures that the corrected inputs $\tilde{\mathbf{u}}_{1:K}$ do not deviate too much from the optimal inputs $\hat{\mathbf{u}}_{1:K}$ as computed in the life-cycle optimization step. The weighing matrices $\mathbf{W}_1$ and $\mathbf{W}_2$ are of relevance for optimization in a stochastic setting in which case they could be based on the (estimated) uncertainty in the inputs and outputs of the life-cycle and the black box models. In a deterministic case, as discussed in this paper, they can be used to weigh the magnitudes of inputs of a different physical nature such as pressures and flow rates. The prediction of the output $\tilde{\mathbf{y}}_{k:k+N}$ over the control horizon is performed with the aid of the identified (i.e. data-driven) model. Because the SubID method results in a model with a (small) number of internal state variables $\mathbf{x}$, it is necessary to specify initial conditions $\mathbf{x}_k$ at the start of the minimization of V. These can be estimated from the known inputs $\tilde{\mathbf{u}}_{k-1}$ and the measured outputs $\mathbf{y}_{k-1}$ with the aid of a so-called state estimator or observer. Further details of the identification and MPC procedures will be discussed in the example below. It should be noted that because, in our example, the number of inputs is twice the number of outputs, the minimization problem may become ill-posed. Only part of the control input $\tilde{\mathbf{u}}_{k:k+N}$ will then be implemented after which the process from state estimation to input implementation is repeated. As the real reservoir moves away from the state it was in when the linear data-driven model was created, the prediction accuracy of the model

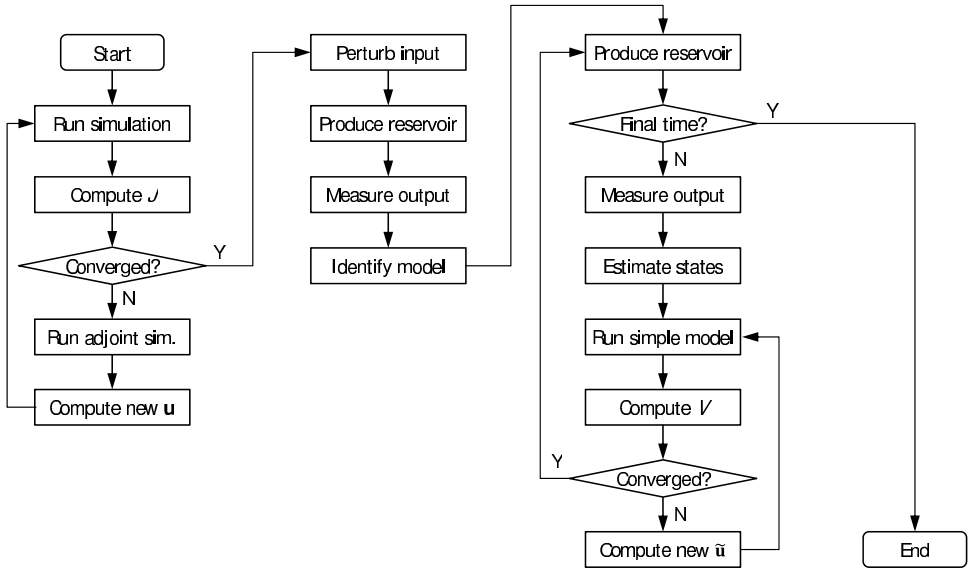

Figure E.2 : Flow chart of the two-level strategy. The left column represents life-cycle optimization using a large-scale eservoir simulation model (performed only once in our example). The second column represents identification of a data-driven model (also performed only once in our example). The third column represents computation of tracking control input using the identified model.

will decrease and re-identification is required. In doing so, the benefit of improved prediction accuracy must be evaluated against the drop in tracking performance during the experiment. However, how to determine the best instant to initiate another re-modeling experiment is not explored in this work, but will be the subject of future research. Fig. E.2 depicts a flow chart of the two-level strategy.

E.5 Example

The reservoir considered in our example is depicted in Fig. E.3. Its geological structure is dominated by two intersecting high-permeable channels. The remaining reservoir properties can be found in Table E.1. The life-cycle of the reservoir covers a period of 11.5 years. Of this reservoir a large-scale model was created to serve as the synthetic 'truth'. In order to provide realistic predictions of short-term dynamic behavior of the reservoir, a very fine spatial discretization around the wells was adopted and a (relatively) very short time step size was chosen of 0.25 days. This truth model was used to generate synthetic (noise-free) production measurements, and to assess the 'true' production performance over the life of the reservoir. A second reservoir model was created which serves as the model to perform life-cycle optimization and

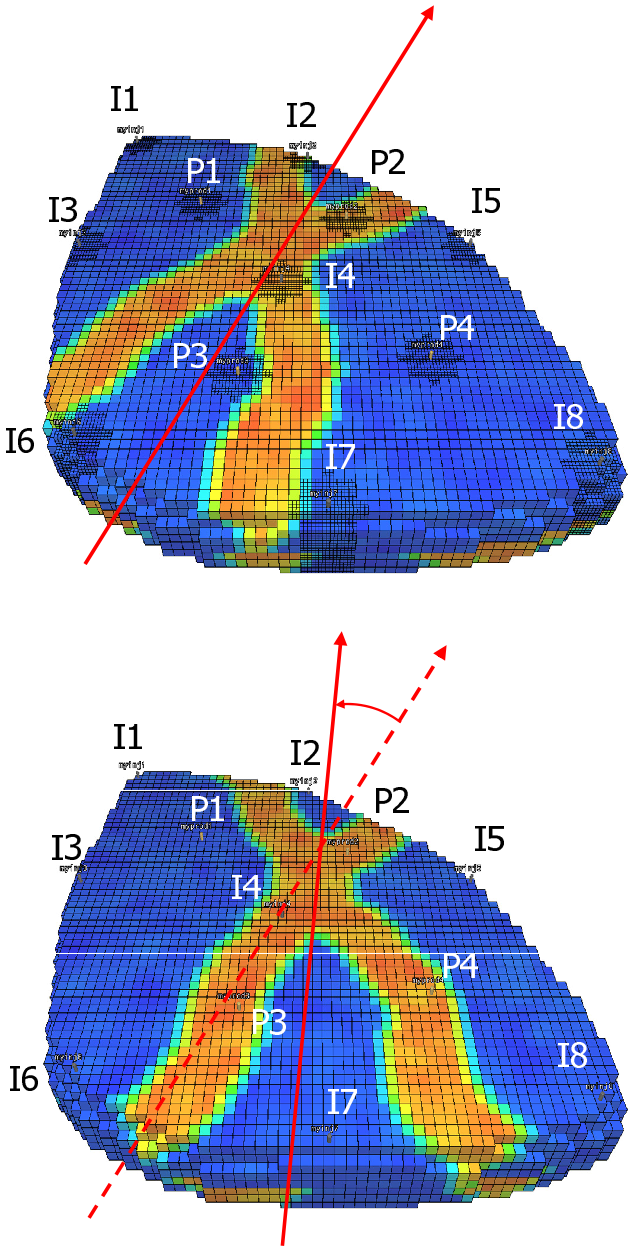

Figure E.3 : (top) 3D reservoir model, used as synthetic 'truth', with 8 injection wells and 4 production wells. Its geological structure involves a network of meandering channels of high permeability. The model on the top is used for life-cycle optimization and differs from the model on the bottom in the direction of the channels, the absence of grid refinement, and the larger time-step size of 30 days.

Table E.1 : *Geological and fluid properties for example*

Property	*Value*	*Units*
Φ	0.20	-
ρ_o (@ 1 bar)	800	kg/m^3
ρ_w (@ 1 bar)	1000	kg/m^3
c_o	$15 \cdot 10^{-5}$	$1/bar$
c_w	$4 \cdot 10^{-5}$	$1/bar$
μ_o	$4 \cdot 10^{-3}$	$Pa \cdot s$
μ_w	$1 \cdot 10^{-3}$	$Pa \cdot s$
p_{cow}	0	bar
S_{wc}	0.20	–
S_{or}	0.05	–
k_{ro}	0.80	–
k_{rw}	0.92	–
n_o	4.75	–
n_w	3.00	–

design the identification experiment. No grid refinement around the wells was used and a time step size of 30 days was adopted. Besides the coarser discretization in space and time, the second model deviates from the 'truth' in its geological structure. In particular it has channels in a slightly different flow direction, such that different wells are inside the high-perm streaks; see Fig. E.3. We used a fully implicit in-house reservoir simulator with adjoint functionality (Kraaijevanger et al. (2007)).

E.5.1 Economic Life-Cycle Optimization

In the control structure as shown in Fig. E.1, the optimal (reference) output $\hat{\mathbf{y}}_{1:K}$ is determined by the life-cycle optimizer using objective function (E.3). We used oil revenues r_o equal to 56.6 $\$/m^3$, water production costs r_{wp} of 6.3 $\$/m^3$, zero water injection costs, and an annual discount rate b equal to 0.1. We solved the life-cycle optimization problem with the aid of a gradient-based algorithm for which the gradients were obtained with the adjoint formalism in the simulator (Kraaijevanger et al. (2007)). We applied rate constraints to the injectors (a maximum rate of 1,590 $\frac{m^3}{day}$) and pressure constraints to the producers (a minimum bottom hole pressure of 375 *bar*, i.e. 25 *bar* below the initial reservoir pressure). Solving the life-cycle optimization problem resulted in an expected maximum NPV of $596 \cdot 10^6$ \$.

E.5.2 System Identification

System identification was performed on the 'true' reservoir. The inputs were the water injection rates of the eight injectors and the bottom-hole pressures of the four producers. The water flooding process is non-linear and as a result the prediction accuracy of a linear model will decrease when the prediction horizon increases. However, in this first experiment, we only once identified a linear model at the start of production for simplicity reasons. The duration of the experiment was chosen using the rule of thumb as used in the process industry that the length should be minimal five times the largest time constant. Through step response analysis on the reservoir model (i.e. not on the 'truth'), the largest time constant was estimated and the minimal duration of the experiment was estimated at 75 days. (The time constants of a strongly dissipative system like an oil reservoir can be interpreted as the half-time in output (e.g. the pressure response in a well) following a step change in the input (e.g. the well rate). For the inputs q_{wi} and p_{wf} to the 'real' reservoir, random binary signals (RBS) were generated. RBS signals were used in this experiment because they cover a wide spectrum of frequencies, which makes them suitable to generate a persistently exciting input. From step responses of the reservoir model to each input, it was found that the response to changes in q_{wi} were much slower than responses to changes in p_{wf}. In order to amplify the low frequency content of excitation signal of the injection rates, the clock period of the RBS signal was set to three sample times (of 0.25 days). The amplitudes of the RBS signals were set to 1,590 $\frac{m^3}{day}$ and 1 bar for q_{wi} and p_{wf} respectively, using the reservoir model to determine that the effect on the outputs was significant.

In order to maintain good economic performance, the RBS signals with zero mean were superimposed upon the preferred inputs which were taken equal to $\hat{\mathbf{u}}$ (i.e. the optimal inputs as obtained from the life-cycle optimization). However, whenever addition of the RBS signal led to infeasibility with respect to the well constraints, the mean value was moved up or down until feasibility was restored. In the identification experiment, the first 25 days of data were omitted after which all initialization effects had died out. The excitation signals and the optimal inputs $\hat{\mathbf{u}}$ can be observed in Fig. E.4. The sampling frequency of the measured outputs $\mathbf{y}$ is determined by the time-step size of the 'truth model', which in this example was equal to 0.25 days. The identification experiment was conducted in open-loop, since the depletion process is inherently stable. Based on these data, an 8th-order SubID model was identified. Fig. E.5 shows the model fit of the model with respect to the measured output data for all four producers. It can be observed that the output of the identified model has a satisfactory accuracy which illustrates that the 8th-order model is capable of representing all relevant dynamics.

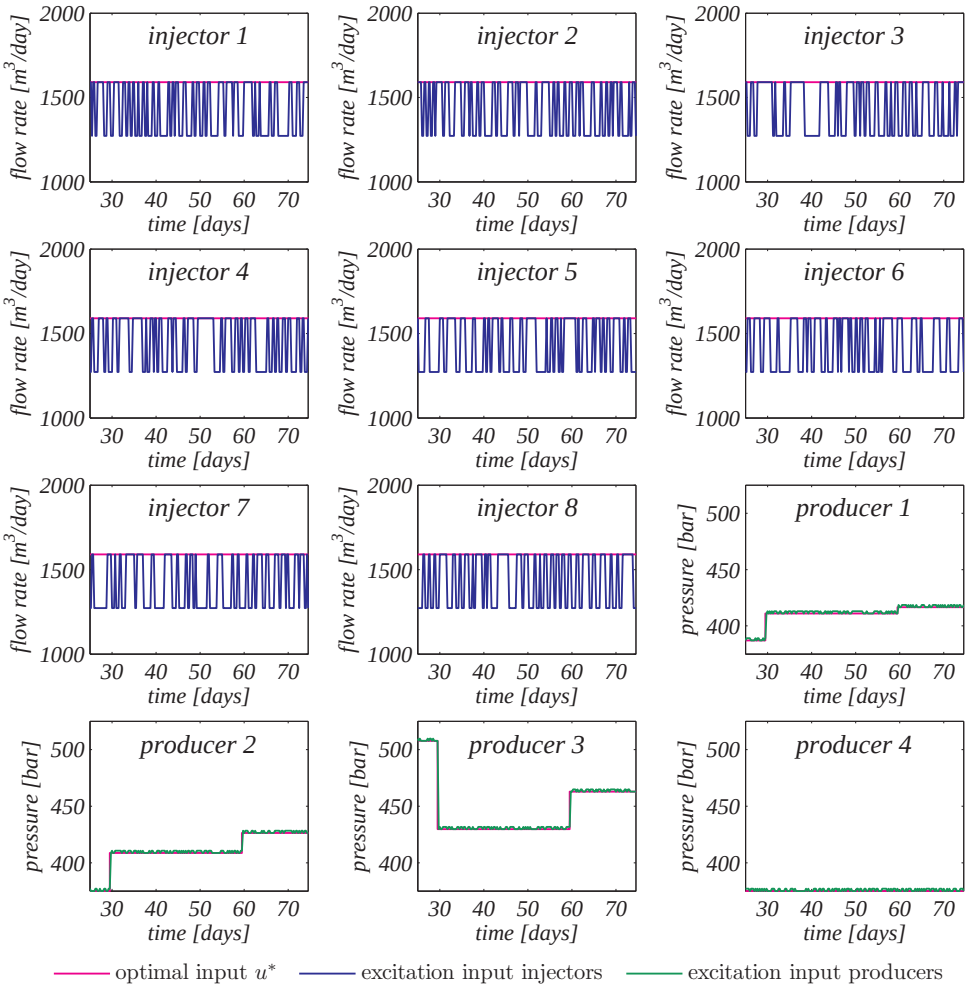

Figure E.4 : Excitation signal for the identification experiment along with optimal inputs $\hat{\mathbf{u}}$ for each input.

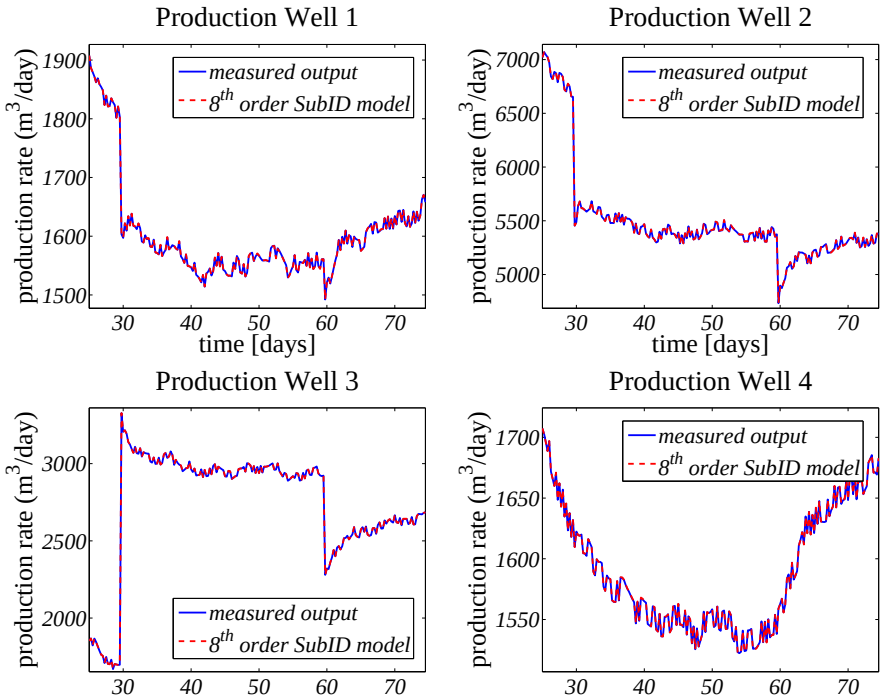

Figure E.5 : Model fit of the 8th-order SubID model with respect to the measured output data.

E.5.3 Model Predictive Control

MPC involves minimization of a cost function as described by equation (E.12). Recall that the outputs are defined as the four total liquid rates in the producers, whereas the inputs are the four bottom hole pressures in the producers and the eight water rates in the injectors. Matrix $\mathbf{W}_1$ (weighing the difference between the optimal long-term outputs $\hat{\mathbf{y}}_{k:k+N}$ and the predicted short-term outputs $\tilde{\mathbf{y}}_{k:k+N}$) was taken as a unit matrix. Weighting matrix $\mathbf{W}_2$ (weighing the difference between the optimal long-term inputs $\hat{\mathbf{u}}_{k:k+N}$ and the predicted short-term inputs $\tilde{\mathbf{u}}_{k:k+N}$) was chosen as a diagonal matrix with zeros and ones in positions corresponding to pressures and flow rates respectively. As a results, $\mathbf{W}_2$ only penalizes deviations of the optimal injection rates and not of the optimal production pressures, such that tracking is mainly realized through changes in the bottom-hole pressures in the production wells. The reason behind this choice was to aim for a higher penalty on changes in produced and injected volumes (with the aid of $\mathbf{W}_1$ and the nonzero elements of $\mathbf{W}_2$ respectively), than on changes in the corresponding pressures. In this experiment, the prediction horizon N was chosen equal to 28, i.e. to one week. Each time step, the minimization problem is solved for the (moving) prediction horizon, which involves two sequential steps: State estimation and quadratic programming (QP).

1. *State Estimation*. In this simulation study, no artificial noise was added to the measurements. As a result, the state estimation problem can be attacked quite straightforwardly using a Luenberger observer (Friedland (1986)); see Appendix E.2 for further details. Note however that alternative choices for state estimation may be considered, e.g. Kalman filtering.

2. *Quadratic Programming*. To solve the minimization of objective function V subject to the inequality constraints on the inputs, a QP problem needs to be solved. In this experiment, a gradient-based QP solver was used, implemented in the in-house reservoir simulator.

We note that the particular algorithmic choices for step 1 and 2 have little impact on the MPC tracking procedure. The controls $\tilde{\mathbf{u}}_{k:k+N}$ as determined by the MPC tracker were re-calculated and applied to the 'real' reservoir at every 0.25 day time step; see Fig. E.6.

E.5.4 Results

We compare the results from inputs $\tilde{\mathbf{u}}$ obtained with the additional MPC layer to results from direct, open-loop application of optimal inputs $\hat{\mathbf{u}}$. Performance is both evaluated in terms of tracking performance and NPV. Tracking performance can be observed in Fig. E.7. In Table E.2, the NPVs of the open-loop application of $\hat{\mathbf{u}}$ and

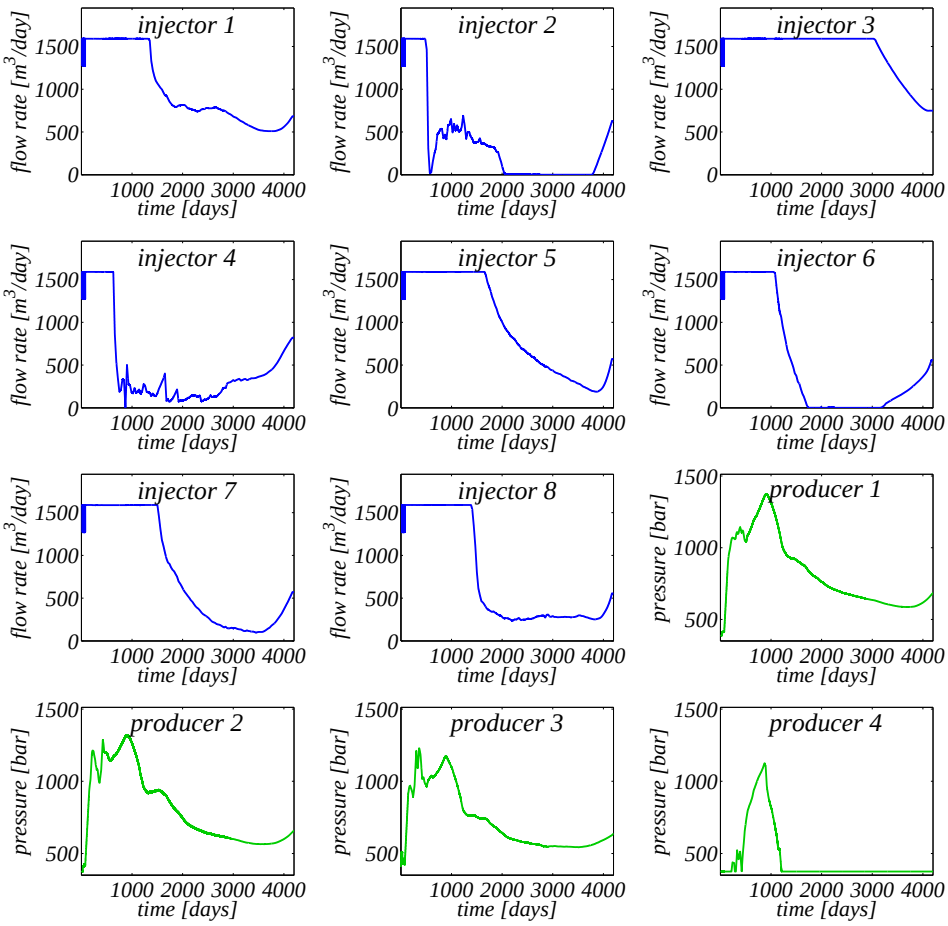

Figure E.6 : Controls $\tilde{\mathbf{u}}$ as determined by the MPC tracker.

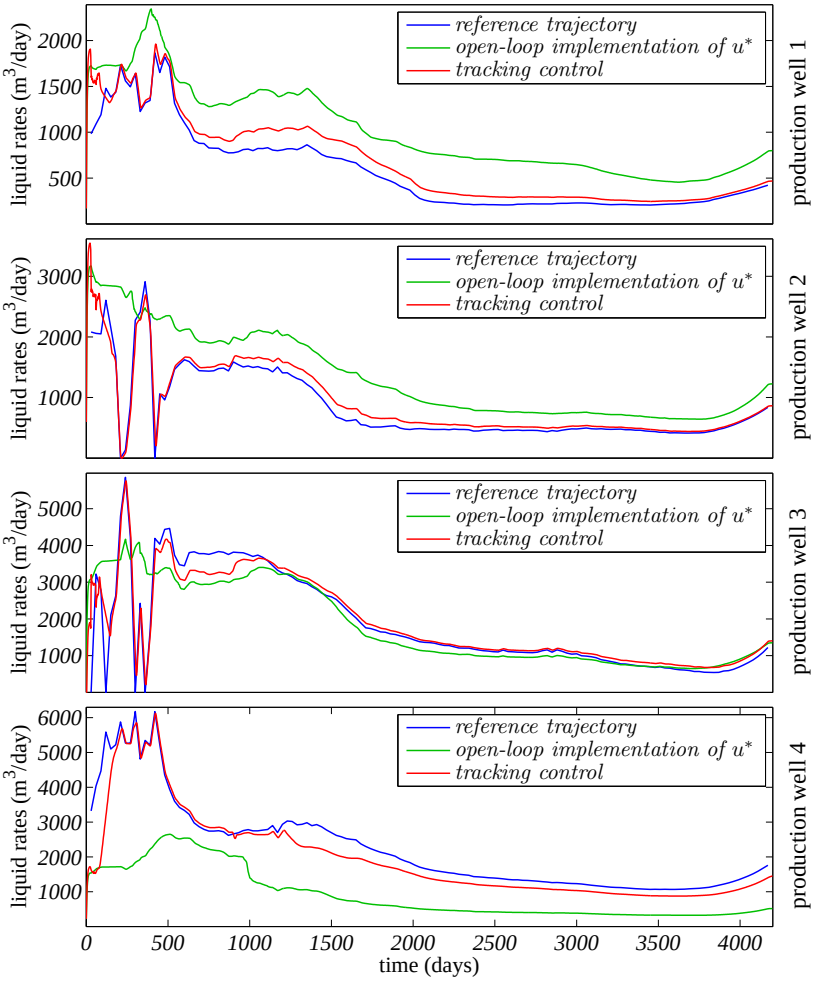

Figure E.7 : Reference and output trajectories for the open-loop application and the tracked case for each of the four production wells over the life of the field.

Table E.2 : *Economic Performance*

	NPV	*% change*
Maximum predicted	596×10^6\$	-
Open-loop application of $\hat{\mathbf{u}}$	558×10^6\$	-6.4%
MPC tracking using $\tilde{\mathbf{u}}$	594×10^6\$	-0.5%

$\tilde{\mathbf{u}}$ are shown in comparison to the expected maximum NPV determined by the life-cycle optimizer. Fig. E.7 depicts the reference and output trajectories for both the open-loop and the MPC tracked case for each of the four production wells over the life of the field. In each of the four plots, four different stages can be identified. In the first 75 days of production, the identification experiment is conducted where the optimal inputs $\hat{\mathbf{u}}$ serve as mean values. During this period the error is large because of the model error between the reservoir model and the 'truth', while the MPC tracker is not active yet. From 75 days to approximately 500 days tracking performance is good due to activation of the MPC tracker. After 500 days tracking performance decreases, however still outperforming open-loop control. This drop is the result of water breakthrough in the production wells, which has a strong nonlinear effect of the dynamics. After approximately 3,000 days tracking improves again, due to the fact that mainly water is produced resulting in a more linear response to the inputs.

E.6 Discussion

E.6.1 Theoretical aspects

In this example we used noise-free measurements which is of course an unrealistic assumption. The SubID and MPC steps can also be performed in a stochastic setting, taking into account measurement noise an model errors, and it is to be expected that increased noise levels will results in a reduced performance of our proposed method. At the other hand, in this example we did only once determine the SubID model used as a basis for the MPC tracker, and we may expect an improved tracking performance when frequent re-estimation of the SubID model is conducted over the length of the field's life-cycle. Moreover, we did not apply any CAHM to update the reservoir model used for the life-cycle optimization. Nor did we use robust optimization, i.e. optimization based on multiple models to reduce the sensitivity to geological uncertainties. Therefore the only way to counteract the negative effects of model inaccuracies on the life cycle performance of the 'true' reservoir was through the actions of the model predictive tracking controller. Based on experiences in the process industry we know that such a tracking control approach is effective when the

disturbances are local in time or space, and can, mathematically, be considered as perturbations around a nominal control trajectory, but with possibly significant cumulative effects. In that case, the long-term model-based optimal result that is used as reference, can still be considered a valid approximation for the real, disturbed, situation. In our example the disturbances resulted from two sources: 1) Near-well bore effects, which were not captured (neither in space nor in time) in the reservoir model used for the life-cycle optimization. 2) A small shift in channel orientation. These model errors result in disturbances which apparently, in this example, were small enough to be rejected by the tracking algorithm. Thus it was possible to realize a life-cycle production response, in the presence of disturbances, that closely resembled the model-optimal results. The reason to use a physics-based model for life cycle optimization is that a data-driven model can never predict water breakthrough or, more in general, saturations. Data-driven models can, however, very well predict pressures over a limited horizon during which the saturations do not change significantly. The effect of small 'disturbances' (in terms of operational events or differences between model and reality) which cause small pressure differences can therefore be 'rejected', i.e. compensated for, by control actions based on a data driven model. Rejection of larger disturbances, which significantly affect the saturations in the reservoir and/or the water breakthrough times in the wells would require more time-consuming updates of the physical reservoir model, e.g. through CAHM and/or geological model revision. In practice it will be difficult to estimate the magnitude of the disturbances, and therefore to know whether the use of a tracking controller on its own will be sufficient to counteract these. Therefore, it seems a logical step to combine tracking control with robust optimization and/or closed-loop reservoir management, resulting in a two-level approach with two feed-back loop as indicated in Fig. 8. In such a setting the lower-level tracking controller would quickly take care of local disturbances, either in space or in time, not captured in the upper-level reservoir model(s), while the more time-consuming CAHM and the use of multiple models would account for larger-scale model errors.

E.6.2 Practical aspects

The creation of a data-driven model requires manipulation of the inputs of the system. In our setting this implies changing the rates or pressures (either at the well head or down hole) in the wells. To maximize the information content in the resulting outputs (i.e. measured pressures and rates) a 'persistently exiciting' input signal is required. The required excitation frequency should be high enough to capture typical near-well bore transients. In our example this translated in a frequency of 0.25 days, i.e. once every six hours. Such a frequency is too high for manual operation but should pose no problems for automatic (computer-operated) surface control valves, as standard in the process industry. The required amplitude is dependent on the signal-to-noise ratio

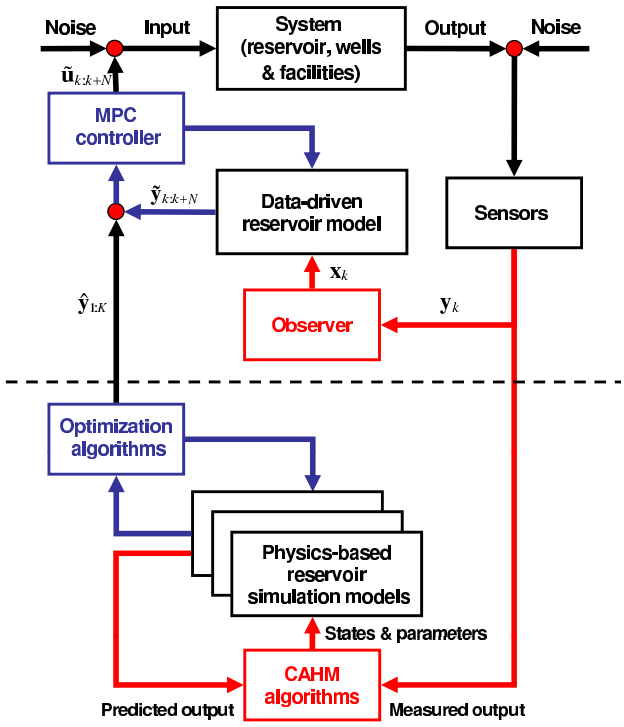

Figure E.8 : Two-level strategy to combine closed-loop reservoir management based on multiple models (bottom part of the figure) with tracking control of production (top part of the figure).

in the measured outputs. This leads to a trade-off between maximizing the excitation amplitude and the measurement time interval which both result in a better signal-to-noise ratio. Note that it is not necessary to implement the input fluctuations as an on-off sequence but that they may consist of a relatively low amplitude fluctuation on top of a steady state signal. This latter feature may make a practical implementation in a producing asset more acceptable. Moreover, in cases where manipulation of producing well parameters is operationally unacceptable, the input fluctuations could be restricted to the water injectors only, at the price of a reduced information content in the measurements.

E.7 Conclusions

The introduction of a two-level optimization and control strategy as described in our paper, combining life-cycle optimization with tracking control, was aimed at rapid attenuation of disturbances caused by small geological and near-wellbore model

errors. For the example considered we conclude that:

- It is possible to obtain a linear data-driven reservoir model through system identification, which gives accurate predictions for a time horizon that is relatively short, but long enough to realize tracking control.

- Tracking control is capable of quickly rejecting the disturbances resulting from small model errors in the form of neglected near-wellbore effects and a slightly erroneous channel orientation.

- The disturbance rejection results in a life-cycle production response that closely resembles the model-optimal results.

Further research is required to assess the range of validity of this approach, in particular in combination with alternative methods to counteract the negative effects of model errors on life-cycle optimization, such as robust optimization or closed-loop reservoir management.

E.8 Nomenclature

b	=	*discount rate,* t^{-1}, $1/year$
c	=	*compressibility,* $m^{-1} \cdot L \cdot t^2$, $1/bar$
j	=	*time step counter for moving horizon*
J	=	*objective function, $*
k	=	*discrete time, or permeability,* L^2, *mD*
K	=	*total number of time steps*
n	=	*Corey exponent*
N	=	*number of time steps in moving horizon*
p	=	*pressure,* $m \cdot L^{-1} \cdot t-2$, *Pa*
q	=	*flow rate,* m^3/d
r	=	*unit revenue/cost,* $\$/m^3$
S	=	*saturation*
t	=	*time, t, d*
$\mathbf{u}$	=	*input vector*
$\tilde{\mathbf{u}}$	=	*data-driven model generated input vector*
$\hat{\mathbf{u}}$	=	*life-cycle model generated input vector*
V	=	*objective function*
$\mathbf{W}$	=	*weighing matrix*
$\mathbf{x}$	=	*state vector*
$\mathbf{y}$	=	*output vector*
$\tilde{\mathbf{y}}$	=	*data-driven model generated output vector*
$\hat{\mathbf{y}}$	=	*life-cycle model generated output vector*
μ	=	*viscosity,* $m \cdot L^{-1} \cdot t^{-1}$, $Pa \cdot s$
ρ	=	*density,* $L^{-3} \cdot m$, kg/m^3
τ	=	*reference time, t, d*
ϕ	=	*porosity*
	=	

Subscripts

cow	=	*capillary (oil/water)*
ro	=	*relative, oil*
rw	=	*relative, water*
t	=	*total*
o	=	*oil*
wf	=	*flowing well bore*
wi	=	*injected water*
wp	=	*produced water*
	=	

Superscripts

T	=	*transposed*

E.9 Glossary

CAHM	=	*computer-assisted history matching*
D-RTO	=	*dynamic real time optimization*
MPC	=	*model predictive control*
NPV	=	*net present value*
QP	=	*quadratic programming*
RBS	=	*random binary signal*
SubID	=	*sub space identification*

E.10 Appendix 1 - Subspace Identification

For a detailed overview of subspace identification methods we refer to Viberg (1995), Van Overschee and De Moor (1996), and Ljung (1999), Section 10.6. Here we provide a brief description. Data driven modeling through subspace methods starts from a system description in state space form, according to:

$$\mathbf{x}_{k+1} = \mathbf{A}\mathbf{x}_k + \mathbf{B}\mathbf{u}_k + \mathbf{w}_k\,, \tag{E.5}$$

$$\mathbf{y}_k = \mathbf{C}\mathbf{x}_k + \mathbf{D}\mathbf{u}_k + \mathbf{v}_k\,, \tag{E.6}$$

where $k \in \mathbb{N}$ is discrete time, $\mathbf{x} \in \mathbb{R}^{n\times 1}$ is the state vector, $\mathbf{u} \in \mathbb{R}^{m\times 1}$ is the input vector, $\mathbf{y} \in \mathbb{R}^{p\times 1}$ is the output vector, $\mathbf{A} \in \mathbb{R}^{n\times n}$ is the system matrix, $\mathbf{B} \in \mathbb{R}^{n\times m}$ is the input matrix, $\mathbf{C} \in \mathbb{R}^{p\times n}$ is the output matrix, $\mathbf{D} \in \mathbb{R}^{p\times m}$ is the direct throughput matrix, and $\mathbf{w} \in \mathbb{R}^{n\times 1}$ and $\mathbf{v} \in \mathbb{R}^{p\times 1}$ are zero-mean stationary stochastic processes representing system and measurement noise respectively. The objective of the identification procedure is to determine, on the basis of input/output data $\{\mathbf{u}_k, \mathbf{y}_k\}_{k=1,\ldots,K}$, a so-called state space realization, i.e. a set of matrices $\{\mathbf{A}, \mathbf{B}, \mathbf{C}, \mathbf{D}\}$, together with the system order, i.e. the dimension n of the state variable $\mathbf{x}$. In subpace identification the most common approach to achieve this is

1. First estimate the so-called extended observability matrix

$$\mathbf{O}_r = \begin{bmatrix} \mathbf{C} \\ \mathbf{CA} \\ \vdots \\ \mathbf{CA}^{r-1} \end{bmatrix}, \tag{E.7}$$

   where r is a finite time-horizon, to be chosen by the user. On the basis of $\mathbf{O}_r$ the pair $\{\mathbf{A}, \mathbf{C}\}$ can be estimated.

2. Next estimate $\{\mathbf{B},\mathbf{D}\}$ through a simple least squares (linear regression) approach.

Step 1
When writing the output equation E.6 for $k,k+1,\ldots,k+r+1$, and denoting the extended vectors

$$\mathbf{u}_{k|r} \stackrel{\Delta}{=} \begin{bmatrix} \mathbf{u}_k \\ \vdots \\ \mathbf{u}_{k+r-1} \end{bmatrix}, \quad \mathbf{v}_{k|r} \stackrel{\Delta}{=} \begin{bmatrix} \mathbf{v}_k \\ \vdots \\ \mathbf{v}_{k+r-1} \end{bmatrix}, \quad \mathbf{y}_{k|r} \stackrel{\Delta}{=} \begin{bmatrix} \mathbf{y}_k \\ \vdots \\ \mathbf{y}_{k+r-1} \end{bmatrix}, \tag{E.8}$$

it follows that

$$\mathbf{y}_{k|r} = \mathbf{O}_r \mathbf{x}_k + \mathbf{S}_r \mathbf{u}_{k|r} + \mathbf{v}_{k|r} \tag{E.9}$$

where the (lower-triangular block-Toeplitz) matrix $\mathbf{S}_r$ is given by

$$\mathbf{S}_r = \begin{bmatrix} \mathbf{D} & \mathbf{0} & \cdots & \mathbf{0} \\ \mathbf{CB} & \mathbf{D} & \cdots & \mathbf{0} \\ \vdots & \vdots & \ddots & \vdots \\ \mathbf{CA}^{r-2}\mathbf{B} & \mathbf{CA}^{r-3}\mathbf{B} & \cdots & \mathbf{D} \end{bmatrix} \tag{E.10}$$

With

$$\mathbf{U} \stackrel{\Delta}{=} \begin{bmatrix} \mathbf{u}_{1|r} & \cdots & \mathbf{u}_{K|r} \end{bmatrix}, \tag{E.11}$$

$$\mathbf{V} \stackrel{\Delta}{=} \begin{bmatrix} \mathbf{v}_{1|r} & \cdots & \mathbf{v}_{K|r} \end{bmatrix}, \tag{E.12}$$

$$\mathbf{X} \stackrel{\Delta}{=} \begin{bmatrix} \mathbf{x}_1 & \cdots & \mathbf{x}_K \end{bmatrix}, \tag{E.13}$$

$$\mathbf{Y} \stackrel{\Delta}{=} \begin{bmatrix} \mathbf{y}_{1|r} & \cdots & \mathbf{y}_{K|r} \end{bmatrix}, \tag{E.14}$$

this becomes

$$\mathbf{Y} = \mathbf{O}_r \mathbf{X} + \mathbf{S}_r \mathbf{U} + \mathbf{V}. \tag{E.15}$$

Estimation of $\mathbf{O}_r$ can now be done through projections - correlations, i.e. by post-multiplying the matrix equation E.10 with a matrix $\mathbf{P}$ such that the terms with $\mathbf{U}$ and $\mathbf{V}$ on the right-hand side disappear (in expected value for $K \to \infty$). Then

$$\mathbf{YP} \approx \mathbf{O}_r \mathbf{XP} \tag{E.16}$$

and the column space of **YP** is equal to the column space of $\mathbf{O}_r$, while the dimension of this column space is determined by the dimension of **x**. By decomposing **YP** in a singular value decomposition (SVD)

$$\mathbf{YP} = \begin{bmatrix} \Phi_1 & \Phi_2 \end{bmatrix} \begin{bmatrix} \Sigma_1 & \mathbf{0} \\ \mathbf{0} & \Sigma_2 \end{bmatrix} \begin{bmatrix} \Psi_1^T \\ \Psi_2^T \end{bmatrix} \tag{E.17}$$

and choosing the decomposition in such a way that the dominant singular values are in Σ_1 and the smaller singular values in Σ_2, the column space of $\mathbf{O}_r$ is estimated by Φ_1 while the corresponding state dimension is given by the number of singular values in Σ_1. From an estimate of $\mathbf{O}_r$ a corresponding estimate of $\{\mathbf{A}, \mathbf{C}\}$ can easily be determined. Note that the SVD actually serves as an order estimation algorithm.

Step 2
With estimates of matrices **A** and **C** available (denoted by $\hat{\mathbf{A}}$ and $\hat{\mathbf{C}}$), matrices **B** and **D** can be found by solving for the linear regression problem

$$\min_{\mathbf{B},\mathbf{D}} \frac{1}{K} \sum_{k=1}^{K} \left\| \mathbf{y}_k - \hat{\mathbf{C}} \left(q\mathbf{I} - \hat{\mathbf{A}} \right)^{-1} \mathbf{B}\mathbf{u}_k - \mathbf{D}\mathbf{u}_k \right\|_2^2 \tag{E.18}$$

in which q denotes the shift operator, $q\mathbf{u}_k = \mathbf{u}_{k+1}$.

Subspace methods of system identification have the advantage that they rely on robust numerical tools such as SVD, they are simply applicable to multiple-input-multiple-output systems, and they incorporate an effective order test.

E.11 Appendix 2 - State Estimation With a Luenberger Observer

An observer is a dynamical system that reconstructs the states of the process under study on the basis of measurements of the process inputs and outputs. For the linear time-invariant process determined by the continuous-time state space model

$$\mathbf{x}_{k+1} = \mathbf{A}\mathbf{x}_k + \mathbf{B}\mathbf{u}_k\,, \tag{E.19}$$

$$\mathbf{y}_k = \mathbf{C}\mathbf{x}_k + \mathbf{D}\mathbf{u}_k\,, \tag{E.20}$$

the (Luenberger) observer has the format

$$\hat{\mathbf{x}}_{k+1} = \mathbf{A}\hat{\mathbf{x}}_k + \mathbf{B}\mathbf{u}_k + \mathbf{L}(\mathbf{y}_k - \hat{\mathbf{y}}_k), \tag{E.21}$$

$$\hat{\mathbf{y}}_k = \mathbf{C}\hat{\mathbf{x}}_k + \mathbf{D}\mathbf{u}_k, \tag{E.22}$$

where $\hat{\mathbf{x}}$ is the estimated state and $\hat{\mathbf{y}}$ is the model output, and the observer is specified by choosing an observer gain $\mathbf{L} \in \mathbb{R}^{n \times p}$. Note that the observer is actually a copy of the original process with a correction term that serves to drive the estimated $\hat{\mathbf{x}}$ towards $\mathbf{x}$ in case that the measured output $\mathbf{y}$ deviates from the model output $\hat{\mathbf{y}}$.

For the estimation error $\tilde{\mathbf{x}} = \mathbf{x} - \hat{\mathbf{x}}$ it can be shown that it satisfies the dynamic equation

$$\dot{\tilde{\mathbf{x}}}_{k+1} = (\mathbf{A} - \mathbf{L}\mathbf{C})\,\tilde{\mathbf{x}}_k \tag{E.23}$$

The observer gain $\mathbf{L}$ is chosen so as to have convergence of the estimation error to zero with sufficient 'speed', while the overshoot of the error response stays limited.

Bibliography

Aanonsen, S.I., Naevdal, G., Oliver, D., Reynolds, A.C., and Valles, B. (2009). The ensemble kalman filter in reservoir engineering - a review. *SPE Journal*, 14(3), 393–412. doi:10.2118/117274-PA.

Alhuthali, A.H., Oyerinde, D., and Datta-Gupta, A. (2007). Optimal waterflood management using rate control. *SPE Reservoir Evaluation & Engineering*, 10(5), 539–551. doi:10.2118/102478-PA.

Almeida, L.F., Tupaca, Y.J., Lazo, J.G., Pacheco, M.A., and Vellasco, M.M.B.R (2007). Evolutionary optimization of smart-wells control under technical uncertainties. In *Latin American & Caribbean Petroleum Engineering Conference*. Buenos Aires, Argentina. doi:10.2118/107872-MS. SPE 107872-MS.

Asheim, H. (1988). Maximization of water sweep efficiency by controlling production and injection rates. In *SPE European Petroleum Conference*. London, United Kingdom. doi:10.2118/18365-MS.

Aziz, K. and Settari, A. (1979). *Petroleum Reservoir Simulation*. Applied Science Publishers.

Barkved, O.I., Buer, K., Kristiansen, T.G., Kjelstadli, R.M., and Kommedal, J.H. (2005). Permanent seismic monitoring of the valhall field, norway. In *International Petroleum Technology Conference*. Doha, Qatar. doi:10.2523/10902-MS. IPTC10902-MS.

Bennet, A.F. (2002). *Inverse Modeling of the Ocean and Atmosphere*. Cambridge University Press, Cambridge.

Brouwer, D.R. and Jansen, J.D. (2004). Dynamic optimization of waterflooding with smart wells using optimal control theory. *SPE Journal*, 9(4), 391–402. doi:10.2118/78278-PA. SPE 78278-PA.

Byrd, Richard H. and Nocedal, Jorge (1990). An analysis of reduced hessian methods for constrained optimization. *Mathematical Programming*, 49(1-3), 285–323. doi:10.1007/BF01588794.

Caers, J., Strebelle, S., and Payrazyan, K. (2003). Interpreters corner - stochastic integration of seismic data and geologic scenarios: A west africa submarine channel saga. *The Leading Edge*, 22(3), 192–196. doi:10.1190/1.1564521.

Calvert, R. (2005). *Insights and Methods for 4D Reservoir Monitoring and Characterization*. Distinguished Instructor (Book 8). Society Of Exploration Geophysicists.

Chen, C., Li, G., and Reynolds, A.C. (2012). Robust constrained optimization of short- and long-term net present value for closed-loop reservoir management. *SPE Journal*, 17(3), 849–864. doi:10.2118/141314-PA.

Chen, T., Gerritsen, M.G., Durlofsky, L.J., and Lambers, J.V. (2009a). Adaptive local-global vcmp methods for coarse-scale reservoir modeling. In *SPE Reservoir Simulation Symposium*. The Woodlands, Texas, U.S.A. doi:10.2118/118994-MS. SPE 118994-MS.

Chen, Y., Oliver, D.S., and Zhang, D. (2009b). Efficient ensemble-based closed-loop production optimization. *SPE Journal*, 14(4), 634–645. doi:10.2118/112873-PA.

Chierici, G.L., Gottardi, G.A., and Guidorzi, R.P. (1981). Identified models for gas storage dynamics. *SPE Journal*, 21(2), 151–159. doi:10.2118/8862-PA.

Conn, A. R., Gould, N. I. M., and Toint, Ph. L. (2000). *Trust-Region Methods*. MOS-SIAM Series on Optimization 1.

de Montleau, P., Cominelli, A., Neylong, K., Rowan, D., Pallister, I., Tesaker, O., and Nygard, I. (2006). Production optimization under constraints using adjoint gradients. In *Proceedings of 10th European Conference on the Mathematics of Oil Recovery (ECMOR X)*. Amsterdam, the Netherlands.

Deutsch, C.V. and Tran, T.T. (2002). Fluvsim: a program for objectbased stochastic modeling of fluvial depositional systems. *Computers & Geosciences*, 28(4), 525535. doi:10.1016/S0098-3004(01)00075-9.

Echeverra Ciaurri, D., Mukerji, T., and Durlofsky, L.J. (2011). *Derivative-free optimization for oil field operations*. SCI 359. Springer-Verlag.

Evensen, G. (2007). *Data assimilation - The Ensemble Kalman Filter*. Springer, Berlin.

Foss, B. and Jensen, J.P. (2011). Performance analysis for closed loop reservoir management. *SPE Journal*, 16(1), 183–190. doi:10.2118/138891-PA. SPE138891-PA.

Friedland, B (1986). *Control System Design An Introduction to State Space Methods*. Mc Graw Hill. Re-issued by Dover.

Gross, L.J. and Small, M.J. (1998). River and floodplain process simulation for subsurface characterization. *Water Resources Research*, 34(9), 2365–2376. doi: 10.1029/98WR00777.

Haimes, Yacov Y. and Li, Duan (1988). Hierarchical multiobjective analysis for large-scale systems: Review and current status. *Automatica*, 24(1), 53–69. doi: 10.1016/0005-1098(88)90007-6.

Heijn, T., Markovinovic, R., and Jansen, J.D. (2004). Generation of low-order reservoir models using system-theoretical concepts. *SPE Journal*, 9(2), 202–218. doi: 10.2118/88361-PA. SPE 88361.

Huesman, A. E. M., Bosgra, O. H., and Van den Hof, P. M. J. (2006). Degrees of freedom analysis of economic dynamic optimal plantwide operation. In *IFAC International Symposium on Dynamics and Control of Process Systems (DYCOPS)*, 165–170. Cancún, Mexico.

Huesman, A.E.M., Bosgra, O.H., and den Hof, P.M.J. Van (2008). Integrating mpc and rto in the process industry by economic dynamic lexicographic optimization; an open-loop exploration. In *AIChE Annual Meeting*. Philadelphia, U.S.A.

Jansen, J.D. (2011). Adjoint-based optimization of multiphase flow through porous media a review. *Computers and Fluids*, 46(1), 40–51. doi: 10.1016/j.compfluid.2010.09.039.

Jansen, J.D., Bosgra, O.H., and Van den Hof, P.M.J. (2008). Model-based control of multiphase flow in subsurface oil reservoirs. *Journal of Process Control*, 18(9), 846–855. doi:10.1016/j.jprocont.2008.06.011.

Jansen, J.D., Brouwer, D.R., Naevdal, G., and Van Kruijsdijk, C.P.J.W. (2005). Closed-loop reservoir management. *First Break*, 23(1), 43–48. doi:10.3997/1365-2397.2005002.

Jansen, J.D., Douma, S.D., Brouwer, D.R., Van den Hof, P.M.J, Bosgra, O.H., and Heemink, A.W. (2009). Closed loop reservoir management. In *SPE Reservoir Simulation Symposium*. The Woodlands, Texas, U.S.A. doi:10.2118/119098-MS. SPE 119098-MS.

Kaleta, M.P., Van Essen, G.M., Van Doren, J.F.M., Bennett, R., van Beest, B.W.H., Van den Hoek, P.J., Brint, J.F., and Woodhead, T.J. (2012). Coupled static / dynamic modeling for improved uncertainty handling. In *SPE Europec*. Copenhagen, Denmark. doi:10.2118/154400-MS.

Kraaijevanger, J.F.B.M., Egberts, P.J.P., Valstar, J.R., and Buurman, H.W. (2007). Optimal waterflood design using the adjoint method. In *SPE Reservoir Simulation Symposium*. Houston, Texas, U.S.A. doi:10.2118/105764-MS. SPE 105764-MS.

Landa, J.L. and Horne, R.N. (1997). A procedure to integrate well test data, reservoir performance history and 4-d seismic information into a reservoir description. In *SPE Annual Technical Conference and Exhibition*. San Antonio, U.S.A. doi: 10.2118/38653-MS.

Li, R., Reynolds, A.C., and Oliver, D.S. (2003). History matching of three-phase flow production data. *SPE Journal*, 8(4), 328–340. doi:10.2118/87336-PA.

Liu, F., Mendel, J.M., and Nejad, A.M. (2009). Forecasting injector/producer relationships from production and injection rates using an extended kalman filter. *SPE Journal*, 14(4), 653–664. doi:10.2118/110520-PA.

Ljung, L (1999). *System Identification - Theory for the User, 2nd ed.* Prentice Hall.

Lorentzen, R.J., Berg, A., Naevdal, G., and Vefring, E.H. (2006). A new approach for dynamic optimization of water flooding problems. In *SPE Intelligent Energy Conference and Exhibition*. Amsterdam, The Netherlands. doi:10.2118/99690-MS.

Luenberger, D. G. (1984). *Linear and nonlinear programming*. Addison-Wesley.

Markovinovic, R., Geurtsen, E.L., and Jansen, J.D. (2002). Subspace identification of low-order reservoir models. In *Proc. XIV International Conference on Computational Methods in Water Resources*, 281–288. Delft, The Netherlands.

Marler, R.T. and Arora, J.S. (2004). Survey of multi-objective optimization methods for engineering. *Structural and Multidisciplinary Optimization*, 26(6), 369–395. doi:369-395. 10.1007/s00158-003-0368-6.

Miettinen, K.M. (1999). *Nonlinear Multiobjective Optimization*. Kluwer Academic Publishers, Boston.

Naevdal, G., Brouwer, D.R., and Jansen, J.D. (2006). Water flooding using closed-loop control. *Computational Geosciences*, 10(1), 37–60. doi:10.1007/s10596-005-9010-6.

Naevdal, G., Johnsen, L.M., Aanonsen, S.I., and Vefring, E.H. (2005). Reservoir monitoring and continuous model updating using ensemble kalman filter. *SPE Journal*, 10(1), 66–74. doi:10.2118/84372-PA.

Oliver, D.S., Reynolds, A.C., and Liu, N. (2008). *Inverse Theory for Petroleum Reservoir Characterization and History Matching*. Cambridge University Press.

Ramirez, W.F. (1987). *Application of optimal control theory to enhanced oil recovery*. Elsevier.

Rowan, G. and Clegg, M.W. (1963). The cybernetic approach to reservoir engineering. In *Proceedings of the 38th Annual Fall Meeting of the SPE of AIME*. New Orleans, USA. doi:10.2118/727-MS. SPE727.

Ruppen, D., Benthack, C., and Bonvin, D. (1995). Optimization of batch reactor operation under parametric uncertainty - computational aspects. *Journal of Process Control*, 5(4), 235–240. doi:10.1016/0959-1524(95)00015-I.

Saputelli, L., Nikolaou, M., and Economides, M.J. (2005). Self-learning reservoir management. *SPE Reservoir Evaluation & Engineering*, 8(6), 534–547. doi: 10.2118/84064-PA. SPE 84064-PA.

Saputelli, L., Nikolaou, M., and Economides, M.J. (2006). Real-time reservoir management: a multi-scale adaptive optimization and control approach. *Computational Geosciences*, 10, 61–96. doi:10.1007/s10596-005-9011-5.

Sarma, P., Aziz, K., and Durlofsky, L.J. (2005). Implementation of adjoint solution for optimal control of smart wells. In *SPE Reservoir Simulation Symposium*. Houston, U.S.A. doi:10.2118/92864-MS.

Sarma, P., Chen, W.H., Durlofsky, L.J., and Aziz, K. (2008). Production optimization with adjoint models under nonlinear control-state path inequality constraints. *SPE Reservoir Evaluation & Engineering*, 11(2), 326–339. doi:10.2118/99959-PA.

Sayarpour, M., Zuluaga, Kabir, C.S., and Lake, L.W. (2009). The use of capacitanceresistance models for rapid estimation of waterflood performance and optimization. *Journal of Petroleum Science and Engineering*, 69, 227–238. doi: 10.1016/j.petrol.2009.09.006.

Srinivasan, B., Bonvin, D., Visser, E., and Palanki, S. (2003). Dynamic optimization of batch processes: Ii. role of measurements in handling uncertainty. *Computers & Chemical Engineering*, 27(1), 27–44. doi:10.1016/S0098-1354(02)00117-5.

Stammeijer, J.G.F., Davidson, M., Hatchell, P.J., and Lopez, J.L. (2013). Instantaneous 4d seismic (i4d) - an innovative concept to monitor offshore water injector wells. In *6th International Petroleum Technology Conference*. Beijing, China. doi: 10.2523/16901-MS. IPTC16901-MS.

Strebelle, S. (2000). *Sequential simulation drawing structures from training images*. Ph.D. thesis, Stanford University, Stanford, California, U.S.A.

Su, H-J. and Oliver, D.S. (2010). Smart-well production optimization using an ensemble-based method. *SPE Reservoir Evaluation & Engineering*, 13(6), 884–892. doi:10.2118/126072-PA.

Sudaryanto, B. and Yortsos, Y.C. (2000). Optimization of fluid front dynamics in porous media using rate control 1. equal mobility fluids. *Physics of Fluids*, 12(7), 16561670. doi:10.1063/1.870417.

Sudaryanto, B. and Yortsos, Y.C. (2001). Optimization of displacements in porous media using rate control. In *SPE Annual Technical Conference and Exhibition*. New Orleans, U.S.A. doi:10.2118/71509-MS.

Tarantola, A. (2005). *Inverse Problem Theory and Methods for Model Parameter Estimation*. SIAM, Philadelphia. doi:10.1137/1.9780898717921.

Tavassoli, Z., Carter, J.N., and King, P.R. (2004). Errors in history matching. *SPE Journal*, 9(3), 352–361. doi:10.2118/86883-PA.

Terwiesch, P., Ravemark, D., Schenker, B., and Rippin, D.W.T. (1998). Semi-batch process optimization under uncertainty: Theory and experiments. *Computers & Chemical Engineering*, 22(1-2), 201–213. doi:10.1016/S0098-1354(96)00359-6.

Thiele, M.R. and Batycky, R.P. (2006). Using streamline-derived injection efficiencies for improved waterflood management. *SPE Reservoir Evaluation & Engineering*, 9(2), 187–196. doi:10.2118/84080-PA.

Thomas, R. and Nicholas, A.P. (2002). Simulation of braided river flow using a new cellular routing scheme. *Geomorphology*, 43(3-4), 179195. doi:10.1016/S0169-555X(01)00128-3.

Van den Hoek, P.J., Al-Masfry, R., Zwarts, D., Jansen, J.D., Hustedt, B., and Van Schijndel, L. (2009). Optimizing recovery for waterflooding under dynamic induced fracturing conditions. *SPE Journal*, 12, 671–682.

Van den Hof, P.M.J., Jansen, J.D., and Heemink, A.W. (2012). Recent developments in model-based optimization and control of subsurface flow in oil reservoirs. In *Proc. 1st IFAC Workshop on Automatic Control in Offshore Oil and Gas Production*. Trondheim, Norway.

Van Essen, G.M., Jansen, J.D., Brouwer, D.R, Douma, S.G., Zandvliet, M.J., Rollett, K.I., and Harris, D. (2010a). Optimization of smart wells in the st. joseph field. *SPE Reservoir Evaluation & Engineering*, 13(4), 588–595. doi:10.2118/123563-PA.

Van Essen, G.M., Jansen, J.D., and Van den Hof, P.M.J. (2010b). Determination of lower and upper bounds of predicted production from history-matched models. In *Proc.12th European Conference on the Mathematics of Oil Recovery (ECMOR XII)*. Oxford, United Kingdom.

Van Essen, G.M., Jimenez, E., Przybysz-Jarnut, J.K., Horesh, L., Douma, S.G., Van den Hoek, P., Conn, A., and Mello, U.T. (2012). Adjoint-based history-matching of production and time-lapse seismic data. In *SPE Europec*. Copenhagen, Denmark. doi:10.2118/154375-MS.

Van Essen, G.M., Van den Hof, P.M.J., and Jansen, J.D. (2009a). Hierarchical long-term and short-term production optimization. In *SPE Annual Technical Conference and Exhibition*. New Orleans, Louisiana, U.S.A. SPE 124332.

Van Essen, G.M., Van den Hof, P.M.J., and Jansen, J.D. (2011). Hierarchical long-term and short-term production optimization. *SPE Journal*, 16(1), 191–199. doi: 10.2118/124332-PA.

Van Essen, G.M., Van den Hof, P.M.J., and Jansen, J.D. (2013). A two-level strategy to realize life-cycle production optimization in an operational setting. *SPE Journal*, 18(6), 1057–1066. doi:10.2118/149736-PA.

Van Essen, G.M., Zandvliet, M.J., Van den Hof, P.M.J., Bosgra, O.H., and Jansen, J.D. (2009b). Robust waterflooding optimization of multiple geological scenarios. *SPE Journal*, 14(1), 202–210. doi:10.2118/102913-PA. SPE 102913-PA.

Van Overschee, P. and De Moor, B. (1996). *Subspace Identification For Linear Systems: Theory, Implementation, Applications*. Kluwer.

Viberg, M. (1995). Subspace-based methods for the identification of linear time-invariant systems. *Automatica*, 31(12), 1835–1851. doi:10.1016/0005-1098(95)00107-5.

Virnovski, G.A. (1991). Water flooding strategy design using optimal control theory. In *Proceedings of the 6th European Symposium on IOR*, 437–446. Stavanger, Norway.

Viseur, S. (1999). Stochastic boolean simulation of fluvial deposits: A new approach combining accuracy with efficiency. In *SPE Annual Technical Conference and Exhibition*. Houston, U.S.A. doi:10.2118/56688-MS.

Walsh, D.M., Buyok, T., Tiang, S., Ralphie, B., and Tan, T.C. (1996). Justification of appraisal in a mature field. In *SPE Asia Pacific Oil and Gas Conference*. Adelaide, Australia. doi:10.2118/37006-MS.

Wang, C., Li, G., and Reynolds, A.C. (2009). Production optimization in closed-loop reservoir management. *SPE Journal*, 14(3), 506–523. doi:10.2118/109805-PA.

Watson, A.T., Gavalas, G.R., and Seinfeld, J.H. (1984). Identifiability of estimates of two-phase reservoir properties in history matching. *SPE Journal*, 24(6), 697–706. doi:10.2118/12579-PA.

Yang, D., Zhang, Q., and Gu, Y. (2003). Integrated optimization and control of the production-injection operation systems for hydrocarbon reservoirs. *Journal of Petroleum Science and Engineering*, 37(1-2), 69–81. doi:10.1016/S0920-4105(02)00311-X.

Yeten, B., Durlofsky, L.J., and Aziz, K. (2002). Optimization of smart well control. In *SPE International Thermal Operations and Heavy Oil Symposium and International Horizontal Well Technology Conference*. Calgary, Alberta, Canada. doi:10.2118/79031-MS.

Zakirov, I.S., Aanonsen, S.I., Zakirov, E.S., and Palatnik, B.M. (1996). Optimization of reservoir performance by automatic allocation of well rates. In *Proceedings of the 5th European Conference on the Mathematics of Oil Recovery (ECMOR V)*. Leoben, Austria.

Zandvliet, M. J., Van Doren, J. F. M., Bosgra, O. H., Jansen, J. D., and Van den Hof, P. M. J. (2008). Controllability, observability and identifiability in single-phase porous media flow. *Computational Geosciences*, 12(4), 605–622. doi: 10.1007/s10596-008-9100-3.

Zandvliet, M.J., Bosgra, O.H., Jansen, J.D., Van den Hof, P.M.J., and Kraaijevanger, J.F.B.M. (2007). Bang-bang control and singular arcs in reservoir flooding. *Journal of Petroleum Science and Engineering*, 58(1-2), 186–200. doi: 10.1016/j.petrol.2006.12.008.

Nomenclature

Greek symbols

Θ	=	*uncertainty space*
Ω	=	*weighting function*
γ	=	*weighting factor*
ε	=	*tolerance of optimality constraint*
θ	=	*vector of uncertain model parameters*
μ	=	*viscosity*
ρ	=	*density*
τ	=	*reference time*
ϕ	=	*porosity*
ω	=	*weighting factor*

Calligraphic letters

$\mathscr{S}$	=	*optimal subset of* $\mathscr{U}$
$\mathscr{U}$	=	*decision variable space*

Capitals

$\mathbf{B}$	=	*basis for redundant DOFs*
$\mathbf{H}$	=	*Hessian matrix*
J	=	*objective function*
K	=	*total number of timesteps*
N	=	*number of time steps in moving horizon*
N_r	=	*total number of realizations*
P	=	*probability*
$\mathbf{Q}$	=	*weight matrix*
$\mathbf{R}$	=	*weight matrix*
V	=	*tracking control objective function*
$\mathbf{W}$	=	*weighing matrix*

Lower case letters

b	=	*discount rate*
$\mathbf{d}$	=	*projected search direction on* $\mathbf{B}$
j	=	*time step counter for moving horizon*
k	=	*time step counter*
n	=	*iteration index*
p	=	*pressure*
q	=	*flow rate*
t	=	*time*
$\mathbf{u}$	=	*input vector*
$\mathbf{u}_\theta^*$	=	*optimal* $\mathbf{u}$ *for* J_1
$\tilde{\mathbf{u}}_\theta^*$	=	$\mathbf{u}$ *optimized for* J_2 *constrained by* $\mathbf{B}$
$\tilde{\mathbf{u}}_\theta$	=	$\mathbf{u}$ *optimized for* J_2 *not constrained by* $\mathbf{B}$
$\mathbf{x}$	=	*state vector*
$\bar{\mathbf{x}}_0$	=	*prescribed value of initial conditions*
$\mathbf{y}$	=	*output vector*

Subscripts

$_1$	=	*primary*
$_2$	=	*secondary*
$_{cow}$	=	*oil/water capillary*
$_d$	=	*deterministic*
$_o$	=	*oil*
$_{RO}$	=	*robust optimization*
$_r$	=	*realization*
$_{wf}$	=	*flowing well bore*
$_{wi}$	=	*injected water*
$_{wp}$	=	*produced water*

Superscripts

*	=	*optimal*
$^-$	=	*mean*
$^\vee$	=	*vector of data-driven model*
$^\wedge$	=	*vector of full-physics life-cycle model*
^{T}	=	*transposed*

List of Publications

Journal papers

Van Essen, G.M., Zandvliet, M.J., Van den Hof, P.M.J., Bosgra, O.H., and Jansen, J.D. (2009). Robust waterooding optimization of multiple geological scenarios. *SPE Journal*, 14(1), 202-210. doi:10.2118/102913-PA. SPE 102913-PA.

Van Essen, G.M., Jansen, J.D., Brouwer, D.R, Douma, S.G., Zandvliet, M.J., Rollett, K.I., and Harris, D. (2010). Optimization of smart wells in the St. Joseph eld. *SPE Reservoir Evaluation & Engineering*, 13(4), 588-595. doi:10.2118/123563-PA.

Van Essen, G.M., Van den Hof, P.M.J., and Jansen, J.D. (2011). Hierarchical long-term and short-term production optimization. *SPE Journal*, 16(1), 191-199. doi:10.2118/124332-PA.

Van Essen, G.M., Van den Hof, P.M.J., and Jansen, J.D. (2013). A two-level strategy to realize life-cycle production optimization in an operational setting. *SPE Journal*, 18(6), 1057-1066. doi:10.2118/149736-PA.

Conference proceedings

Van Essen, G.M., Zandvliet, M.J., Van den Hof, P.M.J., Bosgra, O.H., and Jansen, J.D. (2006). Robust waterooding optimization of multiple geological scenarios. *SPE Annual Technical Conference and Exhibition*. San Antonio, Texas, U.S.A. SPE 102913-MS.

Van Essen, G.M., Van den Hof, P.M.J. and Jansen, J.D. (2009). Hierarchical economic optimization of oil production from petroleum reservoirs. Prepr. *IFAC Internal Symposium on Advanced Control of Chemical Processes* (ADCHEM). Istanbul, Turkey.

Van Essen, G.M., Van den Hof, P.M.J., and Jansen, J.D. (2009). Hierarchical long-term and short-term production optimization. *SPE Annual Technical Conference and*

Exhibition. New Orleans, Louisiana, U.S.A. SPE 124332-MS.

Van Essen, G.M., Jansen, J.D., and Van den Hof, P.M.J. (2010). Determination of lower and upper bounds of predicted production from history-matched models. In Proc.*12th European Conference on the Mathematics of Oil Recovery* (ECMOR XII). Oxford, United Kingdom.

Van Essen, G.M., Rezapour, A., Van den Hof, P.M.J. and Jansen, J.D. (2010). Integrated dynamic optimization and control in reservoir engineering using locally identified linear models. Proc. of the *49th IEEE Conference on Decision and Control* (CDC). Atlanta, Georgia, U.S.A.

Van Essen, G.M., Van den Hof, P.M.J. and Jansen, J.D. (2010). Lexicographic optimization of multiple economic objectives in oil production from petroleum reservoirs. Proc. of the *2010 American Control Conference* (ACC2010). Baltimore, Maryland, U.S.A.

Van Essen, G.M., Van den Hof, P.M.J., and Jansen, J.D. (2012). A two-level strategy to realize life-cycle production optimization in an operational setting. *SPE Intelligent Energy International Conference*. Utrecht, The Netherlands, SPE 149736-MS.

Van Essen, G.M., Jimenez, E., Przybysz-Jarnut, J.K., Horesh, L., Douma, S.G., Van den Hoek, P., Conn, A., and Mello, U.T. (2012). Adjoint-based history-matching of production and time-lapse seismic data. *SPE Europec*. Copenhagen, Denmark. SPE 154375-MS.

Van den Hof, P.M.J., Jansen, J.D., Van Essen, G.M. and Heemink, A. (2013). Model-based optimization and control of subsurface flow in oil reservoirs. Abstract of invited keynote lecture, *Chinese Control Conference*. Xi'an, P.R. China.

Kahrobaei, S., Van Essen, G.M., Van Doren, J.F.M., Van den Hof, P.M.J. and Jansen, J.D. (2013). Adjoint-based history matching of structural models using production and time-lapse seismic data. *SPE Reservoir Simulation Symposium*. The Woodlands, Texas, U.S.A. 163586-MS.

Technical reports

Van Essen, G.M., and Zandvliet, M.J. (2007). St. Joseph Waterooding Optimization Study. *Shell International Exploration and Production*, Technical report EP-2007-5030 (restricted).

Van Essen, G.M. (2008). Improved Pattern and Allocation Factor Estimation in the OFM Waterflooding Template for West-Salym. *Shell International Exploration and Production*, Technical report EP-2008-5034 (restricted).

Summary

The process of depleting an oil reservoir can be poured into an optimal control problem with the objective to maximize economic performance over the life of the field. Despite its large potential, life-cycle optimization has not yet found its way into operational environments. The objective of this thesis is to improve operational applicability of model-based optimization of oil recovery.

The reluctance of oil and gas companies to adopt this technology in their operational environments can mainly be contributed to the large uncertainties that come into play when optimizing production over the entire life of a field and - in effect - the lack of faith that exists in the available methods and models. These uncertainties are of varying nature and originate from different sources. This leads to the main research question of this thesis: Can the performance of model-based life-cycle optimization of oil and gas production in realistic circumstances be improved by addressing uncertainty in the optimization problem?

In this thesis, two approaches to address this research question are presented, related to the choice for a fixed or adaptive operational strategy. For a fixed strategy, three methods are described: hierarchical optimization, robust optimization, and integrated dynamic optimization and feedback control. For adaptive operational strategies, two aspect are investigated in a more exploratory setting: the combination of different data sources and the frequency of sequential model updating and re-optimization.

Hierarchical optimization

The impact of uncertainty on economic performance can be reduced by shortening the life-cycle of the field. Using hierarchical optimization, economic life-cycle performance can be regarded as primary objective, while speeding up the recovery process may serve as secondary objective. It is demonstrated that for optimal operational strategies with resect to the primary objective there exist redundant degrees

of freedom. This allows for improving the secondary objective (speed up) without any sacrifice in economic performance, as is demonstrated through a waterflooding example.

Robust optimization

The concept behind robust optimization is to express the objective function in probabilistic terms, or more specifically in terms of the expected value and variance. Through sampling of the uncertainty space a representative discrete set of model realizations can be created. A waterflooding example shows that optimization of the expected net present value over a set of 100 realizations can greatly improve the robustness of the operational strategy against the considered geological uncertainty.

Integrated dynamic optimization and feedback control

Instead of implementing an optimized operational strategy as is (open-loop), the output of an optimized model can also serve as a reference trajectory over time. A short-term data-driven model can be used in a tracking control setting to realize the reference trajectory in the field. Doing so allows for suppressing the effect of uncertainties and unpredictable events (disturbances) on economic life-cycle performance during execution of an operational strategy. This is demonstrated on a waterflooding example where the geology and unmodelled fast, localized dynamics are treated as undesired disturbances of which the effects are attenuated through tracking control. As a result, economic life-cycle performance is improved considerably compared to an open-loop application of the optimized operational strategy.

Combination of different data sets

Over the life of a field, measurement data from various sources can be gathered. The resolution of the data from different sources can be mapped onto a vertical, horizontal and temporal scale. Currently available measurement techniques only provide high-resolution data in one of these three dimensions. Calibration of a dynamic reservoir model (also known as ”history matching”) using a single source of data generally leaves much freedom in the model parameter space. However, combinations of complementary data sets with high-resolution data on different scales can significantly reduce the uncertainty. An example illustrates that combining 4D seismic data and production data can reduce geological uncertainty more than the individual sets can, which results in a better prediction accuracy.

Increasing the model update frequency

The current frequency at which the sequential model updates (history matching) and

re-optimization of the operational strategy are executed is in the order of every 3 to 5 years. As a result, new information on the subsurface is only used up to years later at which point it may be too late to take mitigating actions against undesired events. A waterflooding example shows that economic performance in the presence of uncertainty rises by increasing the frequency.

The methods laid out in this thesis provide improved economic life-cycle performance under uncertainty in a number of examples. While presented as separate methods, they are not mutually exclusive and could be combined into a single workflow. Although all the examples involve waterflooding as recovery mechanism, the scope for life-cycle optimization may be larger for enhanced (tertiary) oil recovery methods because of the generally higher up- and downside potential of these techniques. Application of the methods on a real petroleum reservoir is still required to evaluate their merit in a truly realistic environment.

Samenvatting

Het depletieproces van een oliereservoir kan worden beschreven als een optimaal regelprobleem met als doelstelling een maximaal economische resultaat over het leven van het veld. Ondanks de potentie ervan is deze levenscyclus optimalisatie nog niet doorgedrongen tot operationele omgevingen. Het doel van dit proefschrift is om de operationele toepasbaarheid van modelgebaseerde optimalisatie van oliewinning te verbeteren.

De weerstand van olie- en gasbedrijven om deze technologie toe te passen in hun operationele omgeving kan voor het grootste deel worden toegeschreven aan de grote onzekerheden die om de hoek komen kijken bij het optimaliseren van de productie over het hele leven van een veld en - als gevolg daarvan - het gebrek aan vertrouwen in de beschikbare methodes en modellen. De onzekerheden zijn variërend van karakter en komen voort uit verschillende bronnen. Dit heeft geleid tot de volgende onderzoeksvraag: Kan de prestatie van modelgebaseerde levenscyclus optimalisatie van olie- en gasproductie in realistische omstandigheden worden verbeterd door onzekerheid mee te nemen in het optimalisatieprobleem?

In dit proefschrift worden twee benaderingen van de onderzoeksvraag gepresenteerd die samenhangen met de keuze voor een vaste of adaptieve operationele strategie. Voor een vaste strategie worden er drie methodes beschreven: hiërarchische optimalisatie, robuuste optimalisatie, en geïntegreerde dynamische optimalisatie en terugkoppeling. Voor adaptieve operationele strategieën worden twee aspecten onderzocht in een meer verkennende context: de combinatie van verschillende bronnen van data en de frequentie van opeenvolgende modelaanpassingen en her-optimalisatie.

Hiërarchische optimalisatie

De impact van onzekerheid op het economisch resultaat kan worden verminderd door het verkorten van de levenscyclus van een olieveld. Bij hiërarchische optimalisatie

kan het economisch resultaat over de levenscyclus worden beschouwd als primaire doelstelling, terwijl het versnellen van het winningsproces kan dienen als secundair doel. Het is aangetoond dat voor optimale operationele strategieën met betrekking tot de primaire doelstelling er overtollige vrijheidsgraden bestaan. Dit maakt het mogelijk om de secundaire doelstelling (versnelling) te verbeteren zonder daarbij het economisch resultaat op te offeren. Dit wordt gedemonstreerd aan de hand van een *waterflooding* voorbeeld.

Robuuste optimalisatie

Het idee achter robuuste optimalisatie is het uitdrukken van de doelfunctie in probabilistische termen, of meer specifiek in termen van verwachtingswaarde en variantie. Doormiddel van het samplen van de onzekerheidsruimte kan een representatieve, discrete verzameling van modelrealisaties worden gecreëerd. Een *waterflooding* voorbeeld laat zien dat optimalisatie van de verwachtingswaarde (in termen van netto reële waarde) over een verzameling van 100 realisaties de robuustheid van een operationele strategie tegen geologische onzekerheid aanzienlijk kan verbeteren.

Geïntegreerde dynamische optimalisatie en terugkoppeling

In plaats van het sec implementeren van een geoptimaliseerde operationele strategie (open-lus) kan de uitvoer van een geoptimaliseerd model ook dienen als een referentietraject over de tijd. Een korte-termijn, data-gedreven model kan gebruikt worden in een volgregeling om dit referentietraject te realiseren in het veld. Dit maakt het mogelijk om de effecten van onzekerheid en onvoorspelbare gebeurtenissen (verstoringen) op het economisch levenscyclus resultaat te onderdrukken tijdens het uitvoeren van een operationele strategie. Dit wordt gedemonstreerd op een *waterflooding* voorbeeld waar de geologie en de niet-gemodelleerde snelle, lokale dynamica worden beschouwd als onwenselijke verstoringen waarvan de effecten worden onderdrukt doormiddel van een volgregeling. Zodoende wordt het economisch (levenscyclus) resultaat sterk verbeterd ten opzichte van een open-lus implementatie van de operationele strategie.

Combinatie van verschillende type data

Over het leven van een veld worden er meetgegevens van verschillende bronnen verzameld. De data resolutie van de verschillende bronnen kan uitgezet worden op een verticale, horizontale en temporele schaal. De op dit moment beschikbare meettechnieken produceren alleen hoge-resolutie data in één van deze drie dimensies. Het kalibreren van een dynamisch reservoir model (ook wel bekend als ”*history matching*”) tegen een enkele bron van data laat nog veel vrijheden toe in de parameterruimte. Het combineren van aanvullende datasets met hoge-resolutie data

op verschillende schalen kan de onzekerheid significant verminderen. Een voorbeeld illustreert dat door het combineren van 4D seismische data en productiedata de geologische onzekerheid sterker gereduceerd wordt dan individuele sets dat kunnen, met een betere voorspellingsnauwkeurigheid tot gevolg.

Verhogen van de frequentie van modelaanpassingen

De huidige frequentie waarop opeenvolgende model aanpassingen (*history matching*) en her-optimalisaties worden uitgevoerd is in de orde van elke 3 tot 5 jaar. Als gevolg daarvan wordt nieuwe informatie over de ondergrond pas jaren later gebruikt, wanneer het te laat kan zijn om nog corrigerende maatregelen te nemen tegen ongewenste gebeurtenissen. Een *waterflooding* voorbeeld laat zien dat het economisch resultaat in de aanwezigheid van onzekerheid verbetert met het verhogen van de frequentie.

De methodes die uiteengezet worden in dit proefschrift laten onder onzekere omstandigheden een verbeterd economisch resultaat over de levenscyclus van een veld zien in een aantal voorbeelden. Ondanks dat zij gepresenteerd zijn als opzichzelfstaande methodes sluiten ze elkaar niet uit en zouden kunnen gecombineerd worden in een alomvattend werkplan. Hoewel in alle voorbeelden *waterflooding* als winningsmethode wordt gehanteerd zou de scope van levenscyclus optimalisatie voor verbeterde (tertiaire) oliewinningstechnieken groter kunnen zijn door het meestal grotere positieve en negatieve potentieel van deze technieken. Het toepassen van de methodes op een echt petroleumreservoir is nog steeds vereist om hun waarde in een waarlijk realistische omgeving te bepalen.

About the author

Gijs van Essen was born on March 20th 1979 in Amersfoort, the Netherlands. He finished secondary school (VWO) in 1997 at the Vallei College in Amersfoort. In August 1997 he started his study Mechanical Engineering at Delft University of Technology. He graduated for his MSc. in October 2005 with a specialization in Systems and Control Engineering. From 2006 until 2010 Gijs was a PhD student jointly at the Delft Center for Systems & Control (DCSC) and the Department of Petroleum Engineering where he conducted research within the Integrated System Approach for Petroleum Production (ISAPP) program. The results of that research are reported in this thesis. In October 2010 started working as a research reservoir engineer in the Quantitative Reservoir Management team at Shell International E & P, working on Assisted History Matching methods. Currently Gijs is working in the Waterflood Global Deployment team.